A Physicochemical and Biophysical Investigation into the Role of Lysyl-Phosphatidylglycerol in the Membrane of Staphylococcus aureus under mild acidic conditions

Rehal, Reg

Awarding institution:
King's College London

Title: A Physicochemical and Biophysical Investigation into the Role of Lysyl-Phosphatidylglycerol in the Membrane of Staphylococcus aureus under mild acidic conditions

Author: Reg Rehal

A Physicochemical and Biophysical Investigation into the Role of Lysyl-Phosphatidylglycerol in the Membrane of *Staphylococcus aureus* under mild acidic conditions

by

Reg Paul Rehal

Mpharm

A thesis submitted for the Degree of

Doctor of Philosophy

in the School of Biomedical and Health Sciences

of King's College London

October 2013

Institute of Pharmaceutical Sciences

King's College London

Abstract

Background: *Staphylococcus aureus* readily colonises human epithelia despite the presence of innate defences including mild acidity and cationic antimicrobial peptides (CAMPs). Reduced sensitivity of *S. aureus* to these defences appears partly due to the increased biosynthesis of lysyl-phosphatidylglycerol (L-PG) in its plasma membrane. The precise mechanisms by which L-PG facilitates tolerance to acidity and CAMPs remain under-investigated, due to the lipid's lability in mild aqueous conditions. This study examines the role of L-PG in responses to epithelial defences and describes the synthesis and characterisation of a stable L-PG analogue designed for use in biophysical experiments to investigate membrane defences in *S. aureus.*

Methods: The genetic regulation of L-PG biosynthesis was studied by assessing changes in *graXRS*, *vraFG* and *mprF* expression in response to mild acidity. The effect of acidity on *S. aureus* membrane lipid composition was quantified by ^{31}P NMR. Monolayers and bilayers formed from *S. aureus* lipid extracts and synthetic lipid models were employed in investigations into the effects of low pH and CAMPs on membrane structure and physicochemical properties. The experimental techniques included neutron diffraction, small-angle neutron scattering, neutron reflectivity, pressure–area isotherms, zeta potential measurements and ^{2}H-NMR.

Results: Increased L-PG synthesis at pH 5.5, to ~50% total phospholipid, correlated with *mprF* and *graRS* expression. The L-PG concentrations at pH 5.5 produced a condensing effect on the bacterial membrane (with both natural and synthetic lipids), making it cationically charged and less permeable to solvent. These membrane changes reduced electrostatic attraction of CAMPs and retarded their ability to partition into the membrane.

Conclusions: L-PG plays an important role in *S. aureus* tolerance to mild acidity by altering plasma membrane charge and lipid packing properties. These membrane alterations also facilitate tolerance to other epithelial defences such as CAMPs, making L-PG biosynthesis a putative target for antimicrobial therapeutics.

Acknowledgements

"A man either lives life as it happens to him, meets it head-on and licks it,

or he turns his back on it and starts to wither away."

Gene Roddenberry, creator of Star Trek

I first and foremost would like to thank my principal supervisor Dr Richard D. Harvey for giving me this fantastic opportunity to do this PhD and for providing me with the freedom to run this project as my own. It has been a long and tough journey with plenty of ups and downs, however he has always stuck by me through thick and thin and I would not be at this final stage without his help and guidance. I also would like to thank my second supervisor Dr Kenneth D. Bruce for his input into my work over the years of my PhD. I must also give my utmost gratitude and appreciation to Dr Piers Gaffney (Imperial College London) for all the practical chemistry training, enlightening talks about chemistry and for help with constructing my chemistry chapter. Without whom there would be no chapter 4 onwards in this thesis!

I must also give special thanks to Dr Robert Barker (Institut Laue-Langevin) for helping me with the silanization process of the silicon substrates I required for neutron reflectivity experiments, and for assisting me with the neutron reflectivity data interpretation. Another special thank you must also go to Dr Damian Rivett (Imperial College London) for providing me with ample assistance during transcriptomic experiments. Also a last special thank you must go to the Biotechnology & Biological Sciences Research Council and King's College London for funding my work and providing me with laboratory space and equipment.

A substantial amount of the work described in this thesis would also not have been possible without the additional help of the following people: Dr Giovanna Fragneto, Dr Bruno Deme and Federica Sebstiani (Institut Laue-Langevin), Professor Robert Thomas (Oxford), Dr Jonathan Edgeworth, Dr James Mason, Dr Vincenzo Abate, Mital Patel, Anam Sacranie and Simran Uppal (King's College London) and Dr Ann Terry (Rutherford Appleton Laboratory). I owe everyone listed here my most sincere gratitude.

I would lastly like to thank my wonderful wife Jasmine Kaur Rehal who has stuck by me for the past four years and our son Rashpal Singh Rehal who was born in the second year of my PhD, both of whom have been my inspiration to carry on during the hardest times. Without the ongoing support and dedication of all my family I surely would not be where I am today!

List of Abbreviations and Symbols

4MW	Four matched water
β_{max}	Mean maximum surface pressure increase after peptide injection
$\mathcal{E}_s$	Scattered circular waveform
$\partial\Sigma/\partial\Omega$	Neutron scattering cross section
ΔV_Q	Quadrupolar splitting of ^{2}H NMR doublet signal
ε_0	Permittivity of vacuum
ε	Dielectric constant
ζ	Electrokinetic potential
η_Q	Electric field gradient asymmetry
θ	Neutron incident angle
ϑ_i	Difference between the ranking of two variables
I	Nuclear spin state
λ	Wavelength
μ	Electrokinetic frequency shift
ω	Nuclear magnetogyric ratio
Π	Surface pressure
ρ	Spearman Rho test value
ρ_n	Scattering length density of a collection of similar nuclei
ρ(r)	Mean vesicle cross sectional scattering length denisty
Υ_0	Subphase surface tension
Υ	Surface tension of subphase after in presence of an amphiphilic molecule
ψ	Lamellar d-spacing
$\aleph_i$	Number of scattering nuclei in a given layer
$\tilde{V}$	Interaction potential between a neutron and a nucleus
ω_Q	Energy separation of a nucleus between the ground state and excited states
μ	Number of gene repeats
ζ	Experimentally determined area per molecule
a_0	Voigt area function peak amplitude
a_1	Voigt area function peak centre
a_2	Voigt area function peak width

a_3	Voigt area function peak shape
A	Limiting area per molecule
aa-PG	Aminoacyl phosphatidylglycerol
A_{ex}	Excess area function
AcOH	Acetic acid
Ala	Alanine/alanyl
al-PC	1-palmitoyl-2-[16-(acryloyloxy)hexadecanoyl]-*sn*-glycero-3-phosphorylcholine
ATP	Adenosine triphosphate
BHI	Brain heart infusion
b_i	Scattering length of an atomic nucleus
B_0	Magnetic field strength
CAMP	Cationic antimicrobial peptide
cDNA	Complementary deoxyribonucleic acid
CL	Cardiolipin
C_Q	Quadrupolar coupling constant
C_T	Cycle threshold value
C^S	Compressibility index
d	Slit width
d_{62}DPPC	D_{62}-1,2 Dipalmitoyl phosphatidylcholine
d_{62}PG	D_{62}-1,2-*O*-dipalmitoyl phosphatidylglycerol
d_{62}3adLPG	D_{62}-1,2-*O*-dipalmitoyl 3-aza-dehydroxy lysyl-phosphatidylglycerol
DMAP	4-(Dimethylamino)pyridine
DMPG	1,2 Dimyristoyl-*sn*-glycero-3-phospho-(1'-*rac*-glycerol)
DP3aLPG	1,2-*O*-dipalmitoyl 3-aza lysyl-phosphatidylglycerol
DP3adLPG	1,2-*O*-dipalmitoyl 3-aza-dehydroxy lysyl-phosphatidylglycerol
DPPG	1,2-*O*-Dipalmitoyl-*sn*-glycero-3-phospho-(1'-*rac*-glycerol)
DPTAP	1,2-Dipalmitoyl-3-trimethylammonium-propane
DSC	Differential scanning calorimetry
DPL-PG	1,2-*O*-Dipalmitoyl lysyl-phosphatidylglycerol
ΔE	Change in energy level
EDC.HCl	*N*-(3-dimethylaminopropyl)-*N'*-ethylcarbodiimide hydrochloride
e*Q*	Quadrupole moment

e^2qQ	Static quadrupolar coupling constant
$F(h)$	Absolute structure factor
$F^M(h)$	Absolute structure factors of a bilayer without magainin 2 F5W
$F^P(h)$	Absolute structure factors of a bilayer with magainin 2 F5W
G	Gaseous phase
Gro	Glycerol chain in phosphatidylglycerol
h	Order of neutron diffraction
HR-ESI+	High resolution electrospray analysis
Hz	Hertz
$I(h)$	Neutron diffraction peak area
k_i	Neutron incident vector
k_r	Neutron reflected vector
k'	Neutron circular scattering vector
K	Mean time taken for the surface pressure to increase by 50% after peptide injection
K^s	Compressional modulus
$L_i(h)$	Neutron diffraction Fourier transformation correctional factors
L_α	Fluid phase
$L_{\beta'}$	Gel phase
L_c	Liquid condensed phase
L_e	Liquid expanded phase
L-PG	Lysyl-phosphatidylglycerol
LUV	Large unilamellar vesicle
Lys	Lysine/lysyl
mRNA	Messenger ribonucleic acid
MIC	Minimum inhibitory concentration
MLV	Multi-lamellar vesicle
MprF	Multiple peptide resistance factor
MRSA	Methicillin resistant *Staphylococcus aureus*
MS	Mass spectrometry
MSSA	Methicillin susceptible *Staphylococcus aureus*
NMR	Nuclear magnetic resonance
NQR	Nuclear quadrupole resonance

n	Number of ranks in Mann Whitney U-test
N_α	Low energy state nuclei
N_β	High energy state nuclei
OD_{600}	Optical density at λ = 600nm
PCR	Polymerase chain reaction
PE	Phosphatidylethanolamine
PG	Phosphatidylglycerol
$P_{\beta'}$	Ripple phase
PO3adLPG	1-*O*-palmitoyl-2-*O*-oleoyl 3-aza-dehydroxy lysyl-phosphatidylglycerol
ppm	Parts per million
PPTS	Pyridinium *p*-toluene sulfonate
Ptd	Glycerol in diacylglycerol
qPCR	Quantitative polymerase chain reaction
q_z or Q_z	Neutron angular momentum transfer perpendicular to the membrane interface
r	Waveform radius
r^2	Correlation coefficient
R_f	Retention factor
RT	Reverse transcription
SAM	Self-assembled monolayer
S_{CD}	Order parameter
SANS	Small angle neutron scattering
SLD	Scattering length density
SMW	Silicon matched water
SUV	Small unilamellar vesicle
TBDMS	T*ert*-butyldimethylsilyl
TCRS	Two-component regulatory system
TFA	Trifluoroacetic acid
THF	Tetrahydrofuran
THP	Tetrahydropyran
TIPS	Triisopropylsilane
TLC	Thin layer chromatography
TMCL	1,1',2,2'-Tetramyristoyl cardiolipin

TMPA	3-(Trimethoxysilyl)propyl acrylate
TRIS	Tris(hydroxymethyl)aminomethane
T_m	Main phase transition temperature
TMDs	Transmembrane domains
tRNA	Transfer ribonucleic acid
V	Electric field gradient
U_i	Calculated experimental Mann Whitney U-test value
U_{crit}	Mann Whitney U-test critical U value
WAXS	Wide angle X-ray scattering
Z	Distance along bilayer normal

All statistical errors reported in both graphs and tables throughout this thesis are to one standard deviation, unless otherwise stated.

Table Of Contents

List of Figures

List of Tables

Chapter 1

Main Introduction

1.1 Bacterial Aminoacyl Phospholipids

Phospholipids are a primary component of cellular plasma membranes which enable cells to exist as discrete morphological structures by forming membranes which separate them from their external environment. However, the role of membrane phospholipids is not limited to this function as they are known to partake in a multitude of cellular activities including energy generation, maintenance of ion gradients, cell division (Rang *et al.* 2003), apoptosis (Fadok *et al.* 2000), drug resistance in prokaryotes (Nishi *et al.* 2004), providing a permeability barrier and the supporting of membrane protein activities (Dowhan 1997). Phospholipid core structures are similar to those of surfactants since they consist of a lipophilic hydrocarbon chain attached to a hydrophilic headgroup (figure 1-1). These structural features allow the phospholipids to assemble into bilayers in an aqueous milieu, possessing a hydrophobic core with the headgroups presenting at the interfaces between the membrane surfaces and their aqueous environment (figure 1-1).

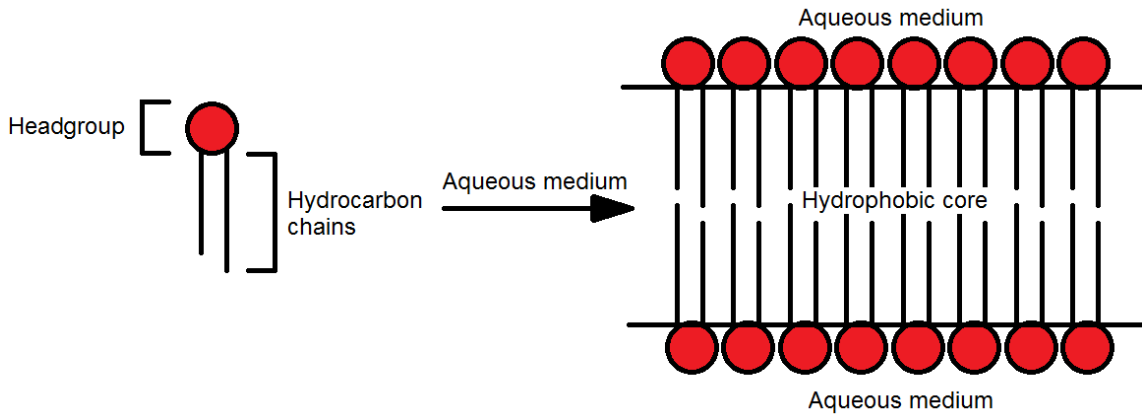

Figure 1-1 Schematic of a lipid molecule and the resulting bilayer when added to an aqueous environment.

The majority of phospholipids found in the cells of living organisms are glycerophospholipid analogues with the exception of sphingomyelin which is a derivative of sphingosine (Drabkin 1958). The major glycerophospholipids found in mammalian membranes are zwitterionic phosphatidylcholines whereas bacterial cells principally contain zwitterionic phosphatidylethanolamine (PE) and/or anionic phosphatidylglycerol (PG) (Roy 2009). With

respect to bacteria, the proportions of PE and PG can vary greatly from species to species and can even show inter-strain differences within the same species groups. This variation in the levels of commonly expressed phospholipids results in bacterial cells with various morphologies (e.g. rods and cocci) and different membrane properties. However, some bacteria have a more diverse phospholipid content and have evolved the ability to modify their phospholipids (most notably PG) with various amino acids forming aminoacyl lipids which alter their membrane surface properties in response to their growth environment (Asselineau 1991).

The first bacterial aminoacyl lipids to be isolated, the aminoacyl PGs (aa-PGs), were discovered in the early 1960s in a small number of Gram positive bacteria (Roy 2009). These aa-PGs were formed from the generation of an ester group between the carboxylic acid group of lysine or alanine, and the 1 position hydroxyl group of the headgroup glycerol of PG (Gould & Lennarz 1967). Later studies also revealed the existence of glycerol 2 position structural isomers of these aa-PGs in *Enterococcus faecalis* (figure 1-2) (Gould & Lennarz 1967, Tocanne *et al.* 1974a, Dossanto *et al.* 1970).

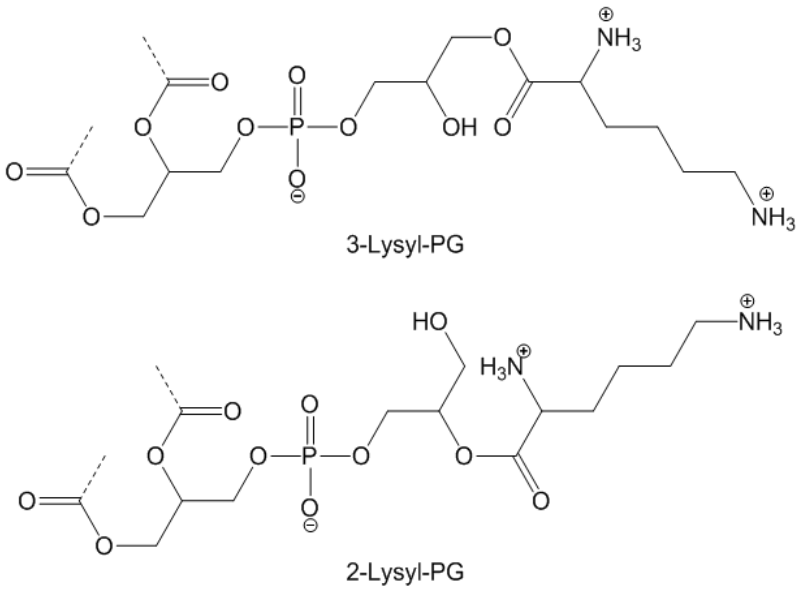

Figure 1-2 Structures of the headgroups of 3-lysyl-PG and 2-lysyl PG.

The screening of several bacterial species (including Gram negatives) later revealed the presence of aa-PGs in a very wide range of bacteria (figure 1-3). In addition, a greater diversity of amino acids such as ornithine (Houtsmuller & Van Deenen 1963), arginine (Dossanto *et al.* 1970) and glycine (Gould & Lennarz 1967) were also found covalently bonded to PG in a variety of species. Most studies which examined the presence and abundance of aa-PGs in bacteria

showed them to be synthesised in the bacterial plasma membranes in response to environmental stresses (e.g. low pH, exposure to cationic antimicrobial peptides or CAMPs, exposure to antibiotics etc.) (Gould & Lennarz 1967, Dossanto *et al.* 1970, Houtsmuller & Van Deenen 1963, Slavetinsky *et al.* 2012). Increased biosynthesis of the aa-PGs has been suggested to alter the physicochemical properties of bacterial plasma membranes facilitating a reduction in their susceptibility to these environmental stresses (Geiger *et al.* 2010).

Although a number of different bacterial aa-PGs were shown to exist, most recent studies have focused on the function and role of lysyl-PG (L-PG) and alanyl-PG in bacterial plasma membranes (Slavetinsky *et al.* 2012). The latter of these two phospholipids is a zwitterionically charged lipid at physiological pH and its function in bacterial membranes is still not fully understood, however, its presence increases the MIC of *Staphylococcus aureus* upon exposure to CAMPs and daptomycin, after *mprF* from *Clostridium perfringens* has been introduced into *S. aureus* (Slavetinsky *et al.* 2012). L-PG however, is a much more widely studied cationic aa-PG and is found in many bacteria (figure 1-3), but it is commonly found at high concentrations (~50% total membrane phospholipid) in the plasma membrane of *S. aureus* when the bacterium is exposed to sub-lethal concentrations of CAMPs or when cultured in a low pH medium (Nishi *et al.* 2004, Gould & Lennarz 1970, Peschel *et al.* 2001). The reason for this high biosynthesis of L-PG in *S. aureus* under these conditions has been the subject of great interest, because *S. aureus* has been found to colonise human epithelial surfaces such as skin and the anterior nares of the nasal cavity which are both low pH environments and possess a high abundance of CAMPs (Lambers *et al.* 2006, Ong *et al.* 2002, Washington *et al.* 2000, Von Eiff *et al.* 2001, Cole *et al.* 1999). Previous studies conducted to understand the role and function of L-PG at such high concentrations in the plasma membrane of *S. aureus* have proven difficult due to the labile nature of L-PG under mild aqueous conditions (*vide infra*) (Danner *et al.* 2008). Therefore the primary aim of the study described in this thesis was to find techniques and strategies to better understand the role and function of L-PG in the plasma membrane of *S. aureus* when the bacterium is grown under a low pH environment or in the presence of CAMPs. This was achieved by examining the behaviour of lipid extracts from *S. aureus* grown at pH 5.5 and 7.4, and biomimetic synthetic lipid models of these *S. aureus* lipid extracts, with biophysical experiments under both pH 5.5 and 7.4 environmental conditions in the absence and presence of a CAMP.

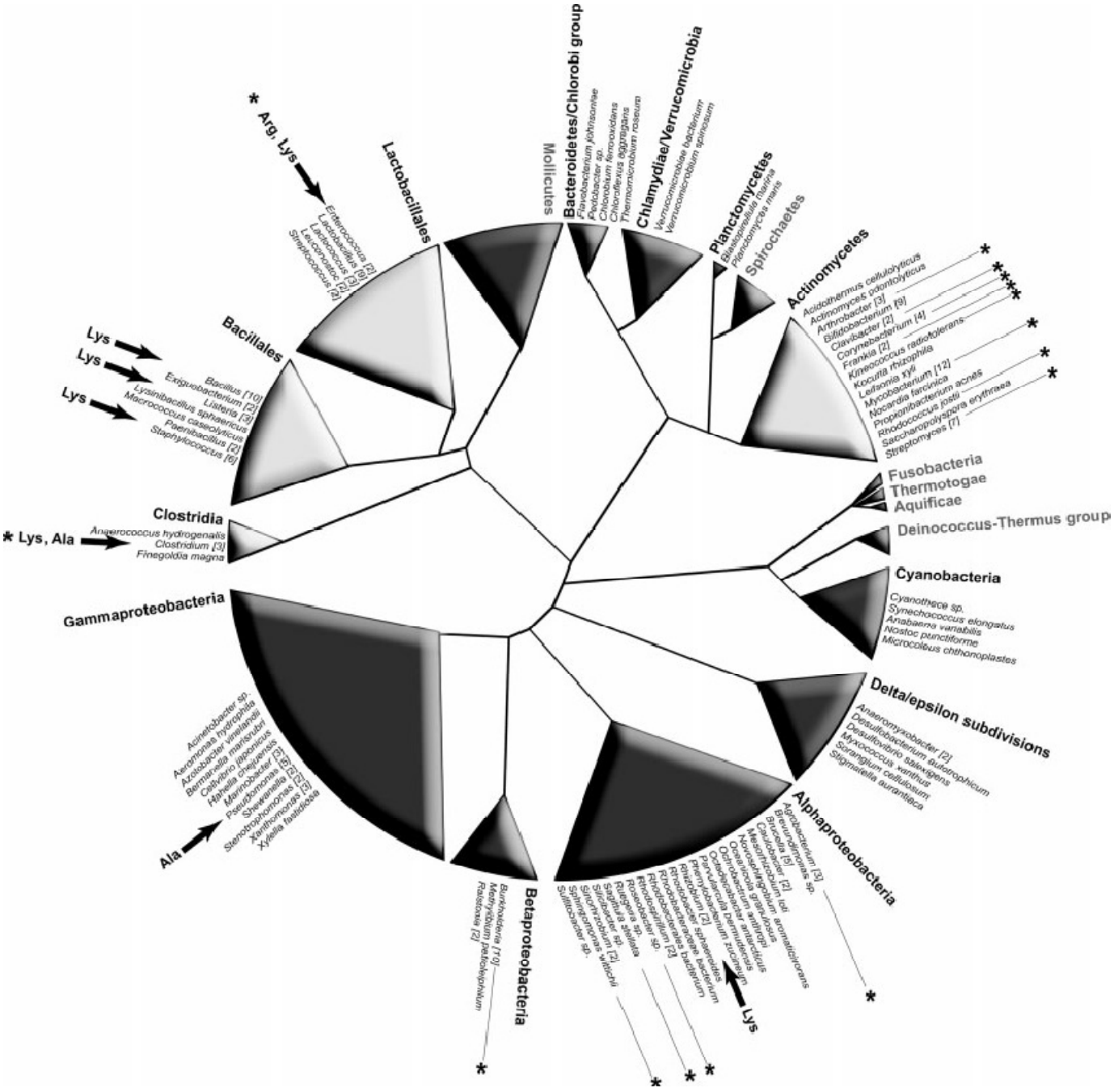

Figure 1-3 Phylogenic map of the distribution of alanyl-PG (Ala) and L-PG (Lys) in all known bacteria expressing these lipids up to the end of 2008. Organisms which contain *mprF* paralogs are highlighted (*). Reproduced from Roy, H., (2009) (Roy 2009).

The initial discovery of L-PG was in the early 1960s (Macfarlane 1962) and it was recognised as one of the major phospholipids in *S. aureus* in addition to PG and cardiolipin (CL) (figure 1-4). The net headgroup charge of L-PG was observed to be +1 as it contains two protonated amines and one phosphate group whereas the headgroups of PG and CL possess net -1 charges (figure 1-4) (Gould & Lennarz 1970, Haines 2009). The function of L-PG in *S. aureus* was unknown at the time of its discovery, however, studies in the 1970s revealed it to

constitute ~30% of the total membrane phospholipid content at physiological pH, increasing at low pH (~pH 5.2) to ~50% total phospholipid (figure 1-4) (Gould & Lennarz 1970). (figure 1-4) (Gould & Lennarz 1970). This finding suggested that the presence of an increased number of protons in the external growth environment of *S. aureus* activated a sensory response from the bacteria resulting in the increased biosynthesis of L-PG. The reason for the increased levels of L-PG in membranes was suggested to be due to lipid ion-pairs being formed between L-PG and PG or CL therefore attenuating the surface anionicity of the plasma membrane thus reducing electrostatic attraction of protons to the membrane outer surface (Gould & Lennarz 1970, Tocanne *et al.* 1974c).

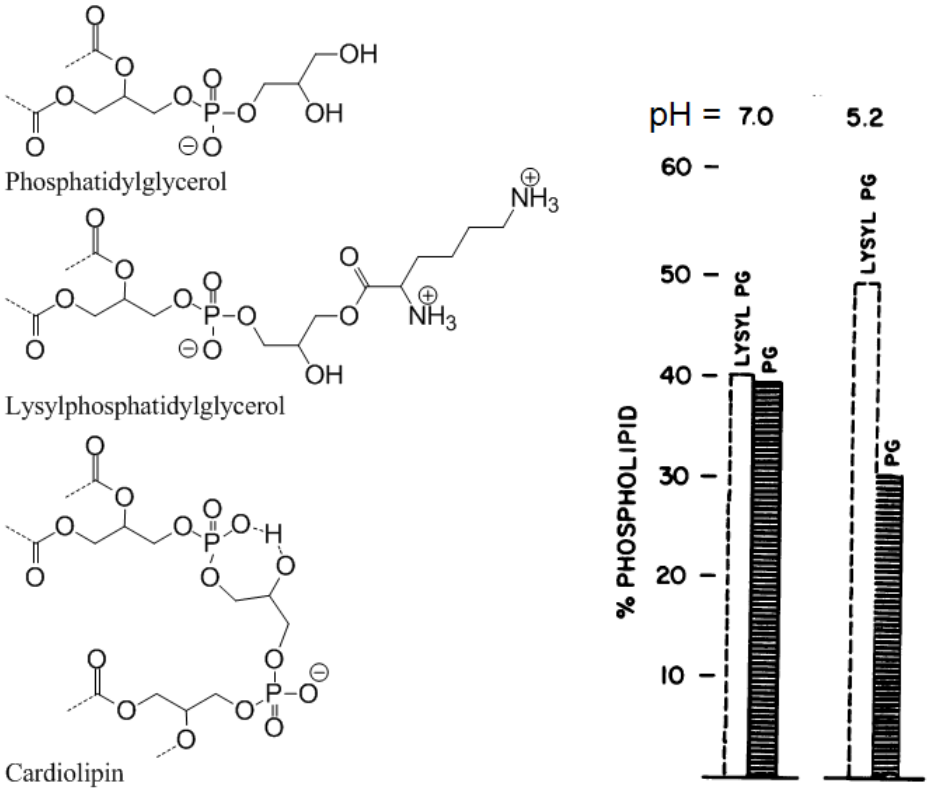

Figure 1-4 Structures of the major phospholipids found in *S. aureus* and an adapted figure from Gould W. and Lennarz J., (1970) (Gould & Lennarz 1970) showing the expression of L-PG and PG in *S. aureus* grown at pH 7.0 and pH 5.2.

1.2 The estimated pKas of L-PG

Although L-PG was estimated to have a +1 charge, it was unknown whether this charge existed at all pH values and therefore in the mid-1970s pKa studies on synthetic L-PG were conducted by the deposition of the lipid as monolayers on subphases of pH 2.0 up to pH 10.0 (Tocanne *et al.* 1974c). The limiting area per molecule of the lipid on each subphase in the liquid condensed phase (~30 mN/m) was then used to construct a pH titration curve of limiting

area per molecule as a function of increasing pH (figure 1-5). The pH titration curve revealed estimated pKa data on the ionisable groups of L-PG of 1-3, 6-7 and >10 and these were assigned to the lipid's phosphate, α-amine and ε-amine group's, respectively (figures 1-5) (Tocanne *et al.* 1974c). Therefore, at physiological pH the headgroup of L-PG was likely to exist in two forms, zwitterionic and cationic, whereas at low pH it would be mainly cationic. Further studies also revealed lipid ion-pair formation between L-PG and PG was greatest at low pH compared to physiological pH as lateral density of monolayers composed of L-PG and PG 1:1 mol/mol was greatest on a pH 5.8 subphase (Tocanne *et al.* 1974c).

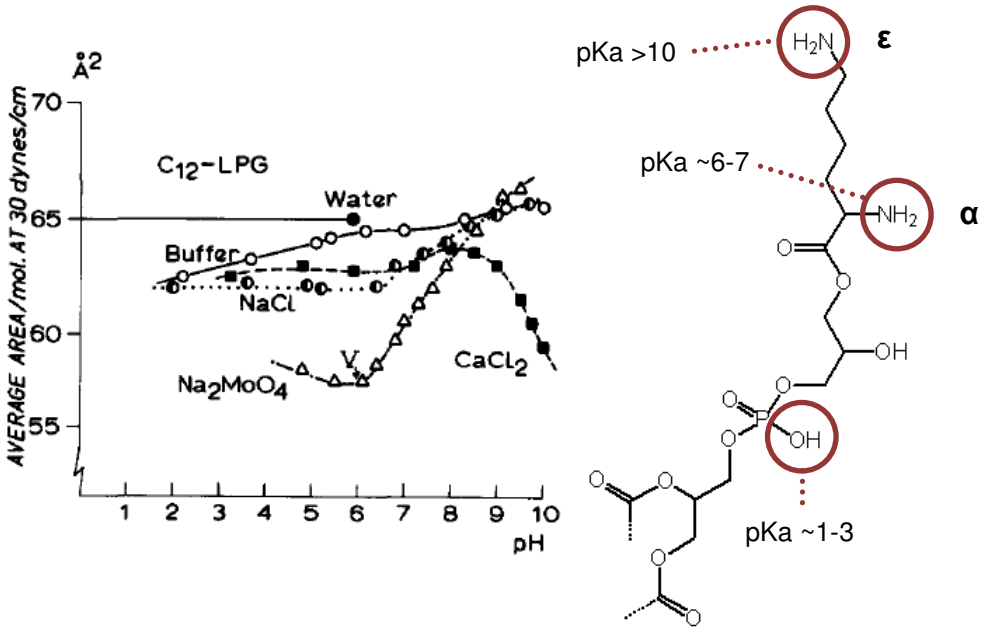

Figure 1-5 Reproduced pH titration curve of synthetic C_{12}-L-PG from Tocanne *et al.*, (1974) (Tocanne *et al.* 1974c) and the molecular structure of the headgroup of L-PG and the pKas of its ionisable groups

1.3 The labile nature of L-PG

Differential scanning calorimetry (DSC) of 100% 1,2-*O*-dipalmitoyl L-PG (DPL-PG) dispersed as vesicles was shown to exhibit a main lipid phase transition temperature (T_m) of between 40.2°C and 40.5°C with a ripple phase between 37°C and 38°C (figure 1-6) (Danner *et al.* 2008). However, a number of higher temperature phase transitions were also detectable in these vesicles and suggested L-PG may be breaking down (Danner *et al.* 2008). The breakdown of L-PG under a mild aqueous environment has been observed previously in several studies; and under low pH conditions (<pH 3.0) hydrolysis of the two acyl hydrocarbon chain esters takes place and at high pH (>pH 5) hydrolysis of the aminoacyl ester occurs (Gould & Lennarz 1970, Danner *et al.* 2008, Tocanne *et al.* 1974c). These L-PG degradation products at

different pHs are shown in the DSC scans of DPL-PG in figure 1-6 where a T_m ~55℃ of palmitate is shown at pH 2.0 and a broad T_m 40℃ - 55℃ of L-PG and PG mixed with lysine is shown at pH 9.0.

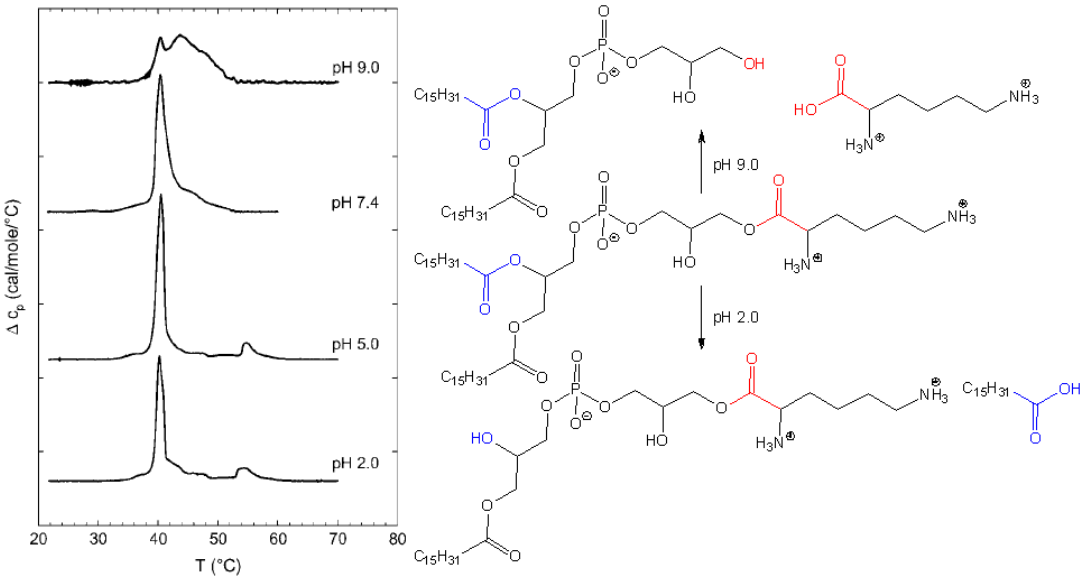

Figure 1-6 Adapted DSC scans from Danner *et al.* (2008) of DPL-PG in numerous pH environments and the structures of the possible breakdown products of DPL-PG at different pHs (Danner *et al.* 2008).

To further highlight the highly labile nature of L-PG under a mild aqueous environment, wide angle X-ray scattering (WAXS) of 100% DPL-PG showed the presence of three different domain structures at 15℃ (figure 1-7) (Danner *et al.* 2008). Two of these domains ($\beta'_{1,2}$) were formed of bilayers, but were found to be contaminated with palmitate (figure 1-7). The remaining domain (β,h) was an interdigitated bilayer of 100% DPL-PG however its abundance was very low suggesting a high degree of DPL-PG breakdown had occurred in the sample (Danner *et al.* 2008).

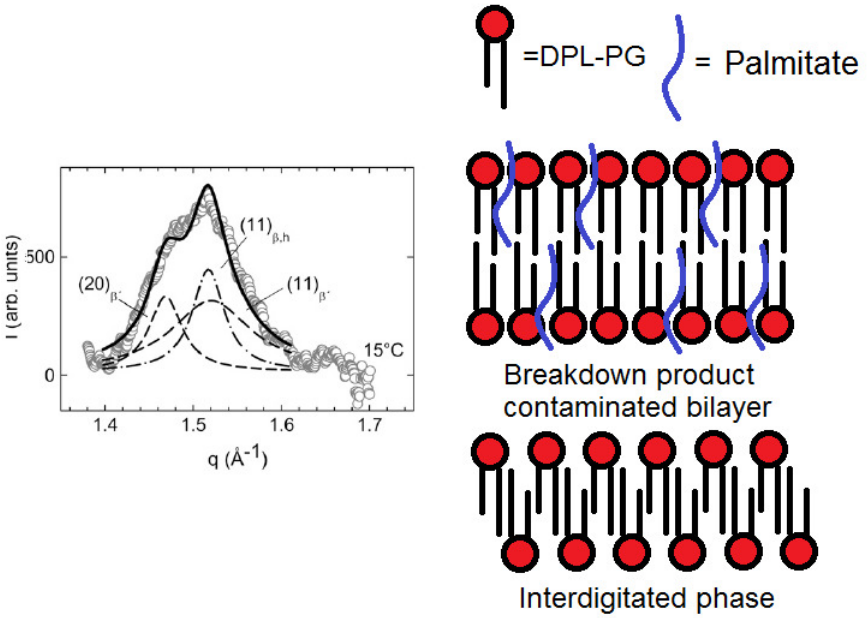

Figure 1-7 Adapted WAXS scan of DPL-PG at pH 5.0 from Danner *et al.* (2008) showing the presence of three domain structures at 15°C and the possible structure of these domains (Danner *et al.* 2008).

The demonstrated high lability of L-PG under mild aqueous conditions makes the lipid difficult to study in experiments with PG and CL and may explain why the literature lacks valid experimental data on the mechanistic role and function of L-PG in the plasma of *S. aureus*. Therefore one of the other aims of this thesis was also to address this problem by synthesising an aqueous stable analogue of L-PG which could be used as an L-PG substitute in synthetic lipid models of the plasma membrane of *S. aureus.*

1.4 Isolation, lipid quantification and surface charge properties of membranes containing L-PG

1.4.1 Protoplasts

In order to examine the changes in plasma membrane outer leaflet surface charge of live *S. aureus* grown at two different pHs, direct access to the bacterial plasma membrane surface is required. The main problem of gaining this access is the presence of a peptidoglycan cell wall which surrounds the surface of the *S. aureus* plasma membrane (figure 1-8).

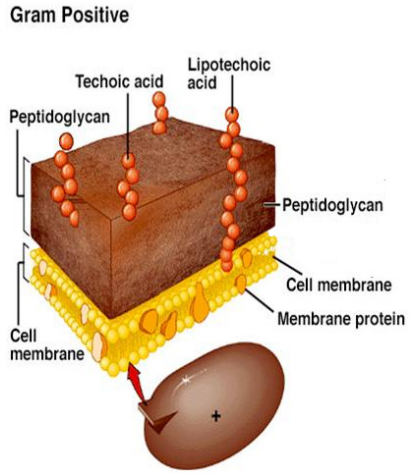

Figure 1-8 Reproduced image from Medimoon Ltd. (2013) showing the membrane structure of *S. aureus* (Medimoon Ltd. 2013).

In a recent study this problem has been avoided by removal of the cell wall of *S. aureus* by enzymatic digestion (Kim *et al.* 2009). This technique involves the use of lysostaphin which is a glycylglycine endopeptidase that specifically targets D-glycine-D-glycine units in the pentaglycine domain of peptidoglycan (Iversen & Grov 1973). The result of this enzyme's activity is the cleavage of the cell wall of *S. aureus* leaving a protoplast of the bacterium remaining and the outer surface of the plasma membrane open for examination. In order to analyse the protoplast surface charge properties zeta potential measurements can be undertaken where zeta potential of a cell, also known as the electrokinetic potential (ζ), is a measure of the surface charge of a cell at the shear plane (figure 1-9) (Fell 2004). The shear plane (or plane of slip) is the distance from the surface of the cell where the solute molecules associated with the cell surface are not bound to it as a moving unit and can move away freely from the cell (Wilson *et al.* 2001). The technique works by creating a potential between two electrodes in an aqueous medium in which the cells are suspended. A laser is then projected between the electrodes and the change in frequency of the detected beam caused by the

movement of the cells is used to calculate their electrophoretic movement. This frequency shift (μ) is then used in the Smoluchowski equation (Hunter 1988) in order to calculate the cells' mean ζ:

$$\zeta = \frac{\eta\mu}{\varepsilon_0\varepsilon} \tag{1}$$

Where, η is the viscosity of the medium, ε_0 is the permittivity of vacuum and ε is the dielectric constant of the medium.

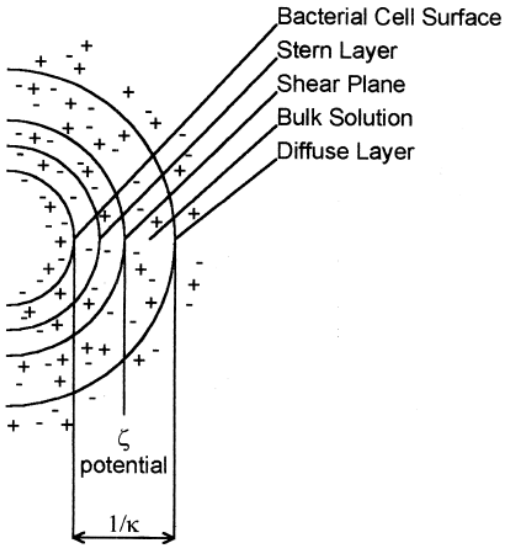

Figure 1-9 Reproduced image from Wilson *et al.* (2001) showing the various solvent layers surrounding a bacterial cell (Wilson *et al.* 2001).

In previous studies of whole cell zeta potential, changes in *S. aureus* zeta potential before and after exposure to the CAMPs LL-37 and hBD3 showed a zeta potential result of -15.0 mV ± 4.0 mV in the absence of the CAMPs and a zeta potential result of -12.9 mV ± 1.9 mV after exposure to the CAMPs (Ouhara *et al.* 2008). The reduction in zeta potential after CAMP exposure was attributed to increased cell wall D-alanylation and upregulation of plasma membrane L-PG content (Ouhara *et al.* 2008). From these results it would appear that zeta potential measurements are sensitive enough to detect changes in the surface charge of *S. aureus* protoplasts caused by changes in plasma membrane L-PG biosynthesis. Therefore zeta potential measurements were used to examine the plasma membrane surface charge presentation of *S. aureus* protoplasts when grown in both pH 5.5 and 7.4 environments.

1.4.2 Polar lipid extraction

In order to perform biophysical experiments on the phospholipids biosynthesised by *S. aureus* in both pH 5.5 and 7.4 growth environments, the lipids must first be extracted from the bacterium. A number of studies utilise the widely accepted methods of Bligh and Dyer (Bligh & Dyer 1959) for polar lipid extraction from bacteria. The technique takes advantage of the different miscibilities of chloroform, methanol and water when mixed in different proportions. The principal of the technique involves solvent phase manipulation and begins with forming a single phase mixture of the bacterial cell (~98% water) and 20 sample volumes of chloroform and methanol; the organic solvents are mixed in the ratio 2:1 v/v, respectively. After formation of the single phase it is separated into two phases by the addition of 8.3 sample volumes of water. The resulting two phase system contains the bacterial phospholipids in the higher density lower organic layer (figure 1-10).

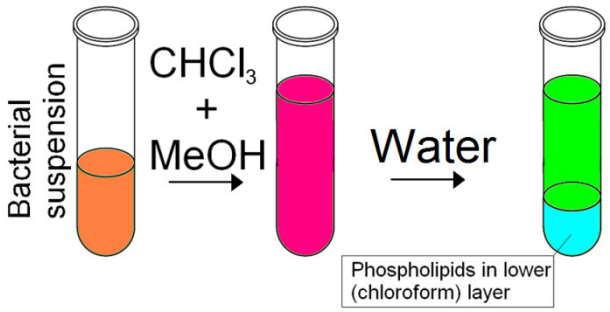

Figure 1-10 Simplified schematic showing the basic principles of the Bligh and Dyer lipid extraction protocol.

A major problem, however, of adapting the original Bligh and Dyer technique to *S. aureus* is the hydrolysis of L-PG when in contact with the aqueous solvent (section 1.3). To try and avoid this problem an acid-modified version of the technique has been formulated, which involves the addition of 0.13 sample volumes of 2N HCl to the bacterial pellet before extraction and the use of only pH 2.0 saline when adding the aqueous phase to the single phase mixture (figure 1-10) (Foreman-Wykert *et al.* 2000). Maintaining low pH conditions throughout the lipid extraction process stabilises the headgroup of the L-PG molecule and limits its degradation. Therefore the acid-modified polar lipid extraction protocol was used in this thesis in order to obtain polar lipid extracts from *S. aureus*.

1.4.3 Identification and quantification

Identification of phospholipids from biological extracts is traditionally performed by normal phase two dimensional thin layer chromatography (TLC) (Rouser *et al.* 1970). This system is ideally suited to performing this task due to the difference in bonding strengths and polarities of the phospholipid headgroups with the silica adsorbent (Snyder 2008). The fundamentals of the technique involve competition of the localised phospholipids with the polar eluting solvent for the silanol groups of the silica adsorbent. Depending on the strength of localisation of the phospholipid and the developing solvent, the phospholipid will migrate in the direction of the developing solvent by a certain distance (retention factor, R_f) (Snyder 2008). Normally, phospholipids cannot be developed by a single solvent but require a multi-solvent mixture due to the strong localisation of the phospholipid headgroups to the silica. With respect to the phospholipids found in *S. aureus*, a previous study has suggested the best developing mobile phase for the horizontal direction is chloroform–methanol–ammonium hydroxide 33% (65:25:5 v/v/v) and then chloroform–acetone–acetic acid–methanol–water (45:16:9:8:4 v/v/v/v/v) for the vertical direction (Mukhopadhyay *et al.* 2007). The developed results give a chromatogram as shown in figure 1-11.

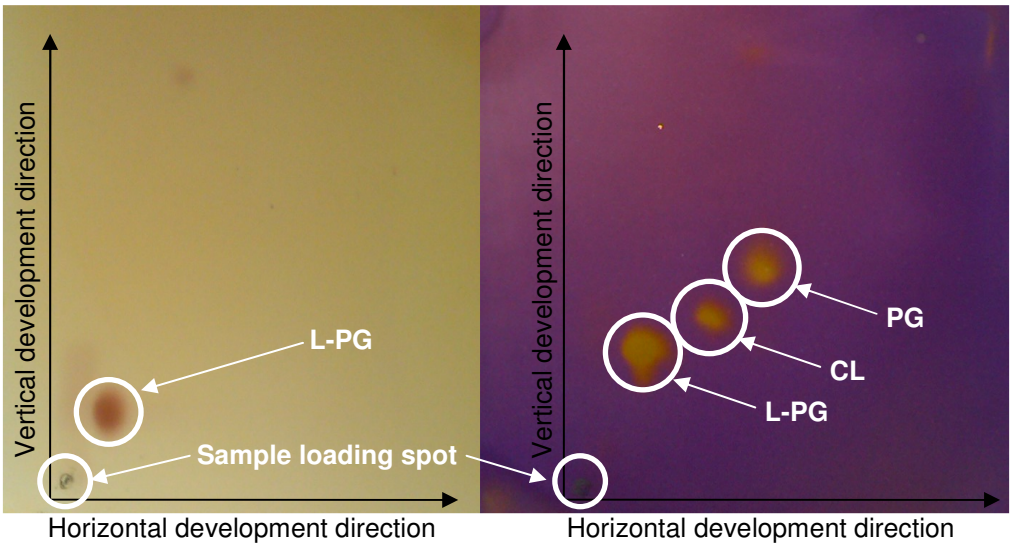

Figure 1-11 Chromatogram of the separated lipids from *S. aureus* 476; ninhydrin stain (left) and potassium permanganate stain (right). L-PG = Lysylphosphatidylglycerol, PG = phosphatidylglycerol and CL = cardiolipin.

The staining agents for the TLC chromatograms are highly diverse depending on what information is being sought after. However a large number of studies utilise a Dittmer-Lester reagent as the mixture forms a blue complex with the phosphorous of the phospholipids (Vaskovsky & Kostetsky 1968, Diltmer & Lester 1964). Other commonly used staining reagents

are ninhydrin which visualises amine or amide containing lipids and potassium permanganate which visualises compounds with oxidisable groups (Skipski *et al.* 1964).

Relative quantification of the lipids from TLC chromatograms is carried out either by densitometry or by TLC spot digestion. Densitometric methods depend on charring of the phospholipid spots using copper reagents or strong acids such as sulphuric acid (Gustavsson 1986). The TLC chromatograms are then digitally scanned and the TLC spots are analysed by their density in order to extrapolate a relative quantification (Gustavsson 1986). The phosphodigestion method requires the TLC spots to be scrapped into individual vials and digested by a chloro-peroxide agent which liberates the phosphate from the phospholipid. Ammonium molybdate salts and ascorbic acid are then added after digestion in order to form a phospho-molybdate complex which absorbs at λ 830 nm (Mrsny *et al.* 1986). Spectroscopic analysis then determines the relative quantification of the phospholipids from the different absorbances of the phospho-molybdate complexes in the individual lipid samples.

Although the lipid identification and quantification methods described are assumed as 'gold standard' they do however lead to inaccurate results. The TLC separation utilises strong acids and bases in order to increase polarity of the mobile phase and allow the phospholipids to migrate. These strong acid-base properties of the developing agents can lead to degradation of the phospholipids, especially L-PG as it is already has a labile ester group. Additionally, TLC development can take up to 2-3 hours for good spot separation which increases the time the lipids are in contact with the mobile phase and increases the likelihood of lipid degradation. The densitometric quantification requires an even spread of the staining agent over all spots, and enough sample and staining agent to provide a good resolution development. Both of these aspects are difficult to achieve and uneven staining can result in density inaccuracies between phospholipid spots, and overloaded or inadequately loaded sample onto the TLC plate can lead to gross over or under estimations of phospholipid quantities, respectively. Phosphodigestion requires the use of harsh non-environmentally friendly oxidising agents which can be potentially hazardous to the user, especially when heated to ~100-200°C. This method also requires a substantial amount of time before full digestion of the phospholipid (up to 24 hours) (Mrsny *et al.* 1986) and the molybdate reaction adds a further time constraint (~2-3 hours). Contamination of the sample with acidic compounds e.g. phosphoric acids, can often hinder the accuracy of this assay as these can also form molybdate complexes.

Recently, more sophisticated high-throughput techniques have been trialled to overcome the problems associated with the traditional methods for phospholipid identification and quantification. One such method is ^{31}P NMR, where the resonance signal of naturally occurring isotopic phosphorous-31 in individual phospholipids is directly examined from a lipid extract in order to identify and relatively quantify the lipids in the extract. The reason ^{31}P in phospholipids can be used to examine these aspects is because ^{31}P has an atomic nucleus which has a nuclear spin that allows it to behave as a magnetic bar (Williams & Fleming 2008). This nuclear spin (I) is equal to ½, which means that ^{31}P nuclei can take up one of two orientations when placed in an applied magnetic field; high energy (opposing the direction of the applied field) or low energy (with the direction of the applied field) (Williams & Fleming 2008). In general, the difference in the energy levels (ΔE) of nuclei with I = ½ is governed by:

$$\Delta E = \frac{h\omega B_0}{2\pi} \tag{2}$$

where, ω is the magnetogyric ratio, h is Planck's constant and B_0 is the strength of the applied magnetic field.

To assess the distribution of nuclei in the high energy state (N_β) and in the lower energy state (N_α) the Boltzmann equation can be applied:

$$\frac{N_\beta}{N_\alpha} = e^{-\frac{\Delta E}{kT}} \tag{3}$$

Therefore if a radio-frequency signal is applied to the system and it matches the frequency at which the nuclear magnets naturally spin in, in the magnetic field B_0, then a shift in the N_β/N_α ratio occurs and more nuclei are promoted to the N_β level (Williams & Fleming 2008). This resonance frequency (161.9 MHz for ^{31}P) is given by:

$$v = \frac{\gamma B_0}{2\pi} \tag{4}$$

On discontinuation of the applied radio-frequency the nuclei revert back to their N_α state however the relaxation releases energy in the form of an emitted radio frequency which is

detected. This detected radio signal is then analysed by Fourier transformation (Williams & Fleming 2008) to give a resonance peak in an NMR spectrum (figure 1-12).

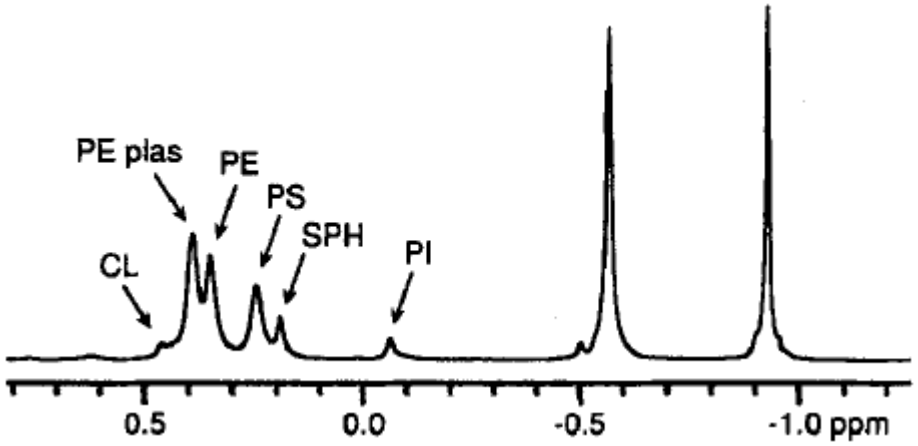

Figure 1-12 ^{31}P NMR spectrum of rat liver and brain lipid extracts. Reproduced from Metz and Dunphy (1996) (Metz & Dunphy 1996).

The appearance of a resonance signal in the NMR spectrum tends to vary substantially depending on the chemical and magnetic environment surrounding that atom. This is because the surrounding atoms or chemical groups also act as magnets and will exert a magnetic field on the atom of interest which alters the energy required to promote the atom to the N_β state. A surrounding atom or chemical group can either have a shielding effect where the neighbouring atom is electron donating or a deshielding effect where the neighbouring atom is electron withdrawing (Williams & Fleming 2008). If the surrounding groups are electron donating the atom of interest becomes more magnetically shielded which results in the influence of the applied magnetic field of the instrument to be weaker on the atom of interest and the radio-wave energy required to promote it to a N_β state reduced. Therefore the emitted radio-wave energy is also reduced on relaxation of the atom leading to the NMR signal appearing more positive (upfield) in the NMR spectrum (e.g. PI in figure 1-12). Electron withdrawing groups reduce the magnetic shielding around the atomic nuclei thus the signal appears more negative or downfield (e.g. CL in figure 1-12). This change in chemical shift of ^{31}P NMR signals was highly advantageous for the identification of phospholipids in *S. aureus* lipid extracts as all the lipids in *S. aureus*, namely L-PG, PG and CL, all showed up with different chemical shift values due to the various chemical environments surrounding their phosphate groups.

Although qualitative information can be extracted from ^{31}P NMR, relative quantitative information can also be extracted from the ^{31}P NMR spectrum. Studies by Metz and Dunphy (1996) on rat brain and liver lipid extracts (figure 1-12) demonstrated that the integrated area of a single ^{31}P NMR resonance signal was related to the abundance of that assigned lipid in the actual sample (Metz & Dunphy 1996). However, one problem that can be encountered with this method is resonance signal overlap of more than one phospholipid appearing at similar resonances in the ^{31}P NMR spectrum. This problem can be overcome by fitting Voigt area functions (figure 1-13) to the overlapping signals which allow deconvolution of these resonance signals; an example of this deconvolution is shown in figure 1-13 with a methicillin resistant *S. aureus* (MRSA) phospholipid extract.

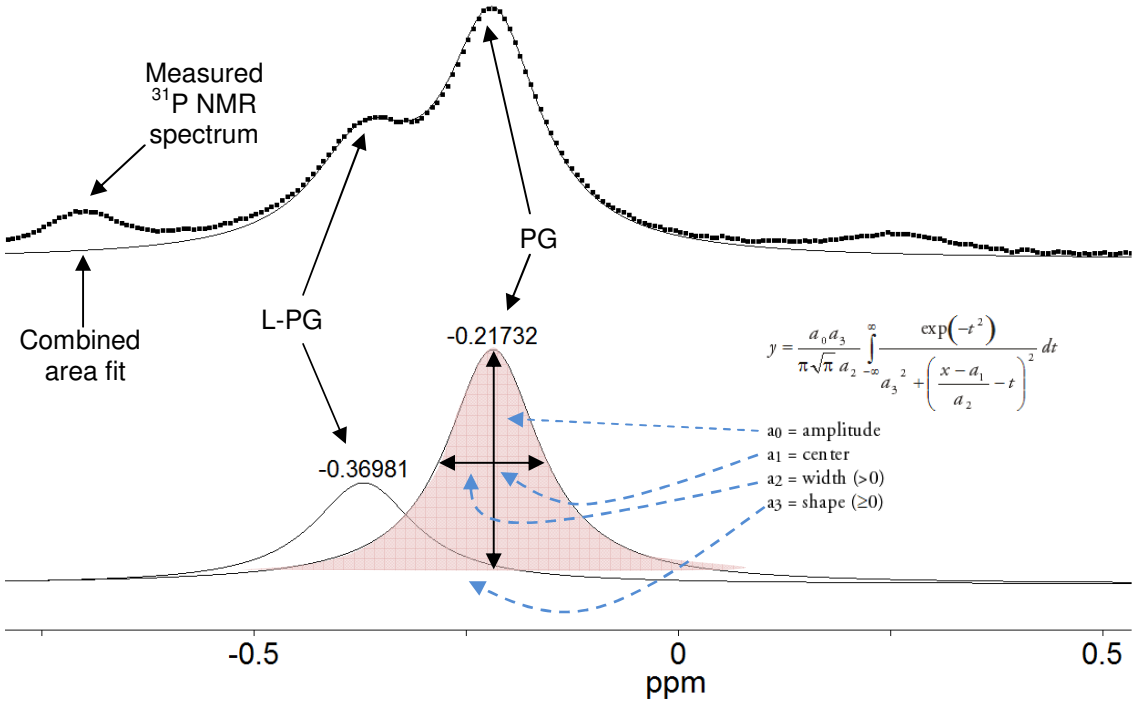

Figure 1-13 ^{31}P NMR spectrum of a lipid extract from MRSA NCTC8352 grown in a pH 7.4 environment (top), the associated Voigt area profile of the fitted peaks (bottom) and the equation of the Voigt area function to deconvolute the overlapping resonance signals.

The use of ^{31}P NMR to identify and relatively quantify phospholipids will be explored in this thesis with lipid extracts from *S. aureus* as the technique requires no harsh reagents and the lipids can be analysed directly from the natural lipid extract without any pre-treatments. Samples can be made up in a deuterated chloroform–methanol mixture (2:1 v/v) with a small quantity of pH 2.0 saline to stabilise the L-PG in the sample. In addition to this, the time taken to analyse the sample is relatively low (~2 hours) in comparison to TLC methods and no further assays are required to gain all the qualitative and relative quantitative information required.

Therefore this technique safeguards against the breakdown of L-PG to preserve as much as possible for analysis.

1.4.4 Reconstituted membrane lipid charge properties

The surface charge properties of biomembranes containing L-PG can be analysed using protoplasts however the lipid content of the plasma membrane of *S. aureus* only constitutes ~22-36% of the membrane whereas the rest is made up of intrinsic membrane proteins and small amounts of RNA (Ward & Perkins 1968). Of the lipidic component, the phospholipids make up ~77-92% depending on the *S. aureus* strain and the environment it is grown in (Ward & Perkins 1968). Therefore, it is likely the membrane surface charge properties of the protoplasts will be heavily influenced by the extracellular regions of the membrane proteins presenting at the bilayer surface. To try and compensate for this problem the lipid extracts from *S. aureus* can be reconstituted as vesicles, and this can apply to synthetic biomimetic lipid mixtures as well. These vesicles can then be analysed by measuring their zeta potentials in order to find their surface charge presentation at the slipping plane without the influence of membrane proteins.

The formation of vesicles using phospholipids can be achieved in numerous ways, however, the use of *S. aureus* lipid extracts limits the types of techniques that can be utilised. Normally to form vesicles of a consistent size distribution, lipids are dissolved in a volatile organic solvent (e.g. chloroform) and placed in an inert container (e.g. glass) with a large surface area. The organic solvent is then extracted using high pressure inert gas (e.g. nitrogen) or by reduced pressure evaporation (Woodle & Papahadjopoulos 1989). This removal of the organic solvent leaves a lipid film on the surfaces of the vehicle (figure 1-14A). To disperse the lipids as vesicles, an aqueous medium is added to the vehicle which begins to solvate the headgroups of the lipids in the lipid film and causes them to peel away from the surface of the vehicle and spontaneously form multi lamellar vesicles (MLVs) (figure 1-15B) (Woodle & Papahadjopoulos 1989). To aid in dispersion of the vesicles sonication energy can be used to bombard the sample which also reduces the MLV structures into unilamellar vesicles of a uniform size distribution (figure 1-15C) (Woodle & Papahadjopoulos 1989).

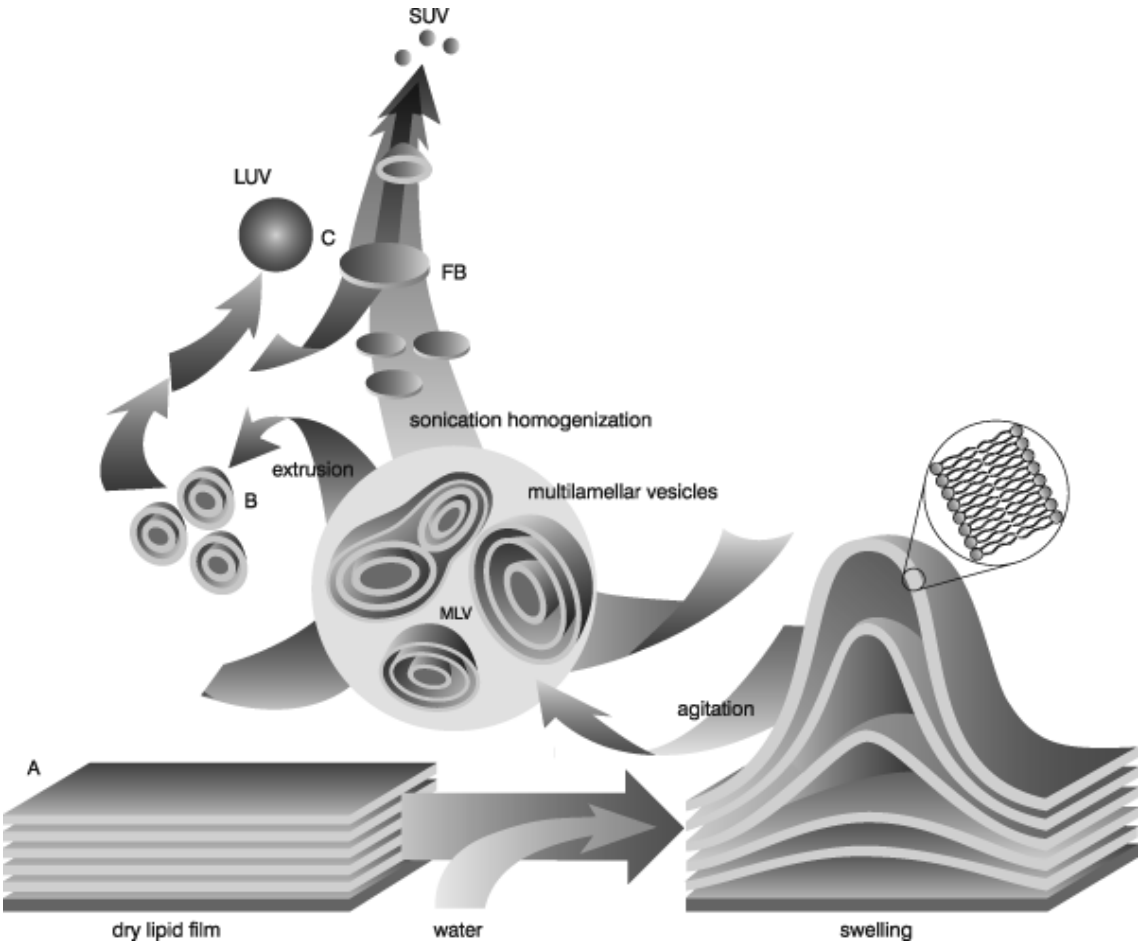

Figure 1-14 Preparation of vesicles. (A) Lipids are combined and dried under reduced pressure or high pressure gas transfer. On hydration unilamellar or multilamellar vesicles are formed (B and C). Figure reproduced from Avanti Polar Lipids, Inc (2013) (Avanti Polar Lipids Inc. 2013b).

The problem with bombarding *S. aureus* lipid extracts with sonication energy to form unilamellar vesicles of a uniform size distribution is the increased possibility of L-PG breakdown due to the high heat and vibrational energy input of the sonication device. This is undesirable and can be avoided by preparing the vesicles by freeze-thaw cycling which involves freezing the aqueous suspension containing the dispersed MLVs and then rapidly heating the sample to melting point (Traïkia *et al.* 2000); this process is repeated several times to obtain a vesicle population size of uniform distribution, however the overall mixture will still consist of different sized MLVs. The overall morphology and lamellarity of the vesicles is of little relevance when recording zeta potentials as the electrophoretic mobility of the vesicles will be the same for MLVs, large unilamellar vesicles (LUV) and small unilamellar vesicles (SUV) and therefore the use of this preparation technique is suitable for preparing *S. aureus* lipid extracts as MLVs.

1.5 Surface pressure–area isotherms of phospholipids

Examination of the pKas of L-PG conducted by Tocanne *et al.* (1974) looked at the limiting area per molecule of L-PG on subphases of different pHs and differing salt concentrations (Tocanne *et al.* 1974b). The areas were recorded from a surface pressure of ~30 mN/m however a vast amount of important information can be gathered from the surface pressure–area isotherm of the lipid as well. To prepare a monolayer film of phospholipids (Langmuir film) the lipids are dissolved in a volatile solvent (e.g. chloroform) and deposited dropwise on to an aqueous subphase. As the volatile solvent evaporates the amphiphilic properties of the lipids (figure 1-1) cause them to align themselves at the air–water interface with the headgroups immersed in the subphase and the hydrophobic hydrocarbon chains positioned in the air. However, if low concentrations of the lipid are used the lipids tend to spread across the surface of the subphase and the distances between the lipids is normally too high to assess interactions between them; this is known as the gaseous phase (figure 1-15) (Harkins, Debye 1952). Therefore barriers can be placed on the subphase and closed to reduce the area on which the lipids are spread, thus leading to compression of the monolayer (figure 1-15).

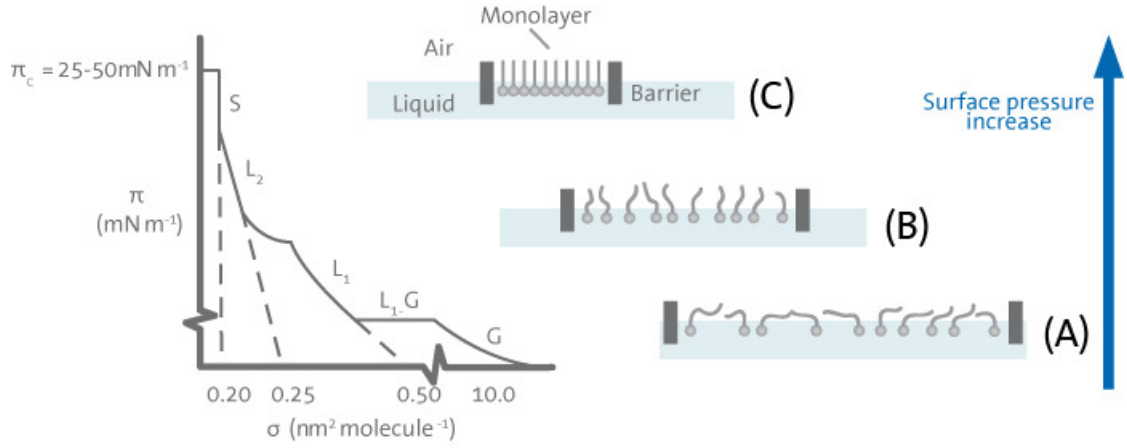

Figure 1-15 *S*urface pressure–area isotherm of a Langmuir film in different phases. Figure reproduced from KSV NIMA (2013) (KSV NIMA 2013). *G* = Gaseous phase, L_n = liquid phase and *S* = liquid condensed phase. A = schematic of lipids in the gaseous phase, B = schematic of lipids in the liquid phase and C = schematic of lipids in the solid or liquid condensed phase.

The compression of the monolayer leads to elimination of water molecules from the subphase surface and a reduction in the surface tension of the liquid surface. Changes in surface tension can then be related to the surface pressure (*Π*) of the subphase exerted by the lipids: (Langmuir 1917)

$$\Pi = \Upsilon_0 - \Upsilon \quad (5)$$

where Y_0 is the surface tension of the subphase in the absence of the Langmuir film and Y is the surface tension of the subphase with the monolayer present.

The recording of the surface pressure changes as the monolayer area decreases and forms what is known as a surface pressure–area isotherm (Gaines 1966). This isotherm varies widely between different amphiphiles and can describe the structural changes the amphiphile goes through in order to reach a solid phase (Harkins and Debye 1952). For example, fatty acids tend to show a 1st order directly proportional change between surface pressure and area which indicates the molecules do not undergo any intermediate phases on compression and orientate themselves increasingly more perpendicular to the air–water interface as the area of the monolayer is reduced (figure 1-16) (KSV NIMA 2013). However, phospholipids tend to undergo two liquid phases and the isotherms show a distinct region described as a 'horizontal phase transition' before they reach a solid phase (figure 1-16) (KSV NIMA 2013).

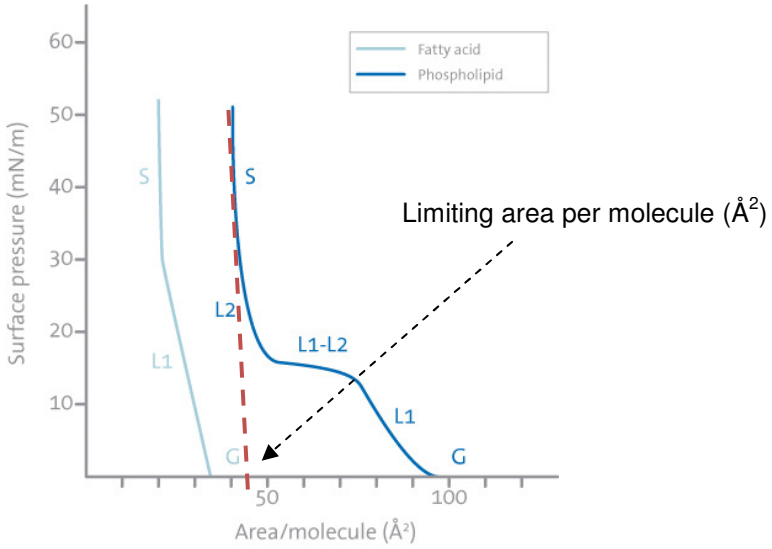

Figure 1-16 *S*urface pressure–area isotherms of a fatty acid with a single hydrocarbon chain and a phospholipid with two hydrocarbon chains. Figure reproduced from KSV NIMA (2011) (KSV NIMA 2013). *G* = Gaseous phase, L_n = liquid phase and *S* = liquid condensed phase.

Extrapolation of the monolayer limiting area per molecular is performed by fitting a tangent to the phase of interest and then extrapolating that tangent to the x-ordinate (figure 1-16, red hashed line) (Gaines 1966).

The measured limiting areas per molecule of different amphiphiles can vary widely and is dictated by the balance between attractive and repulsive forces between neighbouring amphiphiles and the amphiphile and the subphase (Gaines 1966). In addition to this, the type and size of the associated counter ions can also affect molecular areas as well as salts dissolved in the subphase (Gaines 1966). Attractive forces can include hydrogen bonding, electrostatic attraction and Van der Waals interactions, whereas repulsive forces include electrostatic repulsion, steric hindrance and loss of entropy in the system (Gaines 1966).

With regard to the lipids extracted from *S. aureus*, assessment of isotherms of these lipid mixtures of the bacteria grown at different pHs could reveal important interactions which might be occurring between the lipids, such as ion-pair formation between L-PG and PG or CL causing a drop in limiting area per molecule (Tocanne *et al.* 1974c). Such lipid interactions have been recognised previously with monolayers composed of 1,2-dipalmitoyl-3-trimethylammonium-propane (DPTAP, cationic) and 1,2 dimyristoyl-*sn*-glycero-3-phospho-(1'-*rac*-glycerol) (DMPG, anionic), where the lipids individually gave a much higher molecular area compared to a 1:1 mol/mol mixture of both lipids (figure 1-17) (Sung *et al.* 2010). This reduction in molecular area suggested the ionic electrostatic interaction between the lipids was substantially larger than any repulsive forces and the lipids were able to come into closer proximity to one another.

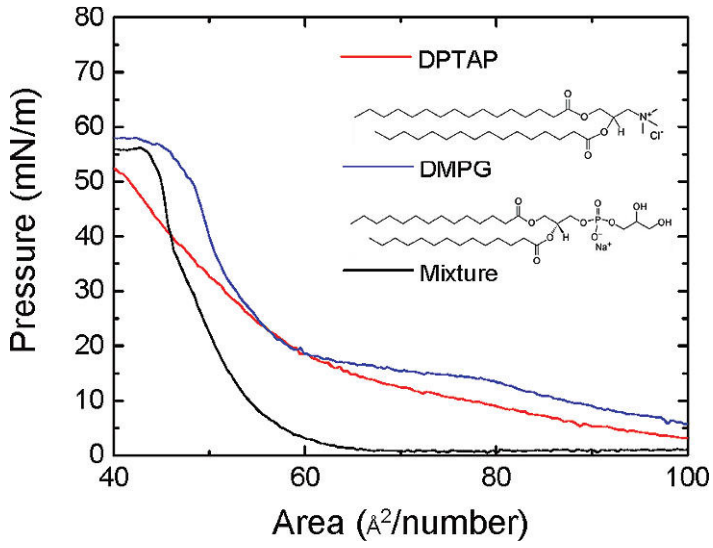

Figure 1-17 Reproduced image from Sung *et al.* (2010) of the molecular structures and *Π-A* isotherms of (a) DPTAP, (b) DMPG, and (c) 1:1 mol/mol DPTAP–DMPG (Sung *et al.* 2010).

A problem with using lipid extracts from *S. aureus* is the lack of detail of the molecular weights of the lipid species present and the unknown total amount of the sample which actually contains phospholipids, as the lipid extracts will contain some lipidic and non-lipidic hydrophobic contaminants (e.g. membrane pigments and glycolipids). These unresolved details of the natural lipid extracts reduce the confidence in the data obtained with them and they cannot be analysed any further than the calculation of their compressibility index (C^S) (Gaines 1966) which is defined by:

$$C^S = -\frac{1}{A}\left(\frac{\partial s}{\partial \pi}\right)_T \tag{6}$$

Where, A is the molecular area and $\partial s/\partial \pi$ is the slope of the phase of interest at a given temperature.

The compressibility index gives an indication of the lateral elasticity of a monolayer at a given temperature and can be converted to its reciprocal K^S, known as the compressional modulus. The compressional modulus is a more useful parameter as it gives details of the monolayer lateral rigidity and can demonstrate an increase or decrease in the monolayer viscosity as a result (Gaines 1966). This parameter will be important to assess in both natural lipid extracts and synthetic biomimetic models of *S. aureus* plasma membrane lipids, as an increase in cationic lipid content with mixtures of PG and CL could either increase or decrease rigidity of the monolayer and therefore show if the plasma membrane of *S. aureus* laterally expands or contracts with greater cationic lipid content.

1.6 ^{2}H Nuclear magnetic resonance spectroscopy

As described in Section 1.4.3 some atomic nuclei have a spin state of ½ which allows their energy to be split by an applied magnetic field however some atomic nuclei (e.g. deuterium) have a spin state of >½ where their energies are split by an electric field gradient (V) emanating from within the material itself (Adams *et al.* 2007). This latter phenomenon, discovered in the late 1950s, is known as nuclear quadrupole resonance (NQR) (Pound 1950). The NQR phenomenon of deuterium influences it's NMR signals due to differences in quadrupolar coupling of deuterium in different chemical environments (Vermeer *et al.* 2007). For a nucleus which has a spin state >½ its electric field tends not to be spherical but rather

elliptical or prolate and it possesses an electrical quadrupole moment (e*Q*) (Suits & Slichter 1984). The e*Q* value is normally a fixed determined value and is not required to be sought from every experiment. The *V* value, however, varies considerably depending on the charge distribution around the nucleus and is different for individual atoms in the material (Levitt 2013). The value of *V* depends on local symmetry around the atom, bond distances, bond angles, long range structure, coupling to neighbouring atoms and the kinetic dynamics of the material (Adams *et al.* 2007, Suits & Slichter 1984, Levitt 2013). Due to the fixed value of e*Q*, the variations in *V* can be directly related with e*Q* to the quadrupolar coupling constant (C_Q): (Adams *et al.* 2007)

$$C_Q = \frac{eQV}{h} \tag{7}$$

and the electric field gradient asymmetry (η_Q):

$$\eta_Q = \frac{V_{xx} - V_{YY}}{V_{zz}} \tag{8}$$

Where, *h* is Planck's constant

The fluctuation in η_Q generally changes by a negligible degree in ^{2}H NQR due to the fixed dimensions of the nucleus and therefore C_Q is a more relevant factor as coupling to the atom of interest can vary substantially depending on the characteristics of the neighbouring atoms (Adams *et al.* 2007). Thus, both parameters can be related to each other through ω_Q, which is the quadrupolar energy separation of the nucleus between the ground state and excited state, and what is essentially measured in ^{2}H NMR: (Adams *et al.* 2007, Levitt 2013)

$$\omega_Q(\beta_{PL}, \gamma_{PL}) = \frac{\omega_Q^{PAS}}{2}(3\cos^2\beta_{PL} - 1 + \eta_Q \sin^2\beta_{PL}\cos 2\gamma_{PL}) \tag{9}$$

where,

$$\omega_Q^{PAS} = \frac{3\pi C_Q}{2I(2I-1)} \tag{10}$$

β_{PL} and γ_{PL} are constants.

Due to the first order nature of ^{2}H NMR, C_Q causes the magnetic resonance signal of a deuterium nucleus to be reflected about the origin of the spectrum (Levitt 2013). This is due to the presence of a negative and positive excited state of the electric field. The separation of the two ^{2}H NMR signals caused by C_Q can be calculated by eq. (9) and equates to $2\omega_Q$ (figure 1-18) (Levitt 2013). Thus a ^{2}H NMR signal in a specific electro-chemical environment will appear with both negative and positive signals.

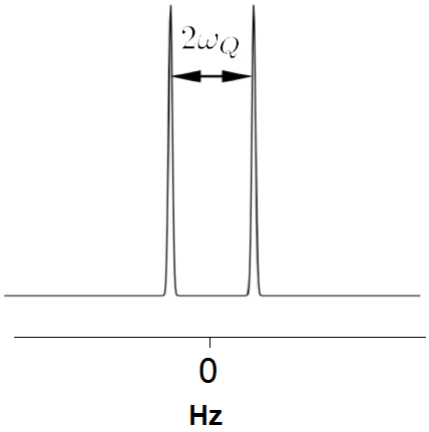

Figure 1-18 Example of a ^{2}H NMR spectrum showing the signal separation of a single deuterium signal.

With regard to membranes, the ^{2}H NMR signal from a deuterium labelled fatty acid chain of a phospholipid can reveal a large amount of information on its phase transition and its membrane order parameters (Vermeer *et al.* 2007). The variations in V between deuterium atoms in a lipid hydrocarbon chain amplify in the presence of free rotation and greater mobility (Davis 1983). Therefore the greatest separation in ^{2}H NMR relaxation signals will be detected when the membrane is in the L_α phase as the CD_2 and CD_3 groups of the lipid chains have substantial rotational possibilities and greater space for lateral movement (Vermeer *et al.* 2007). However, when the membrane is in the $L_{\beta'}$ phase the hydrocarbon chains tend to be more rigid and less disordered, thus reducing their lateral movement and free rotation giving rise to an averaged signal from individual CD_2 and CD_3 groups which cannot be distinguished as easily (Vermeer *et al.* 2007). An example of this phenomenon is shown in figure 1-19 for d_{62}-1,2 dipalmitoyl phosphatidylcholine (d_{62}DPPC).

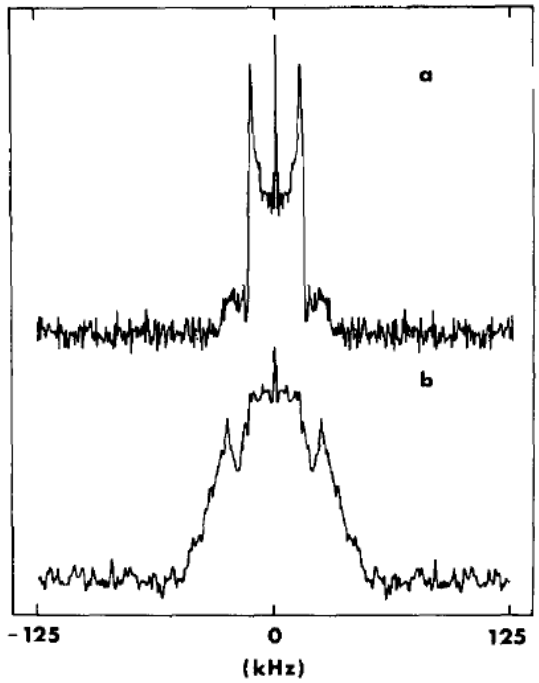

Figure 1-19 ^{2}H NMR spectra of d_{62}DPPC at (a) 43°C and (b) 37°C; Image reproduced from Davis J. H. (1983) (Davis 1983).

The resolution changes in the ^{2}H NMR spectrum can easily be used to identify the phase transition temperature of a lipid or lipid mixture by simple observation of the changes in shape of the spectra as a function of increasing temperature. This will be useful for studying the $L_{\beta'}$ to L_{α} phase change in synthetic biomimetic *S. aureus* model membranes as the suspected ion-pairing effect between L-PG and PG or CL may change the order of the lipids in the membrane at higher temperatures resulting in an alteration in T_m of the membrane.

Above the lipid T_m the resolution of the ^{2}H NMR spectrum is high enough to resolve the signals from individual CD_x groups along the hydrocarbon lipid tails of deuterium labelled phospholipids. This high level of detail can permit the fitting of the integrated area de-Paked individual CD_x groups by a Voigt area function similar to that shown in figure 1-13 for ^{31}P NMR (Schafer *et al.* 1995, Sternin *et al.* 1983). The quadrupolar splitting of the deuterium doublet signal (ΔV_Q) can then be used to calculate the hydrocarbon chain order parameter (S_{CD}) of the deuteriums in a CD_x group using: (Vermeer *et al.* 2007)

$$\Delta V_Q = \frac{3}{2} e^2 qQ . S_{CD} \tag{11}$$

Where, e^2qQ is the static quadrupole coupling constant and is equal to ~168 kHz for a C-D bond in a hydrocarbon chain (Vermeer *et al.* 2007).

The S_{CD} of each CD_x group in the lipid hydrocarbon chain can then be plotted against the respective carbon number in the hydrocarbon chain to assess the degree of order each CD_x group is experiencing in the bilayer. This was of particular importance for this thesis when using synthetic lipids to make biomimetic models of *S. aureus* membranes, as increases in L-PG membrane content could cause changes in membrane ordering through the higher incidence of putative ion-pairs with PG or CL.

1.7 Neutron scattering techniques for studying membranes

1.7.1 Neutron diffraction

The mathematical interpretation of neutron diffraction data is explained in greater detail in chapter 3.2.6, some theoretical background information is given here. Neutron diffraction is a powerful technique used to decipher the molecular structure of static ordered systems (e.g. crystallised proteins) (Wilson & Myles 2006). This can also be applied to membranes of low mobility that can form lamellar stacks in order to act as diffraction gratings (Schoenborn & Knott 1996). The principles of neutron diffraction are analogous to the diffraction of photons as neutron movement is generally interpreted as a waveform (Bragg 1959). When polarised light or neutrons make contact with an aperture of similar dimensions to its wavelength (λ), its wavefront spreads out into a spherical form; this is the principal of diffraction (Bragg 1959). However, if a second slit is in close proximity to the first, the waves from each slit will coincide and can combine (figure 1-20). If the waves are in-phase, that is to say the maxima and minima coincide at the same points, the amplitude of the wave will increase by a factor of two. However if they are out-of-phase then the opposite will occur and the wave will cease to exist. The in-phase phenomenon is known as an order of diffraction and in neutron diffraction these orders provide structural details of the diffracting material (figure 1-20) (Bragg 1959).

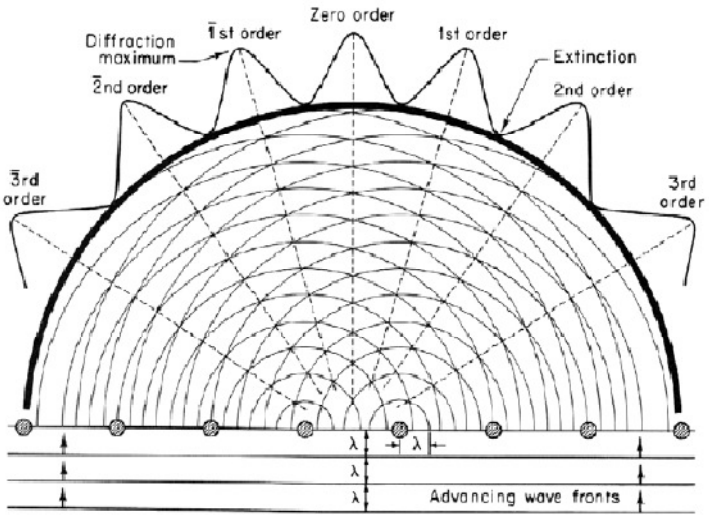

Figure 1-20 Schematic to demonstrate orders of diffraction from two slits. Image reproduced from Schwartz, L.H., (1977) (Schwartz 1977).

The orders of diffraction are governed by Braggs law (Bragg 1959):

$$n\lambda = 2dsin\theta \tag{12}$$

Where, *n* is the order of diffraction, *d* is the width of the slit and *θ* is the angle of diffraction

This principle can be directly applied on to lipid bilayers using neutrons, where the lamellar membrane stacks are analogous to the slits and the incoming neutron beam acts as the light source (figure 1-21) (Schoenborn & Knott 1996). The incident intensity of the neutron is similar to the diffracted intensity and therefore the neutron is described as 'elastic' as no energy is transferred or gained, which allows for thermal low energy neutrons to be utilised as little energy is expended (Fragneto & Rheinstädter 2007). The incident angle (*θ*) is generally fixed for a sample, which is scanned through diffraction angles of *θ*-2*θ* in order to detect Bragg reflections. The resolved Bragg reflections then provide details on the number of orders of diffraction and the angular position of the peaks (bilayer separation including water layer). The integrated intensity of the Bragg reflections is proportional to the square root of the structure factor modulus (Fragneto & Rheinstädter 2007). This factor is most important as it allows construction of the z-axis scattering length density (SLD) profile of the bilayer normal.

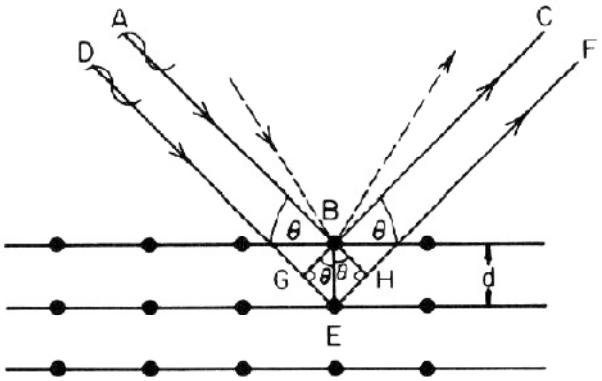

Figure 1-21 Schematic of a neutron incident beam (A + D) hitting the first two bilayers of a lamellar stack (black dots with lines) and the diffracted beam (C + F). Image reproduced from Schwartz, L.H., (1977) (Schwartz 1977).

This system can potentially be used with *S. aureus* lipid extracts as well as synthetic lipids in order to gain details of the bilayer structure with varying amounts of L-PG. In addition to this, selectively deuterium labelling parts of the synthetic lipids can give an indication if a hydrogenated CAMP can partition into bilayers containing different concentrations of a synthetic L-PG analogue. The highlighting of molecules in neutron diffraction is made possible due to the differing neutron scattering lengths of deuterium (6.67×10^{-5} Å) and hydrogen (-3.74×10^{-5} Å) which means they appear differently when diffracting neutrons (Fragneto & Rheinstädter 2007).

1.7.2 Neutron reflectivity

Extrapolation of bilayer parameters from neutron reflectivity using fitted SLD curves is described in full detail in Chapter 6.2.3, some theoretical background information is given here. Neutron reflectivity, unlike neutron diffraction, requires only a single deposited bilayer in order to obtain the bilayer's thickness and structural details. The system can also incorporate different buffers which can change the charge properties of the lipid headgroups whereas no buffering is available in neutron diffraction as hydration comes in the form of increasing humidity. Similar to photons, neutrons can reflect off a surface at a given angle (θ). The reflected beam is elastic and is received at the detector at the same angle of incidence (figure 1-22) (Fragneto-Cusani 2001).

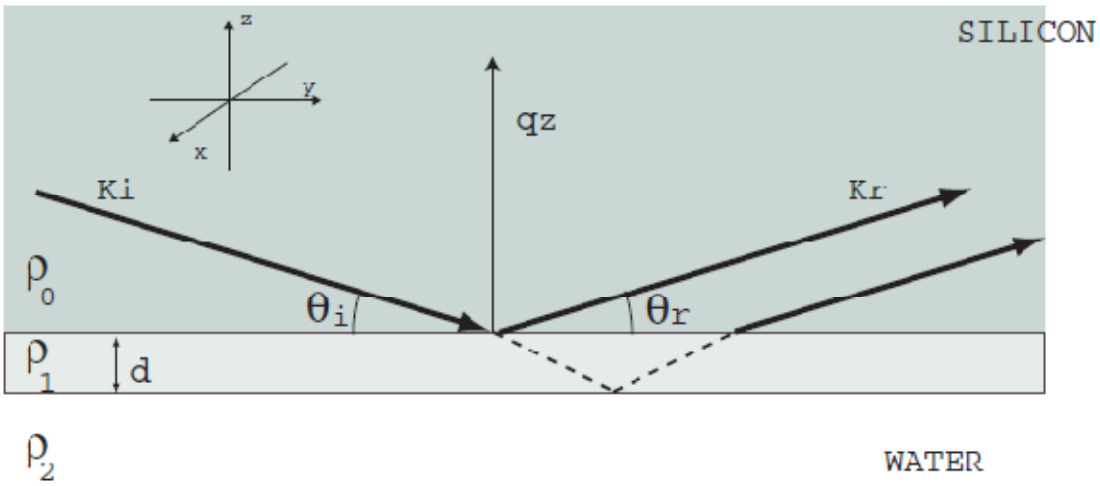

Figure 1-22 Reflection of an incident beam from two flat interfaces; k_i and k_r are the incident and reflected wave vectors (for reflectivity $k_i = k_r$); q_z is the component of the momentum transfer perpendicular to the membrane interface. Reproduced from Fragneto G. (2001) (Fragneto-Cusani 2001).

The difference in wave vector between k_i and k_r (figure 1-22) is what is measured in neutron reflectivity experiments, however, it is better expressed as the angular momentum transfer perpendicular to the membrane interface (q_z) (Fragneto-Cusani 2001):

$$q_z = 2k_i = \frac{4\pi}{\lambda}\sin\theta \tag{13}$$

Where, λ is the wavelength of the neutron beam.

The angle θ is highly dependent on the neutron refractive index of the material being analysed and in most cases total external reflection is required to gain the most structural information of

the material. To ensure no internal reflection occurs, θ angles are always lower than the critical angle of reflection and as most materials have a neutron refractive index just slightly less than air or a vacuum, total external reflection is generally observed (Fragneto-Cusani 2001). Because the neutron refractive index of a material is related to θ, q_z can be directly correlated to the neutron SLD of a material (ρ_n) in a uniform layer, eq. (15) (Fragneto-Cusani 2001). What this therefore permits, is the breakdown of a bilayer into separate layers perpendicular to the surface of the bilayer (e.g. bulk solvent, bilayer headgroups, bilayer hydrocarbon core, solvent between substrate and bilayer headgroups and etc.). The properties of these layers such as lateral density, atomic make up and bilayer normal thickness can then be determined. The layer thickness can be determined through the Fresnel reflectivity parameter (R_k) (Imae *et al.* 2011), and an example of this in a three layer system (Fragneto-Cusani 2001) would be:

$$R_k \approx \frac{16\pi^2}{q_z^4}[(\rho_1 - \rho_0)^x + (\rho_2 - \rho_1)^x + x(\rho_1 - \rho_0)(\rho_2 - \rho_1)\cos q_z d] \quad (14)$$

Where, d is the thickness of the layer and x is the number of layers - 1.

Whereas the SLD of each layer, which gives information on the layer lateral density and atomic make up, can be determined by:

$$\rho_n = \sum b_i \aleph_i \quad (15)$$

Where, b_i is scattering length of the atomic nuclei in the layer and $\aleph_i$ is the number of nuclei per volume in that layer (Fragneto-Cusani 2001).

The values for b_i are known for most materials and do not tend to fluctuate however $\aleph_i$ is highly variable depending on the material being examined and for a bilayer can vary substantially depending on the bilayer lateral density and the presence of non-membrane components partitioned into it (e.g. CAMPs). Therefore neutron reflectivity can be a highly useful analytical tool for the examination of bilayers containing synthetic L-PG analogues as their presence with PG or CL can vastly alter the lateral density and thickness of the bilayer possibly due to ion-pair formation between the oppositely charged lipids. In addition, non-membrane components (e.g.

CAMPs) in this type of bilayer can easily be tracked using selective labelling with isotopes (e.g. deuterium and hydrogen) in a similar fashion to the neutron diffraction experiments. The isotopic labelling can highlight the CAMP in the bilayer and give information on where it preferably resides in the bilayer.

1.7.3 Small angle neutron scattering

Small angle neutron scattering (SANS) is different from diffraction and reflectivity techniques since there is no requirement for the sample to be deposited onto a substrate and the neutron beam is directed to a sample containing a dispersion of vesicles composed of the lipids of interest. There are no fixed angles or wavelength of irradiation unlike diffraction and reflectivity, and a range of neutron wavelengths is employed (Jackson 2008). Each vesicle acts as a collection of *'point scatterers'* (atoms the vesicle is composed of) and each scatterer will scatter an incoming neutron beam heading on trajectory *k* by angle *θ*, which results in the neutron wave being dispersed into a scattered circular waveform (δ_s) heading on a vector trajectory of *k'* (figure 1-23) (Pynn 1990). Similar to reflectivity and diffraction the technique employs elastic neutrons and energy is neither absorbed nor gained by the scattered neutron.

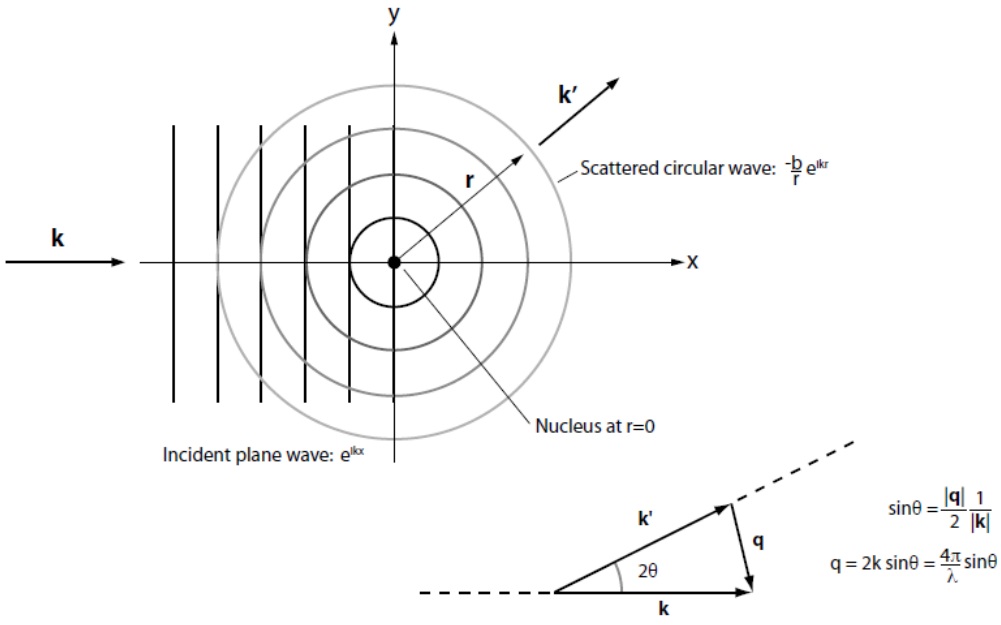

Figure 1-23 Neutron scattering from an atomic nucleus. Image reproduced from Pynn, R., (1990) (Pynn 1990).

The scattered circular waveform (ψ_s) (Jackson 2008) caused by the collision of a neutron with a nucleus of interest can be summarised by the quantum mechanics term:

$$\psi_S = -\frac{b}{r}e^{ikr} \tag{16}$$

Where, *b* is the scattering length of the nucleus and *r* is the waveform radius.

Although the scattered waveform is described as circular, it still migrates along a scattering vector (*k'*) which can be resolved into a three dimensional term by inclusion of the nuclear momentum term from eq. (13), into eq. (16):

$$\psi_S = -\sum\left(\frac{b_i}{r}\right)e^{ikr}e^{iq.r} \tag{17}$$

However as shown in figure 1-24, the actual neutron scattering pattern from an individual nucleus is not a linear migration but rather a cross-sectional scattering through two angles (Φ, θ) (figure 1-24) (Squires 2012).

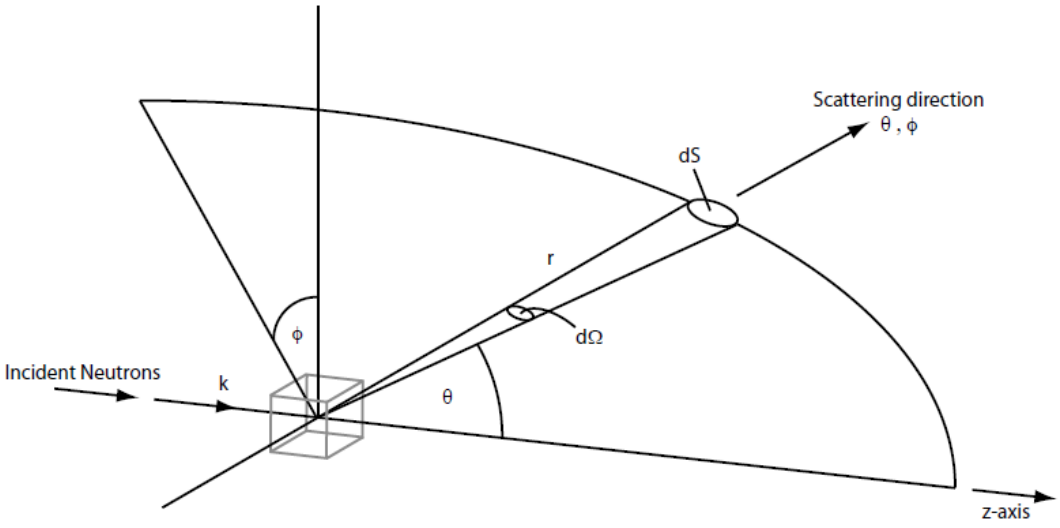

Figure 1-24 Neutron scattering geometry. Image reproduced from Squires, G. L., (2012) (Squires 2012).

Therefore the coherent cross-sectional scattering of a nucleus, which contains the structural information regarding the nucleus, is what is actually detected in SANS (Jackson 2008), and thus eq. (16) is transformed into eq. (17), through incorporation of the neutron cross-sectional scattering ($\partial\sigma/\partial\Omega$):

$$\frac{\partial\sigma}{\partial\Omega}(q) = \frac{1}{N}\left|\sum_{i}^{N} b_i e^{i\boldsymbol{q}.\boldsymbol{r}}\right|^2 \tag{18}$$

Where, N is the number of scattering nuclei.

However, it is near impossible to track the cross-sectional scattering of individual nuclei as the overlap between signals is vast due to them being in very close proximity to each other. Therefore in SANS it is more sensible to resolve the normalised macroscopic cross-sectional scattering emanating from the vesicle structures as a whole (Jackson 2008). Thus the scattering length per nucleus (b_i) in term 18 can be replaced by the vesicle mean SLD (ρ(r)), which gives the Rayleigh-Gans equation (Jackson 2008):

$$\frac{\partial\sum}{\partial\Omega}(q) = \frac{N}{V}\frac{\partial\sigma}{\partial\Omega}(q) = \frac{1}{\tilde{\mathrm{V}}}\left|\int_{2} \rho(\boldsymbol{r}) e^{i\boldsymbol{q}.\boldsymbol{r}} d\boldsymbol{r}\right|^2 \tag{19}$$

Where, $\tilde{V}$ is the interaction potential between the neutron and nucleus and $\partial\Sigma/\partial\Omega$ is the macroscopic cross sectional scattering.

The macroscopic cross sectional scattering modulus in eq. (19) is the main information gained from SANS experiments and is interpreted as a function of the scattering moment, Q_z. However, one of the problems with this parameter is it is equivalent to the square of the integration modulus of the SLD and therefore all phase information is lost as a result and the SLD profile of the macroscopic cross section cannot be constructed (Jackson 2008). Therefore fitting of the data with various best fit lines to reconstruct the SLD profile is normally conducted to overcome the loss of phase information.

The use of SANS in this thesis is helpful because it provides details of how a vesicle bilayer may alter in thickness and adjacent bilayer separation when synthetic lipid mixtures of a L-PG

analogue and PG are varied in molar ratio in both pH 5.5 and 7.4 environments with and without the presence of a CAMP. Therefore SANS can primarily be used to support the data found in reflectivity and diffraction experiments and provide details of how the lipids act in vesicular membranes which is more analogous to the natural state of the *S. aureus* plasma membrane.

1.8 Genetic pathways of L-PG regulation

As discussed, the upregulation of L-PG biosynthesis in the plasma membrane of *S. aureus* under low pH growth conditions is suspected to alter the charge and biophysical properties of the plasma membrane in order to help the bacterium to survive in this environment, which is principally being investigated in this thesis. However, the biosynthesis of L-PG in the plasma membrane of *S. aureus* has previously been shown to be under genetic control when the bacterium was exposed to sub-lethal concentrations of CAMPs (Falord *et al.* 2012, Li *et al.* 2007a, Li *et al.* 2007b, Meehl *et al.* 2007). To date, no gene expression based studies have been conducted on *S. aureus* to examine the genetic pathways linked to the upregulation of L-PG biosynthesis in the bacterium grown at low pH. Therefore, this thesis also investigated the genetic pathways linked to L-PG upregulation in the plasma membrane of *S. aureus* when the bacterium is grown in a low pH environment (pH 5.5).

The biosynthesis of L-PG (figure 1-25) begins at the bacterial cytoplasmic membrane by a membrane bound transesterase which catalyses the condensation of lysine at the α-carboxyl group with the terminal hydroxyl of the glycerol moiety in PG (Gould & Lennarz 1967, Lennarz *et al.* 1966). The lysine is donated to the transesterase in a tRNA bound form which is thought to be specific only for this process and bound to the primary site of the tRNA (Nesbitt & Lennarz 1968, Ernst & Peschel 2011). This transesterase, multiple peptide resistance factor (MprF), is a bifunctional transmembrane protein consisting of two process specific domains (Ernst *et al.* 2009). The first domain of MprF is a synthase which catalyses the reaction of lysine with PG to form a cytoplasmic facing L-PG molecule. The second domain of MprF is a floppase which relocates the newly synthesised L-PG to the outer leaflet of the plasma membrane (Ernst *et al.* 2009).

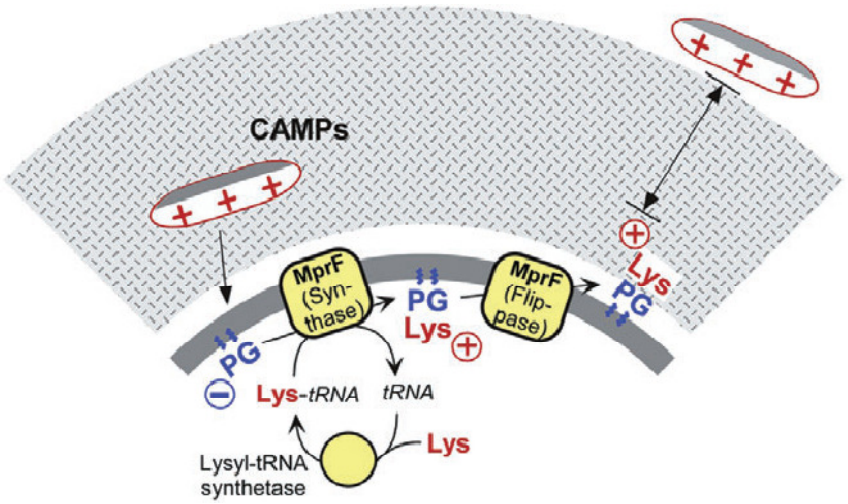

Figure 1-25 Figure reproduced from Ernst *et al.* (2009) showing the *in vivo* biosynthesis of L-PG by *S. aureus* (Ernst *et al.* 2009).

MprF tends to vary in its substrate specificity depending on which bacteria it is isolated from. For example, MprF from *S. aureus* is specific for lysine only and will not accept any other amino acid (Staubitz *et al.* 2004) however the MprF synthase domain of *E. faecium* will accept arginine, alanine and lysine as substrates (Roy & Ibba 2009). In the case of *Listeria monocytogenes* its MprF has flexibility for different phospholipids and can bind lysine to both PG and CL (Thedieck *et al.* 2006).

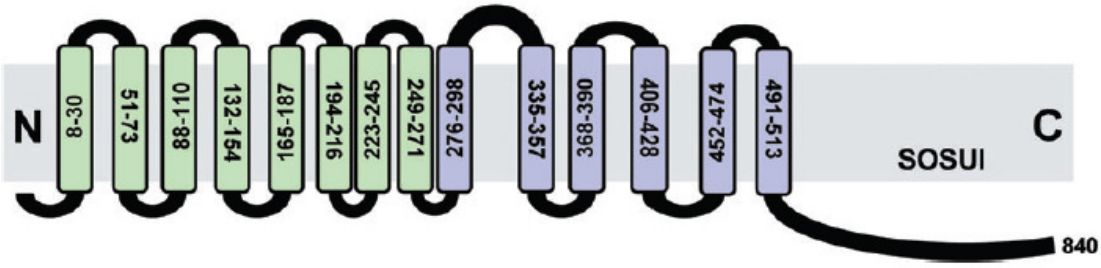

Figure 1-26 Figure reproduced from Ernst *et al.* (2009) showing the proposed structure of MprF in *S. aureus* with the synthase domain (blue) and floppase domain (green) (Ernst *et al.* 2009).

With respect to the structure of MprF in *S. aureus*, as shown in figure 1-26, it consists of 14 transmembrane domains (TMDs) which are located in the plasma membrane. The first six C-terminal TMDs of MprF form the synthase domain of the enzyme and gene knock-out experiments have shown aa-PG production ceases in its absence (Ernst *et al.* 2009). The eight remaining N-terminal TMDs are the floppase domain where newly biosynthesised cytoplasmic L-PG is flopped out onto the outer leaflet of the plasma membrane from the inner leaflet (Ernst *et al.* 2009). The eight N-terminal TMDs are not required for L-PG biosynthesis and in their

absence L-PG biosynthesis still occurs, however the bacterium accumulates high levels of L-PG in its inner plasma membrane leaflet (Ernst *et al.* 2009). The actual mechanism by which the 'floppase' operates is unknown as it has no obvious ATP binding sites which suggests it may function through proton motive force, however this is unsubstantiated to date (Ernst *et al.* 2009).

In 2008 it was found that certain clinical isolates of *S. aureus* showed reduced sensitivity to the lipopeptide antibiotic daptomycin (Ho *et al.* 2008, Jung *et al.* 2008). These strains all possessed a fully functioning MprF enzyme however they contained point mutations which appeared to make the enzyme more functional with a higher turnover rate than the wild type (Ernst & Peschel 2011). For example, Yang *et al.* (2009) found a serine-to-leucine substitution at position 295 of the MprF synthase domain which resulted in *S. aureus* 703 being less susceptible to the effects of daptomycin, however substitution back to serine resulted in the bacterium being susceptible to the antibiotic (Yang *et al.* 2009). Similarly in other studies, point mutations in MprF have also been found where the enzyme turns over greater amounts of L-PG onto the plasma membrane outer leaflet in *S. aureus* (Ernst & Peschel 2011). However majority of these studies showed floppase domain point mutations which suggested these polymorphs of MprF may enhance the rate of transportation of L-PG to the outer membrane leaflet of the bacterium (Friedman *et al.* 2006, Kosowska-Shick *et al.* 2009).

According to previous studies MprF has no sensory domains and is not autoregulating and therefore cannot upregulate L-PG on its own (Peschel *et al.* 2001). Later studies however revealed MprF forms the end part of a much larger cascade of genetically regulated processes (figure 1-27).

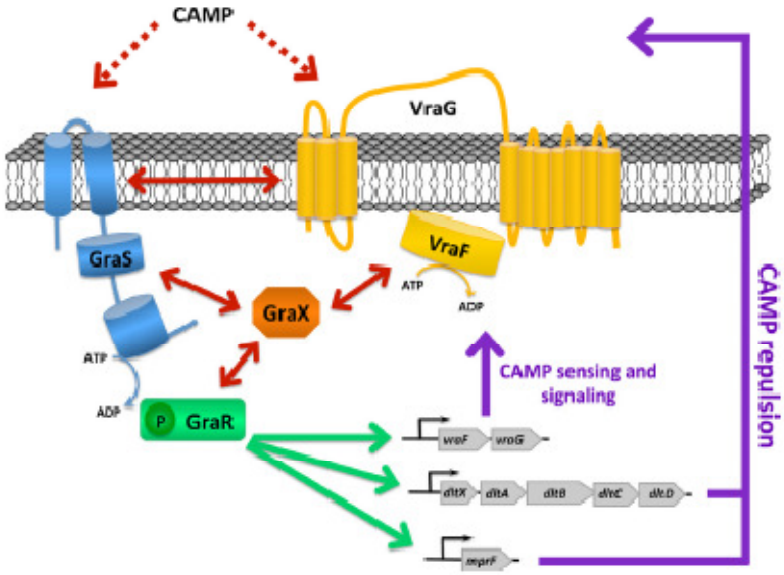

Figure 1-27 Figure reproduced from Falord *et al.,* (2012) showing the *in vivo* cascade of events leading to MprF upregulation (Falord *et al.* 2012).

Studies by Meehl *et al.,* (2007) uncovered the presence of four main sensory two-component regulatory systems (TCRS) present on the plasma membrane of *S. aureus* which were all tested for sensitivity to CAMPs and vancomycin (Meehl *et al.* 2007). One of these TCRS was found to be sensitive to these antimicrobial agents and was expressed between genes 716 to 720 of MRSA COL. The upregulation in expression of this gene cluster in response to these agents supported earlier research suggesting genes 716 and 717, also known as *graR* and *graS* respectively, were genes coding for a vancomycin sensor (GraS) and regulator (GraR) system associated with the plasma membrane of *S. aureus* (figure 1-27) (Cui *et al.* 2005). The structure of GraRS is a two-component histidine kinase sensor (GraS) with a cytoplasmic response regulator (GraR). GraS is a membrane bound sensor consisting of two membrane bound domains and GraR is an ATP activated internal regulator of the *mprF, dltABCD* and *vraFG* operons (Falord *et al.* 2012). The structure of GraS contains a nine residue extraceullar loop which consists of a number of negatively charged amino acids, which is thought to bind vancomycin and CAMPs to activate the sensor and catalyse the phosphorylation of GraR (Li *et al.* 2007a). Later research, showed genes 719 and 720 from MRSA COL to be the genes for a two-component ABC transporter, namely *vraF* and *vraG* respectively (Falord *et al.* 2012). The role of this two-component transporter pump was thought to be for influx and efflux of substances required for homeostasis (Cui *et al.* 2005), however due to the unusually small truncated structure of the pump section (VraG) it was later found to be for efflux of

peptidoglycan/teichoic acid precursors after phosphorylation by VraF (Meehl *et al.* 2007). Studies using MRSA COL showed the bacterium to be sensitive to vancomycin and CAMPs to a similar degree as *graR* knockout mutants, when *vraG* was knocked out and indicated that GraRS was not being activated in the absence of VraG (Falord *et al.* 2012). This finding suggested the 198 amino acid extra-cellular loop of VraG (figure 1-27) predominately bound vancomycin and CAMPs and activated the GraRS system which in turn positively upregulated its own synthesis through GraR (positive feedback loop) (Falord *et al.* 2012). The final gene in the cluster between 716 to 720 of MRSA COL was 718 which was assigned to be *graX*, the expressed protein of this gene (GraX) was suggested to act as an intermediary to maintain balance of the resistance system however this theory is unsubstantiated to date (Falord *et al.* 2012).

The pathways governing L-PG regulation have only been studied with CAMPs or vancomycin and no other external stimuli. Therefore this thesis will look at this regulatory pathway under physiological pH and mild acidic conditions (pH 5.5) to clarify if the increase in plasma membrane L-PG biosynthesis in *S. aureus* under mild acidic conditions is a result of upregulation in the expression of *graXRS* and *vraFG*.

1.9 Cationic antimicrobial peptide interactions with membranes containing L-PG

A large proportion of the research dedicated to the study of L-PG in membranes has focused on exposure of the membranes of bacteria to CAMPs or antibiotics in whole cell studies. In all cases, exposure to CAMPs and certain antibiotics (mainly vancomycin and daptomycin) results in an increase in L-PG biosynthesis in *Bacillus anthracis* (Samant *et al.* 2009), *Bacillus subtilis* (Hachmann *et al.* 2009, Salzberg & Helmann 2008), *L. monocytogenes* (Thedieck *et al.* 2006), *Mycobacterium tuberculosis* (Maloney *et al.* 2009), *S. aureus* (Nishi *et al.* 2004, Peschel *et al.* 2001, Ernst *et al.* 2009, Staubitz *et al.* 2004) and *Rhizobium tropici* (Sohlenkamp *et al.* 2007). The increase in membrane L-PG biosynthesis appears to contribute to the resistance of these bacteria to CAMPs and these certain antibiotics. The mechanism through which L-PG does this is thought to be due to the formation of a membrane charge barrier to these agents or a dampening of the membrane anionicity which would reduce the

electrostatic attraction of CAMPs and cationic antibiotics to the plasma membrane (figure 1-25) (Nishi *et al.* 2004).

Although the work in this thesis principally looks at how high concentrations of L-PG in the plasma membrane of *S. aureus* helps the bacterium to adapt to low pH environments found on human skin and the anterior nares of the nasal cavity, it should also be remembered these epithelial surfaces also contain CAMPs (Ong *et al.* 2002, von Eiff *et al.* 2001, Cole *et al.* 1999). The presence of CAMPs and a low pH environment on these epithelial surfaces suggest *S. aureus* is able to survive in the presence of both of these environmental stresses. With respect to the previous research conducted with CAMPs and changes in L-PG biosynthesis in *S. aureus*, it appears that upregulation of L-PG in the bacterial plasma membrane plays a major role in the resistance of these bacteria to the cytolytic effects of CAMPs (Nishi *et al.* 2004, Peschel *et al.* 2001). Therefore this thesis also looked at how *S. aureus* lipid extracts and biomimetic synthetic models of the plasma membrane of *S. aureus* in both physiological and low pH environments (pH 5.5) were adapted, with different concentrations of L-PG, to also cope with the presence of a CAMP. In order to keep this work relevant, a biomimetic innate immune system defensive CAMP analogue was used, magainin 2 F5W (GIGKWLHSAKKFGKAFVGEIMNS). This 23 amino acid peptide is derived from a CAMP found in *Xenopus Laevis* (Ludtke *et al.* 1996, Ludtke *et al.* 1995, Zasloff *et al.* 1988). On contact with anionically charged membranes the peptide adopts an amphiphilic α-helical structure and can partition into a membrane (Ludtke *et al.* 1996, Ludtke *et al.* 1995). Then, providing the membrane bound concentration of the peptide is sufficient the peptide can cause membrane thinning or pore formation (Ludtke *et al.* 1996, Ludtke *et al.* 1995). Both of these cytolytic mechanisms of magainin 2 F5W were ideal to assess the resistance of reconstituted membranes made from *S. aureus* lipid extracts and synthetic lipid models of these extracts. Therefore, experiments were performed in both pH 5.5 and 7.4 environments with lipid extracts from *S. aureus* grown at pH 5.5 and 7.4 and synthetic lipid models to represent these lipid extracts. The results from these experiments provided several mechanisms of how L-PG at high concentrations in the plasma membrane of *S. aureus* helped the bacterium to survive on low pH human epidermal surfaces.

Chapter 2

The regulation of lysyl-phosphatidylglycerol biosynthesis in *Staphylococcus aureus* in response to mild acidic conditions

2.1 Introduction

The increase in biosynthesis of lysyl-phosphatidylglycerol (L-PG) in the plasma membrane of *Staphylococcus aureus* in response to cationic antimicrobial peptides (CAMPs) and mildly acidic growth environments has been established (Nishi *et al.* 2004, Gould & Lennarz 1970, Peschel *et al.* 2001, Ernst *et al.* 2009). The genetic pathway linked to the upregulation of L-PG in response to CAMPs has also been established and L-PG biosynthesis appears to be under the control of the gene cluster consisting of *graXRS* and *vraFG*, known as the 'five-component system' (Falord *et al.* 2012, Meehl *et al.* 2007). Although the genetic regulation of L-PG biosynthesis has been investigated on exposure of *S. aureus* to CAMPs, increased plasma membrane L-PG biosynthesis of the bacterium in mildly acidic growth environments has not. Therefore this chapter will examine the changes in messenger ribonucleic acid (mRNA) expression of *graXRS, vraFG* and *mprF* in six different *S. aureus* strains when reducing their growth environment pH from 7.4 to 5.5.

As explained in chapter 1.8 the 'five-component system' in *S. aureus* principally operates by GraRS detecting the presence of CAMPs in its external growth environment (Falord *et al.* 2012). This detection subsequently, via GraR phosphorylation, results in the increased expression of *graXRS* and *vraFG* and the upregulation of the membrane bound lysyl-transesterase, multiple peptide resistance factor (MprF), hence resulting in increased L-PG biosynthesis (Falord *et al.* 2012, Li *et al.* 2007a, Li *et al.* 2007b, Meehl *et al.* 2007). The 9 residue extracellular loop of GraS contains three aspartate residues (pKa ~4.1), which the cationic groups of CAMPs are presumed to interact with in order to activate GraS (Li *et al.* 2007a, Li *et al.* 2007b). It is possible high proton concentrations in a pH 5.5 environment may also interact with GraS in a similar fashion resulting in increased expression of *graS* and the other genes in the 'five-component system' cluster. Therefore this provided grounds to investigate the changes in

graXRS and *vraFG* expression in *S. aureus* grown under a pH 5.5 environment compared to a pH 7.4 environment.

In a more recent study, VraFG, the ATP activated peptidoglycan building block exporter pump of the 'five-component system,' (Meehl *et al.* 2007) has been suggested to play a role in the sensing of CAMPs through their binding to the 198 residue extra-cellular loop of VraG (Falord *et al.* 2012). The binding of CAMPs to VraG activates GraR resulting in the upregulation of both *vraFG* and *mprF* expression and increased biosynthesis of L-PG (chapter 1.8) (Falord *et al.* 2012, Meehl *et al.* 2007). The upregulation of *vraFG* expression will also be investigated in this study with respect to changes in the pH growth conditions of *S. aureus* to observe if excess environmental protons will also upregulate *vraFG* expression.

In general, examination of gene expression can be performed either by quantification of the end protein product or by extraction and quantification of mRNA. Quantitative proteomics is normally carried out by extraction of the protein of interest and then quantification by densitometric methods after western blot separation or mass spectrometry (MS). The difficulty of using western blot and densitometry is that it requires an antibody to identify the protein of interest which is difficult to obtain without a purified version of the protein (Renart & Sandoval 1984). With respect to GraXRS, VraFG and MprF, it is hard to find clean versions of these proteins, as several of these proteins are membrane bound and are not commercially available therefore designing an antibody for these proteins is a complicated and uneconomical process. Relative protein quantification between cells grown in two different environments with MS does not require antibodies however for the most accurate relative quantification the proteins of interest require isotopic or isobaric-tag labelling to differentiate them in their respective growth conditions (Aebersold & Mann 2003, Walther & Mann 2010). Isotopic labelling of proteins can be an expensive process and isobaric-tag labelling can give inaccurate results if all tag reactions have not reached completion (Walther & Mann 2010), therefore MS was not performed for relative protein quantification of GraXRS, VraFG and MprF. Relative quantification of mRNA expression of *graXRS, vraFG* and *mprF* was selected to avoid these problems associated with the protein quantification methods and was performed using reverse transcription (RT) of mRNA of the genes *graXRS, vraFG* and *mprF* to cDNA and then amplification of the cDNA to a detectable level using the polymerase chain reaction (PCR) (Livak & Schmittgen 2001). Quantification of the amplified cDNA at the set threshold level was

performed using the asymmetrical cyanine dye, *N',N'*-dimethyl-*N*-[4-[(*E*)-(3-methyl-1,3-benzothiazol-2-ylidene)methyl]-1-phenylquinolin-1-ium-2-yl]-*N*-propylpropane-1,3-diamine (SYBR Green I), which intercalates with DNA to form a DNA–SYBR Green I complex. The formed DNA–SYBR Green I complex absorbs blue light ($\lambda_{excitation}$ 494 nm) and emits green light ($\lambda_{emission}$ 521 nm) to which the intensity of the emitted green light is detected and used to determine the concentration of the DNA present in the sample (Qiagen 2013). The concentration of DNA at the specific threshold was then used to calculate the relative concentration of each gene. These relative quantifications of the mRNA expression of *graXRS, vraFG* and *mprF* were then compared between both pH 5.5 and 7.4 growth environments in order to observe how pH affected the expression of these genes and to assess if the 'five-component system' was involved in the upregulation of L-PG in *S. aureus* grown under a low pH environment.

2.2 Materials and Methods

2.2.1 Materials

Brain heart infusion (BHI) media was used for all bacterial cultures and was purchased from Oxoid, UK. Concentrated hydrochloric acid (12.4 M, 38.0%), ethanol (99.9%), d-chloroform with 0.03% (v/v) tetra-methyl silane (≥99.8 %D atom), ethylenediaminetetraacetic acid (≥98.0%) and sodium chloride ACS reagent (≥99.0%) were all purchased from Sigma-Aldrich, UK, and used as supplied. Methanol and saturated phenol were purchased from Fisher Scientific, UK, and used as supplied. 1,2-*O*-dipalmitoyl-*sn*-glycero-3-phospho-(1'-*rac*-glycerol) sodium salt (DPPG), 1,2-*O*-dipalmitoyl-sn-glycero-3-[phospho-rac-(3-lysyl(1-glycerol))] chloride salt (DPL-PG) and 1,1',2,2'-tetramyristoyl cardiolipin ammonium salt (TMCL) were all purchased with >99.0% purity from Avanti Polar Lipids, USA. All reagents and pre-prepared silica columns for mRNA isolation came as part of the ISOLATE RNA Mini kit columns system (Bioline, UK) and were used following manufacturer's instructions. DNase I and its associated reaction buffer was purchased from Fermentas, Ontario, Canada and used according to manufacturer's instructions. SYBR Green I was purchased from Qiagen international and used with a Rotagene 6000 (Qiagen) for PCR experiments. Designed primers were all purchased from Invitrogen international and used as supplied. Large scale centrifugation (~400 mL) was conducted on a Beckman Coulter J2-21 centrifuge (Beckman Coulter, UK), and smaller scale centrifugation was conducted on either a Beckman Coulter Allegra X-12 (10-50 mL) or a

Beckman Coulter Microfuge 16 (< 5mL), (Beckman Coulter, UK). ^{31}P NMR spectra were acquired using a Bruker 400 (Bruker, Karlsruhe, Germany). *S. aureus* strains were kindly donated by Dr Jonathan Edgeworth (St. Thomas' Hospital, London) and key biological designations are summarised in table 2-1.

Table 2-1 *S. aureus* strains used for transcriptomics and lipid extractions.

Strain	Sequence type	Spa type	Van MIC$^{\alpha}$ (µg/mL)
MSSA 476	ST1	T183	<0.5
MRSA G32	ST239	T032	>1.5
MRSA G33	ST22	T032	<0.5
MRSA G35	ST22	T032	<0.5
MRSA H64	ST36	T018	<0.5
MRSA H66	ST36	T018	<0.5

MSSA = Methicillin susceptible *S. aureus*
MRSA = Methicillin resistant *S. aureus*
$^{\alpha}$ Vancomycin minimum inhibitory concentration (*in vitro*)

2.2.2 Phospholipid extraction and quantification

A strain of *S. aureus* from table 2-1 was pre-cultured from a cryovial in 50 mL BHI broth for 18 h at 37°C with continuous agitation at 100 rpm. One mL of the pre-culture was then used to inoculate 400 mL of BHI at either pH 7.4, or adjusted to pH 5.5 with concentrated hydrochloric acid. The culture was then incubated in 400 mL BHI for 18 h at 37 °C with constant agitation at 100 rpm. After 18 h, the bacterial suspension was centrifuged at 10,000 rpm for 20 min at 4 °C and the resulting pellet was then washed twice with 50 mL physiological saline adjusted to either pH 5.5 or 7.4 (depending on growth pH), by vortexing the pellet until it was fully resuspended and then centrifuging again at 10,000 rpm for 20 min at 4 °C. Two grams of the washed pellet was then vortexed for 5 min with 40 mL of chloroform–methanol (2:1 v/v) and 0.26 mL of 2 M HCl to create a single phase. The mixture was then incubated for 90 min at 37 °C with 100 rpm agitation prior to the addition of 16.6 mL pH 2.0 saline to create two phases. The two phase mixture was then further vortexed for 5 min and then centrifuged at 3,750 rpm for 30 min at 20 °C. The upper aqueous phase was removed and any insoluble cell debris at the interface discarded. The bottom organic layer was then added to 13.2 mL methanol and 16.6 mL of pH 2.0 saline (acidified with concentration HCl) and centrifuged again at 3,750 rpm for 30 min at 20 °C. The upper aqueous layer was removed and any residual solvents were evaporated under reduced pressure and the resultant lipid film dissolved in d-

chloroform–methanol–pH 2.0 saline (2:1:0.1 v/v/v). The lipid extraction method was then repeated in triplicate with all *S. aureus* strains (table 2-1) to obtain a mean relative abundance of the phospholipids in each *S. aureus* strain.

^{31}P NMR was performed on the lipid extract samples in addition to DPPG, L-PG and TMCL standards at 298.1 °K and 161.98 MHz, spectra were decoupled against ^{1}H at 400 Mhz. All samples were scanned for 3000 cycles at 10 µs pulses. Spectral peaks corresponding to the *S. aureus* phospholipids were then compared by chemical shift to those obtained from the lipid standards and were then fitted with a Voigt area function as described in chapter 1.4.3 using the program Peakfit Version 4.12 (Systat software, San Jose, USA), to determine relative quantities of the phospholipids present (Systat software 2012). Cardiolipin fitted areas were divided by a factor of two to take into account the presence of two phosphate groups in the lipid. To assess if a significant difference existed between phospholipid expression in *S. aureus* under pH 5.5 growth conditions in comparison to pH 7.4 growth conditions, a one tailed Mann Whitney U-test was performed on L-PG expression obtained for both pH conditions in each strain:

$$U_i = n_1 n_2 + \frac{n_1(n_1 + 1)}{2} - R_i \tag{20}$$

where, n_i is the sample set size and R_i is the sum of the ranks in the respective sample.

A one tailed Mann Whitney U-test was utilised as this showed if a significant increase in L-PG biosynthesis occured at pH 5.5 compared to pH 7.4. The lowest U_i value was compared to the critical *U* value (U_{crit}) at the 95% significance level (Lehmann & D'Abrera 1975), and if U_i was found to be greater than the U_{crit} the change in L-PG expression at the different pHs would not be considered significant.

2.2.3 Transcriptomics

2.2.3.1 RNA extraction and conversion to cDNA

A pre-culture in BHI broth at pH 7.4 of 100 µL of a *S. aureus* strain from table 2-1 was used to inoculate 40 mL of BHI broth at either pH 7.4 or adjusted to pH 5.5 with concentrated HCl. The inoculated broth was then incubated at 37 °C for 18 h with constant agitation at 100 rpm. After incubation, 100 µL of the broth was used to inoculate a further 40 mL of sterile BHI broth at either pH 5.5 or 7.4 depending on previous growth conditions and was incubated until

the population achieved an OD_{600} of 0.5-0.7 (late exponential stage). RNA was then extracted using the method of Franca *et al.,* (2012) by firstly diluting the culture to an OD_{600} of 0.3 using BHI adjusted to the appropriate pH. An aliquot (2 mL) of the bacterial suspension was centrifuged at 10,000 rpm and 20 ℃ for 5 min and the supernatant was discarded. The resultant pellet was resuspended in 900 µl of RNase free water–lysis buffer R–saturated phenol 1:4:4 v/v/v, and 400 mg of acid-washed 0.2 mm diameter glass beads purchased from Sigma-Aldrich, UK, were added. The sample was then homogenised for 35 s at 6.0 m/s using a FastPrep™ homogeniser (MPBio, UK). After homogenisation, the sample temperature was reduced to 0 ℃ in an ice–water bath and the homogenisation was repeated. The sample was then centrifuged for 5 min at 16,000 rpm at 20 ℃, and ~700 µL of the supernatant was transferred into a 1.5 mL volume micro-centrifuge tube containing an equal volume of ice-cold ethanol at 0 ℃. The sample, afterwards, was fractionated on the pre-prepared silica columns provided in the ISOLATE RNA mini kit and the RNA was eluted into 45 µl of RNase free water. All samples were subsequently treated with 2 µl of DNase I and 5 µl of reaction buffer prior to incubation at 37 ℃ for 30 min. DNase I was then inactivated by the addition of 5 µl of 25 mM EDTA and incubated at 65 ℃ for 10 min resulting in DNA-free RNA. The RNA extraction method was repeated in triplicate for all *S. aureus* strains (table 2-1). The concentration of RNA extracted from the samples was measured using a Picodrop™ Microlitre spectrophotometer (GRI Ltd., Braintree, UK) and 1 µg total RNA was reverse transcribed using random hexamers in the High Capacity RNA-to-cDNA kit with RNase inhibitor (Applied Biosystems) according to the manufacturer's instructions.

2.2.3.2 Quantitative PCR

Quantification of cDNA was determined by quantitative PCR (qPCR) using SYBR Green I and a Rotagene 6000 following manufacturer protocols. Primer sequences to amplify regions of the genes of interest are shown in table 2-2. Sequences for the *graR, graX* and *vraG* primers were designed on Primer-BLAST (Ye *et al.* 2012). The designed primers were validated by sequencing of the amplified product (*Macrogen Ltd.*, Seoul, Korea) and database matching using BLASTN (Altschul *et al.* 1997). DNA standards for qPCR reactions were formulated by dilution of a known quantity of DNA (0.1 µg). The efficiencies of the qPCR reactions were all found to be within 0.30 – 0.35. All C_T values were taken at a defined threshold of 0.1.

Table 2-2 Primer sequences used for qPCR

Primer name	DNA sequence (5' – 3')	Target	Ref.
qRT-*mprF*-F	TTGTAGGTTTCGGTGGCTTT	*mprF*	Yang *et al.,* 2012
qRT-*mprF*-R	GATGCATCGAAAACATGGAA		
*graS*sybr-F	TGAAATCTCGCATGAACTGG	*graS*	Meehl *et al.,* 2007
*graS*sybr-R	ATGGCGTTTCCGCTAAATCT		
qPCR*graR*-F	AGAAAAACGTACATTGACTTGGCA	*graR*	This study
qPCR*graR*-R	AACAAATGCTTCATCATCCCA		
qPCR*graX*-F	GCAGGTGGAACAGGATATATTGGTA	*graX*	This study
qPCR*graX*-R	TTGCTGCAACAACCTGTTCGTAATG		
*vraF*sybr-F	GTCTGGTGGACAAAGGCAAC	*vraF*	Meehl *et al.,* 2007
*vraF*sybr-R	TCGATTTGCATAGCTTGCTG		
qPCR*vraG*-F	GGAAGGCTCACAAGTCGGAA	*vraG*	This study
qPCR*vraG*-R	TGCAAGCTCATAACTTCGTCG		
LT*nuc*-F	AAATTACATAAAGAACCTGCGACA	*nuc*	Thomas *et al.,* 2007
LT*nuc*-R	GAATGTCATTGGTTGACCTTTGTA		

All experimentally determined C_T values for each gene were normalised against the specific heat-stable DNA nuclease gene, *nuc* (Thomas *et al.* 2007). The normalisation transformation was performed using the $2^{-\Delta\Delta C}{}_T$ method (Livak & Schmittgen 2001, Schmittgen & Livak 2008), in order to calculate the mean ΔC_T value of each gene:

$$\Delta C_T = \frac{\sum_{\mu max}^{0} 2^{-\left(\frac{C_{Ti}-C_R}{C_R}\right)}}{\mu_{max}} \qquad (21)$$

Where, C_{Ti} is the C_T value of the gene of interest, C_R is the C_T value of the reference gene and μ is the number of replicates.

To examine if any relationships existed between changes in individual gene expression and L-PG expression, the difference in ΔC_T values was calculated between pH 5.5 and 7.4 growth conditions for each gene ($\Delta\Delta C_T$) and the change in L-PG expression between pH 5.5 and 7.4 growth conditions ($\Delta L\text{-}PG$) was also calculated. The variables were then assessed against each other for correlations using a Spearman Rho test (ρ):

$$\rho = \frac{1 - 6\sum \vartheta_i}{n(n^2 - 1)} \tag{22}$$

where, n is the sample size and ϑ_i is the difference in ranking between the two variables.

The strength of the relationship between $\Delta\Delta C_T$ values of two genes or between $\Delta\Delta C_T$ of a gene and $\Delta L\text{-}PG$ was assessed by the divergence of ρ from 0 to ±1 at the 95% significance level, where a ρ value of 1 and $P<0.05$ indicated a strong significant positive correlation between both variables and a significant ρ value of -1 and $P<0.05$ indicated a strong significant negative correlation between both variables.

2.3 Results and discussion

2.3.1 Phospholipid quantification

Prior to the analysis of the bacterial lipid extracts, standards of DPL-PG, DPPG and TMCL were examined in order to detect their chemical shift value in a ^{31}P NMR spectrum (figure 2-1).

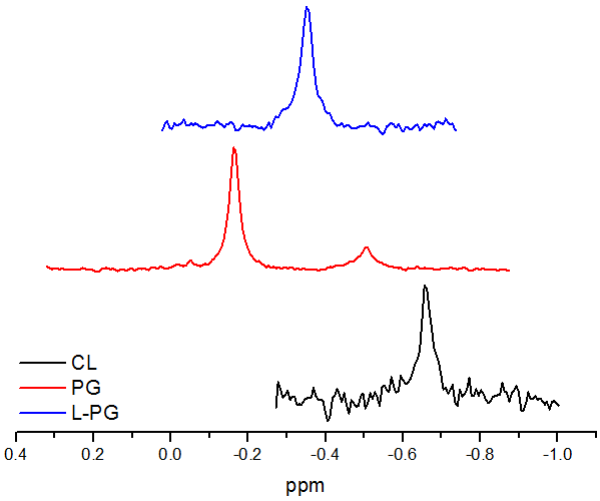

Figure 2-1 ^{31}P NMR spectra of the standards of DPL-PG, DPPG and TMCL.

The resonance signals of both DPL-PG and TMCL appeared as singlets which suggested their phosphates adopt a single charge state under the slightly acidic conditions employed (figure 2-1). It would be expected that the signal for TMCL would be split for each of its two phosphates, however this is not the case. Since the negative charge in TMCL under the mildly acidic conditions used is shared between both of its phosphate groups due to an internal hydrogen bond, both phosphates experience the same magnetic environment therefore a single resonance signal appeared in the ^{31}P NMR spectrum shown in figure 2-1 (Haines 2009). Two resonance signals would also be expected for DPL-PG under the mildly acidic conditions employed, due to the existence of ionised and unionised phosphate in the lipid in this environment (L-PG phosphate pKa ~1-3, (Tocanne *et al.* 1974c)), however this was also not observed. The lack of two resonance signals for DPL-PG appeared to be the result of constant shielding of the phosphate by either association with a proton from the dissolving solution or by association with either of the protonated amine groups of the lipid's headgroup. Therefore the appearance of one resonance signal for DPL-PG was due to the phosphate always presenting as unionised and gave rise to only one resonance signal. The only resonance signal for which

a split was detected, was DPPG, where a small additional upfield signal was observed (figure 2-1). The presence of an additional resonance signal in the DPPG spectrum suggested the phosphate of DPPG was experiencing two different magnetic environments, possibly due to association with different counter-ions.

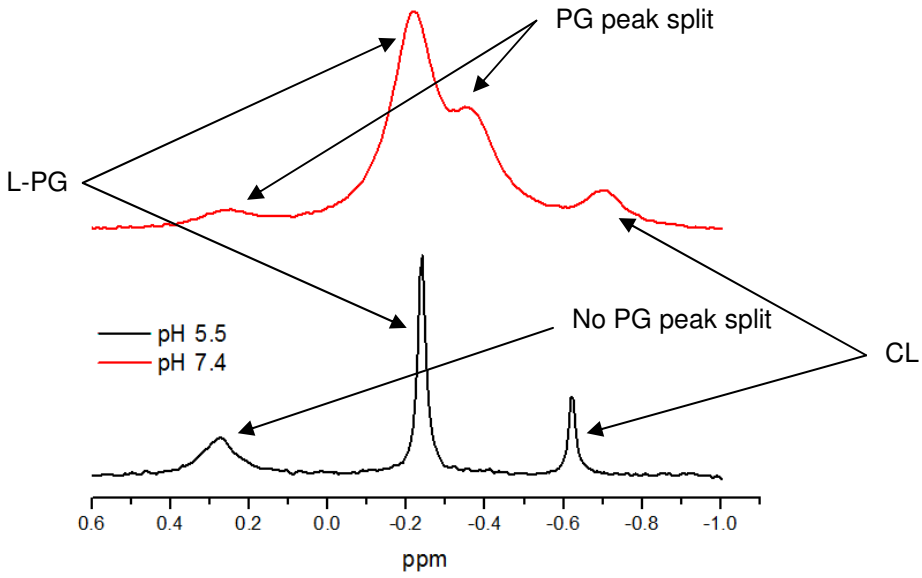

Figure 2-2 ^{31}P NMR spectra of MRSA G32 lipid extracts, showing the splitting of the PG peak.

The ^{31}P NMR spectra obtained for the natural lipid extracts from all the *S. aureus* strains varied markedly in position and intensity of the PG peaks (e.g. figure 2-2). This large variation in PG peak appearance was likely to have been due to the uncontrolled types of counter-ions present in the lipid extract which may have had different densities and different shielding effects on the PG phosphate. However, these inconsistencies in the appearance of the PG resonance signals posed little problem for the relative lipid quantification of PG. This was because each peak of PG was easily identified by chemical shift then fitted separately and also summed in the final analysis to give an accurate relative quantification of the PG in the lipid extract.

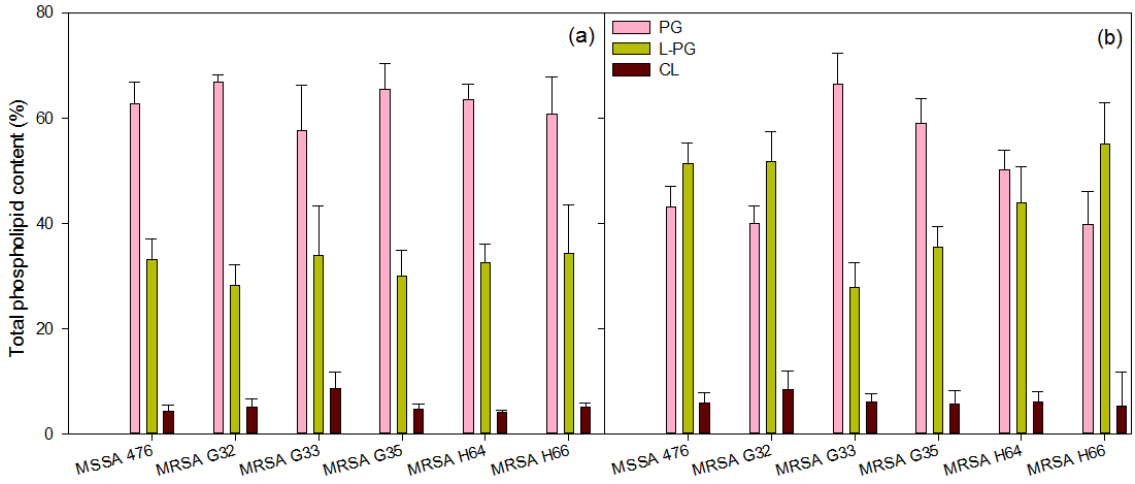

Figure 2-3 Mean relative phospholipid content of six *S. aureus* strains grown at (a) pH 7.4 and (b) pH 5.5.

The phospholipid content of the six *S. aureus* strains used in this study can be split into two groups based on their expression of L-PG, PG and CL at pH 5.5 compared to pH 7.4. The first group, consisting of MRSA G33 and G35, showed no significant difference in phospholipid expression at pH 5.5 compared to pH 7.4 ($U_{1,2}>U_{crit}$, $P > 0.05$, figures 2-3a & b). Whereas, the second group consisting of MSSA 476 and MRSA G32, H64 and H66 showed a significant upregulation of L-PG and a decrease in PG biosynthesis at pH 5.5 compared to pH 7.4 ($U_{1,2}<U_{crit}$, $P < 0.05$, figures 2-3a & b). Observation of the growth yield of *S. aureus* in the first group saw a final wet weight of ~0.2 g from 400 mL BHI growth media, compared to ~0.4 g at pH 7.4. Such a low yield at pH 5.5 suggested the bacteria had low tolerance to the pH 5.5 growth conditions which resulted in them expending substantial energy to survive at pH 5.5, hampering their ability to grow as rapidly as the first group. The second group gave final growth yields of ~0.5 g wet weight from 400 mL BHI growth media at both pH 7.4 and 5.5 and displayed L-PG content close to ~50% total phospholipid content at pH 5.5 (figure 2-3b) which is consistent with previous findings of *S. aureus* growth at low pH (Gould & Lennarz 1970). The ability of this second group to grow well under the pH 5.5 conditions suggested that the greater amount of L-PG in the bacterial plasma membrane may have helped the bacteria to grow more rapidly in the low pH environment (Gould & Lennarz 1970).

The finding that both MRSA and MSSA strains biosynthesised L-PG close to ~50% total phospholipid content at low pH suggested that upregulation in L-PG biosynthesis may be a sensory response by the bacteria to excess protons in its growth environment. Therefore L-PG may play an adaptive role in the survival of *S. aureus* to low pH environments (e.g. skin) rather

than primarily as a resistance mechanism against cationic antimicrobial peptides (CAMPs) as formerly suggested (Nishi *et al.* 2004, Peschel *et al.* 2001).

L-PG content of most *S. aureus* strains has previously been shown to be ~10-20% total phospholipid content when grown at pH 7.4, and increases to ~38% when under threat from CAMPs (Short & White 1971). The L-PG expression of all *S. aureus* strains grown at pH 7.4 in this study (~30%) is marginally higher than that reported in previous studies (Nishi *et al.* 2004, Kim *et al.* 2009, Ernst *et al.* 2009, Staubitz *et al.* 2004, Koprivnjak *et al.* 2002, Sievers *et al.* 2010). As mentioned in chapter 1.4.3, most bacterial lipid extraction protocols are based on the Bligh and Dyer technique (Bligh & Dyer 1959) which utilises a pH 7.4 extraction method where L-PG is highly labile (Danner *et al.* 2008). Additionally, TLC analysis of phospholipids requires harsh polar reagents which can further denature L-PG. In this study, L-PG was stabilised by extracting the lipid at low pH and any subsequent analysis of the phospholipids were performed at low pH with non-polar solvents. Therefore, the greater L-PG expression of the bacteria grown at pH 7.4 reported in this study may be due to the L-PG stabilising low pH environment in which the lipid was maintained (Gould & Lennarz 1970, Foreman-Wykert *et al.* 2000)

2.3.2 Transcriptomics

The genetic pathway governing regulation of L-PG biosynthesis is thought to be mediated through *graXRS* and *vraFG* expression (Falord *et al.* 2012, Li *et al.* 2007a, Li *et al.* 2007b, Meehl *et al.* 2007, Cui *et al.* 2005). To assess if any of the genes g*raXRS* and *vraFG* were co-expressed when exposing the bacteria to pH 5.5 conditions in comparison to pH 7.4, all six genes of interest in the *S. aureus* strains (table 2-1) were assessed for direct correlations between each other. As shown in figures 2-4a and b, both *graS* and *graR* were the only two genes to have a strong direct correlation between one another with respect to their expression at pH 5.5 compared to pH 7.4 suggesting that both genes were co-expressed. The finding of co-expression of *graS* and *graR* is in agreement with previous studies (Meehl *et al.* 2007), and therefore subsequent correlations with *graS* were assumed to be the same for *graR*.

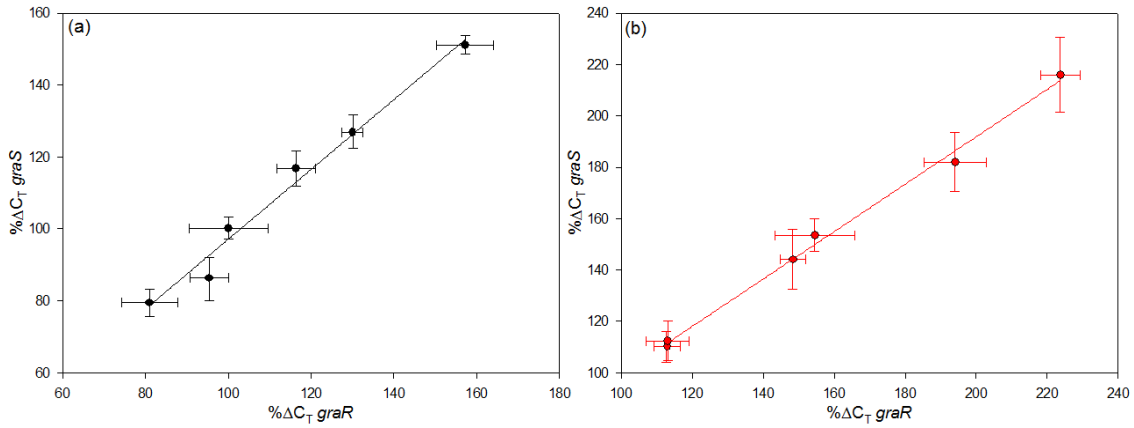

Figure 2-4 %ΔC_T values of *graR* vs. *graS* of all six strains of *S. aureus* grown at (a) pH 7.4 [ρ = 0.98, P = 0.01] and (b) pH 5.5 [ρ = 0.99, P = 0.01]

The sensing of CAMPs in the external growth environment of *S. aureus* and the associated increase in L-PG biosynthesis is thought partly to be through the TCS sensory histidine kinase, GraRS, which is the product of *graS* (and *graR*) expression (Meehl *et al.* 2007). Therefore, to examine if a correlation existed between the changes in *ΔL-PG* and changes in *graS* expression ($\Delta\Delta C_T$ *graS*) at the two pHs, the Spearman's Rho test was performed between *ΔL-PG* and $\Delta\Delta C_T$ *graS,* as shown in figure 2-5.

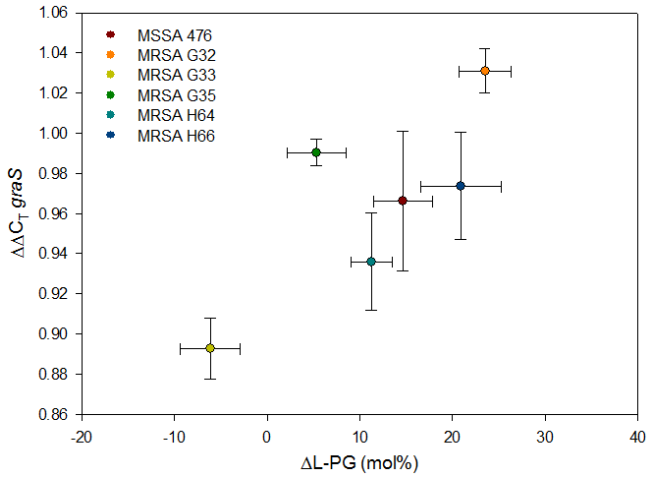

Figure 2-5 *ΔΔC$_T$ graS* vs. *ΔL-PG* of all six strains of *S. aureus* grown at pH 5.5 vs. pH 7.4 (ρ = 0.68, P = 0.18)

The observed relationship between *ΔL-PG* and *ΔΔC$_T$ graS* (figure 2-5) illustrated only a moderate positive correlation existed between the changes in *graS* and L-PG expression as pH was reduced from 7.4 to 5.5 (ρ = 0.68), and the relationship was not significant (P = 0.18). The moderate correlation between the changes in expression of *graS* and L-PG suggested there may be other genetic pathways which regulate L-PG biosynthesis, or that there may be different availabilities and regulation of the lysyl-tRNA in the bacteria required for L-PG biosynthesis (Ernst & Peschel 2011). Additionally, it is also possible some L-PG may have broken down in the natural lipid extracts and resulted in under calculation of the plasma membrane L-PG content. Therefore due to L-PG being synthesised by MprF, the change in *mprF* expression (*ΔΔC$_T$ mprF*) at the two different pHs was assessed against *ΔΔC$_T$ graS* as shown in figure 2-6.

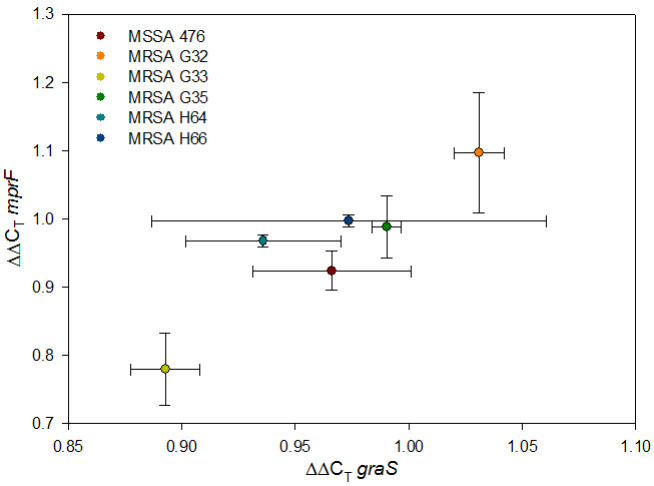

Figure 2-6 *ΔΔC$_T$ graS* vs. *ΔΔC$_T$ mprF* of all six strains of *S. aureus* grown at pH 5.5 vs. pH 7.4 (ρ = 0.89, P = 0.03)

A significant positive correlation (ρ = 0.89, P = 0.03) was found to exist between the changes in *graS* and *mprF* expression when decreasing the pH of the growth media (figure 2-6). The significant positive correlation proposed that between sensing of the low pH environment and the synthesis of L-PG there were little other influencing regulatory factors between MprF and GraS. This result also suggested that between MprF and final L-PG biosynthesis an intermediate regulatory genetic stage may be present or there may be the presence of *S. aureus* strains which provide lysyl-tRNAs at different rates to MprF. A polymorphic version of MprF may also have been present in some of the *S. aureus* strains. Polymorphic versions of MprF have been found previously for daptomycin resistant MRSA strains which possessed point mutations in the synthase domain of MprF and could turnover L-PG much more rapidly compared to the wild-type enzyme (Yang *et al.* 2009, Julian *et al.* 2007, Murthy *et al.* 2008b). To help support the possibility of one or more of these theories being true the correlation between Δ*L-PG* and $\Delta\Delta C_T$ *mprF* was examined. As shown in figure 2-7 a positive correlation existed between Δ*L-PG* and $\Delta\Delta C_T$ *mprF* (ρ = 0.77), which although was stronger than the positive correlation between $\Delta\Delta C_T$ *graS* and Δ*L-PG* (ρ = 0.68), was not significant (P = 0.10). Therefore, this strongly suggested an additional regulatory genetic process may be present, a potential polymorphic variant of MprF may have existed in some of the *S. aureus* strains or there may also have been a difference between availability and provision of lysyl-tRNAs between strains. It should also be noted that the non-significant correlation between Δ*L-PG* and $\Delta\Delta C_T$ *mprF* may also be due to breakdown of L-PG in the lipid extracts, therefore creating inaccuracy in the estimation of L-PG biosynthesis at the two pHs.

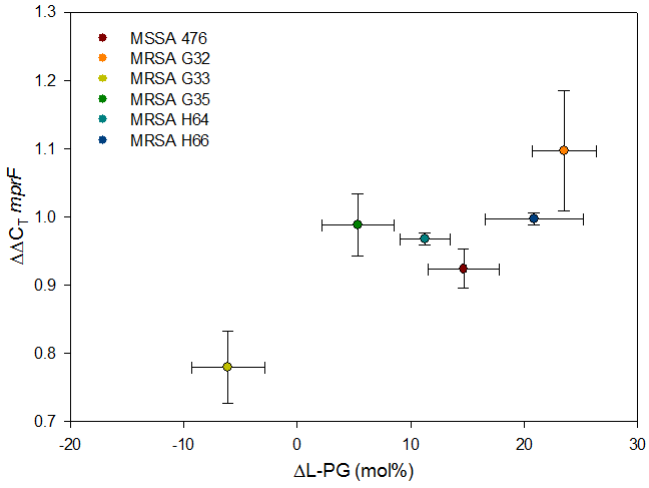

Figure 2-7 Δ*L-PG* vs. $\Delta\Delta C_T$ *mprF* of all six strains of *S. aureus* grown at pH 5.5 vs. pH 7.4 (ρ = 0.77, P = 0.10)

With respect to the sensitivity of *S. aureus* to CAMPs, GraR requires a functioning VraG in order to regulate *mprF* expression and in the absence of *vraG* little to no upregulation in L-PG biosynthesis occurs on exposure to CAMPs (Falord *et al.* 2012). Therefore, to examine if VraG was also required for changes in L-PG biosynthesis when *S. aureus* was exposed to a low pH environment $\Delta\Delta C_T$ *mprF* and $\Delta\Delta C_T$ *graS* were assessed against changes in *vraG* expression at pH 5.5 in comparison to pH 7.4 ($\Delta\Delta C_T$ *vraG*) (figures 2-8a and b).

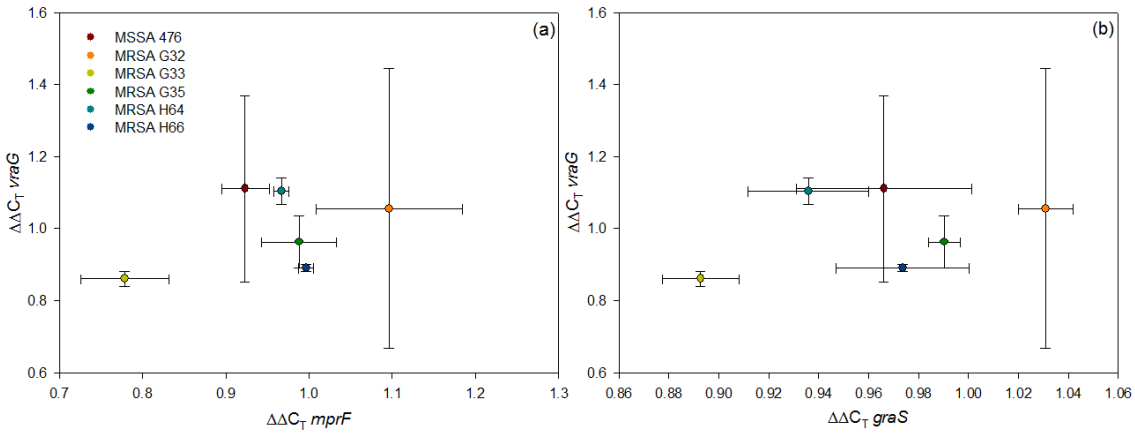

Figure 2-8 (a) $\Delta\Delta C_T$ *vraG* vs. $\Delta\Delta C_T$ *mprF* (ρ = 0.03, P = 1.00) and (b) $\Delta\Delta C_T$ *vraG* vs $\Delta\Delta C_T$ *graS* (ρ = 0.14, P = 0.80), of all six strains of *S. aureus* grown at pH 5.5 vs. pH 7.4.

The data illustrated in figures 2-8a & b showed there were weak positive correlations, which were not significant, between changes in *vraG* expression and changes in *graS* (ρ = 0.14, P = 0.80) and *mprF* (ρ = 0.03, P = 1.00) expression as pH of the growth environment was reduced. The weak correlations between $\Delta\Delta C_T$ *vraG* and both, $\Delta\Delta C_T$ *mprF* and $\Delta\Delta C_T$ *graS* indicated that expression of VraG was not affected to a high degree in the bacterial membrane at pH 5.5 compared to pH 7.4. Therefore, VraG would appear to be little involved in the regulation of L-PG biosynthesis when the bacterium is cultured in a mildly acidic pH environment and suggests GraRS may be able to be directly activated by excess environmental protons.

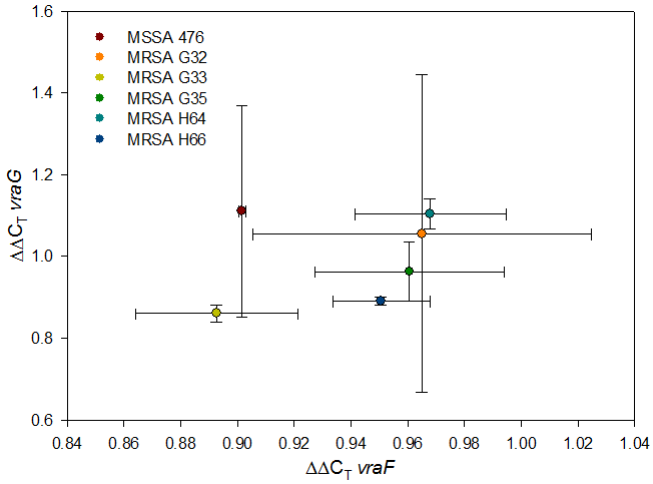

Figure 2-9 *ΔΔC$_T$ vraF* vs. *ΔΔC$_T$ vraG* (ρ = 0.43, *P* = 0.42) of all six strains of *S. aureus* grown at pH 5.5 vs. pH 7.4.

VraG operates via phosphorylation by the intra-cellular ATPase VraF (Falord *et al.* 2012), however changes in *vraF* expression at pH 5.5 compared to pH 7.4 (*ΔΔC$_T$ vraF*) and *ΔΔC$_T$ vraG* were not found be significantly correlated to each other (ρ = 0.43, *P* = 0.42, figure 2-9). The lack of significant correlation between *ΔΔC$_T$ vraF* and *ΔΔC$_T$ vraG* suggested VraG and/or VraF may have had some degree of measurement anomalies as both genes overlap and should be co-expressed (Meehl *et al.* 2007). To assess if the intra-cellular ATPase VraF had any correlations with *ΔL-PG*, *ΔΔC$_T$ mprF* and *ΔΔC$_T$ graS* were assessed with respect to *ΔΔC$_T$ vraF* (figures 2-10a and b).

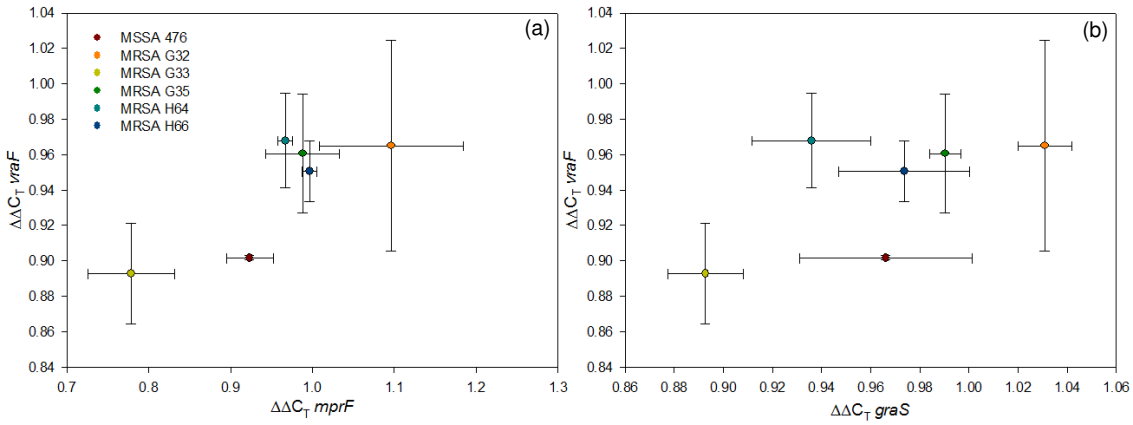

Figure 2-10 (a) *ΔΔC$_T$ vraF* vs. *ΔΔC$_T$ mprF* (ρ = 0.61, *P* = 0.26) and (b) *ΔΔC$_T$ vraF* vs *ΔΔC$_T$ graS* (ρ = 0.43, *P* = 0.42), of all six strains of *S. aureus* grown at pH 5.5 vs. pH 7.4.

Figures 2-10a and b showed a moderate positive correlation, which was not significant, existed between changes in *vraF* expression and both, *graS* (ρ = 0.43, *P* = 0.42) and *mprF* (ρ = 0.61, *P* = 0.26) expression in response to a low pH environment and suggested changes in growth environment pH had little effect on VraF expression. The moderate correlation between *ΔΔC$_T$*

vraF and both, $\Delta\Delta C_T$ *mprF* and $\Delta\Delta C_T$ *graS* supported the earlier finding that VraG may not be required for L-PG upregulation in response to a low pH environment, as the VraF ATPase is also not upregulated to such a high degree at low pH in comparison to GraS and MprF.

The final gene examined in the *graXRS* and *vraFG* cluster with respect to changes in environmental growth pH was *graX*, however the role of GraX is largely unknown and has been suggested to be a regulatory protein between GraS, GraR and VraF (Falord *et al.* 2012).

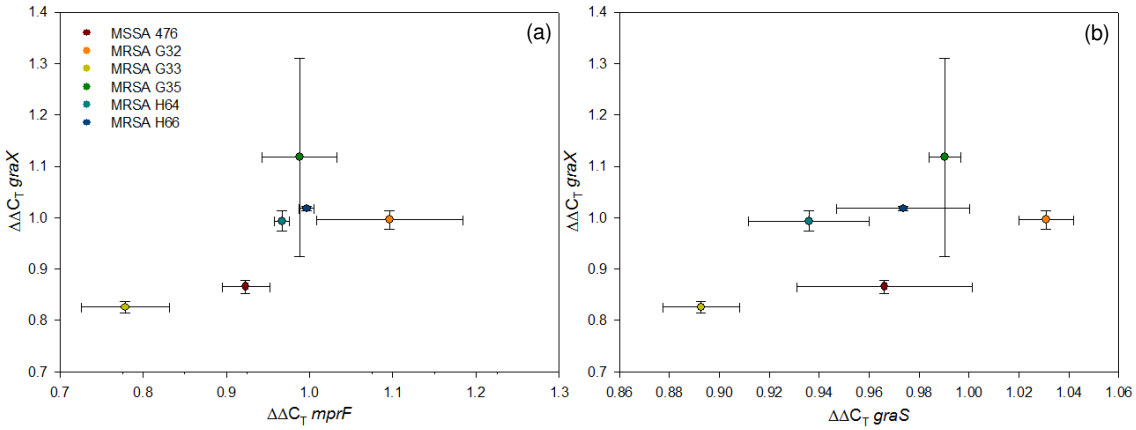

Figure 2-11 (a) $\Delta\Delta C_T$ *graX* vs. $\Delta\Delta C_T$ *mprF* (ρ = 0.71, P = 0.10) and (b) $\Delta\Delta C_T$ *graX* vs $\Delta\Delta C_T$ *graS* (ρ = 0.77, P = 0.10), of all six strains of *S. aureus* grown at pH 5.5 vs. pH 7.4.

As shown in figures 2-11a and b, changes in *graS* (ρ = 0.77, P = 0.10) and *mprF* (ρ = 0.71, P = 0.10) expression at pH 5.5 compared to pH 7.4 showed positive correlations with changes in *graX* expression between both pHs, however the correlations were not significant. Similar to the changes observed in *vraFG* expression at pH 5.5 compared to pH 7.4, *graX* expression changes to a lower degree than either *graS* or *mprF* between these pHs. This suggested that *graX* may have a reduced role in the response of the bacterium to a low pH environment. It is difficult however to substantiate this, as the role of GraX is unclear at present and if it does possess a regulatory role between GraS, GraR and VraF, upregulation of its expression may not be required to such a high degree when the bacterium is grown in a low pH environment.

2.4 Conclusion

This study reports evidence that the upregulation of L-PG in *S. aureus* in response to a mildly acidic environment may be regulated by GraS. The increased expression of *graS* in a pH 5.5 environment was associated with a similar increase in the expression of *mprF*, which may explain why a greater amount of L-PG is found at pH 5.5 in MSSA 476 and MRSA G32, H64 and H66. The roles of VraFG and GraX remain unknown at this current time with respect to *S. aureus* growth at pH 5.5, however, it would appear that VraFG may not play a major role in L-PG biosynthesis when the bacterium is grown in a mildly acidic environment due to the lack of increased *vraFG* expression in comparison to that of *graS* and *mprF* at pH 5.5. This lack of upregulation of the expression of *vraFG* at pH 5.5 is in contrast to findings with *S. aureus* exposed to CAMPs (Falord *et al.* 2012). Although this chapter reports some preliminary data on the regulation of *graRSX* and *vraFG* with respect to changes in environmental growth pH of *S. aureus*, the data must be interpreted with caution. The reference gene, *nuc*, showed little significant difference in expression between both pH growth environments in this study, however previous studies have shown it to change in expression in *S. aureus* under different environmental pressures (e.g. low and physiological pH environments) (Weinrick *et al* 2004). Therefore *nuc* may not be a suitable reference gene for data normalisation. To address this issue in the future, house keeping genes such as *fabD, tpiA*, *gyrA*, etc (Theis *et al.* 2007), which are not known to be affected by environmental growth pH, could be used to normalise the qPCR data. Therefore, before any definitive conclusion can be sought from this chapter, further work must be conducted with a series of house keeping genes in relation to *graRSX* and *vraFG* expression under different pH growth conditions.

The increased biosynthesis of L-PG at low pH in *S. aureus* provides the bacterial plasma membrane with a greater concentration of a cationically charged phospholipid which presumably helps to protect the bacterium from the greater concentration of protons in its growth environment (Gould & Lennarz 1970). However, the effects of the increased biosynthesis of L-PG at low pH on the *S. aureus* plasma membrane are not fully understood since the actual mechanism by which L-PG protects the plasma from higher concentrations of protons remains unsubstantiated. Therefore, this work will now focus on the biophysical characterisation of membranes containing L-PG under mildly acidic conditions.

Chapter 3

Characterisation of *Staphylococcus aureus* plasma membrane lipid extracts

3.1 Introduction

Chapter 2.3.1 showed that when *Staphylococcus aureus* was cultured at pH 5.5, strains methicillin susceptible *S. aureus* (MSSA) 476 and methicillin resistant *S. aureus* (MRSA) G32, H64 and H66 plasma membrane L-PG content increased to ~50% total phospholipid. Such high L-PG concentrations have also previously been reported in *S. aureus* grown in a low pH environment and was suggested to attenuate the anionic membrane surface charge imposed by the other plasma membrane phospholipids, phosphatidylglycerol (PG) and cardiolipin (CL) (Gould & Lennarz 1970). However this theory is unsubstantiated as no surface charge assessment was performed on these bacteria, alas this charge neutralisation mechanism of L-PG in low pH environments remains only an assumption. L-PG has previously been suggested to be cationic with a net +1 charge as it contains two protonated amine groups and a single anionic phosphate group (Peschel *et al.* 2001). However, this headgroup charge depends on environmental pH due to L-PG's α-amine group having an estimated pKa of ~6-7 (Tocanne *et al.* 1974c). In light of this, as PG and CL have net -1 charges, in the pH range 3.0 to 8.0 (Haines 2009), it is likely L-PG could form ion-pairs with these lipids in a pH 7.4 environment, but even more ion-pairs in a low pH environment, i.e. neutralising more membrane surface anionicity at low pH. Therefore, this charge neutralisation theory at low pH and the nature of the effect that changes in L-PG headgroup charge and concentration have on the plasma membrane of *S. aureus* in both low pH and pH 7.4 growth environments were examined. This was conducted by extracting the plasma membrane phospholipids of *S. aureus* grown in pH 5.5 and 7.4 environments and assessing the individual lipid extracts characteristics by a series of biophysical techniques in both pH 5.5 and 7.4 environmental conditions. These techniques principally focussed on how membrane lateral density and surface charge were altered by different L-PG concentrations found in the bacterial plasma membrane under pH 5.5 and 7.4 growth conditions.

In order to examine changes in plasma membrane lateral density and elasticity, the pH 5.5 and 7.4 lipid extracts from *S. aureus* can be formed into monolayers by depositing them at the air–

water interface of aqueous subphases adjusted to either pH 5.5 or 7.4, and then laterally compressing them. Compression of these monolayers can then be used to assess how resistant the monolayers are on different pH subphases to applied lateral force which could then provide information on how laterally dense and rigid the monolayers are when L-PG is present in different charge states and concentrations on both pH subphases (Gaines 1966). Such an experiment has previously been conducted with mixtures of 1,2-*O*-dipalmitoyl-3-trimethylammonium-propane (DPTAP, cationic) and 1,2-*O*-dimyristoyl PG (DMPG, anionic) where an equimolar mixture of the two lipids produced a rigid monolayer with low elasticity through lipid ion-pair formation (Sung *et al.* 2010).

To assess changes in plasma membrane surface charge of the bacterium grown in pH 5.5 and 7.4 environments, zeta potential measurements can be employed with both natural lipid extracts and protoplasts of live bacteria. The zeta potentials of pH 5.5 and 7.4 lipid extracts from *S. aureus*, formulated as mutli-lamellar vesicles (MLVs) in both pH 5.5 and 7.4 buffers, would provide information as to what the surface charge presentation is for the lipid components of the bacterial plasma membrane in different pH buffers. Zeta potentials of live *S. aureus* protoplasts in both pH 5.5 and 7.4 growth environments can then be used to ascertain the actual zeta potential of the bacterial plasma membrane in order to try and validate the *S. aureus* plasma membrane MLV model zeta potential results.

In order to gain atomic details of the bilayer structures of these lipid extracts from *S. aureus* grown under pH 5.5 and 7.4 environments, neutron diffraction can be employed (Pabst *et al.* 2010). Differences between bilayer thicknesses, scattering length densities (SLD) and lamellar repeat spacings (d-spacing) of lipid extracts from MSSA 476 can be examined with this technique. These derived bilayer parameters could then provide insight into how the hydrocarbon and headgroup conformations of the polar lipids in the plasma membrane of *S. aureus* change between the bacterium grown at pH 5.5 compared to at pH 7.4.

The amalgamation of all of the results from these biophysical techniques should provide details as to how L-PG helps the plasma membrane of *S. aureus* to adapt to mildly acidic pH environments. This is important as *S. aureus* has been found to colonise human epithelial surfaces such as skin and the anterior nares of the nasal cavity, which are both mildly acidic environments (Lambers *et al.* 2006, Washington *et al.* 2000, von Eiff *et al.* 2001).

3.2 Materials and methods

3.2.1 Materials

Tris(hydroxymethyl)aminomethane (>99.0%), concentrated hydrochloric acid (~38%), glacial acetic acid, sodium sulphate (>99.0%), deuterium oxide (99.9%) and sucrose (≥99.5%) were all purchased from Sigma-Aldrich UK, and used as supplied. Enzymes, DNase and lysostaphin, for protoplast formation were both purchased from MP Biomedicals Europe and lysozyme also for protoplast formation was purchased from Sigma-Aldrich UK; all enzymes were used as supplied. Brain heart infusion for growing *S. aureus* was purchased from Oxoid, UK. Organic solvents for lipid preparation and general cleaning, chloroform, ethanol and methanol were all purchased from Fisher scientific, UK. Cleaning solvents for neutron diffraction, chloroform (99.5%), methanol (99.9%) and acetone (99.9%) were all purchased from Sigma-Aldrich, international and used as supplied. Silicon discs for neutron diffraction experiments were obtained from Silicon Materials (Kaufering, Germany); diameter 50.8mm ± 0.50 mm, thickness 275 µm ± 20 µm, resistivity 1-5 Ωcm and single side polished finish. Large scale centrifugation (~400 mL) was conducted on a Beckman Coulter J2-21, UK, and smaller scale centrifugation was conducted either on a Beckman Coulter Allegra X-12 (10-50 mL) or a Beckman Coulter Microfuge 16 (<5 mL), (Beckman Coulter, UK). All zeta potential measurements were performed on a Malvern Zetasizernano ZS, (Malvern, Worcester, UK) using Zetasizer custom software v7.03 (Malvern, Worcester, UK).

3.2.2 *S. aureus* protoplast formation and characterisation

Protoplasts were prepared in triplicate by the same general method (Kim *et al.* 2009) with all six *S. aureus* strains from chapter 2.2.1, namely MSSA 476 and MRSA G32, G33, G35, H64 and H66. *S. aureus* was grown for ~3-4 h to OD_{660} = 0.7 (mid-exponential phase) in 10 mL of brain heart infusion media (BHI) at pH 5.5 or 7.4, adjusted with concentrated HCl, and then centrifuged at 10,000 rpm for 15 min at 4 °C. The formed pellet was then resuspended, by vortex mixing, in 10 mL of 50 mM Tris(hydroxymethyl)aminomethane (TRIS)–glacial acid (AcOH) 1:1 mol/mol adjusted to either pH 5.5 or 7.4 depending on growth conditions and then re-centrifuged at 10,000 rpm for 15 min at 4 °C. The resultant pellet was resuspended a second time, in 10 mL hypertonic buffer which consisted of 1M sucrose and 50 mM TRIS–AcOH 1:1 mol/mol adjusted to the appropriate pH (either pH 5.5 or 7.4). The enzymes lysozyme (200 µg), lysostaphin (100 µg) and DNase (25 µg) were then added sequentially, to 1 mL of the bacterial suspension in hypertonic buffer. The bacterial suspension with enzymes was then incubated at 37 °C with gentle agitation of 100 rpm for 4 h after which the cells were washed with hypertonic buffer at the pH of growth by centrifuging the bacteria at 3,750 rpm for 15 min at 25 °C and then resuspending the formed pellet in fresh 1 mL hypertonic buffer at the appropriate pH. To confirm the presence of protoplasts and complete removal of the cell wall of the bacteria, Gram staining was performed on all of the samples. Zeta potential measurements were then collected of all protoplast samples in hypertonic buffer and the change in zeta potential of the protoplasts from pH 5.5 compared to pH 7.4 growth conditions were then assessed against the change in L-PG content of the bacteria grown at both pHs. Quantitative L-PG data for all the *S. aureus* strains used were obtained from chapter 2.3.1. In order to assess if a significant difference existed between the zeta potential of protoplasts grown at pH 5.5 compared to pH 7.4, a Mann Whitney U-test was conducted on the data using eq. (20) (chapter 2.2.2). The lowest U_i value was compared to the critical U value (U_{crit}) at the 95% significance level (Lehmann & D'Abrera 1975). If $U_i > U_{crit}$ then it was assumed that there was no significant difference between the zeta potential of protoplasts grown at pH 5.5 compared to pH 7.4, however if $U_i < U_{crit}$ then it was assumed a significant difference existed between the between the zeta potential of protoplasts grown at pH 5.5 compared to pH 7.4.

3.2.3 *S. aureus* polar lipid extracts

The polar lipids of MSSA 476 and MRSA G32, G33, G35, H64 and H66 were extracted using the acid-modified Bligh and Dyer extraction method as described in chapter 1.4.2 (Foreman-Wykert *et al.* 2000).

3.2.4 Isotherms of *S. aureus* polar lipid extracts

Solutions of *S. aureus* lipid extracts were formed by dissolving 1 mg of a *S. aureus* lipid extract in 1 mL of chloroform. Each 1 mg/mL bacterial lipid solution (60 µL) was then spread dropwise over the surface of a 500 cm^2 (20 cm × 25 cm) KN2003 Langmuir trough (NIMA technologies, Coventry, UK) containing an aqueous subphase of 10 mM TRIS–AcOH 1:1 mol/mol adjusted to either pH 5.5 or 7.4 with concentrated HCl. The lipid monolayer was then equilibrated for 15 min prior to data acquisition to allow all residual chloroform to evaporate and then isotherms were collected through ten cycles at 22.7 °C with a barrier opening and closing speed of 25 cm^2/min. The maximum surface pressure of the monolayer was set to 40mN/m and the minimum surface pressure was set to 0 mN/m. This method was conducted with all bacterial lipid extracts of *S. aureus* strains MSSA 476 and MRSA G32, G33, G35, H64 and H66. In order to normalise the data, the surface pressure–area isotherms collected from a pH 5.5 or 7.4 lipid extract on a pH 7.4 subphase were averaged and then normalised by setting all the maximum surface pressures (40 mN/m) as the same limiting area per molecule and noting down the change in scale of each bacterial isotherm. Then due to the same pH lipid extract sample being used on the pH 5.5 subphase these isotherms were then normalised by employing the same scaling factor collected on the pH 7.4 subphase. All normalised bacterial lipid extracts are shown in Appendix II. The mean limiting area per molecule for each bacterial lipid extract (A) was then calculated by taking a tangent to the liquid condensed phase of the isotherm at ~30 mN/m and extrapolating the tangent to the x-ordinate. Mean lipid molecular weights were calculated using the relative quantitative phospholipid content of each bacterial strain (Section 2.3.1) and estimated lipid weights of 1300, 900 and 700 for CL, L-PG and PG, respectively (Peschel *et al.* 2001, Durham & Kloos 1978). The compressional moduli (K^s) (Gaines 1966) of each bacterial lipid extract was calculated using:

$$K^s = -A\left(\frac{\delta \Pi}{\delta A}\right)_T \qquad (23)$$

where, Π is the surface pressure of the bacterial lipid extract (mN/m).

The compressional modulus is a quantitative measure of a monolayer's overall elasticity as a function of area per molecule (Gaines 1966). When $K^s = 0$, the monolayer is considered to be rigid and not laterally elastic, whereas positive deviations of K^s from 0 indicate the monolayer has a certain degree of elasticity depending on the value of K^s (Gaines 1966).

Assessment of significant differences between compressional moduli and limiting area per molecule of each pH lipid extract on the different pH subphases was conducted using a one-tailed Mann Whitney U-test, eq. (20) as described above (3.2.2).

3.2.5 Multi-lamellar vesicles of *S. aureus* polar lipid extracts

Two 10 mg samples of a specific *S. aureus* strain lipid extract were each dissolved in 5 mL of chloroform and then evaporated to dryness under reduced pressure over 24 h. The resultant bacterial lipid films were then dispersed as vesicles, by vortex mixing, in 5 mL of 10 mM TRIS–AcOH 1:1 mol/mol adjusted to either pH 5.5 or 7.4 with concentrated HCl. Multi-lamellar vesicles (MLVs) of the bacterial lipid extracts were then formed by freeze-thaw cycling at -200 °C to 50 °C, five times, using a liquid nitrogen bath and a warmed water bath. The bacterial MLVs were then annealed at 25 °C for 60 min and zeta potential measurements were then taken. This method was conducted in triplicate with all lipid extracts from *S. aureus* strains MSSA 476 and MRSA G32, G33, G35, H64 and H66. Assessment of significant differences between MLV zeta potential results of both pH lipid extracts in both pH subphases was conducted using a one tailed Mann Whitney U-test, eq. (20) as outlined above (3.2.2).

3.2.6 Neutron diffraction of *S. aureus* lipid extracts

Two silicon discs were prepared for neutron diffraction by initially cleaning them by 5 min of bath sonication (Branson bath sonicator 3510, Danbury, USA) in chloroform, then acetone and then methanol, and then treating them under UV light for 30 min with a UV/Ozone ProCleaner™ Plus (BioForce Nanosciences, Ames, USA). Bacterial lipid extracts from MSSA 476 separately grown at pH 5.5 and 7.4 were then prepared as oriented multilayers on the silicon discs by dissolving 10 mg of the bacterial lipid extracts in 1 mL of chloroform and then coating the two silicon discs evenly with these bacterial lipid solutions. The silicon discs were then put in a low pressure atmosphere to ensure that all the chloroform was evaporated, to leave only the bacterial lipids coating the polished face of the silicon discs. The coated silicon

discs were then placed over a saturated Na_2SO_4 bath for 24 h at 50 °C in a sealed vessel to achieve ~85% humidity. A coated silicon disc was then mounted on to a goniometer placed in a sealed temperature-controlled aluminium chamber. The humidity and sample contrasts were controlled by varying the H_2O and D_2O content of the internal bath reservoir at different temperatures (21-25 °C), with a constant external temperature of 25 °C. Neutron diffraction was then performed on the D16 neutron diffractometer at the Institut Laue-Langevin (Grenoble, France) at λ = 4.741 Å. Strong reflections were measured for short times (~30 min) whereas weaker ones were measured for ~2-3 hours to improve signal-noise of the higher orders of diffraction. The neutron diffraction profiles (Intensity vs. 2θ) collected for each sample were then fitted with an exponential function using Sigmaplot V 12.0 (Systat Software, San Jose, California, USA) to remove off-specular reflectivity and incoherent scattering. The corrected neutron diffraction orders were then individually modelled with a Voigt area function to calculate the neutron diffraction peak area ($I(h)$), amplitude (a_0), centre (a_1), width (a_2) and shape (a_3) parameters:

$$I(h) = \frac{a_0 a_3}{\pi\sqrt{\pi}\, a_2} \int_{-\infty}^{\infty} \frac{\exp\left(-t^2\right)}{a_3{}^2 + \left(\frac{x - a_1}{a_2} - t\right)^2}\, dt \qquad (24)$$

Where, h is the order of neutron diffraction.

The mean value of a_1 from each order of neutron diffraction was then used to calculate the lamellar repeat spacing (d-spacing, ψ):

$$\psi = \lambda \times \frac{2 \sin\theta}{h} \qquad (25)$$

To reconstruct the one dimensional bilayer SLD profile, the absolute bilayer structure factors ($F(h)$) of each order of neutron diffraction were required. $F(h)$ is related to the intensity of the neutron diffraction order, $I(h)$, using: (Saxena & Schoenborn 1977)

$$|F(h)| = \frac{\sqrt{I(h)}}{\sqrt{L_1(h)L_2(h)L_3(h)}} \tag{26}$$

Where, $L_1(h)$ is the angular velocity term 1/sin 2θ, $L_2(h)$ is a factor correcting for sample mosaicity and $L_3(h)$ is a factor correcting for sample absorption and geometry (Saxena & Schoenborn 1977).

The correctional factors $L_2(h)$ and $L_3(h)$ were corrected for by using the D16 instrument software FORTRAN, (Institut Laue-Langevin,Grenoble, France), however $L_1(h)$ was corrected for whilst calculating the structure factors (Leonard *et al.* 2001). Due to the sample being centrosymmetric, the sign of $F(h)$ for each order could have been positive or negative. Therefore to determine the sign of $F(h)$, contrast variation was employed with both H_2O and D_2O contrasts where the linear dependence of $F(h)$ at a given order, h, was determined versus D_2O content (Appendix AI.I) (Worcester & Franks 1976). Following $F(h)$ sign assignment the Patterson map or SLD profile of the bilayer in real space perpendicular to the bilayer interface, $p(z)$,was calculated using: (Pebaypeyroula, *et al.* 1994, Buldt *et al.* 1979)

$$p(z) = \frac{2}{\psi}\sum_{h=1}^{h_{max}} F(h)\cos\left(\frac{2\pi hz}{\psi}\right) \tag{27}$$

Where, z is the direction perpendicular to the bilayer surface plane (bilayer normal).

3.3 Results

3.3.1 Assessment of zeta potentials of protoplasts and MLVs of *S. aureus* lipid extracts

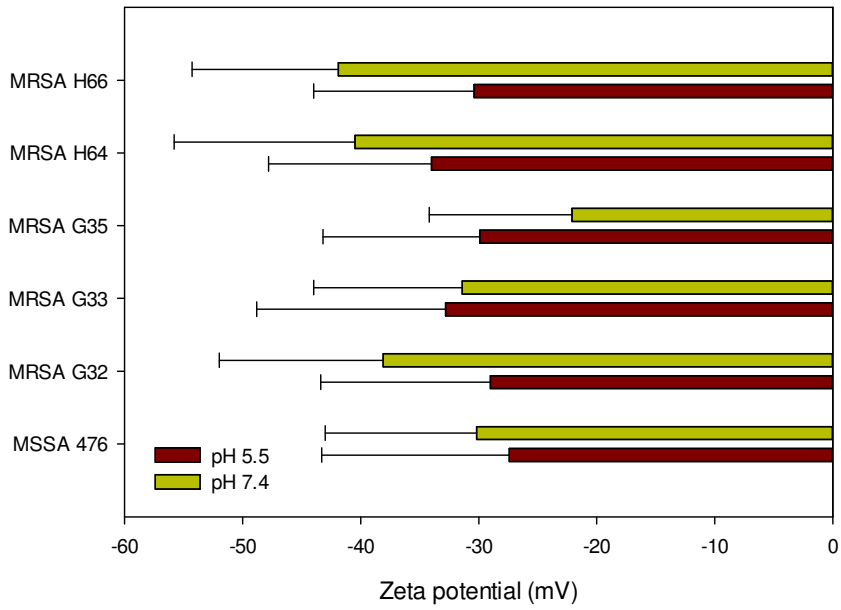

Figure 3-1 Zeta potential results of protoplasts of MSSA 476 and MRSA G32, G33, G35, H64 and H66, grown under pH 5.5 and 7.4 environments.

The mean zeta potential results shown in figure 3-1 demonstrate that all the *S. aureus* protoplasts had anionically charged surfaces. However, MSSA 476 and MRSA G32, H64 and H66 when grown under a pH 5.5 environment showed a reduction in mean zeta potential anionicity compared to when grown at pH 7.4 (figure 3-1). This reduction in zeta potential anionicity under the pH 5.5 growth environment suggested that there was a dampening of the anionic surface charge of the outer leaflet of the plasma membrane, presumably due to an increase in the plasma membrane L-PG content of these strains at pH 5.5 (chapter 2.3.1). To support these findings, zeta potentials of MRSA G33 and G35 protoplasts (figure 3-1), which do not upregulate their plasma membrane L-PG content when grown under a pH 5.5 environment (chapter 2.3.1), did not show the same reduction in zeta potential anionicity when grown at pH 5.5. In order to assess whether a statically significant difference existed between all the *S. aureus* protoplast zeta potentials at pH 5.5 compared to pH 7.4, the zeta potential results at each pH were subjected to a one tailed Mann-Whitney U-test. A result of $U_{1,2}<U_{crit}$ ($P < 0.05$) was found, which suggested a reduction in protoplast zeta potential occurs when *S. aureus* protoplasts are grown in a pH 5.5 environment compared to a pH 7.4.

From the high anionicity of the zeta potential results of all the *S. aureus* protoplasts in figure 3-1 it might be construed that their plasma membranes contained very little L-PG in their outer leaflets. However, the plasma membrane of *S. aureus* also contains a significant number of integral proteins which also would contribute to the protoplast zeta potentials (Ward & Perkins 1968), therefore this may have caused the high anionicity of the recorded protoplast zeta potentials.

To investigate if a significant relationship existed between the change in protoplast zeta potentials under both pH growth environments, and the change in mol% L-PG content of the bacteria grown under both pH environments (chapter 2.3.1), linear regression analysis was performed between the change in both variables as shown in figure 3-2.

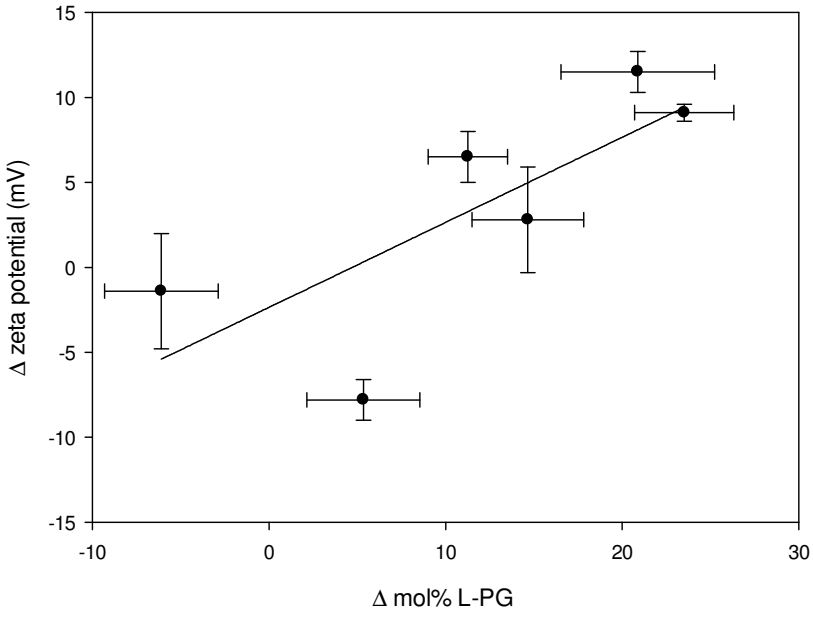

Figure 3-2 The change in mol% L-PG content of six *S. aureus* strains under a pH 5.5 growth environment compared to a pH 7.4 growth environment vs. the change in protoplast zeta potential results of the same six *S. aureus* strains under a pH 5.5 growth environment compared to a pH 7.4 growth environment. $f(x) = 0.5x - 2.35$ ($r^2 = 0.58$).

Figure 3-2 showed a weak positive correlation ($r^2 = 0.58$) existed between changes in protoplast zeta potentials and mol% L-PG content under pH 5.5 growth conditions compared to pH 7.4 (r^2 calculated by linear regression analysis in Microsoft Excel 2007). This positive correlation between changes in protoplast zeta potentials and changes in mol% L-PG content between both pH growth environments suggested that as plasma membrane L-PG biosynthesis increases in *S. aureus*, dampening of protoplast zeta potential anionicity also increases.

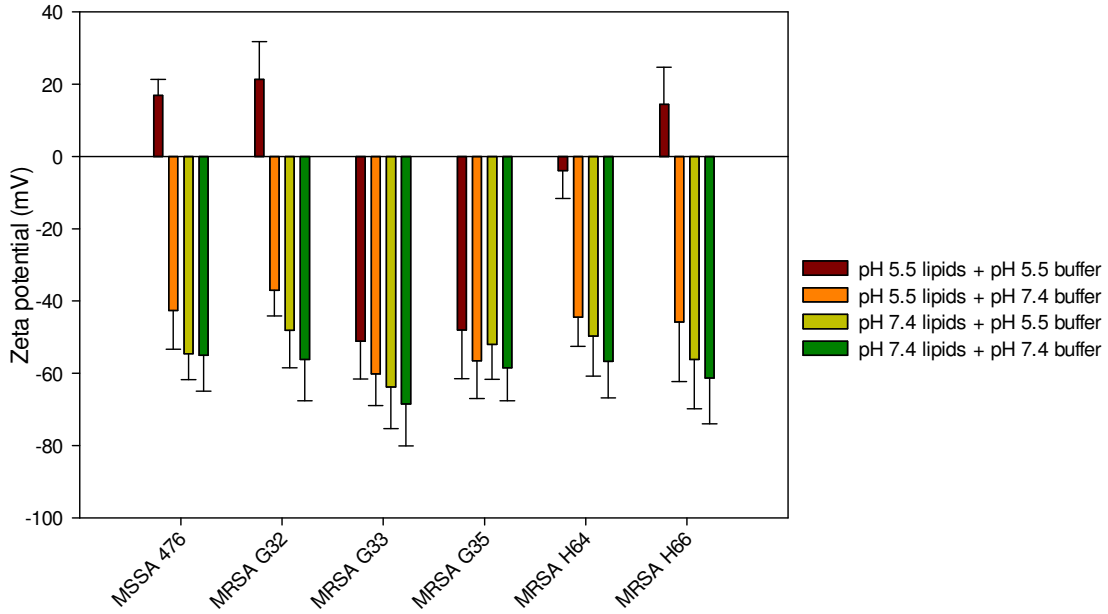

Figure 3-3 Zeta potential results of MLVs of lipid extracts of all six *S. aureus* strains grown at either pH 5.5 or 7.4 in buffers of either pH 5.5 or 7.4.

The MLVs of all the pH 7.4 *S. aureus* lipid extracts exhibited highly negative zeta potential results (between -50 to -70 mV) in a pH 7.4 buffer (figure 3-3). The high zeta potential anionicity of these MLVs indicated that the pH 7.4 lipid extracts were mainly formed from anionic lipids (e.g. PG and CL) which is consistent with the ^{31}P NMR phospholipid quantification data of *S. aureus* grown at pH 7.4 (chapter 2.3.1). However, when these pH 7.4 lipid extracts were dispersed as MLVs in a pH 5.5 buffer, figure 3-3 showed that there was a significant ~10 mV positive increase in the zeta potentials compared to the pH 7.4 buffer ($U_{1,2}<U_{crit}$, $P < 0.05$). This relatively high zeta potential positive shift of ~10mV was attributable to greater neutralisation of membrane PG and CL by the change in the charge state of L-PG from partly zwitterionic and cationic at pH 7.4 to fully cationic at pH 5.5 (Tocanne *et al.* 1974b). Figure 3-3 further supported this presumed change in L-PG charge state in the different pH environments, where the MLVs of the pH 5.5 lipid extracts in a pH 7.4 buffer gave highly negative zeta potential results however in a pH 5.5 buffer gave cationic zeta potential results for MSSA 476 and MRSA G32 and H66. The cationicity of these latter MLVs in a pH 5.5 environment was presumably due to cationic L-PG being >50% total phospholipid in these strains (chapter 2.3.1).

The mean MLV zeta potential result of the MRSA H64 pH 5.5 lipid extract gave a slightly negative result (~ -3 mV) in the pH 5.5 buffer as shown in figure 3-3, however this was not

unexpected as this extract contained ~45% L-PG as total phospholipid as shown in chapter 2.3.1 which presumably was not enough L-PG to form a positively charged outer leaflet in a pH 5.5 buffer. However, a zeta potential result of ~ -3 mV would suggest the bilayer surface of the MLVs were effectively neutral.

Figure 3-3 also showed very little change in zeta potential results of the MLVs of pH 5.5 lipid extracts of MRSA G33 and G35, compared to their pH 7.4 extracts. However, as shown in chapter 2.3.1, the mol% L-PG content of these pH 5.5 extracts were ~30% total phospholipid and therefore this level of L-PG expression was similar to when the bacteria were grown at pH 7.4, hence the zeta potentials of these pH 5.5 extracts were not significantly different from those of the pH 7.4 extracts in both pH buffers ($U_{1,2}>U_{crit}$, $P > 0.05$).

3.3.2 *S. aureus* polar lipid extract monolayer study

Extraction of the polar lipids from *S. aureus* and comparison of their surfaces properties as monolayers at the air–water interface was associated with several problems. Firstly, the Bligh and Dyer extraction method, although specific for polar lipids, gives no guarantee of complete purity and therefore it was unknown how pure the lipid extracts actually were. Secondly, the molecular weights of the phospholipid mixtures were unknown as both, counter ions of various molecular weights maybe have been associated with the lipids and the fatty acid chain lengths may have varied widely between the *S. aureus* strains used (Durham & Kloos 1978, White & Frerman 1968). Lastly, the presence of amphiphilic contaminants could have interfered with the lateral compressional behaviour of the lipid monolayers which may have resulted in artefacts being present in the surface area-pressure isotherms. To try and minimise these issues, the lipid extracts were grouped into pH 5.5 and 7.4 grown bacteria separately and no direct comparisons were made between the two pH growth conditions from which the lipids were extracted.

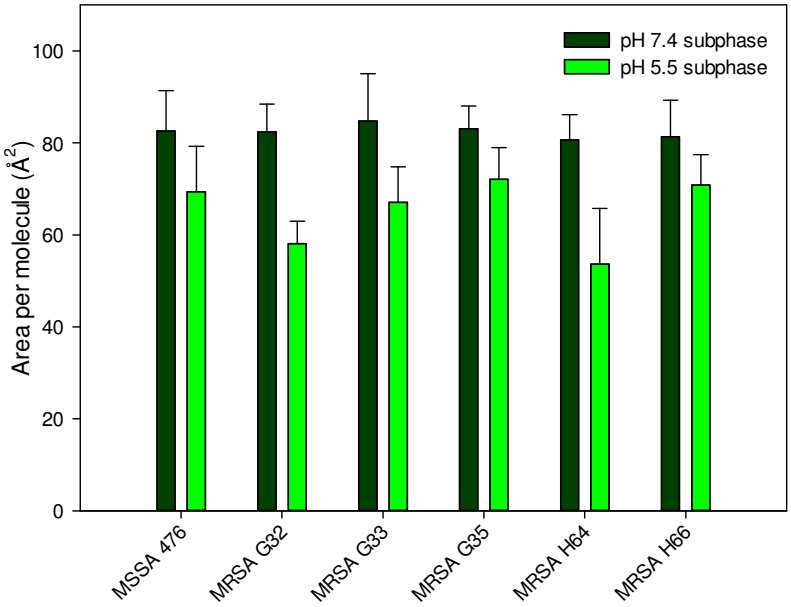

Figure 3-4 Extrapolated limiting area per molecule data from all *S. aureus* pH 7.4 lipid extracts on pH 5.5 and 7.4 subphases.

The pH 7.4 lipid extracts of all six *S. aureus* strains possessed ~30 mol% L-PG content as shown in chapter 2.3.1 with the rest of the phospholipid content being made up of CL (~5 mol%) and PG. In all the pH 7.4 lipid extracts, figure 3-4 showed a significant reduction in mean limiting area per molecule of the monolayers by ~10-27 Å^2 in the liquid condensed phase when reducing the subphase pH from 7.4 to 5.5 ($U_{1,2}<U_{crit}$, $P < 0.05$). This reduction in limiting area per molecule at pH 5.5 was likely to be the result of increased cationic L-PG at this pH, causing greater ion-pair formation between L-PG and PG or CL, thus bringing the lipids into closer proximity of each other, i.e. the monolayers became more laterally condensed at pH 5.5 (Sung *et al.* 2010).

To assess if the greater probability of lipid ion-pairs formed between L-PG and PG or CL at pH 5.5 compared to pH 7.4 also increased the rigidity of the monolayer, the compressional moduli of the pH 7.4 lipid extracts were calculated and compared on both pH subphases.

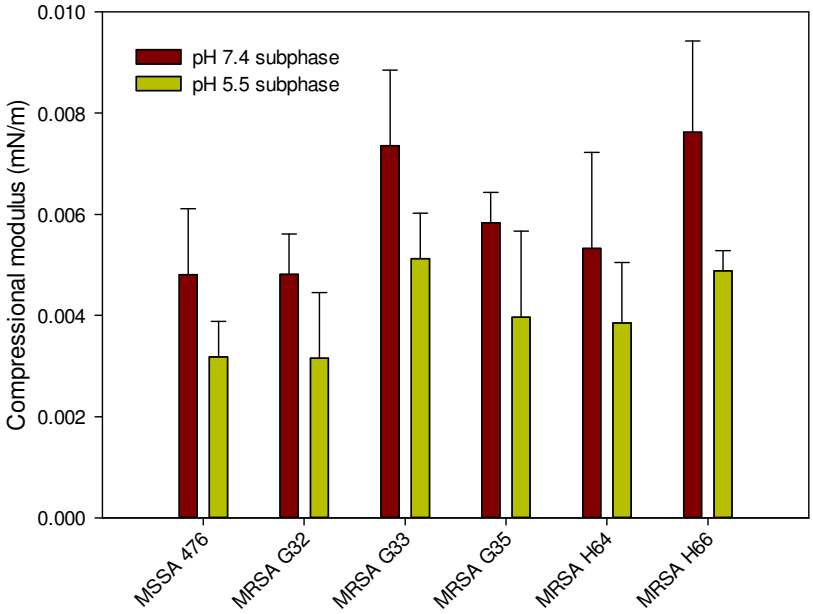

Figure 3-5 Compressional moduli of all *S. aureus* lipid extracts of bacteria grown at pH 7.4 on pH 5.5 and pH 7.4 subphases.

All of the pH 7.4 lipid extracts on a pH 5.5 subphase showed lower compressional moduli compared to the pH 7.4 subphase (figure 3-5), which indicated that the monolayers on the pH 5.5 subphase were significantly less elastic than on the pH 7.4 subphase ($U_{1,2}<U_{crit}$, $P < 0.05$). This significant reduction in monolayer elasticity at pH 5.5 suggested that the presumed increase in lipid ion-pairs at this pH, created more rigid and less elastic monolayers which were more resistant to lateral compression than the same monolayers on a pH 7.4 subphase (Gaines 1966).

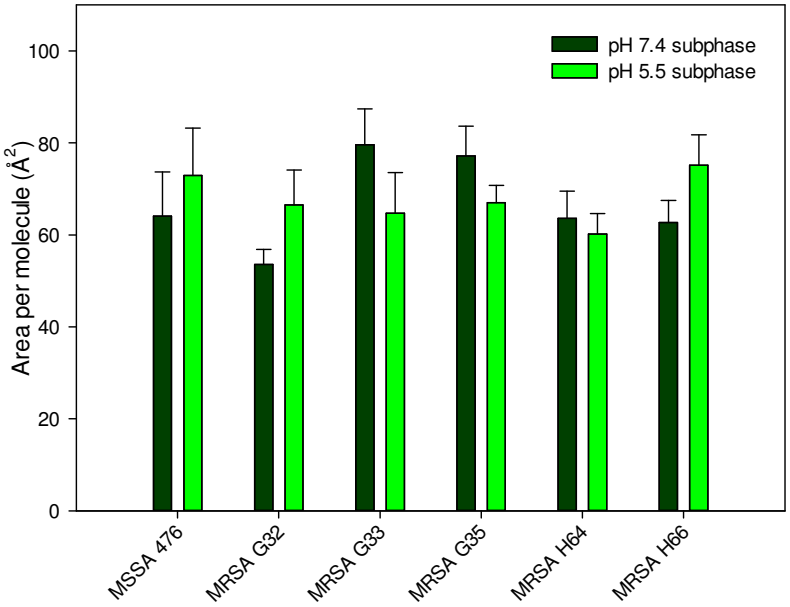

Figure 3-6 Extrapolated limiting area per molecule data from all *S. aureus* pH 5.5 lipid extracts on pH 5.5 and 7.4 subphases.

In contrast to the pH 7.4 lipid extracts, the pH 5.5 lipid extracts showed an increase in limiting area per molecule in *S. aureus* strains MSSA 476 and MRSA G32 and H66 on a pH 5.5 subphase compared to a pH 7.4 subphase (figure 3-6). This increase in limiting area per molecule of these lipid extracts on a pH 5.5 subphase proposed that the substantial L-PG content of these lipid extracts (~50 mol%, chapter 2.3.1), which was presumably in a cationic state, resulted in greater mean limiting areas per molecule compared to a pH 7.4 subphase. Such a result was not unexpected, as the assumed fully cationic L-PG was in excess in these lipid extracts thus lipid-lipid electrostatic charge repulsion between non-ion-paired L-PG molecules was likely to have been high resulting in larger limiting areas per molecule (Gaines 1966).

The mean area per molecule of the MRSA H64 pH 5.5 lipid extract, was similar for both pH 5.5 and 7.4 subphases as shown in figure 3-6. This result was also not unexpected as MRSA H64 grown at pH 5.5 was found to contain ~45 mol% L-PG (chapter 2.3.1) and therefore the presence of excess cationic L-PG in this lipid extract on a pH 5.5 subphase would have been unlikely.

The limiting areas per molecule for the pH 5.5 lipid extracts from MRSA G33 and G35 on both pH subphases (figure 3-6), were similar to those found for the pH 7.4 lipid extracts on both pH subphases (figure 3-4). However, this was to be expected as both MRSA G33 and G35 upregulate their L-PG content by negligible amounts when present in a pH 5.5 environment compared to a pH 7.4 environment (chapter 2.3.1).

Due to the inconsistent results of MRSA G33 and G35, a significant difference between all the strains pH 5.5 lipid extracts limiting areas per molecule on a pH 5.5 subphase compared to a pH 7.4 subphase was not found ($U_{1,2}>U_{crit}$, $P > 0.05$). However, on omission of these strains a significant difference was present ($U_{1,2}<U_{crit}$, $P < 0.05$). Therefore with the exception of strains MRSA G33 and G35, it would appear that the presence of >50 mol% cationic L-PG in a monolayer with PG and CL results in an increase in lipid area per molecule.

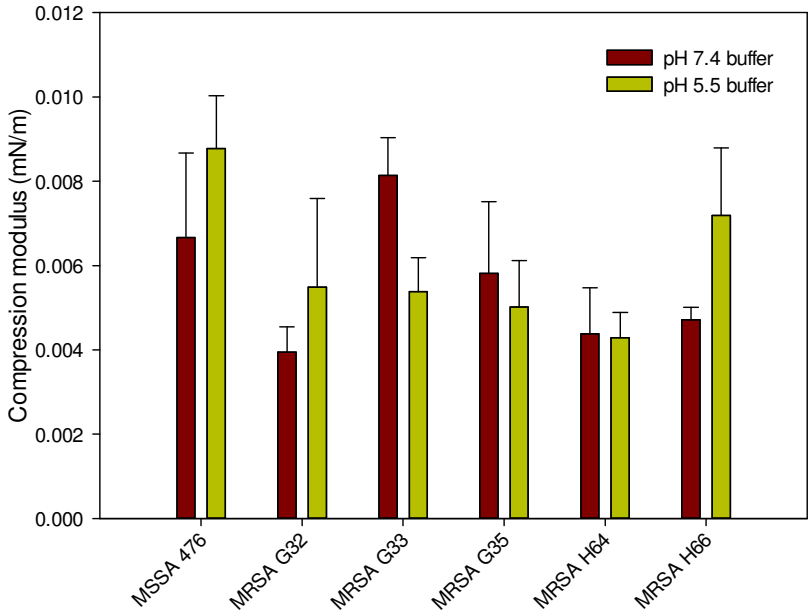

Figure 3-7 Compressional moduli of *S. aureus* lipid extracts from bacteria grown at pH 5.5 on pH 5.5 and 7.4 subphases.

The compressional moduli shown in figure 3-7 of the pH 5.5 lipid extracts of MSSA 476 and MRSA G32 and H66 showed that there was a significant increase in monolayer elasticity when the lipids were deposited on a pH 5.5 subphase compared to a pH 7.4 subphase ($U_{1,2}<U_{crit}$, $P < 0.05$). This result was possibly due to the lateral electrostatic repulsion between headgroups of the excess cationic L-PG in these lipid extracts, therefore making the monolayers more elastic and less resistant to lateral compression (Gaines 1966). The monolayer of the pH 5.5 lipid

extract from MRSA H64 showed a reduction in elasticity on a pH 5.5 subphase compared to a pH 7.4 subphase (figure 3-7), however this appeared to be the result of the L-PG content of this lipid extract being ~45 mol% (chapter 2.3.1), therefore excess cationic L-PG in this monolayer would have been negligible. The elasticity of the pH 5.5 lipid extracts from MRSA G33 and G35 were analogous to extracts from the bacteria grown at pH 7.4 on both pH subphases (figures 3-5 and 7), however as explained earlier, this is expected due to these strains expressing similar levels of phospholipids in both pH 5.5 and 7.4 growth environments (chapter 2.3.1).

3.3.3 Neutron diffraction of *S. aureus* lipid extracts

To prepare the MSSA 476 lipid extracts of the bacteria grown at pH 5.5 and 7.4 for neutron diffraction, bilayer stacks of the lipids were formed which acted as diffraction gratings as described in chapter 1.7.1. Normally in neutron diffraction, to hydrate bilayer stacks the humidity of their surrounding environment is increased which increases adjacent bilayer separation and neutron diffraction peak intensity (Darkes & Bradshaw 2000). In particular, the increase in adjacent bilayer separation results in a greater lamellar d-spacing (Ψ) and due to $\Psi \propto \theta$ the neutron diffraction peak in the neutron diffraction profile moves to higher angles (Darkes & Bradshaw 2000). However, as shown in figure 3-8, the first order of neutron diffraction of the pH 7.4 lipid extract did not consistently move to higher angles with increasing humidity but rather fluctuated unpredictably in position and in intensity with increasing humidity. This anomalous swelling behaviour of the pH 7.4 lipid extract bilayers was also observed in the pH 5.5 lipid extract bilayers and in all orders of neutron diffraction of each lipid extract. The result of this anomalous bilayer swelling in both pH lipid extracts, was bilayer d-spacing results which were not well correlated with increasing humidity (figures 3-9a and b), where normally a directly proportional relationship is observed between d-spacing and increases in humidity (Darkes & Bradshaw 2000).

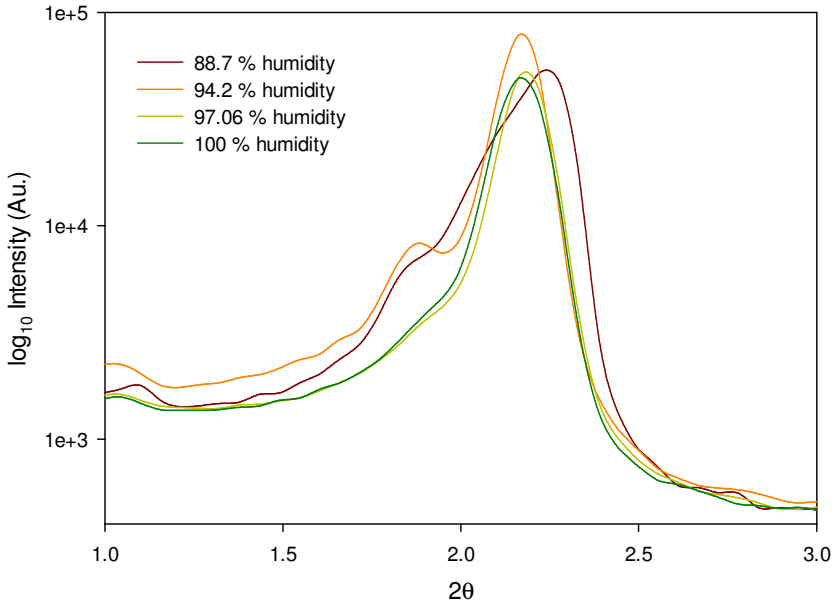

Figure 3-8 First orders of neutron diffraction of the pH 7.4 lipid extract from MSSA 476 with increasing humidity; contrast = D_2O.

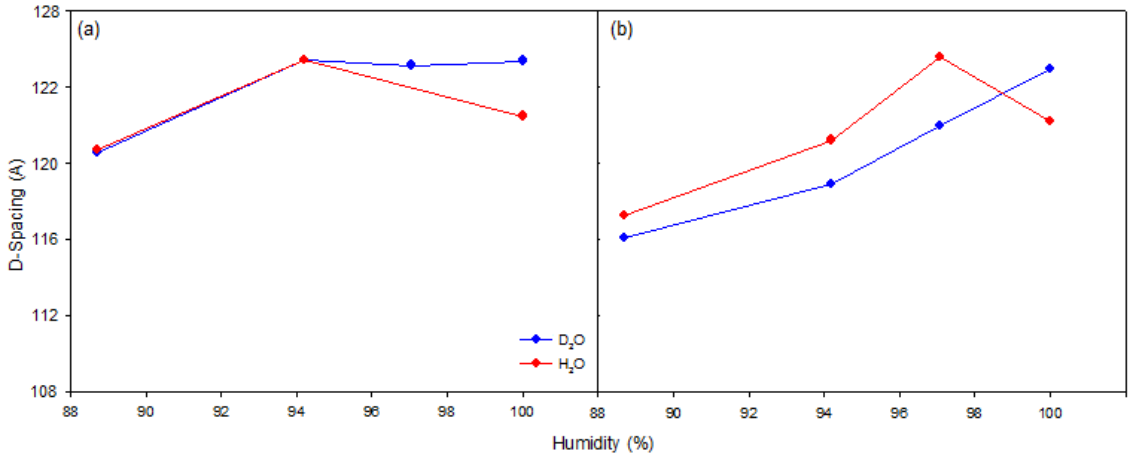

Figure 3-9 D-spacing profiles of the lipid extracts from MSSA 476 grown at (a) pH 7.4 and (b) pH 5.5, with increasing humidity in both H_2O and D_2O contrasts.

The anomalous bilayer swelling profiles in figures 3-9a and b were attributed to the possible breakdown of L-PG under mild aqueous conditions. Such L-PG breakdown has been reported previously in X-ray diffraction studies where the ester group linking lysine to the terminal glycerol hydroxyl group of PG was shown to be labile under mild aqueous conditions (Danner *et al.* 2008). With respect to the actual d-spacing values of both pH lipid extracts (figures 3-9a and b), these were relatively high which was expected due to the lipids in the extracts being charged and therefore electrostatic charge repulsion between adjacent bilayer surfaces would have been high, creating large water layers between the adjacent bilayers (Pozo Navas *et al.* 2005).

Although the first order of neutron diffraction shown in figure 3-8 fluctuated unpredictably with respect to diffraction angle and increasing humidity, at low humidity a small shoulder was observed at ~0.93°. This shoulder was also found in all orders of neutron diffraction exclusively in the pH 7.4 lipid extract which suggested a second lamellar phase may have been present. However, at greater humidities this second lamellar phase was not observed and may possibly have been masked by the high intensity signal of the predominant lamellar phase.

In order to examine the bilayer structure along the bilayer normal, the SLD profiles of the bilayers from the pH 5.5 and 7.4 lipid extracts were constructed for samples at 100% humidity only, as this humidity gives the greatest structural details of the bilayer (Darkes & Bradshaw 2000). The resolution of the SLD profiles was highly dependent on the number of orders of diffraction collected, and in both lipid extracts a maximum of three diffraction orders were detected therefore the SLD profiles were of low resolution. However, the low resolution of the SLD profiles was not an unusual find as the bilayers existed in the L_α phase which contains lipids with high mobility and therefore a large amount of coherent scattering is lost due to the erratic scattering of the highly mobile lipids (Pabst *et al.* 2010).

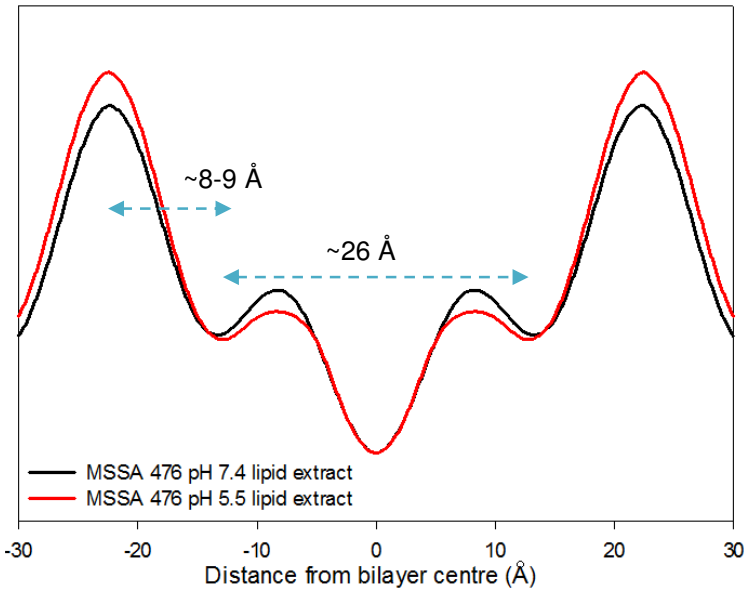

Figure 3-10 SLD profiles of MSSA 476 lipid extracts from bacteria grown at pH 5.5 and 7.4.

The SLD profiles of both pH 5.5 and 7.4 lipid extracts (figure 3-10) show that both bilayers were of comparable thickness. The hydrocarbon regions of both bilayers had a thickness of ~26 Å which indicated the branched C_{15} hydrocarbon chains of the lipids in both lipid extracts were in the L_α phase (White & Frerman 1968). The SLD of the hydrocarbon regions of both pH lipid

extracts were similar across the whole span of the hydrocarbon core and suggested both bilayers existed with a similar lateral density. The thicknesses of the headgroup regions of both lipid extract bilayers were ~8-9 Å (figure 3-10) and was consistent with a mean headgroup thickness consisting of L-PG (10-12 Å), PG (6-7 Å) and CL (~7-8 Å) (Armen *et al.* 1998, Pascher *et al.* 1987) in both bilayers. This headgroup thickness was also consistent with previous findings of L-PG existing in a loop structure due to an internal ionic bond between its protonated ε or α-amine and its phosphate group (El Mashak & Tocanne 1979). The SLD of the pH 5.5 lipid extract headgroup region at ~22 Å from the bilayer centre was marginally greater in intensity compared to the pH 7.4 lipid extract headgroup region (figure 3-10). The higher intensity SLD of the headgroup region in the pH 5.5 lipid extract may have been due to the greater content of L-PG in this lipid extract (chapter 2.3.1), which can form more ion-pairs with PG and CL, hence increasing the mass density and the SLD of this headgroup region.

3.4 Discussion

The lipid extracts from all the *S. aureus* strains when grown at pH 7.4 contained ~30% L-PG according to the ^{31}P NMR results presented in chapter 2.3.1. Monolayers formed from these pH 7.4 extracts on a pH 7.4 subphase showed greater elasticity compared to that of the same lipids on a pH 5.5 subphase. This reduction in compressibility of the pH 7.4 lipid extract on a pH 5.5 subphase suggested that a change in the charge state of L-PG had occurred from partly zwitterionic and cationic at pH 7.4 to close to fully cationic on the pH 5.5 subphase, presumably due to full protonation of the α-amine of L-PG which has a pKa of ~6-7 (Tocanne *et al.* 1974c). This putative increase in cationic L-PG at pH 5.5 appeared to result in the formation of more ion-pairs between L-PG and PG or CL in the pH 7.4 lipid extract which caused the monolayer to become laterally more dense hence reducing its elasticity (Sung *et al.* 2010). With respect to the plasma membrane of *S. aureus*, these results suggest the membrane of the bacterium would become more rigid and laterally dense when the bacterium is exposed to a low pH environment which presumably would hinder the diffusion of protons from the external growth environment into the bacterial cytoplasm.

In contrast, the pH 5.5 lipid extracts from *S. aureus* gave monolayers which were more elastic in strains MSSA 476 and MRSA G32 and H66 on a pH 5.5 subphase compared to a pH 7.4 subphase. However, these lipid extracts had an L-PG content of >50% total phospholipid (chapter 2.3.1) and therefore the monolayers on a pH 5.5 subphase would have had an excess of cationic L-PG. This excess cationic L-PG on a pH 5.5 subphase was shown to make the monolayers more compressible due to the electrostatic charge repulsion between excess cationic L-PG headgroups (Gaines 1966). However, although a minor reduction in monolayer lateral density was found with these extracts at pH 5.5, the MLVs of these extracts in a pH 5.5 buffer gave positively charged zeta potentials which suggested the high concentration of cationic L-PG in these extracts changed the surface charge of the MLVs to positive at pH 5.5. In relation to the *S. aureus* plasma membrane in a pH 5.5 environment, these results insinuate that majority of the plasma membrane of *S. aureus* exists as a laterally dense structure due to the high concentration of L-PG present in it at pH 5.5 (~50 mol%, chapter 2.3.1). However the bacterium also appears to synthesise a small excess of L-PG to cause its plasma membrane outer leaflet surface to become cationically charged. This excess of L-PG in the plasma membrane presumably forms a charge barrier, therefore reducing the affinity of protons towards

the membrane's outer leaflet surface. To try and correlate these natural lipid extract MLV zeta potential results with the actual plasma membranes of live *S. aureus*, protoplasts were also examined for their zeta potential results in both pH 5.5 and 7.4 environments. A significant reduction between zeta potential results of protoplasts in a pH 5.5 environment compared to a pH 7.4 environment were found in MSSA 476 and MRSA G32, H64 and H66. This reduction in zeta potential at pH 5.5 suggested that the bacteria may be upregulating their plasma membrane L-PG content in response to the low pH environment which was dampening the headgroup charges of PG and CL in the plasma membrane outer leaflet. Therefore the protoplast and MLV zeta potential data both supported the assumption that L-PG may attenuate the anionic surface charge presentation of the outer leaflet of the plasma membrane of *S. aureus* in response to a mild acidic pH environment (Gould & Lennarz 1970).

The neutron diffraction SLD profiles gave detailed information into the molecular properties of the bilayers formed from MSSA 476 pH 5.5 and 7.4 lipid extracts. The pH 5.5 lipid extract, in particular, supported the presence of ion-pairs existing between L-PG and PG or CL due to an increase in headgroup SLD. However, the principal finding from the neutron diffraction was from the bilayer swelling profiles of both pH lipid extracts. These swelling profiles showed the bilayers to have erratic swelling behaviour with increasing humidity and strongly suggested that L-PG may have been hydrolysing back to lysine and PG at high humidity (Danner *et al.* 2008). The presumed breakdown of L-PG and the resulting change in bilayer surface charge presentation most likely interfered with the electrostatic and Van der Waals forces which govern adjacent bilayer separation (Pozo Navas *et al.* 2005, Lis *et al.* 1982), thus possibly causing the erratic d-spacing profiles. This result ultimately reduces the confidence in all the results obtained with the natural lipid extracts, as L-PG could have been breaking down in all samples exposed to an aqueous environment.

3.5 Conclusion

The results presented in this chapter suggest that the role of L-PG in the adaptation of *S. aureus* to a mild pH environment is to make the plasma membrane more laterally dense and change the membrane outer leaflet surface charge to positive. However, it is difficult to substantiate these roles of L-PG due to the unknown purity of the lipid extracts and the possibility L-PG may have been breaking down once exposed to an aqueous environment (Danner *et al.* 2008). Therefore the results from this chapter require validation using synthetic lipid models in similar assays. However, due to the possibility of L-PG being labile under mild aqueous conditions a chemically stable biomimetic analogue of L-PG would be required in order to substitute L-PG in subsequent experiments. Therefore this work will now focus on the synthesis of biomimetic chemically stable L-PG analogues and then use these analogues in biophysical experiments to characterise the membrane properties of *S. aureus* grown in mildly acidic conditions.

Chapter 4

Synthesis of novel lysyl-aza-phosphatidylglycerol analogues

4.1 Introduction

The breakdown of lysyl-phosphatidylglycerol (L-PG) under mild aqueous conditions has previously been documented as shown in figure 4-1 (Gould & Lennarz 1970, Danner *et al.* 2008). L-PG can breakdown into numerous products when exposed to mild aqueous conditions, such as lysine, phosphatidylglycerol (PG), lyso-PG and lyso-L-PG (figure 4–1). However, the major breakdown products of L-PG are to lysine and PG, even under manufacturer recommended storage conditions of -20 ℃ as shown in figure 4-1 (Avanti Polar Lipids Inc. 2013a).

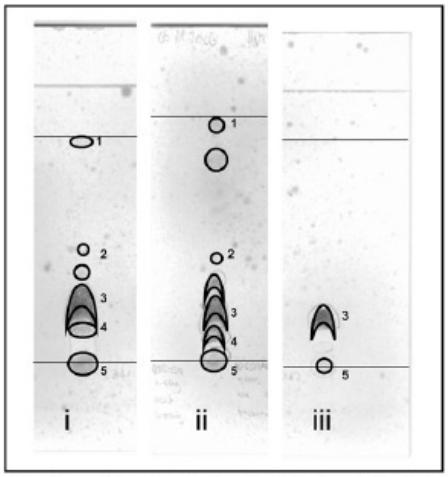

[1] free fatty acids, [2] DPPG, [3] lysyl-DPPG, [4] lyso-lipid, [5] lysine

Detection of degradation products of lysyl-DPPG before (*i*) and after (*ii*) x-ray experiments at pH 5.0 compared with lysyl-DPPG standard (*iii*); detection with molybdenic acid.

Figure 4-1 TLC plate adapted from Danner *et al.* (2008) showing the breakdown of L-PG (Danner *et al.* 2008).

L-PG readily hydrolyses to lysine and PG under mild aqueous conditions because the ester formed between the distal hydroxyl group of PG and the carboxylic acid group of lysine is labile (Danner *et al.* 2008) (figure 4-2). The reason this ester is so labile is because firstly, the protonated lysyl-α-NH_2 of L-PG exerts a negative electron withdrawing inductive effect on the lysyl-ester group in L-PG thus increasing its electrophilicity making it more labile to nucleophilic attack (Hentzen *et al.* 1972). Secondly, both the protonated (and non-protonated) lysyl-α-NH_2

and glycerol 2-OH of L-PG can form intramolecular hydrogen bonds to the lysyl-ester group which could also increase the electrophilicity of the ester group (figure 4-2) (Bruice & Fife 1962).

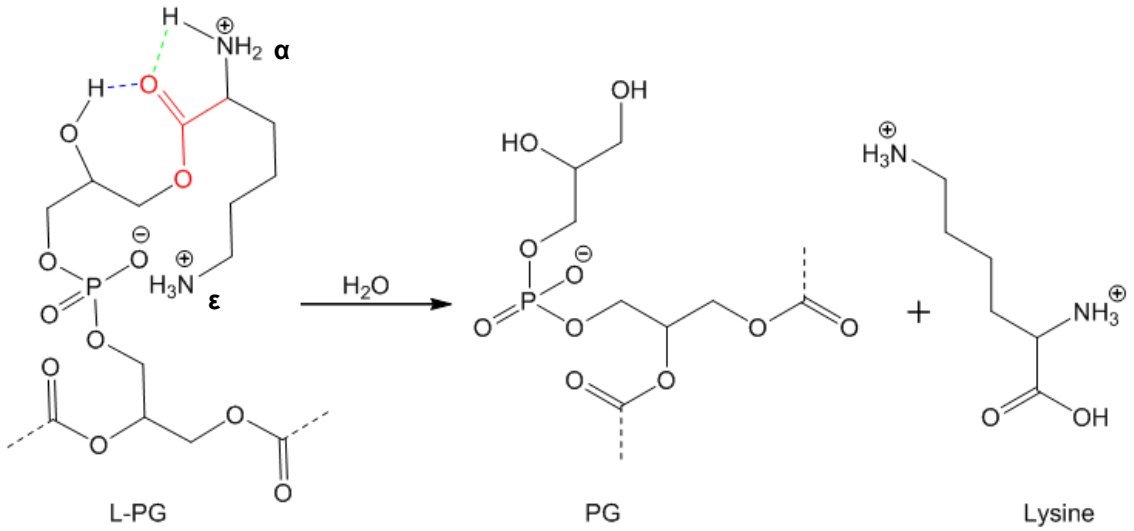

Figure 4-2 Schematic to show the breakdown of L-PG; labile ester (red) and internal hydrogen bonds (blue and green)

The highly labile ester of L-PG makes it difficult to study in biophysical experiments and has resulted in the mechanism of action of the lipid in the plasma membrane of *Staphyloccocus aureus* to be theoretical at best. Therefore, to overcome these problems associated with the lability of L-PG and study the function and behaviour of the lipid *in vitro*, non-labile analogues of L-PG were synthesised. The approach taken in this work was to substitute the labile ester of L-PG for a group which retained majority of the structural features of L-PG. Therefore an amide group was selected to substitute the labile ester in L-PG as an amide is less susceptible to hydrolysis due to the reduced electrophilicity of its carbonyl-carbon and the amine product of its hydrolysis is a poor leaving group (Yoshioka, Stella 2000).

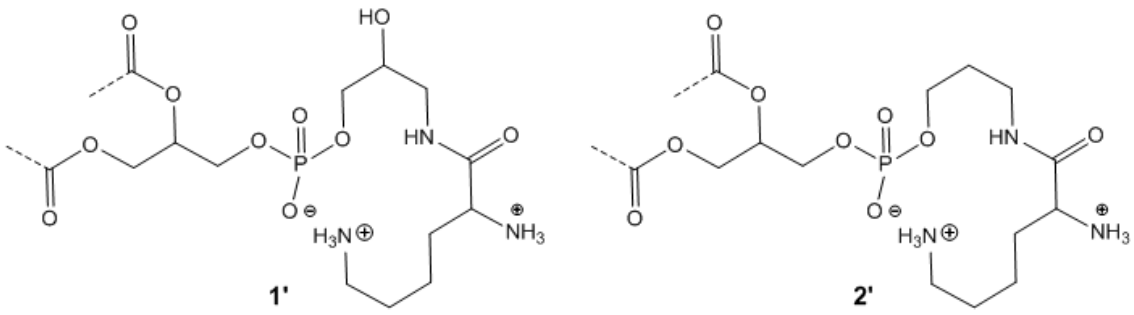

Figure 4-3 Structures of L-PG analogues containing amide groups; 3-*N*-lysyl-1-*O*-(phosphatidyl)-3-aza-3-deoxy-*rac*-glycerol **1'** and 3-*N*-Lysyl-1-*O*-(phosphatidyl)-3-aza-2,3-dideoxyglycerol **2'**.

The substitution of an amide group in L-PG to give 3-*N*-lysyl-1'-*O*-(*rac*-phosphatidyl)-3-aza-3-deoxy-*rac*-glycerol **1'** (figure 4-3), retains majority of the structural characteristics of L-PG. However one drawback of this substitution is the bond angle at the amide nitrogen of **1'** increases to 120° compared to 109° in the ester of native L-PG, due to the sp^2 hybridisation of the nitrogen atom (Kotz *et al.* 2009). The increase in bond angle of the amide in **1'** over the natural L-PG could impose conformational and packing constraints on the lipid headgroup in biophysical assays and must be taken into account when handling *in vitro* results relating to **1'**.

In order to synthesise **1'** the headgroup region of the lipid requires a 3-aminopropane-1,2-diol molecule to link the lysine and phosphate groups together. However, the use of 3-aminopropane-1,2-diol requires a secondary hydroxyl specific protecting group to prevent phosphate and lysyl migration products during synthesis. Although secondary hydroxyl protection is possible, it would require a more complex synthesis and could hinder progression to biophysical assays. Therefore to overcome this problem, an analogue lacking the 2-OH of the natural glycerol unit (3-*N*-Lysyl-1-*O*-(phosphatidyl)-3-aza-2,3-dideoxyglycerol, **2'**) was also synthesised as shown in figure 4-3. The linking molecule between lysine and phosphate in **2'** is a 3-aminopropan-1-ol molecule which lacks a secondary hydroxyl group and therefore no phosphate or lysyl migration can occur.

Previous studies of *S. aureus* lipid extracts showed the most abundant phospholipid fatty acid in *S. aureus* plasma membranes was a branched methyl (anteiso) C_{15} fatty acid (~35-40%) (Durham & Kloos 1978). The presence of phospholipids containing branched C_{15} fatty acids in the plasma membrane of *S. aureus* suggested that the membrane was in the L_α phase (Kaneda 1991). Although C_{15} branched methyl analogues of **1'** and **2'** are more biomimetic with respect to studying L-PG in *S. aureus*, it does not allow for sufficient biophysical assessment of the lipid headgroup behaviour. This is because lipidic headgroup interactions can be been masked by Van der Waals and steric interactions between the branched methyl groups of neighbouring lipid fatty acid chains (Rand 1981). As an alternative to branched fatty acids, unsaturated fatty acids could have been used for **1'** and **2'**, however these fatty acids can also suffer with the same interfering interactions as branched fatty acids (Rand 1981). Therefore to try and minimise the interactions caused by the fatty acid chains, saturated palmitoyl fatty acids were selected as they have a low lateral cross-sectional area and form highly ordered bilayers at

ambient temperatures (Silvius 1982). The use of palmitoyl fatty acids also has the added advantage of forming $L_{\beta'}$ phase bilayers at temperatures <35 °C, which should give higher resolution data in neutron experiments as bilayers formed from these lipids tend to have lower kinetic mobility (Ranck *et al.* 1977).

The synthesis of 1,2-*O*-dipalmitoyl versions of **1'** and **2'** still required a control in order to substantiate data obtained from the lipids above the main phase transition temperature (T_m). Therefore, a 1-*O*-palmitoyl-2-*O*-oleoyl analogue of **2'** (T_m < 2 °C) was also synthesized, and used as a comparator for the 1,2-*O*-dipalmitoyl versions of the lipids above T_m.

The synthesis of native L-PG has already been performed by various methods however they all follow a similar synthetic route which will now be discussed in relation to the synthesis of **1'** and **2'** (Tocanne *et al.* 1974a, Molotkov & Bergelso 1968, Bonsen *et al.* 1967). Synthesis of the headgroup of L-PG starts with 2,3-isopropylidene-1-*O*-benzylglycerol deprotected under mild acidic conditions to yield 1-*O*-benzylglycerol (figure 4-4, step i) (Bonsen *et al.* 1967). The 1-*O*-benzylglycerol is then reacted with 4-toluenesulfonyl chloride at the primary hydroxyl of the 1-*O*-benzylglycerol to give 1-*O*-benzyl-3-*p*-toluenesulfonylglycerol (figure 4-4, step ii) (Bonsen *et al.* 1967). The tosylation of 1-*O*-benzylglycerol is unselective for both the primary and secondary hydroxyl groups of 1-*O*-benzylglycerol and can also undergo hydroxyl migration as well (figure 4-4) (Zagorevskii & Kirsanova 1970). This can then yield 1-*O*-benzyl-2-*p*-toluenesulfonylglycerol and 1-*O*-benzyl-2,3-*p*-bis-toluenesulfonylglycerol as contamination products, thus lowering the yield of the required 1-*O*-benzyl-3-*p*-toluenesulfonylglycerol (figure 4-4). Therefore the tosylation of the primary hydroxyl of 1-*O*-benzylglycerol can result in substantial product wastage and lengthy purification before successive steps can be followed for the rest of the headgroup synthesis.

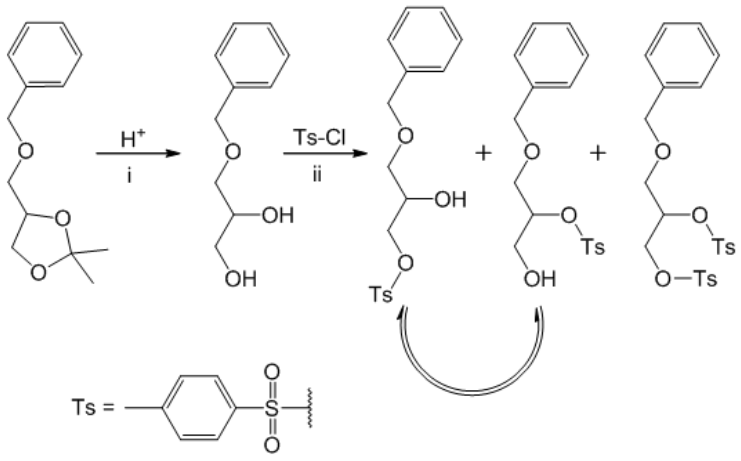

Figure 4-4 Adapted schematic from Bonsen, P., (1967) to show the synthesis of 1-*O*-benzyl-*p*-toluenesulfonylglycerol (Bonsen *et al.* 1967) and also the possible 1-*O*-benzyl-2-*p*-toluenesulfonylglycerol and 1-*O*-benzyl-2,3-*p*-di-toluenesulfonylglycerol contaminants after tosylation of 1-*O*-benzylglycerol.

Subsequently, the 1-*O*-benzyl-3-*p*-toluenesulfonylglycerol is tert-butyl-ether protected at the glycerol 2-hydroxyl using liquid isobutene and sulphuric acid, and then converted to the photolabile 1-*O*-benzyl-2-*O*-tert-butyl-glycerol 3-iodohydrin in the presence of sodium iodide (figure 4-5, steps i and ii) (Tocanne *et al.* 1974a, Bonsen *et al.* 1967). The formed 1-*O*-benzyl-2-*O*-tert-butyl-glycerol 3-iodohydrin can only be handled in dark conditions, due to the risk of iodide decomposition (Srivastava & Jain 2007), and thus is difficult to purify by chromatographic fractionation as all fractionation steps need to be conducted in the absence of light. Next, 1-*O*-benzyl-2-*O*-tert-butyl-glycerol 3-iodohydrin undergoes S_N2 displacement by the carboxylic acid anion of *N,N'*-di-boc-lysine (figure 4-5, step iii). The iodide group serves as a useful ester generating agent as iodide is easily displaced by strong nucleophiles (Hoffman 2004). For the synthesis of the headgroups of **1'** and **2'** this type of chemistry, although compatible, was not utlised due to the substantial number of synthetic and purification steps that would have been required and the careful handling requirements necessary for the preparation of 1-*O*-benzyl-2-*O*-tert-butyl-glycerol 3-iodohydrin. Therefore to synthesise the headgroup of **1'** and **2'** peptide chemistry can be utlised, where an amide is first formed between *N,N'*-di-boc-lysine and 3-aminopropane-1,2-diol or 3-aminopropane-1-ol using carbodiimide chemistry (Ulrich 2008). Modifications can then made to the hydroxyl groups of the headgroup of **1'**, to ensure the secondary hydroxyl group is sufficiently protected using a tetrahydropyranyl acetal before coupling with phosphate.

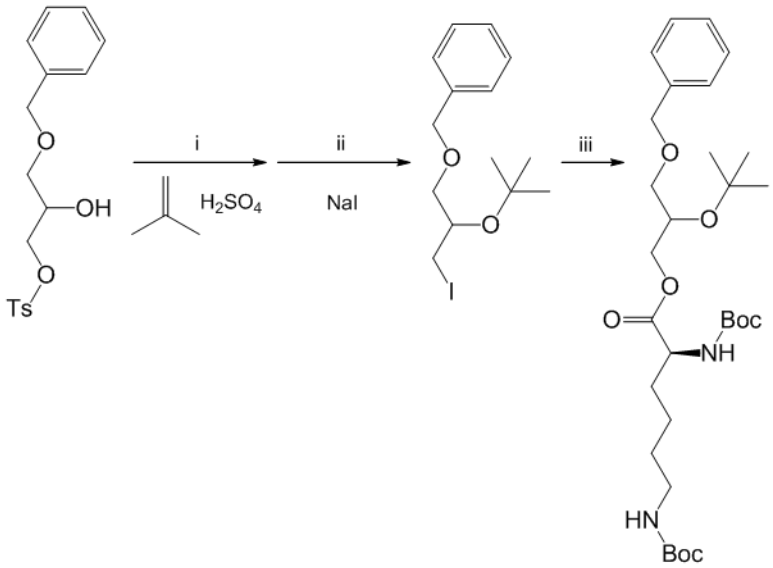

Figure 4-5 Adapted reaction scheme from Bonsen, P., (1967) to show the synthesis of 1-*O*-benzyl-2-*O*-tert-butyl-glycerol 3-iodohydrin (steps i & ii) and then the formation of 1-*O*-benzyl-2-*O*-*t*-butyl-3-*N,N'*-di-boc-lysylglycerol (step iii) (Bonsen *et al.* 1967).

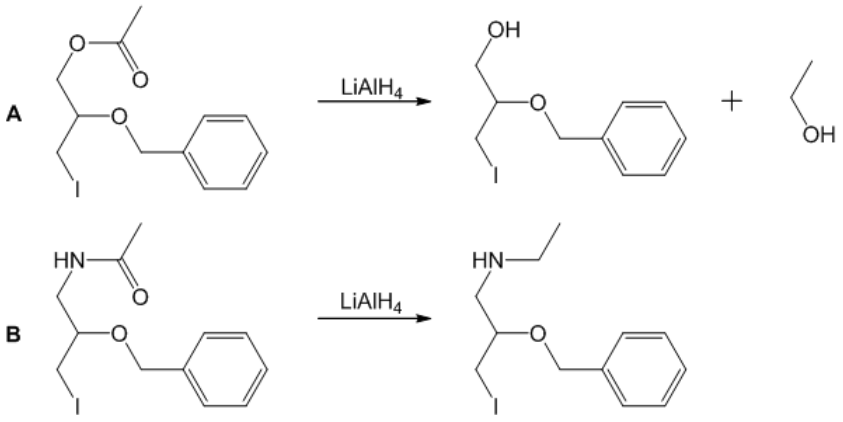

Figure 4-6 Reaction of $LiAlH_4$ with an (A) ester and an (B) amide.

Molotkov *et al.* (1968) suggested an alternative synthesis of the L-PG headgroup, where glycerol was acetate ester protected at the 1-hydroxyl position, benzyl ether protected at the 2-hydroxyl position and iodide substituted at the 3-hydroxyl position, to form 2-(benzyloxy)-3-iodopropyl acetate (figure 4-6A) (Molotkov & Bergelso 1968). The 2-(benzyloxy)-3-iodopropyl acetate was then reacted with $LiAlH_4$ to reduce the 1-acetate ester to a primary alcohol (figure 4-6A), leaving a primary alcohol to react with *N,N'*-di-boc-lysine in order to form an ester. This L-PG headgroup synthesis strategy would have been unsuitable for the preparation of **1'** and **2'** as the amide would reduce to a secondary amine (figure 4-6B) (Fox & Whitesell 1997).

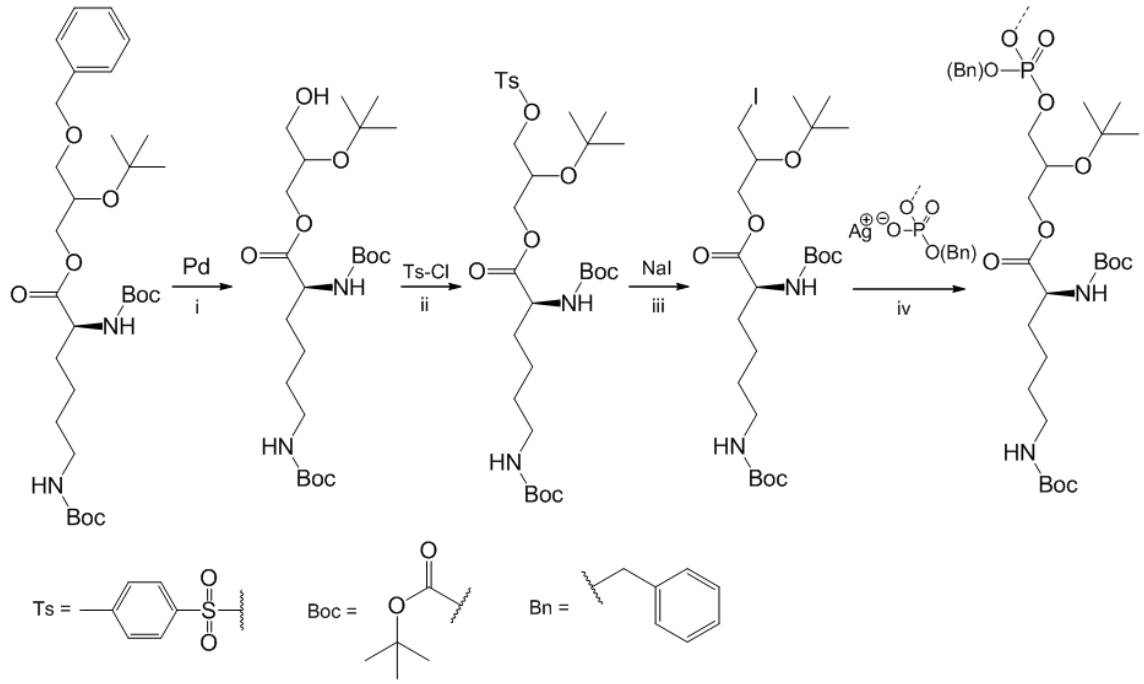

Figure 4-7 Adapted reaction scheme from Bonsen, P., (1967) to show the synthesis of 2-*O*-*t*-butyl-3-*N,N'*-di-boc-lysylglycerol (step i), 1-*O*-*p*-toluenesulfonyl-2-*O*-*t*-butyl-3-*N,N'*-di-boc-lysylglycerol (step ii), 3-*N,N'*-di-boc-lysyl-2-*O*-*t*-butylglycerol 1-Iodohydrin (step iii) and fully protected L-PG (step iv) (Bonsen *et al.* 1967).

Continuation of the synthetic pathway in figure 4-5 showed that after displacement of iodide from 1-*O*-benzyl-2-*O*-tert-butyl-glycerol 3-iodohydrin by *N,N'*-di-boc-lysine the molecule underwent benzyl deprotection using a palladium catalyst, then tosylation and finally iodohydrin formation at the glycerol 1-hydroxyl group (figure 4-7, step i-ii). This iodohydrin product then underwent S_N2 substitution at the CH_2 next to the iodide with a diacylglycerol benzyl protected silver phosphate derivative (figure 4-7, step iv) (Tocanne *et al.* 1974a, Bonsen *et al.* 1967). Although this chemistry could also have been applied to the synthesis of **1'** and **2'** in order to couple the headgroup and phosphate regions of **1'** and **2'**, there are a substantial number of steps that are required to prepare the molecule for phosphorylation, and these steps are complex and could have resulted in substantial product loss. Therefore this chemistry was not undertaken for the synthesis of **1'** and **2'** as yields of the final product were likely to have been low and the large number of synthetic steps involved are uneconomical and overly time consuming.

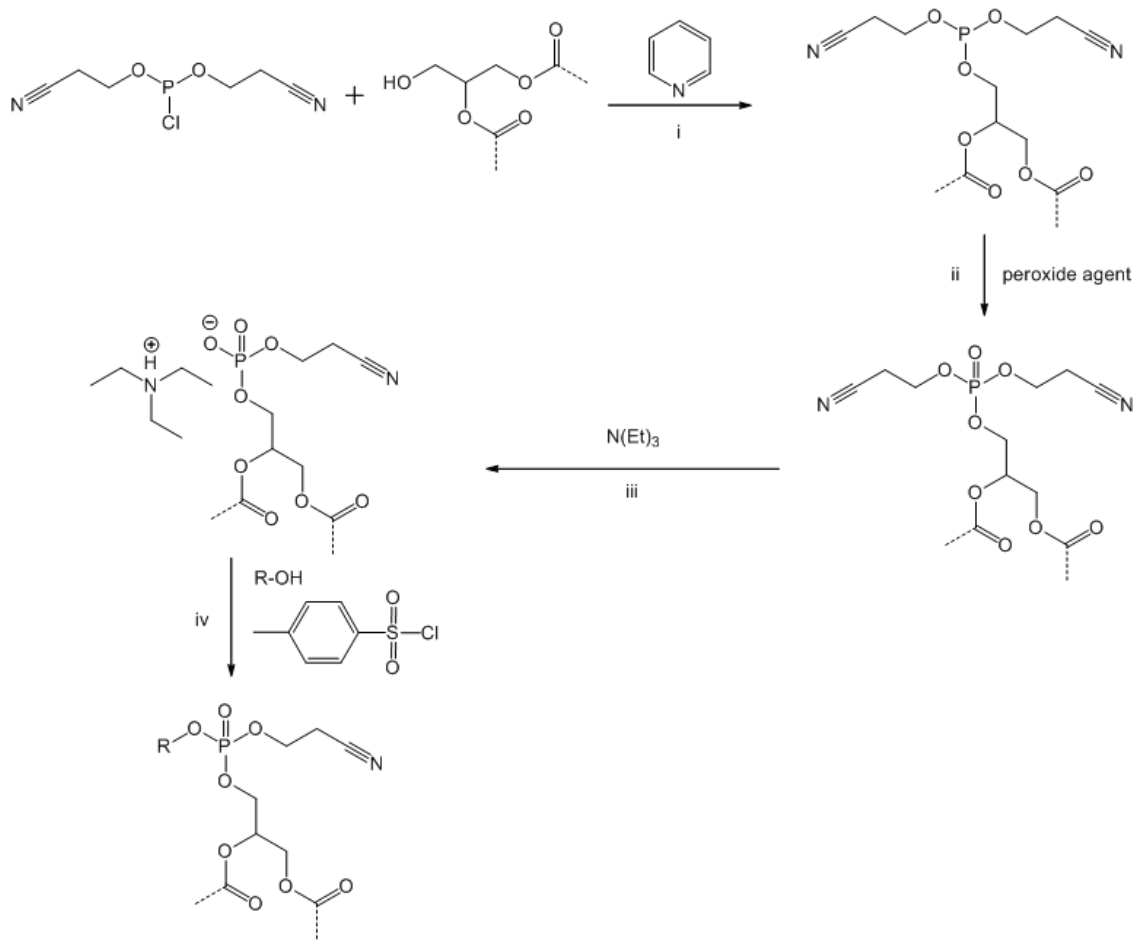

Figure 4-8 Reaction scheme showing the formation of a diacylglycerol phosphochlorodite (step i), the oxidation of the diacylglycerol phosphochlorodite to a diacylglycerol phosphotriester (step ii), the deprotection of one of the cyanoethanol groups of the diacylglycerol phosphotriester (step iii) and finally the coupling of a hydroxyl nucleophilic to the diacylglycerol phosphodiester (step iv).

To couple the lipid headgroup region with the diacylglycerol phosphate in **1'** and **2'**, an oligonucleotide synthesis approach was undertaken where phosphotriester coupling was utlised (Reese & Pei-Zhuo 1993, Gaffney & Reese 2001). The use of a phosphotriester sees dicyanoethyl phosphorochlorodite reacted first with the 3-hydroxyl of a diacylglycerol to displace chloride from the phosphochlorodite (figure 4-8, step i) and then the product is oxidised and separated from its by-products (figure 4-8, step ii). After product purification, the second nucleophile (lipid headgroup nucleophile) is coupled to the phosphate by unblocking a cyanoethyl group under basic conditions (figure 4-8, step iii) and employing a condensing agent (e.g. *p*-toluenesulfonyl chloride). The use of a condensing reagent activates the intermediate phosphate diester salt by forming a phosphosulfonyl anhydride, whereby the sulfonyl group is easily displaced by a good nucleophile (figure 4-8, step iv). This chemistry has previously proven successful in the synthesis of phosphatidylinositols (Gaffney & Reese 2001) and could

therefore theoretically be used for the phosphate coupling in the synthesis of **1'** and **2'**, to give the final protected lipids.

4.2 Results and discussion

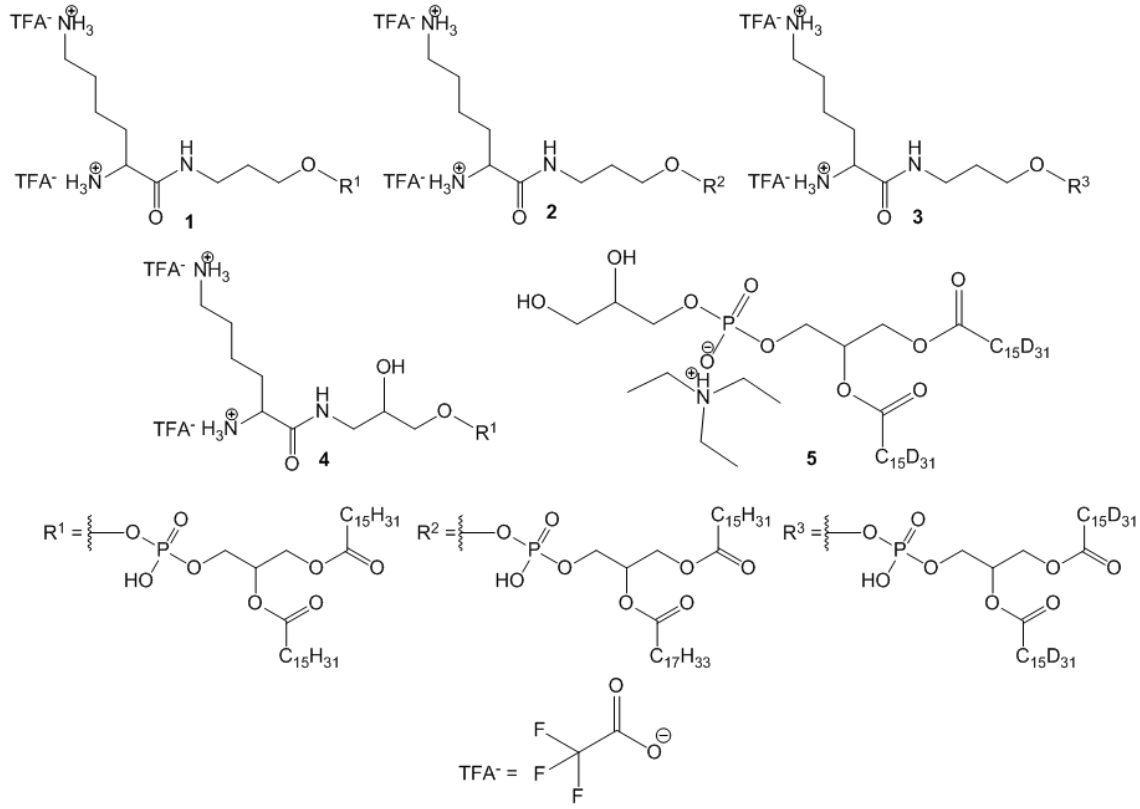

Figure 4-9 Structures and systematic names of the L-PG analogues containing amide groups; 3-*N*-Lysyl-1-*O*-(1,2-*O*-dipalmitoyl-*rac*-phosphatidyl)-3-aza-2,3-dideoxyglycerol **1**, 3-*N*-Lysyl-1-*O*-(1-*O*-palmitoyl-2-*O*-oleoyl-*rac*-phosphatidyl)-3-aza-2,3-dideoxyglycerol **2**, 3-*N*-Lysyl-1-*O*-(D_{62}-1,2-*O*-dipalmitoyl-*rac*-phosphatidyl)-3-aza-2,3-dideoxyglycerol **3** and 3-*N*-lysyl-1-*O*-(1,2-*O*-dipalmitoyl-*rac*-phosphatidyl)-3-aza-3-deoxy-*rac*-glycerol **4**. Additionally, the structure of 1-*O*-(D_{62}-1,2-di-*O*-palmitoyl-*rac*-phosphatidyl)-*rac*-glycerol **5**.

The synthesis of 3-*N*-Lysyl-1-*O*-(1,2-*O*-dipalmitoyl-*rac*-phosphatidyl)-3-aza-2,3-dideoxyglycerol **1**, 3-*N*-Lysyl-1-*O*-(1-*O*-palmitoyl-2-*O*-oleoyl-*rac*-phosphatidyl)-3-aza-2,3-dideoxyglycerol **2**, 3-*N*-Lysyl-1-*O*-(D_{62}-1,2-*O*-dipalmitoyl-*rac*-phosphatidyl)-3-aza-2,3-dideoxyglycerol **3**, 3-*N*-lysyl-1-*O*-(1,2-*O*-dipalmitoyl-*rac*-phosphatidyl)-3-aza-3-deoxy-*rac*-glycerol **4** and 1-*O*-(D_{62}-1,2-di-*O*-palmitoyl-*rac*-phosphatidyl)-*rac*-glycerol **5** can be separated into four stages (figure 4-9). In the first stage, the preparation of the required 3-*N*-(*N'*,*N''*-di-Boc-*rac*-lysyl)-3-aminopropan-1-ol or 2 hydroxy protected 3-*N*-(*N'*,*N''*-di-Boc-*rac*-lysyl)-3-aminopropan-1,2-diol was undertaken for the lipid headgroup. The second stage involved the preparation of 1,2-*O*-diacyl-3-*O*-phosphate-*rac*-glycerol, di(2-cyanoethyl) ester molecules for the lipid hydrocarbon and phosphate groups (Martin *et al.* 1994, Lok 1978). In the third stage, the

lysyl headgroup units (or 1,2-*O*-isopropylidene-*rac*-glycerol for **5**) were coupled with the hydrocarbon chain phosphate units to give the fully protected lipids (Gaffney & Reese 2001). In the final stage, all of the protecting groups were removed to give **1, 2, 3, 4** and **5**.

4.2.1.1 3-*N*-(*N'*,*N"*-di-Boc-*rac*-lysyl)-3-aminopropan-1-ol and *rac*-2-(tetrahydro-2*H*-pyran-2-yloxy)-3-(*N'*,*N''*-di-Boc-*rac*-lysylamino)-propan-1-ol

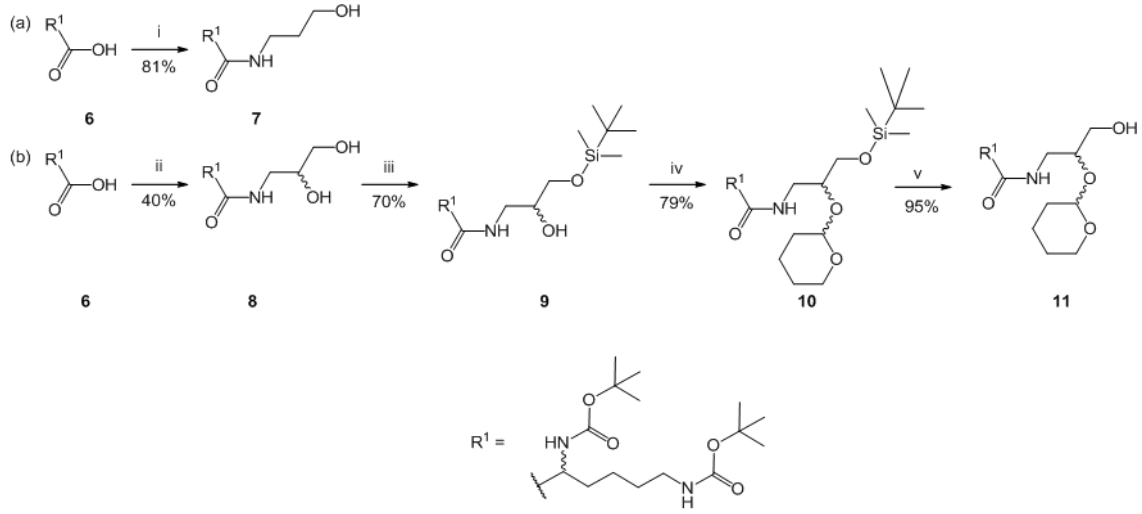

Scheme 1 *Reagents and conditions*: i, 3-aminopropan-1-ol, EDC.HCl, DMAP, *N*-hydroxysuccinimide, room temp., 10 min; ii, *rac*-3-aminopropane-1,2-diol, EDC.HCl, triethylamine, DMAP, room temp., 24 h; iii, *tert*-butyldimethylsilyl chloride, DMAP, pyridine, room temp., 60 min; iv, pyridinium *p*-toluene sulfonate, 3,4-dihydro-2*H*-pyran, room temp,. 24 h; v, tetra-butylammonium fluoride, 0 °C., 10 min.

To begin to prepare both 3-*N*-(*N'*,*N"*-di-Boc-*rac*-lysyl)-3-aminopropan-1-ol **7** and *rac*-2-(tetrahydro-2*H*-pyran-2-yloxy)-3-(*N'*,*N''*-di-Boc-*rac*-lysylamino)-propan-1-ol **11**, *N,N'*-di-Boc-*rac*-lysine **6**, dicyclohexylamonium salt was washed with aqueous $KHSO_4$ to form the conjugate acid of **6**. Initial attempts of coupling without washing steps resulted in large excesses of *N*-(*N*,*N'*-di-Boc-*rac*-lysyl)-dicyclohexylamide contaminating the product and substantially reduced product yields. After mild acid washing of **6**, the assumed conjugate acid of **6** in CH_2Cl_2 was treated with a slight excess of 3-aminopropan-1-ol for the synthesis of **7**, in the presence of *N*-(3-dimethylaminopropyl)-*N'*-ethylcarbodiimide hydrochloride (EDC.HCl), a catalytic quantity of 4-(dimethylamino)pyridine (DMAP) and *N*-hydroxysuccinimide (scheme 1a) (Anderson *et al.* 1964, Wey *et al.* 2007). This reaction gave a yield of ~81% of **7** which was required later for the synthesis of **1**, **2** and **3**. Early attempts to synthesize **7** using *N,N'*-dicyclohexylcarbodiimide were difficult to separate from the reaction by-product *N,N'*-dicyclohexylurea even after repeated crystallisation from acetonitrile, filtration and aqueous washing steps (Sheehan & Hess 1955). This problem was illustrated in the ^{13}C NMR spectrum of **7** (figure 4-10), where the signals at δ_C

25.0, 25.6 and 33.9 may be assigned to the resonance of the CH and CH_2 carbons in the hexyl rings of *N,N'*-dicyclohexylurea. Therefore EDC.HCl was used in preference to form **7** due to its aqueous soluble urea by-product being easily extractable by aqueous washing steps (Sheehan *et al.* 1961).

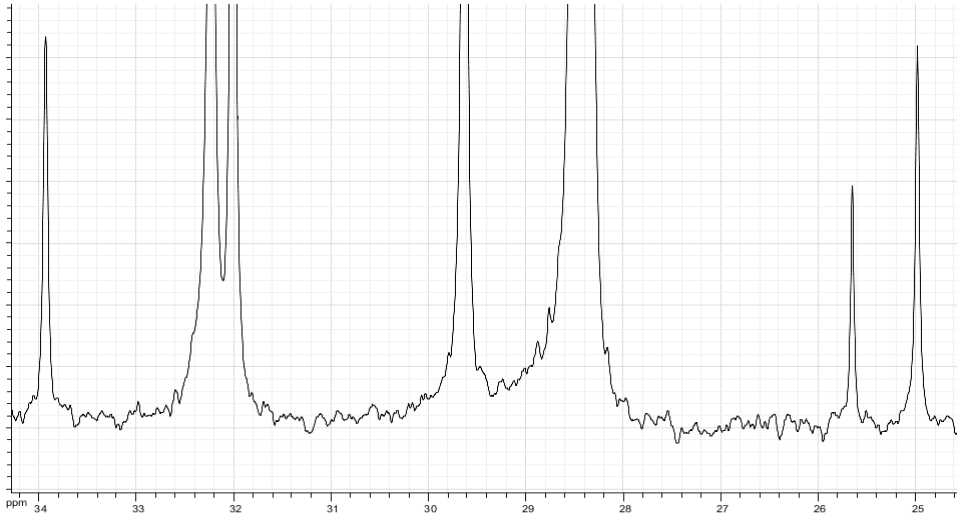

Figure 4-10 Region δ_C 24–33 of ^{13}C NMR spectrum (in $CDCl_3$) of **7** with *N,N'*-dicyclohexylurea contamination; δ_C 25.0, 25.6, 33.9 are the dicyclohexylurea ***C***H_2 and ***C***H signals.

Synthesis of **11**, initially saw the presumed conjugate acid of **6** in ethyl acetate, treated with excess *rac*-3-aminopropan-1,2-diol, EDC.HCl, a catalytic quantity of DMAP and triethylamine to give *rac*-3-*N*-(*N',N''*-di-Boc-*rac*-lysyl)-3-aminoproprane-1,2-diol **8** (scheme 1b, step ii). However, the reaction gave a low yield of **8** (~40%) which was attributed to the poor solubility of *rac*-3-aminopropane-1,2-diol in organic solvents; *rac*-3-aminopropane-1,2-diol is only miscible with water and short chained alcohols. Although the synthesis of **8** could have been conducted under aqueous conditions, *N,N'*-di-Boc-*rac*-lysine is sparingly soluble in aqueous environments (Sheehan *et al.* 1961). Early attempts to synthesise **8** with co-solvent mixtures of ethanol and CH_2Cl_2, resulted in large excesses of the *N*-(*N*,N'-di-Boc-*rac*-lysyl)-ethyl ester being formed. This finding suggested the ethanol may not have functioned properly as a phase transfer agent and *rac*-3-aminopropane-1,2-diol was still in the aqueous phase leaving only ethanol to react with **6** in the organic phase. Therefore, to increase the organic solubility of *rac*-3-aminopropane-1,2-diol, excess triethylamine was added to the reaction to ensure the amine of *rac*-3-aminopropane-1,2-diol was not protonated in the aqueous phase. The addition of triethylamine resulted in greater yields of **8** despite *rac*-3-aminopropane-1,2-diol still being poorly soluble in ethylacetate, however the yield of **8** only reached ~40% at best. The amide

coupling reaction of **8** was monitored by TLC and after 24 hours no remaining succinimidyl ester intermediate was observed which suggested the reaction had reached completion. However, use of a carbodiimide catalyst for such a long duration results in the formation of *N*-acylurea due to a competing side reaction, which also may have contributed to the low yield of **8** (Ulrich 2008). Following the synthesis of **8** an early attempt to clean the crude product was conducted by aqueous solvent extraction. However due to the high polarity of the amino-propane-diol group and high hydrophobicity of the protected lysyl groups, **8** exhibited behaviour similar to a surfactant and caused emulsification of the organic and aqueous phases during aqueous washing steps. Therefore, **8** was purified by normal phase-column chromatographic methods.

The purified **8** was later azeotropically dried from dry pyridine and treated in dry pyridine with a slight excess of *tert*-butyldimethylsilyl (TBDMS) chloride and a catalytic amount of DMAP in an inert atmosphere (scheme 1b, step iii) (Wuts & Greene 2006, Corey & Vemkates 1972). This reaction yielded *rac*-1-*tert*-butyldimethylsilyloxy-2-hydroxy-3-(*N',N''*-di-Boc-*rac*-lysylamino)-propane **9** (scheme 1b). The large steric bulk of the silyl protecting group in **9** ensured the majority of the protecting group was on the primary hydroxyl group of **8** (Wuts & Greene 2006), however due to the use of an excess of Tbmds chloride a small amount of *rac*-1,2-bis-(*tert*-butyldimethylsilyloxy)-3-(*N',N''*-di-Boc-*rac*-lysylamino)-propane was formed as well. Fortunately *rac*-1,2-bis-(*tert*-butyldimethylsilyloxy)-3-(*N',N''*-di-Boc-*rac*-lysylamino)-propane was substantially more hydrophobic, R_f (EtOAC–hexane, 7:3 v/v) 0.89, in comparison to **9** (R_f 0.38) and therefore was easily separated from **9** by normal phase column chromatography with an elution gradient of ethylacetate–hexane. To verify the chromatographic isolation of the silyl 1-*O*-isomer of **9** and none of the silyl 2-*O*-isomer the ^{1}H and ^{13}C NMR spectra of **8** and **9** were overlapped in the regions of the resonance signals of the aminopropane 2-CH(OH) and 3-CH_2O- groups (figures 4-11a and b). The ^{1}H NMR spectra displayed in 4-11a showed the aminopropane CH groups of both **8** and **9** had a chemical shift of δ_H 3.7–3.75 which only slightly changed between both molecules and still integrated to 1H with no splitting. This finding was also observed in the ^{13}C NMR spectra of both **8** and **9** in the region of δ_C 70–71 (figure 4-11b), and therefore was a good indicator that no silyl ether group was present on the aminopropane 2-CH(OH) oxygen atom of **9**. However, the ^{13}C NMR spectrum in figure 4-11c showed a downfield migration of the aminopropane 3-CH_2O- group carbon in **9** (δ_C 65) in comparison to **8** (δ_C 63.2) and suggested the silyl ether was bonded to the oxygen in this group. Also the ^{1}H COSY spectrum of **9** in

$CDCl_3$ (figure 4-11d) showed the presence of a hydroxyl cross peak with the aminopropane 2-CH, which did not appear on addition of MeOD (figure 4-11e). This supported the suggestion that the secondary hydroxyl group on **9** had no silyl ether bonded to it. The ^{13}C NMR CH(OH) signal in figure 4-9b was a doublet for both **8** and **9** which indicated these compounds contained two equal diastereoisomers of **8** and **9** due to the *rac*-3-aminopropane-1,2-diol used.

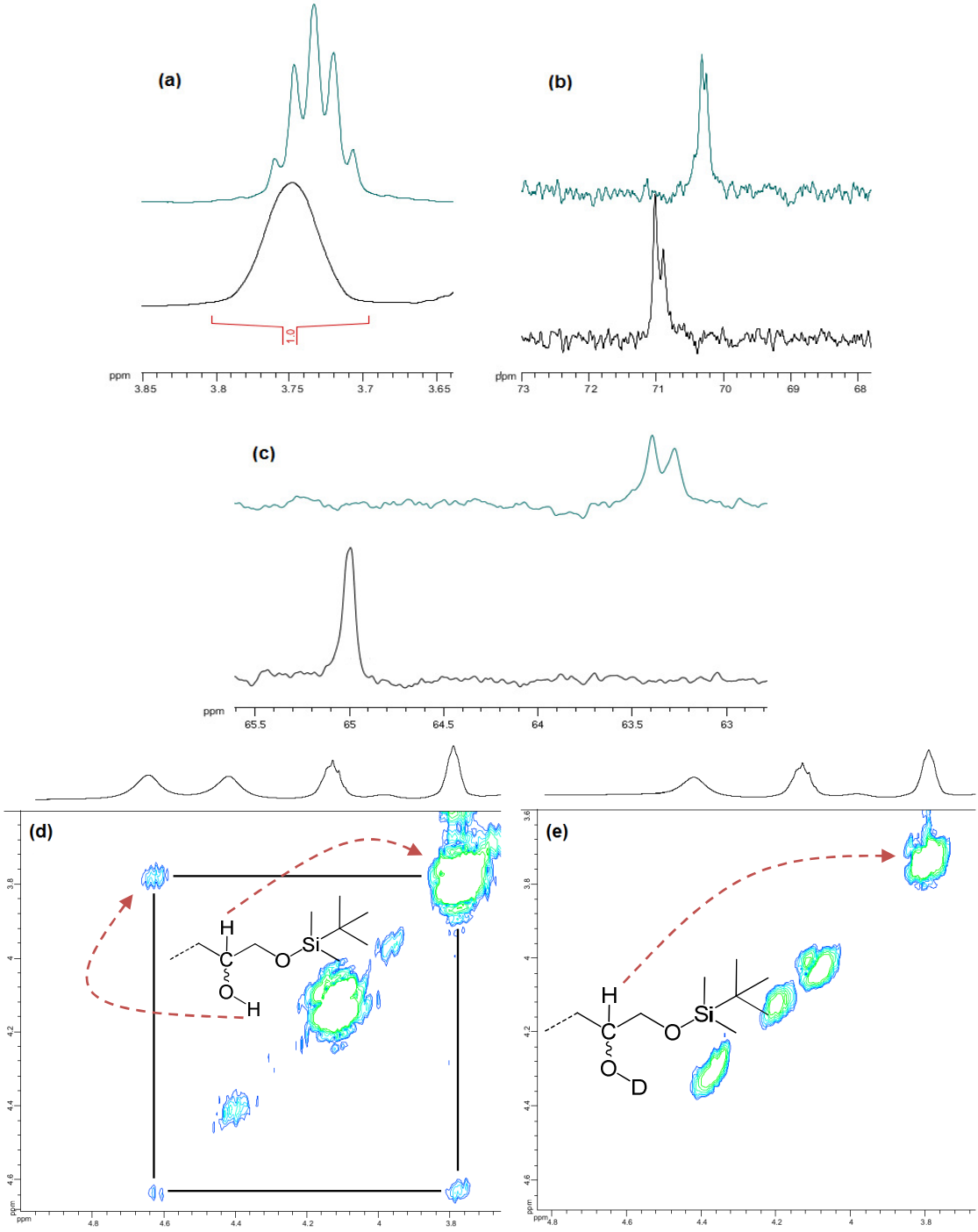

Figure 4-11 Regions δ_H 3.65–3.85, δ_C 63.0–65.5 and δ_C 68.0–73.0 of the ^1H and ^{13}C NMR spectra of **8** (in $CDCl_3$–CD_3OD 2:1 v/v, green) and **9** (in $CDCl_3$, black); (a) δ_H 3.7-3.75 aminopropane 2-C***H***(OH) of **8** and **9**, (b) δ_C 70.0–71.0 aminopropane 2-***C***H(OH) of **8** and **9**, and (c) δ_C 63.2 and 65.0 aminopropane 3-***C***H_2O- of **8** and **9**. Region δ_H 2.60–5.0 of the ^1H COSY spectrum of **9** in (d) $CDCl_3$ and (e) in $CDCl_3$–MeOD 2:1 v/v.

The diastereoisomeric mixture of **9**, without further purification, was next treated with pyridinium *p*-toluene sulfonate (PPTS) and excess 3,4-dihydro-2*H*-pyran in dry CH_2Cl_2 under an inert atmosphere which yielded *N*-(*N,N'*-di-*rac*-1-*tert*-butyldimethylsilyloxy-2-(tetrahydro-2*H*-pyran-2-yloxy)-3-(*N',N''*-di-Boc-*rac*-lysylamino)-propane **10** as a viscous oil (scheme 1b, step iv) (Miyashita *et al.* 1977). Tetrahydropyran (THP) protection of the secondary hydroxyl of **9** was selected as a protecting group for several reasons. First, hydroxyl ether protection has no possibility of migration which was required for **10** after TBDMS deprotection. Second, the preparation of a THP protected hydroxyl can be achieved under mild acidic conditions using PPTS preventing the breakdown of the acid labile TBDMS and carbamate protecting groups of **9** (Corey & Venkates 1972). Third, during global deprotection of the finished lipid the THP acetal should unblock at the same time as the acid-labile Boc carbamates. Lastly, the THP protecting group is robust enough to withstand the further chemistry utlised for synthesise of the rest of the phospholipid.

After the removal of by-products from crude **10** and chromatographic fractionation of **10**, the purified compound gave a high intensity sodiated parent peak of 640.3978 *m/z* with high resolution electrospray where **10** required 640.3964 *m/z*. The good agreement of the experimental electrospray data with the calculated data suggested **10** had been synthesised. However, both ^{1}H and ^{13}C NMR gave multiple peaks for the assigned individual carbon and proton resonance signals in **10** which suggested either a number of impurities were present or that eight chemically distinctive diastereoisomers of **10** were present due to racemic **6** and *rac*-3-aminopropane-1,2-diol being used and also the THP group also having a stereogenic centre. Close observation of both ^{1}H and ^{13}C NMR spectra of **10** suggested that eight diastereoisomers were present as shown in figures 4-12a and b where the ^{1}H NMR signals of the *tert*-butyldimethyl silyl ether (TBDMS) CH_3 groups were separated into two distinct peaks at δ_H 0.08 and 0.9 in **9**, however in **10** these signals separated into 2-3 individual peaks for the separate diastereoisomers. Four diastereoisomers of **9** were also present however splitting of the ^{1}H and ^{13}C NMR resonance signals in **9** was not observed. The lack of NMR peak splits in **9** suggested the presence of the steric overcrowding caused by both the TBDMS and THP protecting groups in **10** may have slowed down molecular rotations around the flexible amino-proprane chain and thus accentuated the difference in resonances of the diastereoisomers in **10** (Williams & Fleming 2008).

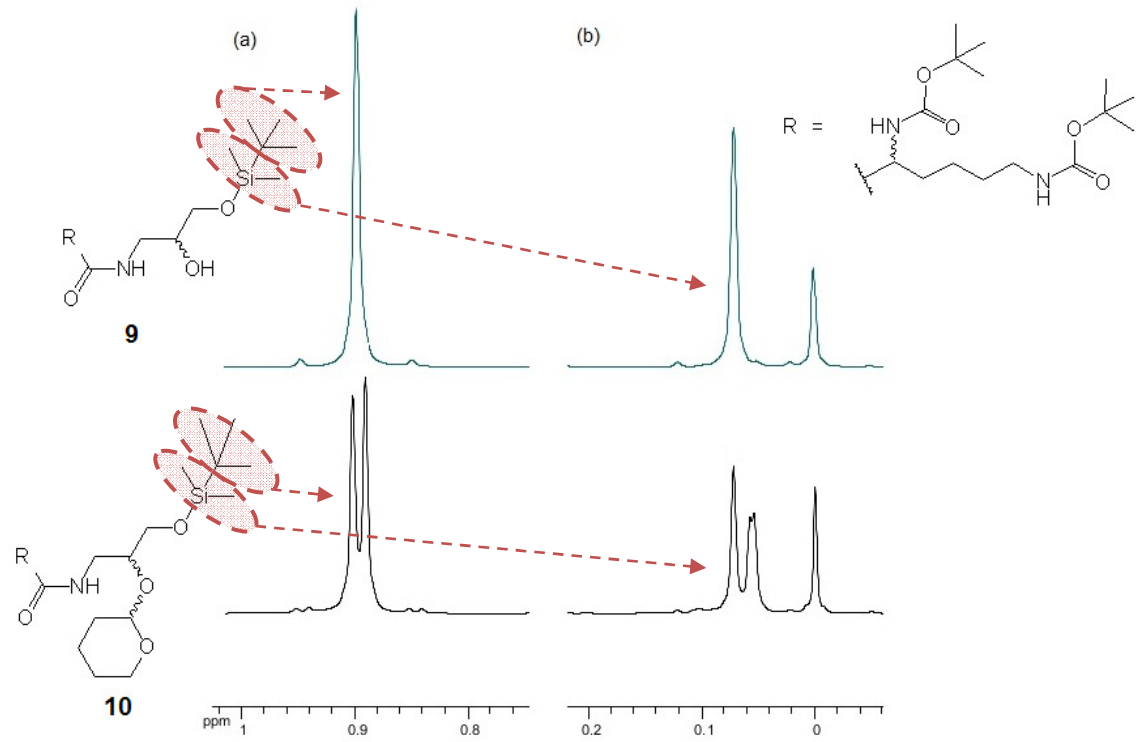

Figure 4-12 Regions δ_H 0–0.20 and 0.80-1.00 of the ^{1}H NMR spectra of **9** (in $CDCl_3$, green) and **10** (in $CDCl_3$, black); (a) δ_H 0.86–0.94 3 × C***H*****$_3$** of TBDMS geminal to the carbon bonded to silicon (b) δ_H 0.04–0.1 2 x C***H*****$_2$** protons of TBDMS geminal to silicon.

To prepare **10** for phosphate coupling, all the diastereoisomers of **10** were together treated with excess tetra-butylammonium fluoride under inert conditions to yield *rac*-2-(tetrahydro-2*H*-pyran-2-yloxy)-3-(*N′,N″*-di-Boc-*rac*-lysylamino)-propan-1-ol **11** (scheme 1b, step v) (Miyashita *et al.* 1977). The efficiency of this deprotection is well documented due to the greater affinity of silicon for fluoride compared to oxygen (Kocienski 2005). However, the formed by-product TBDMS fluoride was hydrolysed under aqueous washing conditions and gave the organic soluble *tert*-butyldimethyl silanol which was mixed with **11** (figure 4-13). Due to the bp of *tert*-butyldimethyl silanol (~139 ℃), it was efficiently distilled off at 50 ℃ under low pressure conditions of 21 mmHg as a colourless oil, therefore rendering **11** free of impurities. The NMR resonance signal splitting of **11** due to the presence of eight diastereoisomers was substantially less pronounced than **10**, which was likely to be due to the reduction in steric bulk and greater freedom of rotation of the aminopropane chain by the removal of the TBDMS ether.

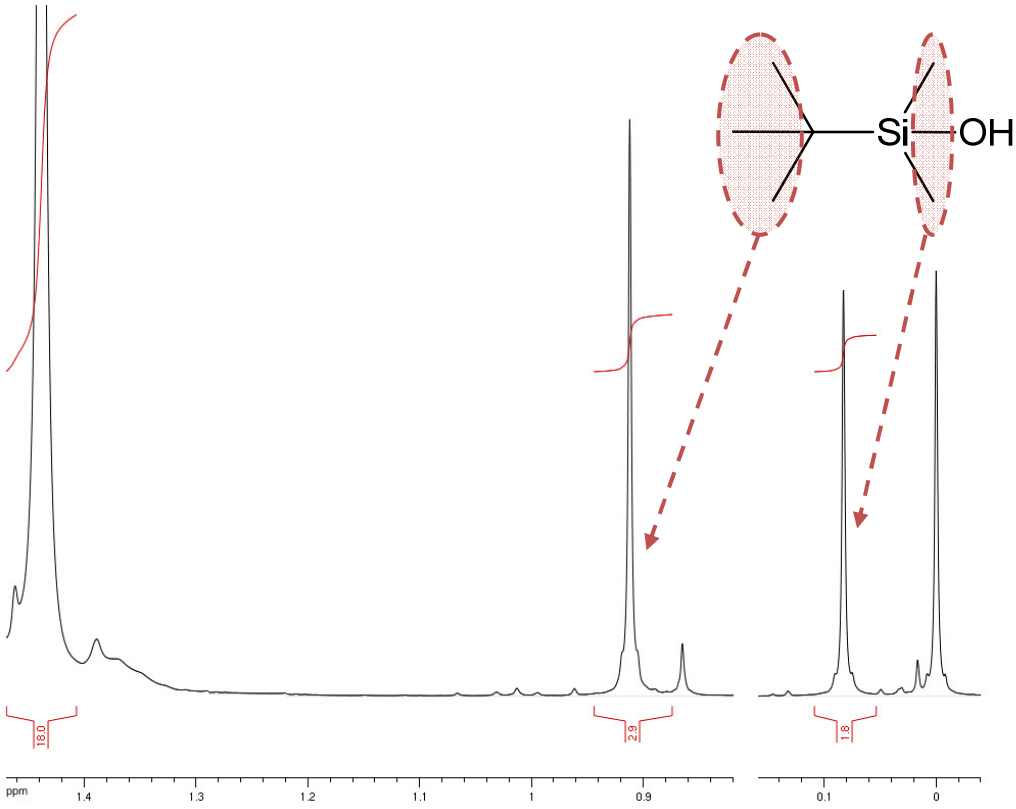

Figure 4-13 Region δ_H 0–0.20 and 0.8–1.4 of the ^{1}H NMR spectrum of **11** (in $CDCl_3$); δ_H 0.09 2 × C***H₃*** geminal to Si in *tert*-butyldimethyl silanol and δ_H 0.92 3 × butyl C***H₃*** groups of *tert*-butyldimethyl silanol. Molecular structure of *tert*-butyldimethyl silanol also shown.

4.2.2 1,2-*O*-Diacyl-3-*O*-phosphate-*rac*-glycerol, di(2-cyanoethyl) esters

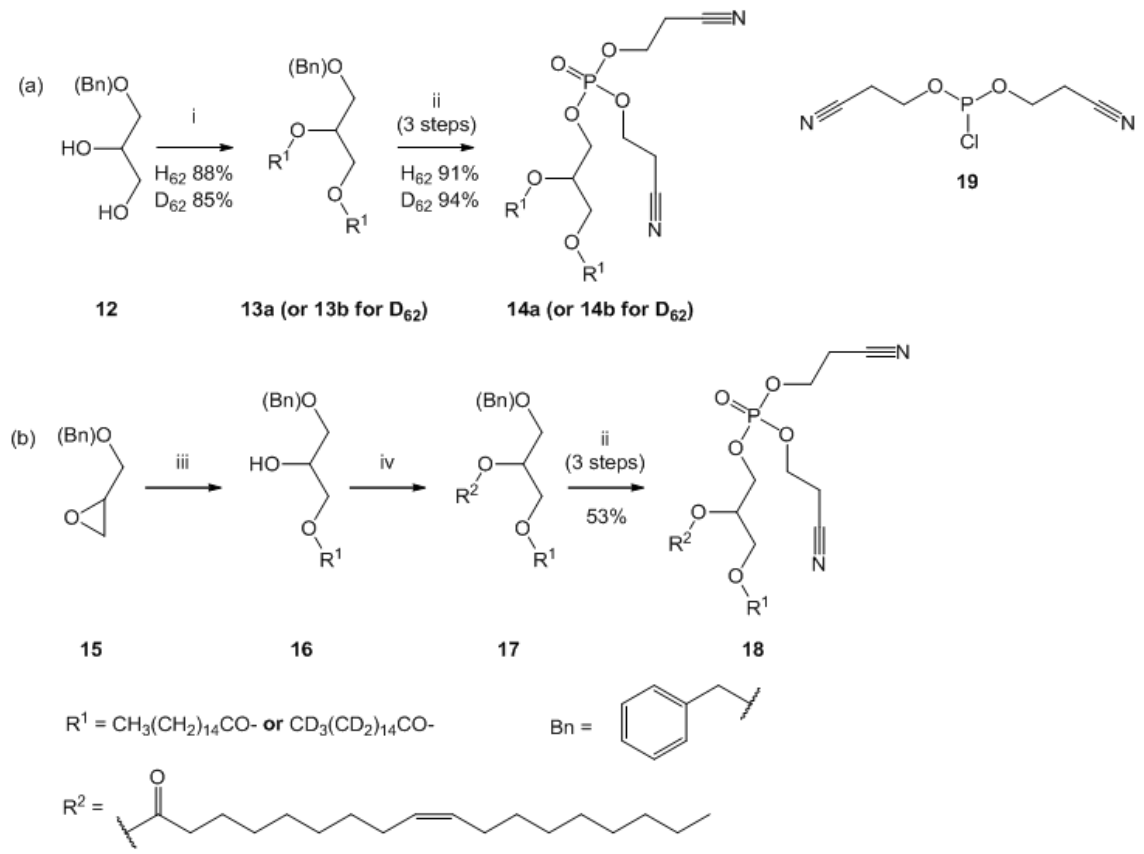

Scheme 2 *Reagents and conditions*: i, DMAP, EDC.HCl, D_{31} or H_{31} palmitic acid, room temp., 24 h; ii, (first step) benzyl deprotection (Lok 1978); (second step) **19**, pyridine, room temp., 15 min; (third step) 6M t*ert*-butyl hydroperoxide, 0 ℃ to room temp., 10 min; iii & iv, Synthesis adapted from Lok CM (1978) (Lok 1978).

The synthesis of both deuterated **13b** and protiated 1,2-*O*-dipalmitoyl-3-*O*-benzyl-*rac*-glycerol **13a** was conducted by the same method (Lok 1978). A solution of 1-*O*-benzyl-*rac*-glycerol **12** in CH_2Cl_2 was treated with palmitic acid (or D_{31}-palmitic acid), EDC.HCl and a catalytic quantity of DMAP (scheme 2a, step i) (Martin *et al.* 1994). This reaction gave the 3-*O*-benzyl protected 1,2-*O*-dipalmitoyl-*rac*-glycerols **13a** and **13b** (scheme 2a). Both **13a** and **13b** fractionated well on normal phase silica from remaining by-products due to their low affinity for silica and therefore eluted with a low ratio of ethylacetate–hexane (1:9 to 2:8 v/v) (Snyder 2008). Electrospray analysis of **13b** showed a sodiated peak of $[M+Na]^+$ 743.9357 *m*/*z*, where **13b** required 743.9321 *m*/*z* which gave good indication that the deuterated palmitoyl hydrocarbon chains had not undergone any hydrogen-deuterium exchange during the reaction. Supporting evidence of the formation of **13a** and **13b** was found in the ^{13}C NMR spectra of both compounds where two peaks were observed at δ_C 173.1 and 173.4 which are similar in chemical shift to the glycerol-esters found in 1,2-*O*-diacylglycerols (figure 4-14) (Lok 1978).

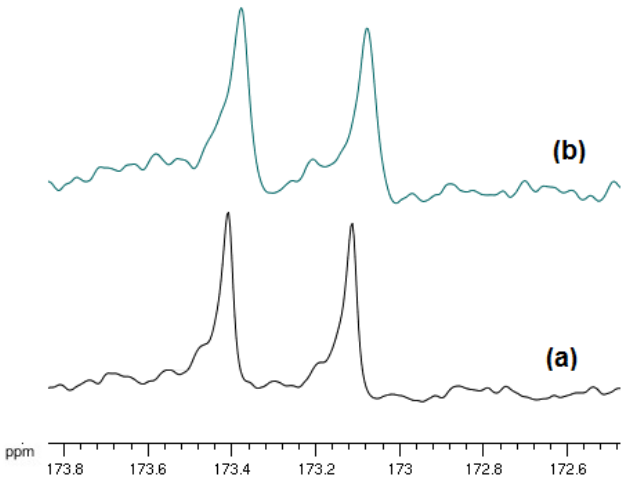

Figure 4-14 Region δ_C 172.6–173.6 of the ^{13}C NMR spectra of **13b** (in $CDCl_3$, green) and **13a** (in $CDCl_3$, black); (a) δ_C 173–173.6, 2 × ***C***O_2 of **13a** and (b) δ_C 173–173.6, 2 × ***C***O_2 of **13b**.

The synthesis of the mixed acyl 1-*O*-palmitoyl-2-*O*-oleoyl-3-*O*-benzyl-*rac*-glycerol **16** was also conducted by similar methods as for the synthesis of **13a** and **b**, however certain modifications were made (Lok 1978). 1-*O*-Benzyl *rac*-glycidyl ether **15** was reacted with a melt of one equivalent of palmitic acid in the presence of a catalytic amount of tetraethylammonium bromide at 100 °C (scheme 2b, step iii). Crystallisation was then performed from a melt of the crude product of **16** at 19 °C in the presence of 0.1 M HCl in order to facilitate the conversion of any glycerol 2-*O*-acyl product of **16** to the primary hydroxyl position, as **16** melts above 22 °C whereas the 2 position structural isomer of **16** melts at <19 °C (Lok 1978). Mono-palmitoyl ester **16** was then fractionationated on normal phase silica to remove any excess palmitic acid present in the crude product. The isolated **16** was confirmed as the correct compound with electrospray analysis with a sodiated parent ion of 681.5424 *m/z* (**16** required 681.5429 *m/z*) and the absence of any glycerol CH hydroxyl peaks at δ_H ~5.04 in the ^{1}H NMR spectrum, which could be assigned to the 2-position structural isomer of **16**. The ^{13}C NMR spectrum of **16** shown in figure 4-15 also showed the presence of only one structural isomer of **16** with a signal at δ_C 174.1 which corresponded to a single ester carbon present in **16** (Lok 1978).

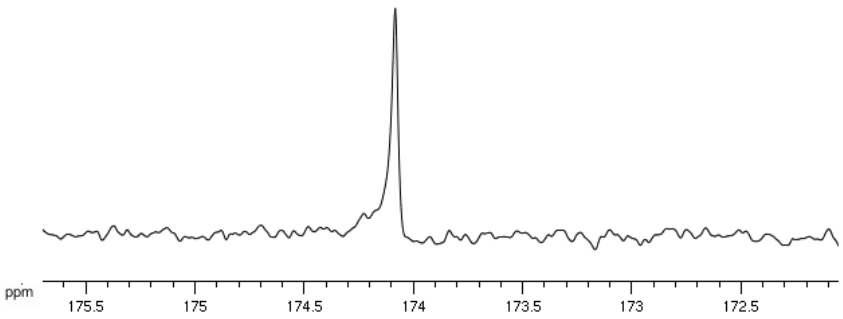

Figure 4-15 Region δ_C 172.5-175.5 of the ^{13}C NMR spectrum of **16** (in $CDCl_3$); δ_C 174.1 1-***C***O_2 of **16**.

In order to add an oleoyl hydrocarbon chain to **16**, **16** was treated with EDC.HCl, DMAP and a slight excess of oleic acid which yielded the 1-*O*-palmitoyl-2-*O*-oleoyl-3-*O*-benzyl-*rac*-glycerol **17** (scheme 2b, step iv). Fully protected diacylglycerol **17** was isolated from its by-products by the same methods as for **13a** and **13b** purification. However it was stored in $CHCl_3$ at -20 ℃ to minimise oxidation of the unsaturated bond in the oleoyl hydrocarbon chain. To confirm the correct isolation of **17** the ^{13}C NMR spectrum was examined in the range of δ_C 173–173.4, where two ester signals identical to that observed in figure 4-15 were present. In addition, the ^{1}H NMR spectrum showed the presence of a second order complex multiplet at δ_H 5.34 which integrated to 2 H and could be assigned to the presence of one unsaturated carbon to carbon bond in **17** (figure 4-16) (Williams & Fleming 2008).

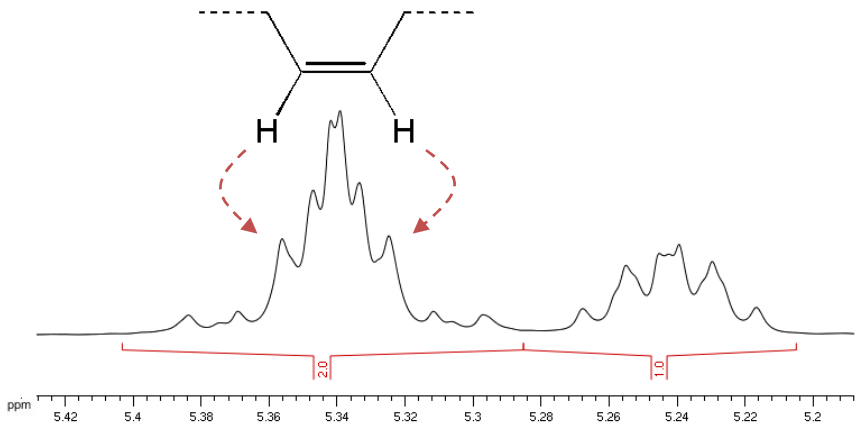

Figure 4-16 Region δ_H 5.20-5.24 of the ^{1}H NMR spectrum of **17** (in $CDCl_3$); region δ_H 5.3–5.4, 1 × R–C***H***=C***H***–R of **17**.

Deprotection of the 3 position benzyl group in **13a**, **13b** and **17** all followed the same method (Lok 1978), but with modifications. 3-Benzyl ethers **13a**, **13b** and **17** were all initially treated with a large excess of boron trichloride under an inert atmosphere at increasing temperature (-

80 ℃ to -40 ℃) (scheme 2a and b, step ii). The initially formed trichloroborane etherates derived from **13a**, **13b** and **17**, were then hydrolysed with water at 0 ℃ (Sorrell 2006). However after phosphorylation of the resultant 3-OH, acyl group migration to the glycerol 3-O position was detected as illustrated in the ^{1}H NMR spectrum of 1,2-*O*-dipalmitoyl-3-*O*-phosphate-*rac*-glycerol, di(2-cyanoethyl) ester **14a** in figure 4-17. The upfield signal in figure 4-17b (δ_H 4.78) was assignable to the glycerol 2-CH proton of 1,3-*O*-dipalmitoyl-2-*O*-phosphate-*rac*-glycerol, di(2-cyanoethyl) ester whereas the downfield signal in figure 4-17a (δ_H 5.27) was the required glycerol 2-CH proton signal of **14a**. From integration of figures 4-17a and b there appeared to be an equal mixture of both structural isomers.

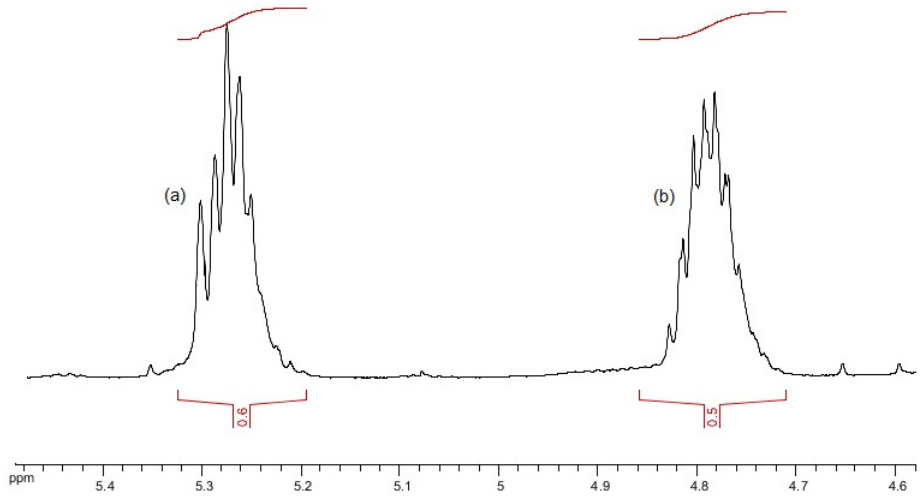

Figure 4-17 Region δ_H 4.6–5.4 of the ^{1}H NMR spectrum of crude 1,2-*O*-dipalmitoyl-3-*O*-phosphate-*rac*-glycerol, di(2-cyanoethyl) ester (in $CDCl_3$); (a) δ_H 5.27 glycerol 2-C***H*** signal of the 1,2-*O*-diacyl isomer and (b) δ_H 4.78 glycerol 2-C***H*** signal of the 1,3-*O*-diacyl isomer.

In order to reduce acyl migration after benzyl deprotection in **14a**, 1,2-*O*-D_{62}-dipalmitoyl-3-*O*-phosphate-*rac*-glycerol, di(2-cyanoethyl) ester **14b** and 1-*O*-palmitoyl-2-*O*-oleoyl-3-*O*-phosphate-*rac*-glycerol di(2-cyanoethyl) ester **18**, the reaction was quenched and washed at 0 ℃ with saturated sodium hydrogen carbonate. The use of sodium hydrogen carbonate in scheme 2a and b, step ii, neutralised the residual hydrochloric acid formed from the hydrolysis of boron trichloride, which was thought to be the migration catalyst. After utilisation of a saturated sodium hydrogen carbonate washing step negligible amounts of the 1,3-*O*-diacyl isomers of **14a** and **b**, and **18** were detected.

To complete the synthesis of **14a**, **14b** and **18**, the crude products from the benzyl deprotection of **13a**, **13b** and **17** were treated with an excess of di(2-cyanoethyl) phosphorochloridite **19** in

dry pyridine (scheme 2a and b, step ii). After pyridine was removed by low pressure evaporation, the intermediate triphosphites of **14a**, **14b** and **18** in CH_2Cl_2 were oxidised with excess *tert*-butyl hydroperoxide at 0 ℃ to yield **14a**, **14b** and **18** (Gaffney & Reese 2001). Separation of **14a** and **b** from their by-products was completed by crystallisation from acetonitrile. However, isolation of **18** from its by-products had to be conducted at -40 ℃ in order to crystallise **18** from acetonitrile as a solid. Electrospray analysis of **14b** showed a sodiated parent ion of 839.9023 *m*/*z* where **14b** required 839.9045 *m*/*z*, which demonstrated the deuterated palmitoyl hydrocarbon chains of **14b** were stable under the reaction conditions employed in scheme 2a, step ii, and no hydrogen-deuterium exchange had occurred. Supporting evidence for the correct isolation of **14a**, **14b** and **18** was found in the proton decoupled ^{13}C NMR spectra of each compound where vicinal phosphorous to carbon coupling was observed resulting in the splitting of the glycerol 3-CH_2 resonance signals of **14a**, **14b** and **18** (figures 4-18d-f) (Kuhl 2008). This signal splitting effect of the glycerol 3-CH_2 signals was not observed in **13a**, **13b** and **17** (figures 4-18a-c), which strongly suggested phosphate was covalently bound to the glycerol 3-CH_2 oxygen of **14a**, **14b** and **18**.

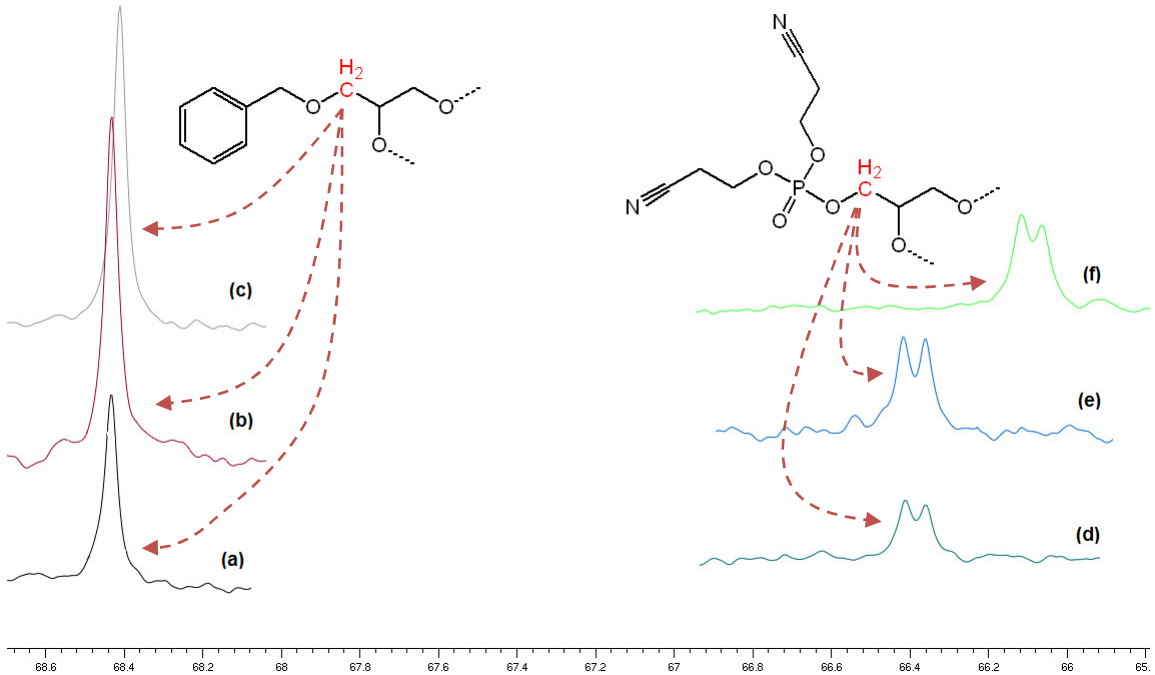

Figure 4-18 Region δ_C 65.0–68.6 of the ^{13}C NMR spectra of (a) **13a**, (b) **13b**, (c) **17**, (d) **14a**, (e) **14b** and (f) **18**, showing the ^{13}C resonance δ_C 68.2–68.6 of the glycerol 3-***C***H_2 of **13a, 13b** and **17**, and the ^{13}C resonance δ_C 65.5–66.5 of the glycerol 3-***C***H_2 of **14a**, **14b** and **18**.

4.2.3 Fully protected lipids

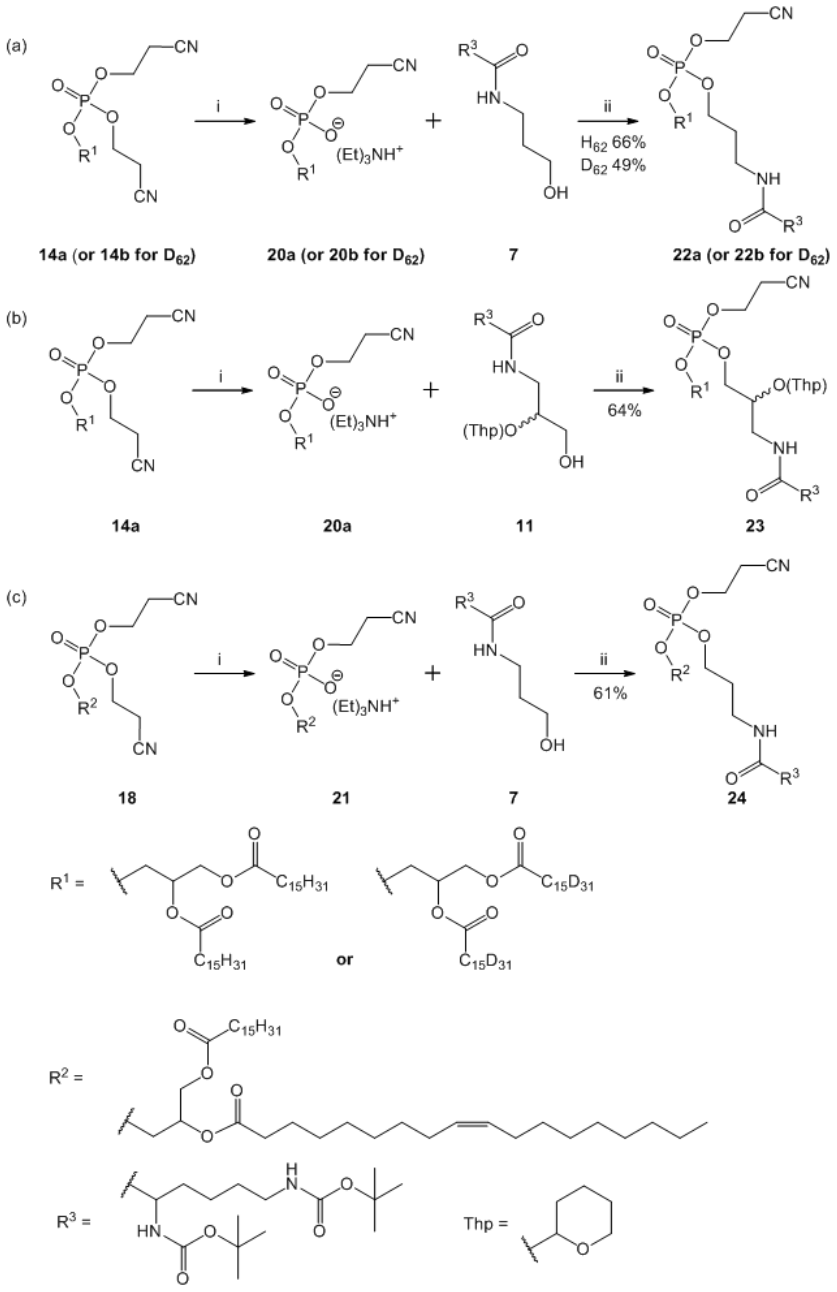

Scheme 3 *Reagents and conditions*: i, triethylamine, acetonitrile, room temp., 16h; ii, 3-nitro-1*H*-1,2,4-triazole, pyridine, 2-mesitylenesulfonyl chloride, room temp., 60 min.

The coupling of **7** or **11** with **14a**, **14b** or **18** was essentially the same for all the coupling reactions (schemes 3a-c). To start with, the 1,2-*O*-diacyl-3-*O*-phosphate-*rac*-glycerol, di(2-cyanoethyl) esters were stirred for 16 hours in an equal volume mixture of triethylamine, acetonitrile and CH_2Cl_2 (schemes 3a-c, step i), which resulted in the formation of 1,2-*O*-dipalmitoyl-3-*O*-phosphate-*rac*-glycerol, (2-cyanoethyl) ester, triethylammonium salt **20a**, 1,2-*O*-D_{62}-dipalmitoyl-3-*O*-phosphate-*rac*-glycerol, (2-cyanoethyl) ester, triethylammonium salt **20b** and 1-*O*-palmitoyl-2-*O*-oleoyl-3-*O*-phosphate-*rac*-glycerol, (2-cyanoethyl) ester,

triethylammonium salt **21** (Gaffney & Reese 2001). **20a**, **20b** or **21** were then separated from any residual solvents and the acrylonitrile by-product by low pressure evaporation (Gaffney & Reese 2001). **20a**, **20b** or **21** were next re-dissolved in dry pyridine and treated with an excess of **7** or **11**, 3-nitro-1*H*-1,2,4-triazole and 2-mesitylenesulfonyl chloride under an anhydrous and inert atmosphere (scheme 3a-c, step ii) (Gaffney & Reese 2001). To ensure close to complete anhydrous conditions all the starting materials were repeatedly azeotroped from dry pyridine and internal surfaces of glassware were dried under vacuum at temperatures >100 °C. The coupling of **7** or **11** with **20a**, **20b** or **21** yielded the fully protected 3-*N*-lysyl-1-*O*-(1,2-*O*-dipalmitoyl-*rac*-phosphatidyl)-3-aza-3-deoxy-*rac*-glycerol **23**, 3-*N*-lysyl-1-(1,2-*O*-dipalmitoyl-*rac*-phosphatidyloxy)-3-aminopropane **22a**, 3-*N*-lysyl-1-(D_{62}-1,2-*O*-dipalmitoyl-*rac*-phosphatidyloxy)-3-aminopropane **22b** and 3-*N*-lysyl-1-(1-*O*-palmitoyl-2-*O*-oleoyl-*rac*-phosphatidyloxy)-3-aminopropane **24**.

Electrospray analysis of **22b** showed a sodiated parent ion of 1172.16 *m*/*z* where **22b** required 1172.14 *m*/*z* and illustrated that negligible deuterium-hydrogen exchange had occurred in **22b** even in the presence of the 2-mesitylenesulfonic acid by-product. Confirmation of the formation of **22a**, **22b**, **23** and **24** was difficult to verify by ^{1}H, ^{13}C and ^{31}P NMR as a large number of the resonance signals were broad, overlapped and multiplets due to the presence of eight diastereoisomers in **22a**, **22b** and **24**, and thirty two diastereoisomers in **23**. Therefore electrospray analysis of **22a**, **22b**, **23** and **24** was relied upon for verification of the isolation of the correct compounds and gave high intensity parent ions of 1109.77 *m*/*z* $[M+Na]^+$, 1172.16 *m*/*z* $[M+Na]^+$, 1209.84 *m*/*z* $[M+Na]^+$ and 1113.71 *m*/*z* $[M+H]^+$, respectively, where **22a**, **22b**, **23** and **24** required 1109.75 *m*/*z*, 1172.14 *m*/*z*, 1209.80 *m*/*z* and 1113.78 *m*/*z*, respectively, and therefore the good agreement between the electrospray analysis and calculated masses was a good indicator the correct compounds had formed. Additionally, TLC of **22a**, **22b**, **23** and **24** all displayed the presence of a single spot when using both potassium permanganate and ninhydrin staining reagents.

The phosphotriester coupling of a hydroxyl containing compound (**7** or **11**) with 2-mesitylenesulfonyl chloride as illustrated in figure 4-19a has a disadvantage of a competing side reaction of the starting hydroxyl containing compound (**7** or **11**) with 2-mesitylenesulfonyl chloride (figure 4-19b). The side reaction shown in figure 4-19b was the more energetically favourable reaction and could have lowered the yields of **22a**, **22b**, **23** and **24**. Therefore to

increase the yield of the phosphotriester coupling, the starting hydroxyl containing compounds (**7** or **11**) were added in large excess (~2 eq.) as well as the catalysts 3-nitro-1*H*-1,2,4-triazole and 2-mesitylenesulfonyl chloride (~5-10 eq.). In particular, 2-mesitylenesulfonyl chloride was added to the reaction mixture slowly dropwise and highly concentrated in a dry CH_2Cl_2 solution to minimize the probability of this secondary reaction (figure 4-19b). The addition of 3-nitro-1*H*-1,2,4-triazole to the phosphotriester coupling also helped drive the reaction forward as it forms a good leaving group for **7** or **11** to displace once bound to the phosphate. The overall yields of **22a**, **22b**, **23**, and **24**, varied from 50-65%, which was less than expected (~70-80% for phosphatidylinositols (Gaffney & Reese 2001)) and suggested the reactions may have not been dry enough and some residual water was present thus reducing the yields of **22a**, **22b**, **23**, and **24**.

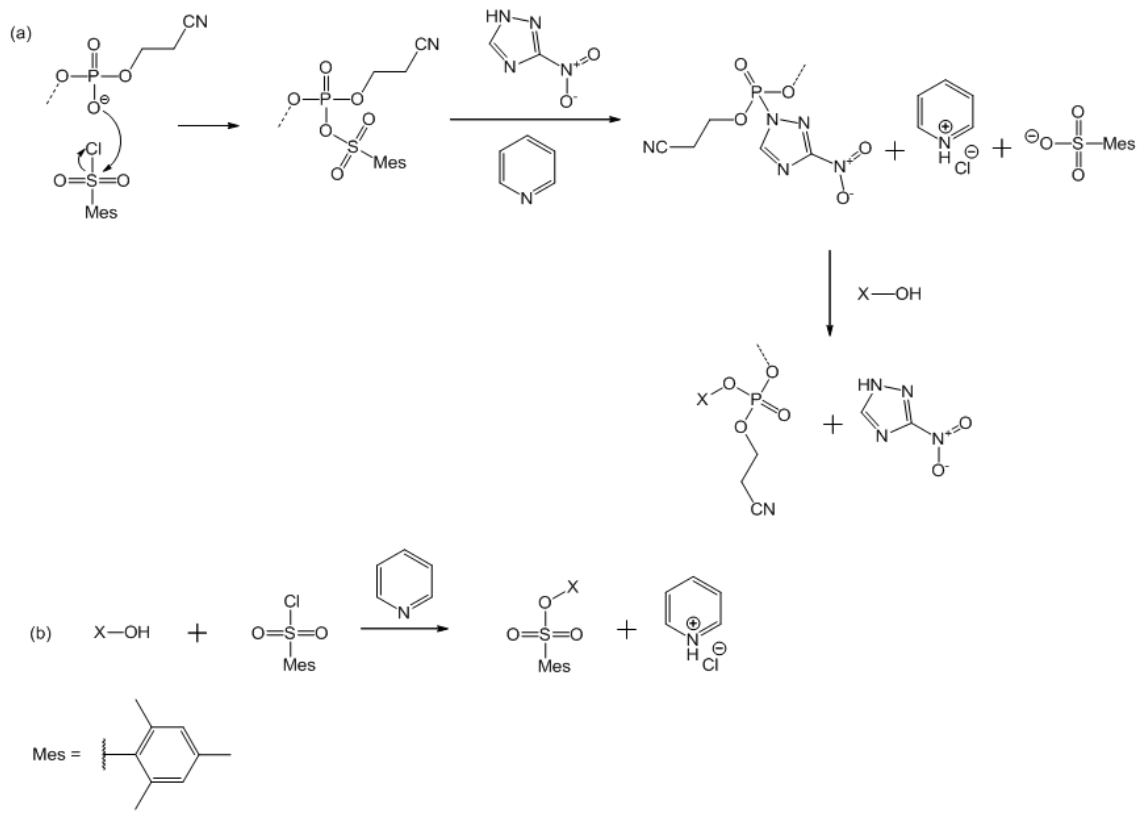

Figure 4-19 (a) Reaction scheme of phosphotriester coupling with a hydroxyl containing compound in the presence of 3-nitro-1*H*-1,2,4-triazole and 2-mesitylenesulfonyl chloride and (b) the competing side reaction of the sulfonation of the hydroxyl containing compound.

An additional synthesis was also performed to produce **5** as it was later required for neutron scattering experiments. The synthesis of **5** began with the formation of fully protected 1-*O*-(D_{62}-1,2-*O*-dipalmitoyl-*rac*-phosphatidyl)-*rac*-glycerol **26** (scheme 4) by coupling a racemic mixture of 1,2-*O*-isopropylidene-glycerol **25** with **20b** by the same method of coupling **7** or **11** with **20a**,

20b or **21** (Gaffney & Reese 2001). The synthesis of **26** has previously been conducted with protiated palmitoyl fatty acid chains rather than deuterated, which made characterisation and confirmation of the synthesis of **26** less complicated (Bruzik *et al.* 1986).

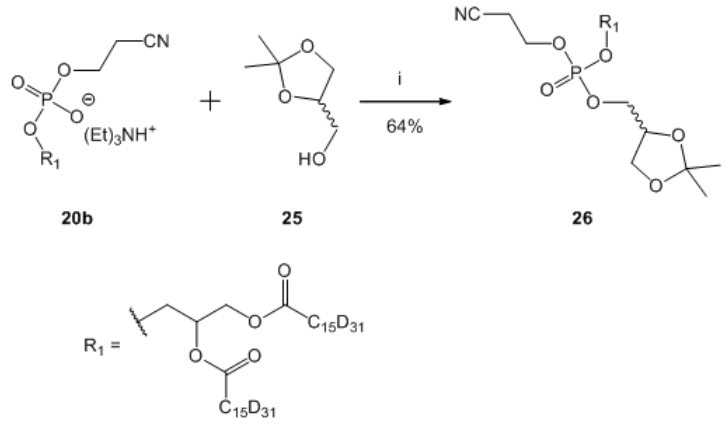

Scheme 4 *Reagents and conditions*: i, 3-nitro-1*H*-1,2,4-triazole, pyridine, 2-mesitylenesulfonyl chloride, room temp., 60 min.

After coupling of **25** with **20b** the removal of excess **25** was performed by aqueous washing of the reaction mixture owing to the high aqueous solubility of **25**. All other by-products of the coupling reaction in scheme 4 were removed by normal-phase chromatographic fractionation of **26**. Confirmation of the isolation of **26** was initially by electrospray where a sodiated parent ion of 900.92 *m*/*z* was found and **26** required 900.95 *m*/*z*. ^{1}H and ^{13}C NMR signals of **26** also closely matched those found for the synthesis of hydrogenated **26** in a previous publication (Bruzik *et al.* 1986). ^{13}C NMR two-bond coupling between phosphorous and both glycerol 3 position CH_2 groups was not found, however due to the presence of eight diastereoisomers in **26** this was not unexpected due to the substantial signal overlap between all the carbon signals of all diastereoisomers present.

4.2.4 Global deprotection

Deprotection of **22a**, **22b**, **23**, **24** and **26** started with the removal of the 2-cyanoethyl ester group in all the fully protected lipids as shown in scheme 3, step i. After removal of the 2-cyanoethyl ester from **22a**, **22b** and **24** the resulting partially unblocked lipids **27a**, **27b** and **29**, respectively, were then treated with a 1:1 mixture of trifluoroacetic acid (TFA) and CH_2Cl_2, and a small amount of triisopropylsilane (TIPS) to trap the *tert*-butyl cations from the Boc groups (scheme 5, step i) (Tarbell *et al.* 1972). Similarly, the 2-cyanoethyl ester of **23** was unblocked, giving **29** which was subjected to a similar deprotection as **22a**, **22b** and **24** but with the addition

of a small amount of water to facilitate THP deprotection as well (scheme 5, step ii) (Kocienski 2005). The full deprotection reactions of **22a**, **22b**, **23**, **24** and **26** yielded the fully uprotected lipids **1**, **2**, **3** and **4** as the bis-trifluoroacetate salts. Phospholipids **1**, **3** and **4** were all successfully crystallised from cold acetone to removal all by-products. However, unsaturated oleoyl lipid **2** required fractionation by reverse phase chromatography on silanized silica due to **2** having a low T_m.

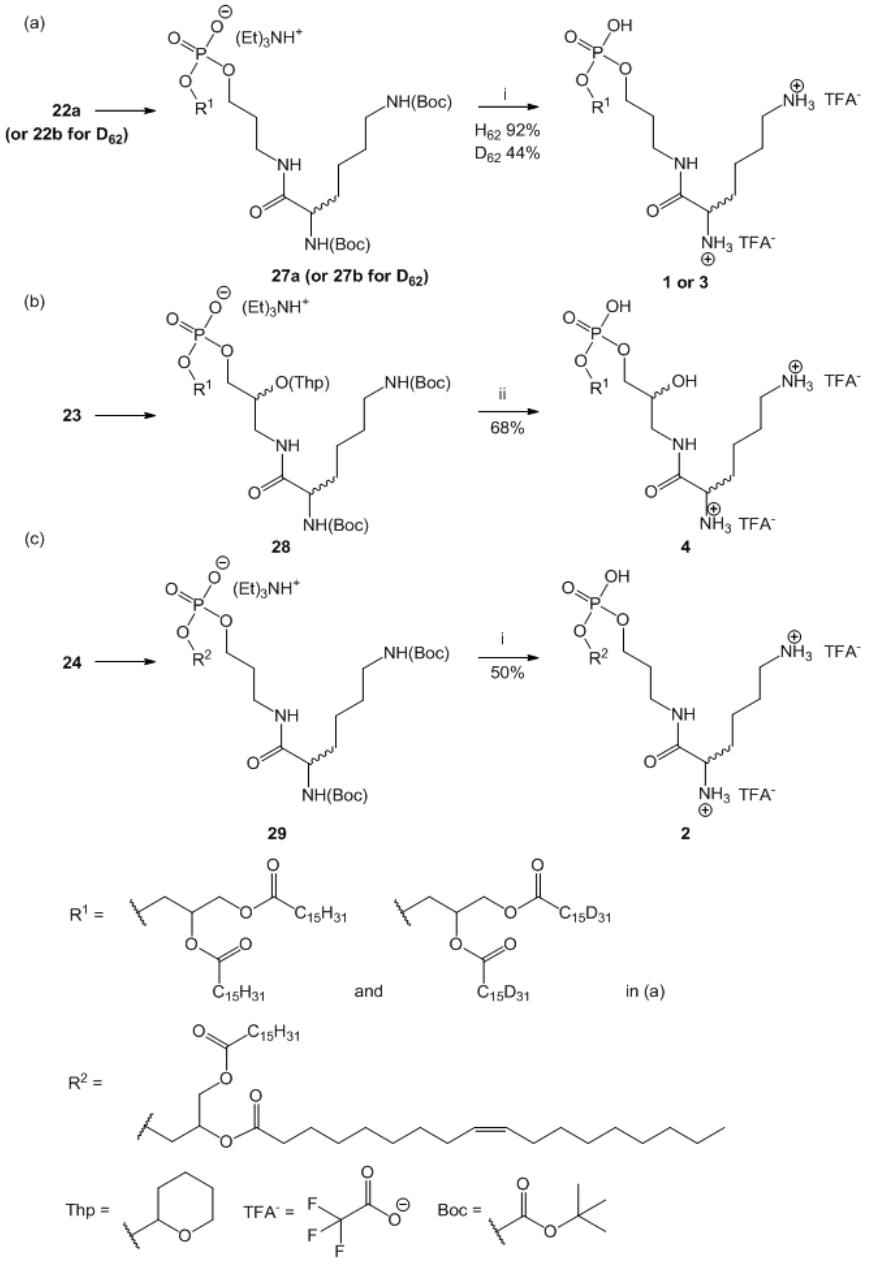

Scheme 5 *Reagents and conditions*: i, TFA, CH_2Cl_2, TIPS, room temp., 1 h; ii, TFA, CH_2Cl_2, H_2O, TIPS, room temp., 4 h.

Electrospray analysis of **3** revealed a parent ion peak of 895.01 *m/z* however **3** required 897.02 *m/z*, and therefore a reported discrepancy of 2 *m/z* was found which suggested some

deuterium-hydrogen exchange had occurred. In the dipalmitoyl hydrocarbon chains of **3** the most labile deuterium atoms are located in the CD_2 groups adjacent to the ester carbonyl groups, as the carbonyl ester groups have a negative inductive effect on these CD_2 groups. Under the highly acidic deprotection conditions employed it was likely some of these CD_2 groups underwent acid catalysed exchanged with protons in the external environment (via the ester enol-tautomer (McMurry 2012)) therefore causing the electrospray mass discrepancy of 2 *m*/*z*. The extent to which the deuterium-hydrogen exchange occurred was measurable from the ^1H NMR spectrum of **3** where resonance signals of the CH_2 groups geminal to the carbonyl ester groups were found at δ_H 2.3-2.4 and integrated to ~0.3 H. This suggested ~15% of the CD_2 groups geminal to the carbonyl ester groups in **3** had exchanged with hydrogen. Such a finding suggested that strongly acidic conditions for unblocking deuterated fatty acid chain lipids should be avoided, or at least minimised.

Full characterisation and confirmation of **1**, **2**, **3** and **4**, was difficult by ^1H, ^{13}C and ^{31}P NMR as the resolved spectra had substantial signal overlaps and broad signals owing to the phospholipids forming lamellar structures thus restricting their molecular motional freedom (Pearce & Komoroski 1993). Nevertheless, ^1H NMR spectra of **1**, **2** and **3** showed no 2-cyanoethyl ester signal at δ_H 2.79 and no *tert*-butyl carbamate CH_3 signals at δ_H 1.43, therefore giving strong indication that **22a**, **22b** and **24** had all been fully deprotected. With respect to **23**, its ^1H NMR spectrum also lacked these signals, but additionally lacked signals for the THP 6-CHO_2 group at δ_H 4.62 and 4.72. Therefore the lack of these signal suggested **23** had been fully deprotected also. Electrospray analysis was also relied upon to try to confirm the presence of the correct compounds where **1**, **2**, **3** and **4** required 834.63 *m*/*z*, 860.65 *m*/*z*, 897.02 *m*/*z* and 850.63 *m*/*z*, respectively, and electrospray found high intensity parent ions of **1**, **2**, **3** and **4** of 834.65 *m*/*z*, 860.65 *m*/*z*, 895.01 *m*/*z* and 850.63 *m*/*z*, respectively. With the exception of **3**, all other compounds showed good agreement between experimental and calculated data for mass spectrometry.

Although it was difficult to characterise **1**, **2** and **3** from their ^1H, ^{13}C and ^{31}P NMR spectra, these were all consistent with the expected structures. However, the downfield signals in the ^1H and ^{13}C NMR spectra of **4** did not appear to be from a single structural isomer and suggested the presence of a possible migration product. The amide group linking the lysyl group to the aminopropane chain in **4** was designed to be a lot less labile than an ester and therefore the

ability for it to migrate to the secondary hydroxyl of the aminopropane was unlikely, especially under acidic conditions which has previously been suggested to stop lysyl migration in L-PG (Tocanne *et al.* 1974a, Yoshioka, Stella 2000). Therefore the only other possible migration product was an acid catalysed phosphate migration from the primary oxygen to the secondary hydroxyl of the aminopropane group. Previous studies have shown 2' to 3' hydroxyl phosphate migration in adenosine mono phosphate under low pH conditions (pH 2.0) due to the formation of an unstable cyclic phosphorane species (Oivanen & Lonnberg 1989). This phosphate migration was certainly possible with **4** under the highly acidic deprotection conditions employed and is demonstrated in figure 4-20.

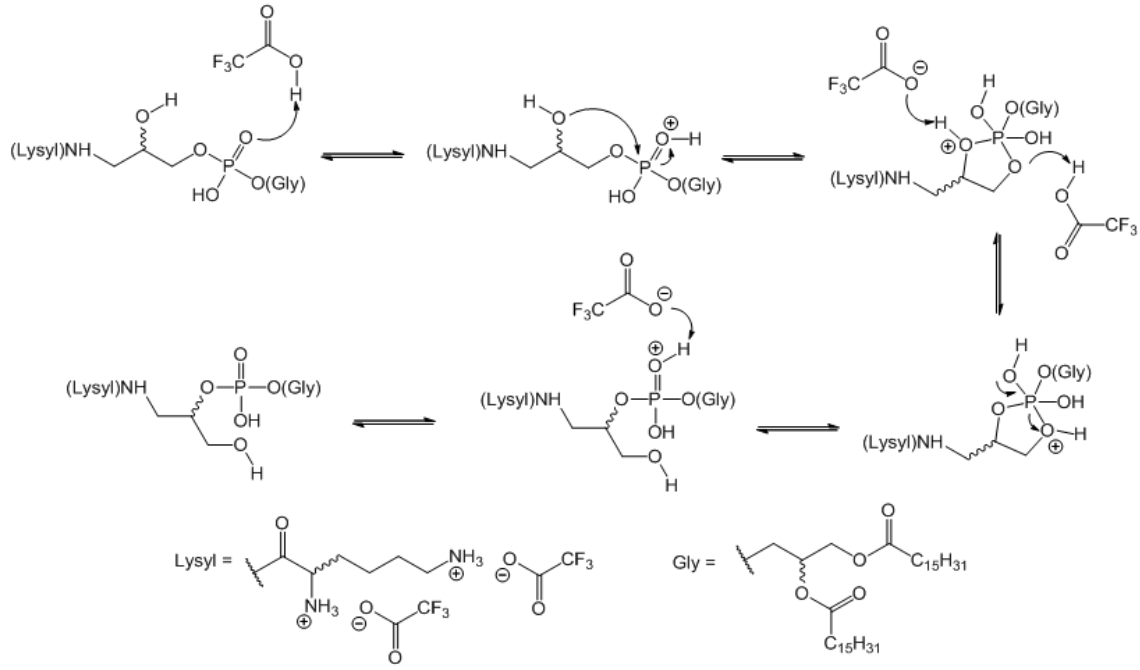

Figure 4-20 Suggested mechanism of the TFA catalysed phosphate migration in **4**.

The ^{13}C-DEPT NMR spectrum of **4** (δ_C 66–69) shown in figure 4-21 also supported the finding of a phosphate migration product in **4** where the signal at δ_C 67.3 resolved to a CH bound to a phosphate group. However the signal at δ_C 67.6 also showed the presence of a CH_2 bonded to a phosphate group.

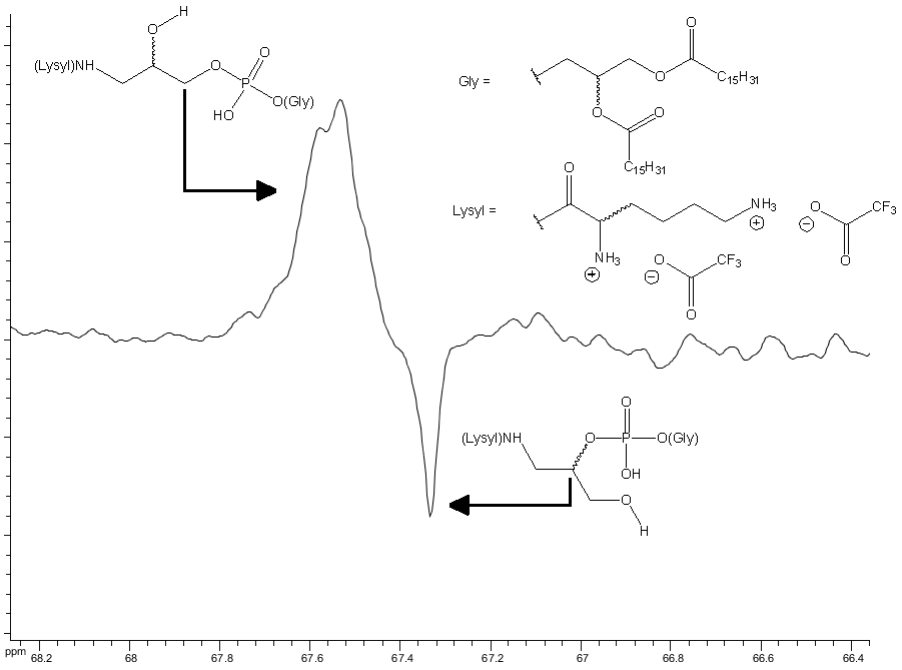

Figure 4-21 Region δ_C 66.4–68.2 of the ^{13}C-DEPT NMR spectrum of **4** (in $CDCl_3$); δ_C 67.3 aminopropane 2-***C***HOP of phosphate 2 position migration product of **4** and δ_C 67.6 aminopropane 3-***C***H_2OP of **4**.

With respect to fully protected phosphatidylglycerol **26**, after 2-cyanoethyl ester removal under basic conditions, this was followed by the addition of acetic acid (70%) and heating to 40 ℃ to remove the acetonide-acetal (Bruzik *et al.* 1986). After three hours **5** was formed as the triethylammonium salt and crystallised from cold acetone. Manufacturer's instructions (Avanti polar lipids, *USA*) of commercial **5**, which comes as the sodium salt, suggest the phospholipid to be dissolved in $CHCl_3$–methanol 2:1 v/v for greatest solubility. However, the use of mixed solvents is highly undesirable for biophysical assays due to differential solvent evaporation when preparing lamellar samples. Therefore **5** was kept as the lipophilic triethylammonium salt and to ensure all the lipid was in this salt form, excess triethylamine was added to **5** after the first crystallisation and then re-crystallised again from acetone. This salt of **5** was fully $CHCl_3$ soluble at all concentrations used in subsequent biophysical experiments.

Electrospray analysis of **5** found a high intensity negative parent ion of 783.89 *m*/*z* where **5** required 783.89 *m*/*z*. The good agreement between the experimental and predicted result showed no deuterium-hydrogen exchange occurred under the acidic conditions employed, which is in contrast to **3** where TFA caused deuterium-hydrogen exchange. The ^{1}H NMR spectrum of **5** also confirmed deprotection of **5** where no 2-cyanoethyl ester peak was observed at δ_H 2.79 and no acetal protecting group CH_3 signals were observed at δ_H 1.36 and 1.44.

4.3 Conclusion

The aim of this synthesis was to synthesise biomimetic analogues of L-PG which were not labile under mild aqueous conditions and was completed successfully with **1**, **2**, **3** and **4**. To assess the stabilities of **1**, **2**, **3** and **4**, the analogues were dispersed in a range of aqueous pH environments (pH 4.0 to 9.0) for different lengths of time and temperatures. Monitoring by TLC showed negligible changes in lipid spot development in all of the phospholipid analogues, unlike figure 4-1. An example of this is demonstrated in the developed TLC plates of **1** under numerous incubation conditions (figure 4-22).

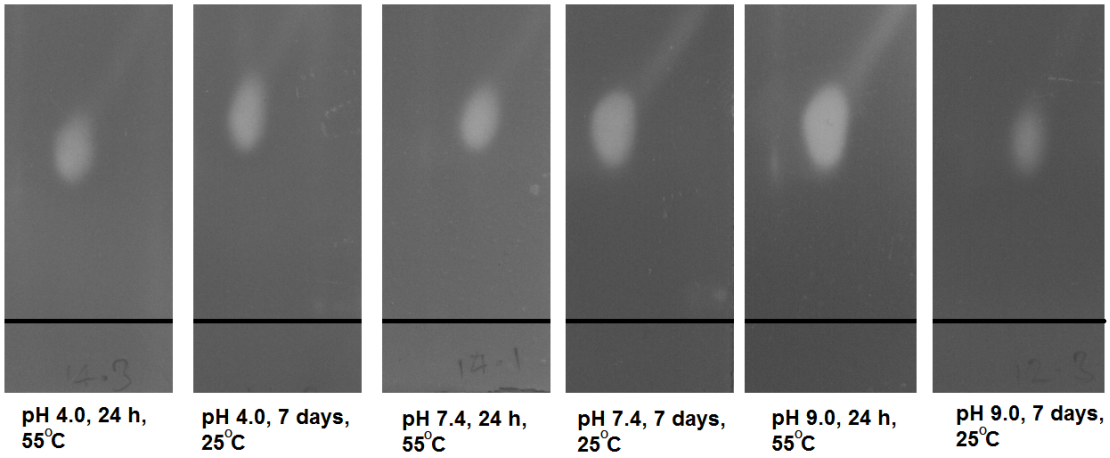

Figure 4-22 Developed TLC plates of **1** under various pH and temperature conditions over several different lengths of time. Mobile phase: $CHCl_3$–MeOH–H_2O–NH_4OH, 65:45:10:5 v/v/v/v, staining agent: $KMnO_4$ stain.

Although **1**, **2**, **3** and **4** were stable under mild aqueous conditions, several important factors have to be taken into consideration whilst using them as L-PG substitutes. Firstly, the amide bonds in **1**, **2**, **3** and **4**, as described earlier, have a different bond angle compared to the ester in L-PG and may exert some conformational constraints on **1**, **2**, **3** and **4**. Secondly, analogues **1**, **2** and **3** all lack a secondary hydroxyl group on their headgroup aminopropane chain which may reduce their lateral headgroup hydrogen bonding abilities when present with other lipids. Lastly, all chemicals used in the synthesis of **1**, **2**, **3**, **4** and **5** were racemic and have produced several diastereoisomers of each lipid whereas L-PG and PG in *S. aureus* are enantiomerically pure. Although there are caveats to be taken into account when using **1**, **2**, **3** and **4** as L-PG substitutes, these amide L-PG analogues provide a starting point to which L-PG in *S. aureus* can be studied in both biophysical and physicochemical assays, to better understand the function and role of L-PG in the plasma membrane of *S. aureus*.

To simplify the naming of **1**, **2**, **3** and **4**, the lipids were renamed 1,2-*O*-dipalmitoyl 3-aza-dehydroxy L-PG, 1-*O*-palmitoyl-2-*O*-oleoyl 3-aza-dehydroxy L-PG, D_{62}-1,2-*O*-dipalmitoyl 3-aza-dehydroxy L-PG and 1,2-*O*-dipalmitoyl 3-aza L-PG, respectively.

4.4 Materials and Methods

4.4.1 Materials

Dichloromethane (≥99.8%), pyridine (≥99%), tetra-hydrofuran (≥99.9%), diethyl ether (≥99%), acetonitrile (99.8%) and triethylamine (≥99%), were purchased from Sigma-Aldrich UK, and stored in septum sealed vessels over baked 4 Å molecular sieves also purchased from Sigma-Aldrich UK. Potassium bisulfate (≥99.9%), anhydrous magnesium sulfate (≥99.5%), *N*-(3-dimethylaminopropyl)-*N'*-ethylcarbodiimide hydrochloride (≥98%), 4-(dimethylamino)pyridine (≥99%), *N*-hydroxysuccinimide (98%), sodium bicarbonate (99.7 - 100.3%), triethylamine (≥99%), *rac*-3-amino-1,2-propanediol (97%), *tert*-butyldimethylsilyl chloride (≥95%), 3,4-dihydro-2*H*-pyran (97%), tetra-butylammonium fluoride (1M in THF), 1-*O*-benzyl-*rac*-glycerol (≥98%), palmitic acid (≥99%), 3-*O*-benzyl *rac*-glycidyl ether (99%), tetra-ethylammonium bromide (98%), oleic acid (≥99%), phosphorus trichloride (99%), chlorotrimethylsilane (≥99%), 3-hydroxypropionitrile (97%), boron trichloride solution (1M in heptane), *tert*-butyl hydroperoxide solution (6M in decane), 2-mesitylenesulfonyl chloride (99%), 1,2-*O*-isopropylidene-*rac*-glycerol (98%), trifluoroacetic acid (99%), tri-isopropylsilane (99%) and glacial acetic acid were all purchased from Sigma-Aldrich UK and used as supplied. *N,N'*-Di-Boc-*rac*-lysine, dicyclohexylammonium salt (96%) was purchased from VWR international. Pyridinium *p*-toluenesulfonate (98%) and 3-nitro-1*H*-1,2,4-triazole (96%) were purchased from VWR international and used as supplied. 3-Amino-1-propanol (97%) was purchased from Fluka AG (UK) and used as supplied. Merck silica gel 60 F_{254} plates were used for normal phase TLC. Sigma-Aldrich UK silica gel 60, particle size 40-63 µm, was used for short column normal phase chromatography; Merck silanized silica gel, particle size 0.063-0.2 mm, was used for reverse phase chromatography. Work up, TLC and chromatography reagents; ethyl acetate, dichloromethane, chloroform, ethanol, hexane, acetone, acetonitrile and methanol were all purchased from Fisher Scientific UK. TLC visualisation reagents were potassium permanganate (3 g $KMnO_4$, 20 g K_2CO_3, 5 mL 5% aq. NaOH, 300 mL H_2O) and ninhydrin (1.5 g ninhydrin, 5 mL glacial acetic acid, 500 mL 95% ethanol). TLC reagent components were all purchased at ≥95% purity from Sigma Alrich UK and used as supplied. TLC plates were

developed by heating for 60 - 120 s with a Bosch 500-2 1600W hot air gun purchased from Fisher Scientific UK. D_{31}-palmitic acid was kindly donated by Professor Robert Thomas, University of Oxford. ^{1}H and ^{19}F NMR spectra were acquired at 400.3 MHz, ^{13}C NMR at 100.7 MHz, and ^{31}P NMR at 162.1 MHz on a Bruker AV400, Germany. Chemical shift values are given in ppm, and *J* values are in *Hz*. NMR abbreviations s, d, t, q, quin, m and b stand for singlet, doublet, triplet, quartet, quintet and broad, respectively. Electrospray ionisation mass spectra were acquired on a Micromass LCT Premier. All reactions were conducted under nitrogen, at room temperature and pressure unless otherwise stated.

NMR hydrogen and carbon designations for lysine and the tetrahydropyran protecting group are as follows:

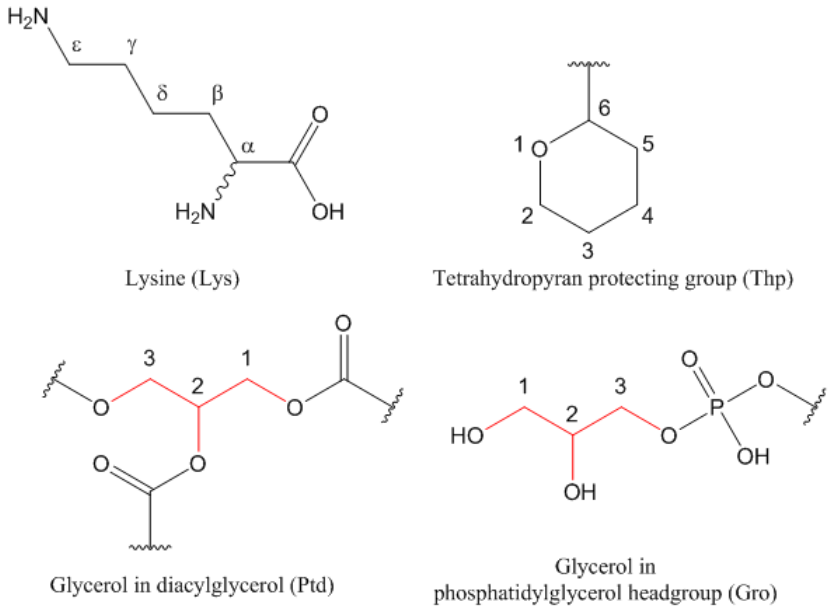

4.4.2 3-*N*-(*N'*,*N"*-Di-Boc-*rac*-lysyl)-3-aminopropan-1-ol 7

N,N'-Di-Boc-*rac*-lysine **6**, dicyclohexylamonium salt (5.54 g, 10.5 mmol) was dissolved in ethyl acetate (50 mL) and washed with aq. 0.1 M $KHSO_4$ (2 × 50 mL). The organic phase was dried ($MgSO_4$) and evaporated under reduced pressure to give a colourless foam (3.47 g, 10.0 mmol, 95%). This material was dissolved in CH_2Cl_2 (20 mL) and to the stirred solution were added *N*-(3-dimethylaminopropyl)-*N'*-ethylcarbodiimide hydrochloride (2.30 g, 12.0 mmol), 4-dimethylaminopyridine (50 mg, 0.4 mmol) and *N*-hydroxysuccinimide (1.38 g, 12.0 mmol). After 10 minutes, TLC showed no starting material remained and 3-aminopropan-1-ol (917 µL, 12.0 mmol) was added. The reaction was monitored by TLC and worked up after the presumed *N,N'*-di-Boc-*rac*-lysine succinimidyl ester could no longer be observed. The organic phase was

washed with aq. $KHSO_4$ (0.1 mM, 2 × 50 mL), sat. aq. $NaHCO_3$ (2 × 50 mL) and brine (2 × 50 mL). The organic layer was then dried ($MgSO_4$), filtered and the solvent evaporated under reduced pressure to afford the *title compound* (3.27 g, 81%) as an off-white foam. *m/z* (HR-ESI+) found $[M+Na]^+$ 426.2577, $C_{19}H_{37}N_3NaO_6$ requires 426.2580; R_f (CH_2Cl_2–EtOH, 9:1 v/v) presumed *N,N′*-di-Boc-*rac*-lysine succinimidyl ester 0.35, *title compound* 0.14; δ_H ($CDCl_3$) 1.38 (2H, quin, *J* 7.8, Lys δ-C***H₂***), 1.44 [18H, s, 2 × C(C***H***$_3$)$_3$], 1.51 (2H, quin, *J* 7.3, Lys γ-C***H₂***), 1.59-1.88 (4H, m, Lys β-C***H₂*** + Pr NCH_2C***H₂***), 3.02-3.19 (2H, m, Lys ε-C***H₂***), 3.27 (1H, bs, Pr OH), 3.43 (2H, q, *J* 6.1, Pr NC***H₂***), 3.65 (2H, q, *J* 6.1, Pr C***H₂***OH), 4.02 (1H, bq, *J* 6.9, Lys α-C***H***), 4.67 (1H, bs, Lys ε-N***H***), 5.21 (1H, bs, Lys α-N***H***), 6.68 (1H, bs, Pr N***H***); δ_C ($CDCl_3$) 22.7 (Lys δ-***C***H_2), 28.4 (3C), 28.5 (3C) [2 × C(***C***H_3)$_3$], 29.6 (Lys γ-***C***H_2), 32.0 (Lys β-***C***H_2), 32.2 (Pr NCH_2***C***H_2), 36.4 (Pr N***C***H_2), 40.0 (Lys ε-***C***H_2), 54.6 (Lys α-***C***H), 59.4 (Pr ***C***H_2OH), 79.1, 79.9 (2 × O***C***Me_3), 155.9, 156.4 (2 × carbamate ***C***=O), 173.4 (amide ***C***=O).

4.4.3 *rac*-3-*N*-(*N′,N″*-Di-Boc-*rac*-Lysyl)-aminoproprane-1,2-diol 8

N,N′-Di-Boc-*rac*-lysine **6**, dicyclohexylamonium salt (8.62 g, 16.3 mmol) was washed as described in experiment 4.4.2 to give a colourless foam (5.37 g, 15.5 mmol, 94%). This material was dissolved in ethyl acetate (30 mL) and to the stirred solution were added *N*-(3-dimethylaminopropyl)-*N′*-ethylcarbodiimide hydrochloride (3.86 g, 20.2 mmol), triethylamine (2.81 mL, 20.2 mmol) and 4-dimethylaminopyridine (50 mg, 0.4 mmol). After 1 hour *rac*-3-aminopropane-1,2-diol (1.56 mL, 20.15 mmol) was added. After a further 24 hours TLC showed the presence of one main product and none of the presumed succinimidyl ester intermediate. Ethyl acetate was then removed under reduced pressure and the residue fractionated twice by chromatography on silica gel (50 g). The column was eluted with ethyl acetate–EtOH (9:1 v/v), the appropriate fractions were combined, and evaporated under reduced pressure to give the *title compound* (2.75 g, 40%) as an off-white foam. *m/z* (HR-ESI+) found $[M+Na]^+$ 442.2511, $C_{19}H_{37}N_3NaO_7$ requires 442.2524; R_f (EtOAc–EtOH, 9 : 1 v/v) presumed *N,N′*-di-Boc-*rac*-lysine succinimidyl ester 0.72, *title compound* 0.48; four equally abundant diastereoisomers of the *title compound* were observed, resulting in several peak splits and non-integer peak integrations δ_H ($CDCl_3$–CD_3OD, 2:1 v/v) 1.40 (2H, quin, *J* 7.8, Lys δ-C***H₂***), 1.44 (9H, s), 1.45 (9H, s) [2 × C(C***H***$_3$)$_3$], 1.50 (2H, quin, *J* 7.3, Lys γ-C***H₂***), 1.61 (1H, dq, *J* 13.9, 4.6), 1.75 (1H, dq, *J* 13.9, 4.6) (Lys β-C***H₂***), 3.07 [2H, t, *J* 6.2, Lys ε-C***H₂***], 3.20-3.45 (2H, m, Pr NC***H₂***), 3.47-3.56 (2H, m, Pr

C***H₂***OH), 3.73 [1H, bquin, *J* 5.3, Pr C***H***(OH)], 4.02 (1H, t, *J* 7.3, Lys α-C***H***); δ_H ($CDCl_3$) includes 4.70 (1H, bs, Pr CH_2O***H***), 4.92 [1H, bs, Pr CH(O***H***)], 5.66 (1H, bs, Lys ε-N***H***), 6.12 (1H, bs, Lys α-N***H***), 7.65 (1H, bs, Pr N***H***); δ_C ($CDCl_3$) 22.6 (Lys δ-***C***H_2), 28.06 (3C), 28.12 (3C) [2 × C(***C***$H_3)_3$], 29.2 (Lys γ-***C***H_2), 31.9 (Lys β-***C***H_2), 39.8 (Lys ε-***C***H_2), 41.8 (Pr N***C***H_2), 54.3-54.9 (m, Lys α-***C***H), 63.30 (0.5C), 63.41 (0.5C) (Pr ***C***H_2OH), 70.34 (0.5C), 70.41 (0.5C) (Pr ***C***H(OH)), 79.91, 79.92 (2 × O***C***Me_3), 156.2, 156.8 (2 × carbamate ***C***=O), 174.1 (amide ***C***=O).

4.4.4 *rac*-1-*tert*-Butyldimethylsilyloxy-2-hydroxy-3-(*N′,N″*-di-Boc-*rac*-lysylamino)-propane 9

To a stirred solution of *rac*-3-*N*-(*N′,N″*-di-Boc-*rac*-lysyl)-3-aminoproprane-1,2-diol **8** (2.75 g, 6.56 mmol) and 4-dimethylaminopyridine (32 mg, 0.26 mmol) in CH_2Cl_2–pyridine (1:1 v/v, 15 mL), was added *tert*-butyldimethylsilyl chloride (1.19 g, 7.87 mmol) dropwise in CH_2Cl_2 (5 mL). After 60 min, TLC showed none of the starting material remained. The reaction was quenched with water (500 µL) and washed with sat. aq. $NaHCO_3$ (2 × 50 mL) and water (2 × 50 mL). The organic layer was dried ($MgSO_4$), filtered and concentrated under reduced pressure. The residue was fractionated by chromatography on silica gel (60 g) eluting with a gradient of EtOAc–hexane and the appropriate fractions (*ca.* EtOAc–hexane 7:3 v/v), were combined, and evaporated under reduced pressure to give the *title compound* (2.46 g, 70%) as a light red viscous oil. *m/z* (HR-ESI+) found $[M+Na]^+$ 556.3375, $C_{25}H_{51}N_3NaO_7Si$ requires 556.3389; R_f (EtOAc-hexane, 7 : 3 v/v) 0.38; eight equally abundant diastereoisomers of the *title compound* were observed, resulting in several peak splits and non-integer peak integrations δ_H ($CDCl_3$) 0.07 [6H, s, Tbdms Si(C***H***$_3)_2$], 0.83 [9H, s, Tbdms C(C***H***$_3)_3$], 1.38 (2H, quin, *J* 7.5, Lys δ-C***H₂***), 1.44 [18H, s, 2 × C(C***H***$_3)_3$], 1.50 (2H, quin, *J* 6.8, Lys γ-C***H₂***), 1.65 (1H, dt, *J* 13.9, 4.7), 1.80 (1H, dt, *J* 13.9, 4.7) (Lys β-C***H₂***), 3.10 (2H, bq, *J* 6.7, Lys ε-C***H₂***), 3.15-3.30 (1H, m, Pr NCH***H***), 3.45 [1H, bs, Pr CH(O***H***)], 3.49-3.67 (3H, m, Pr C***H₂***OSi + Pr NCH***H***), 3.75 [1H, bs, Pr C***H***(OH)], 4.00-4.20 (1H, m, Lys α-C***H***), 4.86 (1H, bs, Lys ε-N***H***), 5.48 (1H, bs, Lys α-N***H***), 6.89 (1H, bs, Pr N***H***); δ_C ($CDCl_3$) -5.4 (2C) [Tbdms Si(***C***$H_3)_2$], 18.3 [Tbdms ***C***$(CH_3)_3$], 22.6 (Lys δ-***C***H_2), 25.9 (3C) [Tbdms C(***C***$H_3)_3$], 28.49 (3C), 28.53 (3C) [2 × C(***C***$H_3)_3$], 29.7 (Lys γ-***C***H_2), 32.2 (Lys β-***C***H_2), 39.9 (Lys ε-***C***H_2), 42.5 (Pr N***C***H_2), 54.3-55.1 (m, Lys α-***C***H), 65.0 (Pr ***C***H_2OSi), 70.91 (0.25C), 71.03 (0.75C) [Pr ***C***H(OH)], 79.1, 79.9 (2 × O***C***Me_3), 155.9, 156.3 (2 × carbamate ***C***=O), 173.2 (amide ***C***=O).

4.4.5 *rac*-1-*tert*-Butyldimethylsilyloxy-2-(tetrahydro-2*H*-pyran-2-yloxy)-3-(*N',N''*-di-Boc-*rac*-lysylamino)-propane 10

rac-1-*tert*-Butyldimethylsilyloxy-2-hydroxy-3-(*N',N''*-di-Boc-*rac*-lysylamino)-propane **9** (2.46 g, 4.61 mmol) and 3,4-dihydro-2*H*-pyran (547 µL, 5.99 mmol) were dissolved in CH_2Cl_2 (5 mL) to which was added pyridinium *p*-toluene sulfonate (116 mg, 0.46 mmol). After stirring for 24 hours, TLC revealed one main product and none of the starting material. The solution was diluted with further CH_2Cl_2 and washed with aq. $KHSO_4$ (0.1 mM, 2 × 50 mL), then sat. aq. $NaHCO_3$ (2 × 50 mL) and brine (2 × 50 mL), dried ($MgSO_4$), filtered and the solvent was evaporated under reduced pressure. The residue was fractionated by chromatography on silica gel (50 g) eluting with a gradient of EtOAc–hexane, the appropriate fractions, (*ca.* EtOAc–hexane 50:50 v/v) were combined and evaporated under reduced pressure to give the *title compound* (2.26 g, 79%) as a red viscous oil. *m/z* (HR-ESI+) found $[M+Na]^+$ 640.3978, $C_{30}H_{59}N_3NaO_8Si$ requires 640.3964; R_f (EtOAc–hexane, 70 : 30 v/v) 0.64; eight equally abundant diastereoisomers of the *title compound* were observed, resulting in several peak splits and non-integer peak integrations δ_H ($CDCl_3$) 0.05 (1.5H, s), 0.06 (1.5H, s), 0.07 (3H, s) [Tbdms $Si(CH_3)_2$], 0.89 (4.5H, s), 0.90 (4.5H, s), [Tbdms $C(CH_3)_3$], 1.38 (2H, quin, *J* 7.7, Lys δ-CH_2), 1.44 [18H, s, 2 × $C(CH_3)_3$], 1.48-1.76 (7H, m, Thp $C^4H_2C^5H_2$ + Lys β-CH + Lys γ-CH_2), 1.76-1.94 (3H, m, Thp C^3H_2 + Lys β-CH), 2.97-3.06 (0.5H, m), 3.24-3.38 (0.5H, m) (Pr NCH), 3.11 (2H, q, *J* 6.7, Lys ε-CH_2), 3.44-3.55 (1H, m, Thp C^6H), 3.55-3.70 (2H, m, Pr NCH + Pr CHOSi), 3.70-3.85 (2H, m, Pr CHOSi + Pr CHOThp), 3.87-3.96 (0.5H, m), 3.97-4.07 (0.5H, m) (Thp C^6H), 4.12 (1H, m, Lys α-CH), 4.50-4.61 (0.5H, m), 4.68-4.74 (0.5H, m) (Thp C^2HO_2), 4.77 (1H, bt, *J* 6.2, Lys ε-NH), 5.26 (1H, bs, Lys α-NH), 6.55 (0.25H, bs), 6.61 (0.25H, bt, *J* 5.4), 7.03 (0.25H, bs), 7.07 (0.25H, bs) (Pr NH); δ_C ($CDCl_3$) -5.5 (1C), -5.4 (1C) [Tbdms $Si(CH_3)_2$], 18.28 (0.5C), 18.32 (0.5C) [Tbdms $C(CH_3)_3$], 19.8 (0.5C), 21.1 (0.25C), 21.3 (0.25C) (Thp C^4H_2), 22.6 (Lys δ-CH_2), 25.2 (0.5C), 25.3 (0.5C) (Thp C^5H_2), 25.8 (1.5C), 25.9 (1.5C) [Tbdms $C(CH_3)_3$], 28.3 (3C), 28.4 (3C) [2 × $C(CH_3)_3$], 29.7 (Lys γ-CH_2), 30.8 (0.5C), 31.3 (0.25C), 31.4 (0.25C) (Thp C^3H_2), 32.2 (0.25C), 32.4 (0.25C), 32.8 (0.25C), 33.0 (0.25C) (Lys β-CH_2), 40.0 (0.5C), 41.1 (0.25C), 41.2 (0.25C) (Pr NCH_2), 40.1 (Lys ε-CH_2), 54.5 (Lys α-CH), 62.9 (0.5C), 64.9 (0.25C), 65.1 (0.25C) (Thp C^6H_2), 64.2 (0.5C), 64.5 (0.5C) (Pr CH_2OSi), 75.2 (0.5C), 78.5 (0.25C), 79.0 (0.25C) (Pr CHOThp), 79.6 (1C), 79.8 (1C) (2 × OCMe_3), 98.3 (0.5C), 101.3

(0.25C), 101.5 (0.25C) (Thp ***C***^{2}HO), 155.6, 156.1 (2 × carbamate ***C***=O), 171.1 (0.5C), 171.8 (0.25C), 172.0 (0.25C) (amide ***C***=O).

4.4.6 *rac*-2-(tetrahydro-2*H*-pyran-2-yloxy)-3-(*N',N''*-di-Boc-*rac*-lysylamino)-propan-1-ol 11

rac-1-*tert*-Butyldimethylsilyloxy-2-(tetrahydro-2*H*-pyran-2-yloxy)-3-(*N',N''*-di-Boc-*rac*-lysylamino)-propane **10** (2.26 g, 3.66 mmol) was dissolved and stirred in THF (5 mL) at 0 °C (ice–water bath) and to this was added dropwise tetra-butylammonium fluoride (1 M, 4.5 mL, 4.39 mmol). After 10 minutes, TLC showed one main product and none of the starting material. The mixture was added to CH_2Cl_2 (50 mL) and washed with water (3 × 50 mL), dried ($MgSO_4$), filtered and the solvent was evaporated under reduced pressure. Residual tert-butyldimethylsilanol was then distilled off at 50 °C/21 mmHg to give the *title compound* (1.75 g, 95%) as a clear viscous oil. *m/z* (HR-ESI+) found $[M+Na]^+$ 526.3084, $C_{24}H_{45}N_3NaO_8$ requires 526.3099; R_f (EtOAc–hexane, 7:3 v/v) 0.11; eight equally abundant diastereoisomers of the *title compound* were observed, resulting in several peak splits and non-integer peak integrations δ_H ($CDCl_3$) 1.38 (2H, quin, *J* 8.1, Lys δ-C***H***$_2$), 1.41-1.47 [18H, s, 2 × C(C***H***$_3$)$_3$], 1.47-1.72 (7H, m, Thp C^4***H***$_2$C^5***H***$_2$ + Lys β-CH***H*** + Lys γ-C***H***$_2$), 1.72-1.91 (3H, m, Thp C^3***H***$_2$ + Lys β-CH***H***), 3.10 (2H, q, *J* 6.7, Lys ε-C***H***$_2$), 3.27-3.45 (1H, m, Pr NCH***H***), 3.45-3.68 (4H, m, Pr NCH***H*** + Pr C***H***$_2$O***H***), 3.72-3.83 (1H, m, Pr C***H***OThp), 3.89-3.96 (2H, m, Thp C^6***H***$_2$), 4.07-4.12 (1H, m, Lys α-C***H***), 4.61 (1H, dd, *J* 5.6, 3.3, Thp C^2***H***O$_2$), 4.91 (1H, bt, *J* 5.8, Lys ε-N***H***), 5.46 (1H, bs, Lys α-N***H***), 6.93 (0.25H, bt, *J* 5.9), 7.01 (0.25H, bs), 7.17 (0.5H, bt, *J* 5.3) (Pr N***H***); δ_C ($CDCl_3$) 20.4 (0.5C), 20.7 (0.25C), 20.8 (0.25C) (Thp ***C***^{4}H$_2$), 22.7 (Lys δ-***C***H$_2$), 25.1 (0.5C), 25.2 (0.5C) (Thp ***C***^{5}H$_2$), 28.4 (3C), 28.5 (3C) [2 × C(***C***H$_3$)$_3$], 29.7 (Lys γ-***C***H$_2$), 31.1 (0.5C), 31.2 (0.25C), 31.3 (0.25C) (Thp ***C***^{3}H$_2$), 32.1 (0.5C), 32.4 (0.5C) (Lys β-***C***H$_2$), 39.9 (Lys ε-***C***H$_2$), 40.6 (0.5C), 40.8 (0.5C) (Pr N***C***H$_2$), 54.6 (Lys α-***C***H), 61.7 (0.5C), 63.1 (0.5C) (Pr ***C***H$_2$OH), 64.1 (0.5C), 64.3 (0.25C), 64.5 (0.25C) (Thp ***C***^{6}H$_2$), 77.6 (0.5C), 78.5 (0.25C), 78.6 (0.25C) (Pr ***C***HOThp), 79.1, 79.9 (2 × O***C***Me$_3$), 99.1 (0.5C), 100.3 (0.5C) (Thp ***C***^{2}HO), 155.9, 156.3 (2 × carbamate ***C***=O), 173.1 (0.5C), 173.2 (0.5C) (amide ***C***=O).

4.4.7 1,2-*O*-Dipalmitoyl-3-*O*-benzyl-*rac*-glycerol 13a

1-*O*-Benzyl-*rac*-glycerol **12** (3.42 g, 18.8 mmol) was added to a stirred solution of 4-dimethylaminopyridine (114 mg, 0.94 mmol), *N*-(3-dimethylaminopropyl)-*N'*-ethylcarbodiimide

hydrochloride (9 g, 46.9 mmol) and palmitic acid (10.6 g. 41.3 mmol) in CH_2Cl_2 (30 mL). After 24 hours, TLC showed the presence of one main product and none of the starting material. The reaction solution was concentrated under reduced pressure and fractionated by chromatography on silica gel (150 g) eluting with a gradient of EtOAc–hexane, the appropriate fractions (*ca.* EtOAc–hexane 10:90 to 20:80 v/v), were combined, and evaporated under reduced pressure to give the *title compound* (10.86 g, 88%) as a white wax. *m/z* (HR-ESI+) found $[M+Na]^+$ 681.5424, $C_{42}H_{74}NaO_5$ requires 681.5429; R_f ($CHCl_3$–EtOH, 96:4 v/v) 0.81; δ_H ($CDCl_3$) 0.88 (6H, t, *J* 6.9, 2 × Palm C***H***$_3$), 1.16-1.38 [48H, m, 2 × Palm (C***H***$_2$)$_{12}$CH$_3$], 1.60 (4H, quin, *J* 7.4, 2 × Palm C***H***$_2$CH$_2$CO$_2$), 2.23 (2H, t, *J* 7.5), 2.32 (2H, t, *J* 7.5) (2 × Palm C***H***$_2$CO$_2$), 3.55-3.63 (2H, m, Ptd 3-C***H***$_2$), 4.19 (1H, dd, *J* 6.5, 11.8), 4.35 (1H, dd, *J* 3.7, 11.8) (Ptd 1-C***H***$_2$), 4.51 (1H, d, *J* 12.1), 4.56 (1H, d, *J* 12.1) (PhC***H***$_2$), 5.24 (1H, tt, *J* 3.8, 6.4, Ptd 2-C***H***), 7.25-7.37 (5H, m, C$_6$***H***$_5$); δ_C ($CDCl_3$) 14.2 (2C) (2 × Palm ***C***H$_3$), 22.7 (2C) (2 × Palm ***C***H$_2$CH$_3$), 24.92 (1C), 25.0 (1C) (2 × Palm ***C***H$_2$CH$_2$CO$_2$), 29.0-30.1 (20C) [2 × Palm (***C***H$_2$)$_{10}$CH$_2$CH$_2$CO$_2$], 32.0 (2C) (2 × Palm ***C***H$_2$CH$_2$CH$_3$), 34.15 (1C), 34.36 (1C) (2 × Palm ***C***H$_2$CO$_2$), 62.7 (Ptd 1-***C***H$_2$), 68.3 (Ptd 3-***C***H$_2$), 70.0 (Ptd 2-***C***H), 73.3 (Ph***C***H$_2$), 127.6 (2C), 127.8 (1C), 128.4 (2C), 137.7 (1C) (***C***$_6$H$_5$), 173.1 (1C), 173.4 (1C) (2 × ester ***C***=O).

4.4.8 1,2-*O*-D_{62}-Dipalmitoyl-3-*O*-benzyl-*rac*-glycerol 13b

D_{31}-palmitic acid (5.0 g. 17.4 mmol) was reacted with 1-*O*-benzyl-*rac*-glycerol **12** as described in experiment 4.4.7. The products were worked up and fractionated to give the *title compound* (4.84 g, 85%) as a white wax. *m/z* (HR-ESI+) found $[M+Na]^+$ 743.9357, $C_{42}H_{12}D_{62}NaO_5$ requires 743.9321; identical TLC, ^{1}H NMR and ^{13}C NMR spectra as 1,2-*O*-dipalmitoyl-3-*O*-benzyl-*rac*-glycerol, except ^{1}H and ^{13}C NMR lack palmitoyl CH_2 and CH_3 peaks.

4.4.9 1-*O*-Palmitoyl-2-*O*-oleoyl-3-*O*-benzyl-*rac*-glycerol 17

The synthesis and purification of 1-*O*-palmitoyl-2-*O*-oleoyl-3-*O*-benzyl-*rac*-glycerol was conducted as described by Lok C. (1978) (Lok 1978). 1-*O*-Benzyl *rac*-glycidyl ether **15** (10.77 g, 65.6 mmol) and palmitic acid (16.8 g, 65.6 mmol) were stirred with tetra-ethylammonium bromide (276 mg, 1.31 mmol) at 100 ℃ (oil bath). After 2 h, TLC showed no 1-*O*-Benzyl rac-glycidyl ether remained and the reaction mixture was then added to CH_2Cl_2 (20 mL) and stirred with 0.1 M HCl in ethanol (1mL, 0.1 mmol) until no 1,2-isomer was detected by TLC. After 4 hours, the mixture was concentrated under reduced pressure and fractionated by chromatography on silica gel (150 g), eluting with a gradient of EtOAc–hexane, the appropriate

fractions (*ca.* EtOAc–hexane 20:80 v/v), were combined, and evaporated under reduced pressure to give the putative 1-*O*-palmitoyl-3-*O*-benzyl-*rac*-glycerol **16** (16.32 g, 59%), δ_H ($CDCl_3$) 3.92-4.04 (1H, m, Ptd 2-C***H***(OH)), 3.07 (1H, bs, Ptd 2-CH(O***H***)); δ_H ($CDCl_3$) 174.1 (1 × ester ***C***=O) (Lok 1978). This material was then added to a stirred solution of 4-dimethylaminopyridine (100 mg, 0.83 mmol), *N*-(3-dimethylaminopropyl)-*N'*-ethylcarbodiimide hydrochloride (7.68 g, 40.0 mmol) and oleic acid (11.3 g. 40.0 mmol) in CH_2Cl_2 (50 mL). After 24 hours, TLC showed the presence of one main product and none of the starting material. The reaction mixture was concentrated under reduced pressure and fractionated by chromatography on silica gel (150 g) eluting with a gradient of EtOAc–hexane, the appropriate fractions (*ca.* EtOAc–hexane 10:90 to 20:80 v/v), were combined, and evaporated under reduced pressure to give the *title compound* (18.1 g, 68%) as a pale yellow oil. *m/z* (HR-ESI+) found $[M+Na]^+$ 707.5605, $C_{42}H_{76}NaO_5$ requires 707.5585; R_f ($CHCl_3$–EtOH, 99:1 v/v) 1-*O*-Benzyl *rac*-glycidyl ether 0.63, 2-*O*-Palmitoyl-3-*O*-benzyl-*rac*-glycerol 0.3, 1-*O*-Palmitoyl-3-*O*-benzyl-*rac*-glycerol 0.35, *title compound* 0.65; δ_H ($CDCl_3$) 0.88 (6H, t, *J* 6.7, Palm C***H***$_3$ + Oleoyl C***H***$_3$), 1.17-1.39 [44H, m, Palm (C***H***$_2$)$_{12}$CH$_3$ + Oleoyl (C***H***$_2$)$_4$CH$_2$CH=CHCH$_2$(C***H***$_2$)$_6$], 1.60 (4H, quin, *J* 7.7, Palm C***H***$_2$CH$_2$CO$_2$ + Oleoyl C***H***$_2$CH$_2$CO$_2$), 2.0 (4H, q, *J* 6.3, Oleoyl C***H***$_2$CH=CHC***H***$_2$), 2.27 (2H, t, *J* 7.5), 2.32 (2H, t, *J* 7.5) (Palm C***H***$_2$CO$_2$ + Oleoyl C***H***$_2$CO$_2$), 3.54-3.63 (2H, m, Ptd 3-C***H***$_2$), 4.19 (1H, dd, *J* 6.2, 12.2), 4.35 (1H, dd, *J* 3.8, 12.0) (Ptd 1-C***H***$_2$), 4.51 (1H, d, *J* 12.0), 4.56 (1H, d, *J* 12.0) (PhC***H***$_2$), 5.24 (1H, tt, *J* 4.2, 6.1, Ptd 2-C***H***), 5.29-5.40 (2H, m, Oleoyl C***H***=C***H***), 7.25-7.37 (5H, m, C$_6$***H***$_5$); δ_C ($CDCl_3$) 14.2 (2C) (Palm ***C***H$_3$ + Oleoyl ***C***H$_3$), 22.7 (2C) (Palm ***C***H$_2$CH$_3$ + Oleoyl ***C***H$_2$CH$_3$), 24.97 (1C), 24.99 (1C) (Palm ***C***H$_2$CH$_2$CO$_2$ + Oleoyl ***C***H$_2$CH$_2$CO$_2$), 27.28 (1C), 27.31 (1C) (Oleoyl ***C***H$_2$CH=CH***C***H$_2$), 28.9-30.1 (18C) [Palm (***C***H$_2$)$_{10}$CH$_2$CH$_2$CO$_2$ + Oleoyl (***C***H$_2$)$_4$CH$_2$CH=CHCH$_2$(***C***H$_2$)$_4$], 31.9 (2C) (Palm ***C***H$_2$CH$_2$CH$_3$ + Oleoyl ***C***H$_2$CH$_2$CH$_3$), 34.19 (1C), 34.28 (1C) (Palm ***C***H$_2$CO$_2$ + Oleoyl ***C***H$_2$CO$_2$), 62.7 (Ptd 1-***C***H$_2$), 68.3 (Ptd 3-***C***H$_2$), 70.0 (Ptd 2-***C***H), 73.3 (Ph***C***H$_2$), 127.7 (2C), 127.8 (1C), 128.4 (2C), 137.7 (1C) (***C***$_6$H$_5$), 129.7 (1C), 130.0 (1C) (Oleoyl ***C***H=***C***H), 172.9 (1C), 173.3 (1C) (2 × ester ***C***=O).

4.4.10 Di(2-cyanoethyl) phosphorochloridite 19

The synthesis and purification of di(2-cyanoethyl) phosphorochloridite was conducted as described by Gaffney P. (2001) (Gaffney & Reese 2001). To a stirred solution of chlorotrimethylsilane (19.2 mL, 150 mmol) in diethylether (125 mL) was added dropwise 3-hydroxypropionitrile (10.1 mL, 148 mmol) in triethylamine (21.3 mL). After 2 h, the reaction

mixture was filtered and concentrated under reduced pressure. The residue was then distilled to give 3-(trimethylsilyloxy)propionitrile (19.24 g) as a colourless liquid, bp 78–80 °C/21 mmHg. This was then dissolved in acetonitrile (65 mL) and phosphorous trichloride (5.32 mL, 61.09 mmol) was added to the stirred solution. After 2 days, the products were concentrated under reduced pressure to yield the *title compound* (13.5 g) as a colourless oil. This material was estimated by ^{31}P NMR spectroscopy to contain ~75 mol% of the *title compound*; δ_P ($CDCl_3$) 138.4 [~20%, ***P***$(O(CH2)_2CN)_3$], 165.0 [~75%, ***P***$Cl(O(CH2)_2CN)_2$], 178.8 [~5%, ***P***$Cl_2(O(CH2)_2CN$]. This material was used without further purification.

4.4.11 1,2-*O*-Dipalmitoyl-3-*O*-phosphate-*rac*-glycerol, di(2-cyanoethyl) ester 14a

To a stirred solution of 1,2-*O*-Dipalmitoyl-3-*O*-benzyl-*rac*-glycerol **13a** (1.5 g, 2.28 mmol) in CH_2Cl_2 (5 mL) was added 1M boron trichloride in heptane (5.01 mL, 5.01 mmol) dropwise over 5 min with a starting temperature of -78 °C (acetone–dry ice-bath) increased to -40 °C (acetonitrile–dry ice-bath). The reaction mixture was then washed with ice cold sat. aq. $NaHCO_3$ (2 × 50 mL), dried ($MgSO_4$), filtered and concentrated under reduced pressure. The residue was taken up in pyridine (10 mL) and to the stirred solution was then added di(2-cyanoethyl) phosphorochloridite **19** (75 mol%, 1.2 g, *ca.* 4.36 mmol). After 15 min, TLC showed none of the starting material remaining and 3-hydroxypropionitrile (100 µL, 1.41 mmol) was added. The mixture was then concentrated under reduced pressure and re-dissolved in CH_2Cl_2 (10 mL) at 0 °C (ice-water bath). 6M *tert*-butyl hydroperoxide in decane (1 mL, 6 mmol) was added to the stirred solution. After 30 min, the solution was washed with aq. sodium thiosulfate (5%, 2 × 50 mL), sat. aq. $NaHCO_3$ (2 × 50 mL) and water (2 × 50 mL). The dried ($MgSO_4$) organic layer was then filtered and evaporated under reduced pressure and the residue crystallized twice from acetonitrile to give the *title compound* (1.56 g, 91%) as a white wax. *m/z* (HR-ESI+) found $[M+Na]^+$ 777.5180, $C_{41}H_{75}N_2NaO_8P$ requires 777.5154; R_f ($CHCl_3$–MeOH, 96:4 v/v) presumed 1,2-*O*-dipalmitoyl-*rac*-glycerol 0.52, presumed 1,2-*O*-dipalmitoyl-3-*O*-phosphite-*rac*-glycerol di(2-cyanoethyl) ester 0.74, *title compound* 0.29; δ_H ($CDCl_3$) 0.88 (6H, t, *J* 6.7, 2 × Palm C***H***$_3$), 1.19-1.37 [48H, m, 2 × (C***H***$_2$)$_{12}$CH$_3$], 1.61 (2H, quin), 1.62 (2H, quin) (*J* 7.1, 2 × Palm CO_2CH_2C***H***$_2$), 2.32 (2H, t, *J* 7.5), 2.35 (2H, t, *J* 7.5) (2 × Palm CO_2C***H***$_2$), 2.80 (4H, t, *J* 6.0, 2 × C***H***$_2$CN), 4.10-4.42 (8H, m, Ptd C***H***$_2$CHC***H***$_2$ + 2 × C***H***$_2$CH$_2$CN), 5.24-5.31 (1H, m, Ptd 2-C***H***); δ_C ($CDCl_3$) 14.2 (2C) (2 × Palm ***C***H$_3$), 19.68 (1C), 19.75 (1C) (2 × ***C***H$_2$CN), 22.7 (2C) (2 × Palm ***C***H$_2$CH$_3$), 24.9 (2C) (2 × Palm CO_2CH_2***C***H$_2$), 29.0-30.0 (20C) [2 × Palm (***C***H$_2$)$_{10}$CH$_2$CH$_2$CO$_2$],

32.0 (2C) (2 × Palm ***C***$H_2CH_2CH_3$), 34.0 (1C), 34.2 (1C) (2 × Palm ***C***H_2CO_2), 61.5 (Ptd 1-***C***H_2), 62.5 (2C) (d, *J* 3.3, 2 × PO***C***H_2CH_2CN), 66.3 (d, *J* 5.0, Ptd 3-***C***H_2OP), 69.18 (0.5C), 69.23 (0.5C) (2 diastereoisomers of Ptd 2-***C***H), 116.4 (2C) (2 × ***C***≡N), 172.9 (1C), 173.3 (1C) (2 × ester ***C***=O); δ_P ($CDCl_3$) -2.4 (***P***O_4).

4.4.12 1,2-*O*-D_{62}-Dipalmitoyl-3-*O*-phosphate-*rac*-glycerol di(2-cyanoethyl) ester 14b

1,2-*O*-D_{62}-Dipalmitoyl-3-*O*-benzyl-*rac*-glycerol **13b** (3.17 g, 4.38 mmol) was treated with 1M boron trichloride in heptane (9.64 mL, 9.64 mmol), di(2-cyanoethyl) phosphorochloridite **19** (75 mol%, 2.30 g, *ca.* 8.37 mmol) and 6M *tert*-butyl hydroperoxide in decane (1.92 mL, 11.53 mmol) as described in experiment 4.4.11. The products were worked up and crystallised to give the *title compound* (3.38 g, 94.3%) as a white wax. *m/z* (HR-ESI+) found $[M+Na]^+$ 839.9023, $C_{41}H_{13}D_{62}N_2NaO_8P$ requires 839.9045; identical TLC, ^1H, ^{13}C and ^{31}P NMR spectra as 1,2-*O*-dipalmitoyl-3-*O*-phosphate-*rac*-glycerol, di(2-cyanoethyl) ester, except ^1H and ^{13}C NMR lack palmitoyl CH_2 and CH_3 peaks.

4.4.13 1-*O*-Palmitoyl-2-*O*-oleoyl-3-*O*-phosphate-*rac*-glycerol di(2-cyanoethyl) ester 18

1-*O*-Palmitoyl-2-*O*-oleoyl-3-*O*-benzyl-*rac*-glycerol **17** (2.0 g, 2.92 mmol) was treated with 1M boron trichloride in heptane (6.43 mL, 6.43 mmol), di(2-cyanoethyl) phosphorochloridite **19** (75 mol%, 1.53 g, *ca.* 5.58 mmol) and 6M *tert*-butyl hydroperoxide in decane (1.28 mL, 7.69 mmol) as described in experiment 4.4.11, with modifications. The final residue was twice crystallized from acetonitrile at -40 °C (acetonitrile–dry ice-bath) to give the *title compound* (1.20 g, 53%) as an off-white viscous oil at room temperature. *m/z* (HR-ESI+) found $[M+Na]^+$ 803.5327, $C_{43}H_{77}N_2NaO_8P$ requires 803.5310; R_f ($CHCl_3$–EtOH, 96:4 v/v) presumed 1-*O*-palmitoyl-2-*O*-oleoyl-*rac*-glycerol 0.33, presumed 1-*O*-palmitoyl-2-*O*-oleoyl-3-*O*-phosphite-*rac*-glycerol di(2-cyanoethyl) ester 0.41, *title compound* 0.20; δ_H ($CDCl_3$) 0.88 (6H, t, *J* 6.7, Palm C***H***$_3$ + Oleoyl C***H***$_3$), 1.20-1.37 [44H, m, Palm (C***H***$_2$)$_{12}$$CH_3$ + Oleoyl (C***H***$_2$)$_4$$CH_2CH$=$CHCH_2$(C***H***$_2$)$_6$], 1.60 (2H, quin, *J* 7.6), 1.62 (2H, quin, *J* 7.9) (Palm C***H***$_2$$CH_2CO_2$ + Oleoyl C***H***$_2$$CH_2CO_2$), 2.0 (4H, q, *J* 6.3, Oleoyl C***H***$_2$CH=CHC***H***$_2$), 2.31 (2H, t, *J* 7.7), 2.34 (2H, t, *J* 7.1) (Palm C***H***$_2$$CO_2$ + Oleoyl C***H***$_2$$CO_2$), 2.81 (4H, t, *J* 6.1, 2 × C***H***$_2$CN), 4.09-4.44 (8H, m, Ptd C***H***$_2$CHC***H***$_2$ + 2 × C***H***$_2$$CH_2$CN), 5.26-5.33 (1H, m, Ptd 2-C***H***), 5.31-5.40 (2H, m, Oleoyl C***H***=C***H***); δ_C ($CDCl_3$) 14.0 (2C) (Palm ***C***H_3 + Oleoyl ***C***H_3), 19.59 (1C), 19.61 (1C) (2 × ***C***H_2CN), 22.6 (2C) (Palm ***C***H_2CH_3 + Oleoyl ***C***H_2CH_3), 24.7 (2C) (Palm ***C***$H_2CH_2CO_2$ + Oleoyl ***C***$H_2CH_2CO_2$), 27.1 (2C) (Oleoyl ***C***H_2CH=CH***C***H_2), 28.8-30.1 (18C) [Palm (***C***H_2)$_{10}$$CH_2CH_2CO_2$ + Oleoyl

($\boldsymbol{C}H_2)_4CH_2CH{=}CHCH_2(\boldsymbol{C}H_2)_4$], 31.8 (2C) (Palm $\boldsymbol{C}H_2CH_2CH_3$ + Oleoyl $\boldsymbol{C}H_2CH_2CH_3$), 33.9 (1C), 34.0 (1C) (Palm $\boldsymbol{C}H_2CO_2$ + Oleoyl $\boldsymbol{C}H_2CO_2$), 61.4 (Ptd 1-$\boldsymbol{C}H_2$), 62.3 (2C) (d, *J* 3.3, 2 × PO$\boldsymbol{C}H_2CH_2CN$), 66.1 (d, *J* 5.4, Ptd 3-$\boldsymbol{C}H_2$), 68.88 (0.5C), 69.14 (0.5C) (2 two diastereoisomers of Ptd 2-$\boldsymbol{C}H$), 116.4 (2C) (2 × $\boldsymbol{C}{\equiv}N$), 129.6 (1C), 129.8 (1C) (Oleoyl $\boldsymbol{C}H{=}\boldsymbol{C}H$), 172.6 (1C), 173.0 (1C) (2 × ester $\boldsymbol{C}{=}O$); δ_P ($CDCl_3$) -2.5 ($\boldsymbol{P}O_4$).

4.4.14 Fully protected 3-*N*-lysyl-1-(1,2-*O*-dipalmitoyl-*rac*-phosphatidyloxy)-3-aminopropane 22a

1,2-*O*-Dipalmitoyl-3-*O*-phosphate-*rac*-glycerol di(2-cyanoethyl) ester **14a** (1.2 g, 1.60 mmol) was dissolved in triethylamine–CH_2Cl_2–acetonitrile (1:1:1 v/v/v; 9 mL) and stirred at room temperature. After 16 h, the mixture was concentrated under reduced pressure, re-dissolved in pyridine (5 mL) and to this solution was added 3-nitro-1*H*-1,2,4-triazole (2.30 g, 16.0 mmol) and 3-*N*-(*N'*,*N''*-Di-Boc-*rac*-lysyl)-3-aminopropan-1-ol **7** (1.0 g, 2.4 mmol). 2-Mesitylenesulfonyl chloride (2.1 g, 9.60 mmol) in CH_2Cl_2 was then added dropwise to the stirred solution over 30 min. After a further 30 min the reaction was quenched with water (50 µL) and washed with sat. aq. $NaHCO_3$ (2 × 50 mL) and brine (2 × 50 mL). The organic layer was dried ($MgSO_4$), filtered and products concentrated under reduced pressure. The residue was fractionated by chromatography on silica gel (50 g). The column was first eluted with EtOAc–hexane (50:50 to 100:0 v/v) and then EtOAc-EtOH (95:5 v/v). Appropriate fractions EtOAc-EtOH 95:5 v/v were combined, and evaporated under reduced pressure to give the *title compound* (1.15 g, 66%) as a yellow wax. *m/z* (HR-ESI+) found $[M+Na]^+$ 1109.77, $C_{57}H_{107}N_4NaO_{13}P$ requires 1109.75; R_f (EtOAc) 0.24; eight equally abundant diastereoisomers of the *title compound* were observed, resulting in several peak splits and non-integer peak integrations δ_H ($CDCl_3$) 0.88 (6H, t, *J* 6.8, 2 × Palm C$\boldsymbol{H}_3$), 1.18-1.35 [48H, m, 2 × ($C\boldsymbol{H}_2)_{12}CH_3$], 1.37-1.41 (2H, m, Lys δ-C$\boldsymbol{H}_2$), 1.44 [18H, s, 2 × C($C\boldsymbol{H}_3)_3$], 1.51 (2H, quin, *J* 7.1, Lys γ-C$\boldsymbol{H}_2$), 1.55-1.68 (5H, m, Lys β-C$\boldsymbol{H}$H + 2 × Palm C$\boldsymbol{H}_2CH_2CO_2$), 1.76-1.86 (1H, m, Lys β-C$\boldsymbol{H}$H), 1.90 (2H, quin, *J* 6.3, Pr $NCH_2C\boldsymbol{H}_2$), 2.32 (2H, t, *J* 7.4), 2.34 (2H, t, *J* 7.4) (2 × Palm C$\boldsymbol{H}_2CO_2$), 2.80 (2H, t, *J* 6.4, C$\boldsymbol{H}_2$CN), 3.11 (2H, q, *J* 6.4, Lys ε-C$\boldsymbol{H}_2$), 3.30-3.45 (2H, m, Pr NC$\boldsymbol{H}_2$), 4.04 (1H, bs, Lys α-C$\boldsymbol{H}$), 4.09-4.39 (8H, m, Ptd C$\boldsymbol{H}_2$CHC$\boldsymbol{H}_2$ + POC$\boldsymbol{H}_2CH_2CN$, Pr C$\boldsymbol{H}_2$OP), 4.72 (1H, bt, *J* 6.5, Lys ε-N$\boldsymbol{H}$), 5.20-5.32 (2H, m, Ptd 2-C$\boldsymbol{H}$ + Lys α-N$\boldsymbol{H}$), 6.74 (1H, bt, *J* 5.3, Pr N$\boldsymbol{H}$); δ_C ($CDCl_3$) 14.1 (2C) (2 × Palm $\boldsymbol{C}H_3$), 19.7 (d, *J* 7.5, $\boldsymbol{C}H_2$CN), 22.7 (3C) (2 × Palm $\boldsymbol{C}H_2CH_3$ + Lys δ-$\boldsymbol{C}H_2$), 24.9 (2 × Palm $\boldsymbol{C}H_2CH_2CO_2$), 28.37 (3C), 28.51 (3C) [2 × C($\boldsymbol{C}H_3)_3$], 28.9-30.0 (22C) [2 × Palm ($\boldsymbol{C}H_2)_{10}CH_2CH_2CO_2$ + Pr $NCH_2\boldsymbol{C}H_2$ + Lys γ-$\boldsymbol{C}H_2$], 31.9

(2C) (2 × Palm ***C***$H_2CH_2CH_3$), 32.08 (0.5C), 32.12 (0.5C) (Lys β-***C***H_2), 34.07 (1C), 34.11 (1C) (2 × Palm ***C***H_2CO_2), 35.21 (0.5C), 37.41 (0.5C) (Pr N***C***H_2), 39.49 (0.75C), 39.59 (0.25C) (Lys ε-***C***H_2), 54.5 (Lys α-***C***H), 61.6 (Pr ***C***H_2OP), 62.1-62.4 (m, ***C***H_2CH_2CN), 65.6-66.2 (m, Ptd ***C***H_2CH***C***H_2), 69.71 (0.5C), 69.79 (0.5C) (Ptd 2-***C***H), 79.1 (1C), 79.9 (1C) (2 × O***C***Me_3), 116.6 (***C***≡N), 156.2 (2 × carbamate ***C***=O), 172.6 (1C), 172.9 (1C), 173.3 (1C) (amide + 2 × ester ***C***=O); δ_P ($CDCl_3$) -1.44 (***P***O_4).

4.4.15 Fully protected 3-*N*-lysyl-1-(D_{62}-1,2-*O*-dipalmitoyl-*rac*-phosphatidyloxy)-3-aminopropane 22b

D_{62}-1,2-*O*-Dipalmitoyl-3-*O*-phosphate-*rac*-glycerol di(2-cyanoethyl) ester **14b** (1.0 g, 1.22 mmol), was treated with 3-nitro-1*H*-1,2,4-triazole (1.75 g, 12.2 mmol), 3-*N*-(*N'*,*N"*-Di-Boc-*rac*-lysyl)-3-aminopropan-1-ol **7** (0.76 g, 1.83 mmol) and 2-mesitylenesulfonyl chloride (1.6 g, 7.32 mmol) as described in experiment 4.4.14. The products were worked up and fractionated to give the *title compound* (680 mg, 49%) as a yellow wax. *m/z* (HR-ESI+) found $[M+Na]^+$ 1172.16, $C_{57}H_{45}D_{62}N_4NaO_{13}P$ requires 1172.14; identical TLC, ^1H, ^{13}C and ^{31}P NMR spectra to previous compound, except ^1H and ^{13}C NMR lack palmitoyl CH_2 and CH_3 peaks.

4.4.16 Fully protected 3-*N*-lysyl-1-(1-*O*-palmitoyl-2-*O*-oleoyl-*rac*-phosphatidyloxy)-3-aminopropane 24

1-*O*-Palmitoyl-2-*O*-oleoyl-3-*O*-phosphate-*rac*-glycerol di(2-cyanoethyl) ester **18** (1.20 g, 1.54 mmol) was treated with 3-nitro-1*H*-1,2,4-triazole (2.21 g, 15.4 mmol), 3-*N*-(*N'*,*N"*-Di-Boc-*rac*-lysyl)-3-aminopropan-1-ol **7** (0.96 g, 2.31 mmol) and 2-mesitylenesulfonyl chloride (2.6 g, 9.24 mmol) as described in experiment 4.4.14. The products were worked up and fractionated to give the *title compound* (1.06 g, 61%) as a viscous yellow oil. *m/z* (ESI+) found $[M+H]^+$ 1113.71, $C_{59}H_{110}N_4O_{13}P$ requires 1113.78; R_f (EtOAc) 0.32; eight equally abundant diastereoisomers of the *title compound* were observed, resulting in several peak splits and non-integer peak integrations δ_H ($CDCl_3$) 0.88 (6H, t, *J* 6.7, Palm C***H***$_3$ + Oleoyl C***H***$_3$), 1.17-1.35 [44H, m, Palm (C***H***$_2$)$_{12}$CH$_3$ + Oleoyl (C***H***$_2$)$_4$CH$_2$CH=CHCH$_2$(C***H***$_2$)$_6$], 1.39 (2H, m, Lys δ-C***H***$_2$), 1.44 [18H, s, 2 × C(C***H***$_3$)$_3$], 1.49 (2H, quin, *J* 6.8, Lys γ-C***H***$_2$), 1.55-1.68 (5H, m, Lys β-C***H***H + Palm C***H***$_2$CH$_2$CO$_2$ + Oleoyl C***H***$_2$CH$_2$CO$_2$), 1.75-1.85 (1H, m, Lys β-C***H***H), 1.91 (2H, quin, *J* 6.0, Pr NCH$_2$C***H***$_2$), 2.01 (4H, q, *J* 6.3, Oleoyl C***H***$_2$CH=CHC***H***$_2$), 2.32 (2H, t, *J* 7.8), 2.35 (2H, t, *J* 7.8) (Palm C***H***$_2$CO$_2$ + Oleoyl C***H***$_2$CO$_2$), 2.80 (2H, t, *J* 6.1, C***H***$_2$CN), 3.10 (2H, q, *J* 6.4, Lys ε-C***H***$_2$),

3.29-3.43 (2H, m, Pr NC***H₂***), 4.03 (1H, bs, Lys α-C***H***), 4.09-4.40 (8H, m, Ptd C***H₂***CHC***H₂*** + POC***H₂***CH_2CN, Pr C***H₂***OP), 4.78 (1H, bt, *J* 6.2, Lys ε-N***H***), 5.23-5.31 (2H, m, Ptd 2-C***H*** + Lys α-N***H***), 5.31-5.40 (2H, m, Oleoyl C***H***=C***H***); δ_C ($CDCl_3$) 14.1 (2C) (Palm ***C***H_3 + Oleoyl ***C***H_3), 19.8 (d, *J* 7.1, ***C***H_2CN), 22.7 (3C) (2 × Palm ***C***H_2CH_3 + Oleoyl ***C***H_2CH_3 + Lys δ-***C***H_2), 24.9 (Palm ***C***$H_2CH_2CO_2$ + Oleoyl ***C***$H_2CH_2CO_2$), 27.2 (1C), 27.3 (1C) (Oleoyl ***C***H_2CH=CH***C***H_2), 28.47 (3C), 28.51 (3C) [2 × C(***C***$H_3)_3$], 28.8-30.1 (20C) [Palm (***C***$H_2)_{10}CH_2CH_2CO_2$ + Oleoyl (***C***$H_2)_4CH_2(CH)_2CH_2$(***C***$H_2)_4$ + Pr NCH_2***C***H_2 + Lys γ-***C***H_2], 31.9 (3C) (Palm ***C***$H_2CH_2CH_3$ + Oleoyl ***C***$H_2CH_2CH_3$ + Lys β-***C***H_2), 33.92 (1C), 34.21 (1C) (Palm ***C***H_2CO_2 + Oleoyl ***C***H_2CO_2), 34.97 (0.5C), 36.23 (0.5C) (Pr N***C***H_2), 38.78 (0.75C), 39.90 (0.25C) (Lys ε-***C***H_2), 54.5 (Lys α-***C***H), 61.6 (Pr ***C***H_2OP), 62.1-62.4 (m, ***C***H_2CH_2CN), 65.8-66.2 (m, Ptd ***C***H_2CH***C***H_2), 68.76 (0.5C) 69.33 (0.5C) (Ptd 2-***C***H), 79.2 (1C), 79.9 (1C) (2 × O***C***Me_3), 116.6 (***C***≡N), 129.7 (1C), 130.0 (1C) (Oleoyl ***C***H=***C***H), 156.3 (2 × carbamate ***C***=O), 172.7 (1C), 173.0 (1C), 173.4 (1C) (amide + 2 × ester ***C***=O); δ_P ($CDCl_3$) -1.45 (***P***O_4).

4.4.17 Fully protected 3-aza-3-deoxy-3-*N*-lysyl-1-*O*-(1,2-*O*-dipalmitoyl-*rac*-phosphatidyl)-*rac*-glycerol 23

1,2-*O*-di-palmitoyl-3-*O*-phosphate-*rac*-glycerol di(2-cyanoethyl) ester **14a** (1.09 g, 1.45 mmol) was treated with *rac*-2-(tetrahydro-2*H*-pyran-2-yloxy)-3-(*N′,N″*-di-Boc-*rac*-lysylamino)-propan-1-ol **11** (875.2 mg, 1.74 mmol), 3-nitro-1*H*-1,2,4-triazole (2.08 g, 14.5 mmol) and 2-mesitylenesulfonyl chloride (1.9 g, 8.70 mmol) as described in experiment 4.4.14. The products were worked up and fractionated by chromatography on silica gel (50 g). The column was eluted with a gradient of EtOAc–hexane. Appropriate fractions which were eluted with EtOAc–hexane (9:1 v/v), were combined, and evaporated under reduced pressure to give the *title compound* (1.11 g, 64%) as a dark yellow wax. *m/z* (HR-ESI+) found $[M+Na]^+$ 1209.8365, $C_{62}H_{115}N_4NaO_{15}P$ requires 1209.7989; R_f (EtOAc–EtOH, 96:4 v/v) 0.81; thirty two equally abundant diastereoisomers of the *title compound* were observed, resulting in several peak splits and non-integer peak integrations δ_H ($CDCl_3$) 0.88 (6H, t, *J* 6.8, 2 × Palm C***H***$_3$), 1.17-1.35 [48H, m, 2 × CH_3(C***H***$_2)_{12}CH_2CH_2CO_2$], 1.38 (2H, m, Lys δ-C***H₂***), 1.44 [18H, s, 2 × C(C***H***$_3)_3$], 1.47-1.57 (6H, m, Lys γ-C***H₂*** + Thp C^5***H***$_2C^4$***H***HC^3***H***H), 1.57-1.71 (5H, m, 2 × Palm C***H***$_2CH_2CO_2$ + Lys β-C***H***H), 1.71-1.90 (3H, m, Lys β-C***H***H + Thp C^4***H***HC^3***H***H), 2.32 (2H, t, *J* 7.6), 2.35 (2H, t, *J* 7.6) (2 × Palm C***H***$_2CO_2$), 2.82 (2H, t, *J* 5.8, C***H***$_2$CN), 3.10 (2H, bq, *J* 6.7, Lys ε-C***H₂***), 3.38-3.62 (3H, m, Pr NC***H***$_2$ + Thp OC^6***H***H), 3.81-4.01 (2H, m, Thp OC^6***H***H + Pr NCH_2C***H***), 4.01-4.44 (9H, m, Lys

α-C***H*** + Pr C***H***$_2$OP + Ptd C***H***$_2$CHC***H***$_2$ + POC***H***$_2$CH$_2$CN), 4.62 (0.5H, s), 4.72 (0.5H, s) (1H, Thp C***H***O$_2$), 4.87 (1H, bs, Lys ε-N***H***), 5.24-5.31 (1H, m, *J* 5.0, Ptd 2-C***H***), 5.38 (1H, bs, Lys α-N***H***), 6.84 (0.25H, bs), 6.94 (0.5H, bs), 7.07 (0.25H, bs) (1H, Pr N***H***); δ_C ($CDCl_3$) 14.1 (2C, 2 × Palm ***C***H3), 19.6 (d, *J* 7.0, ***C***H$_2$CN), 19.63 (0.75C), 19.86 (0.25C) (Thp ***C***^{4}H$_2$), 22.5-23.0 (m, 3C, Lys δ-***C***H$_2$ + 2 × Palm ***C***H$_2$CH$_3$), 24.9 (2 × Palm ***C***H$_2$CH$_2$CO$_2$), 25.2 (0.5C), 25.3 (0.5C) (Thp ***C***^{5}H$_2$), 28.4 (3C), 28.5 (3C) [2 × C(***C***H$_3$)$_3$], 28.9-30.0 [2 × Palm (***C***H$_2$)$_{10}$CH$_2$CH$_2$CO$_2$ + Lys γ-***C***H$_2$], 30.8 (0.75C), 31.0 (0.25C) (Thp ***C***^{3}H$_2$), 30.8 (2C, 2 × Palm ***C***H$_2$CH$_2$CH$_3$), 31.0 (0.75C), 31.1 (0.25C) (Lys β-***C***H$_2$), 34.0 (1C), 34.2 (1C) (2 × Palm ***C***H$_2$CO$_2$), 38.8-39.2 (m, Pr N***C***H$_2$), 40.0 (0.75C), 40.5 (0.25C) (Lys ε-***C***H$_2$), 54.5 (0.75C), 54.7 (0.25C) (Lys α-***C***H), 61.7 (Ptd 1-***C***H$_2$), 62.3 (PO***C***H$_2$CH$_2$CN), 63.2 (0.75C), 64.3 (0.25C) (1C, Thp O***C***^{6}H$_2$), 65.9 (Ptd 3-***C***H$_2$), 67.7 (0.25C), 68.0 (0.75C) (1C, Pr ***C***H$_2$OP), 69.25 (0.5C), 70.01 (0.5C) (Ptd 2-***C***H), 73.7 (0.75C), 75.3 (0.25C) (1C, Pr ***C***HOThp), 78.9 (1C), 79.8 (1C) (2 × O***C***Me$_3$), 99.2 (0.75C), 100.2 (0.25C) (1C, Thp ***C***^{2}HO$_2$), 116.5 (***C***N), 155.9 (1C), 156.2 (1C) (2 × carbamate C=O), 172.3 (0.25C), 172.7 (0.75C), 172.9 (1C), 173.3 (1C) (amide + 2 × ester ***C***=O); δ_P ($CDCl_3$) -1.6 (***P***O$_4$).

4.4.18 Fully protected 1-*O*-(D_{62}-1,2-*O*-dipalmitoyl-*rac*-phosphatidyl)-*rac*-glycerol 26

D_{62}-1,2-*O*-Dipalmitoyl-3-*O*-phosphate-*rac*-glycerol di(2-cyanoethyl) ester **14a** (2.56 g, 3.13 mmol) was treated with 1,2-*O*-isopropylidene-*rac*-glycerol **25** (776 μL, 6.16 mmol), 3-nitro-1*H*-1,2,4-triazole (4.49 g, 31.3 mmol) and 2-mesitylenesulfonyl chloride (4.10 g, 18.78 mmol) as described in experiment 4.4.14. The products were worked up and fractionated by chromatography on silica gel (50 g). Eluting with a gradient of EtOAc–hexane, the appropriate fractions (*ca.* EtOAc–hexane 70:30 to 80:20 v/v) were combined and evaporated under reduced pressure to give the *title compound* (1.54 g, 64%) as a yellow wax. *m/z* (ESI+) found $[M+Na]^+$ 900.92, $C_{44}H_{20}D_{62}NNaO_{10}P$ requires 900.95; R_f (EtOAc–hexane, 50:50 v/v) 0.17; eight equally abundant diastereoisomers of the *title compound* were observed, resulting in several peak splits and non-integer peak integrations δ_H ($CDCl_3$) 1.36 (3H, s), 1.44 (3H, s), [C(C***H***$_3$)$_2$] 2.79 (2H, t, *J* 6.2, C***H***$_2$CN), 3.81 (1H, dd, *J* 5.5, 3.0, Gro 1-OC***H***H), 4.04-4.12 (3H, m, Gro 1-OC***H***H + Gro 3-C***H***$_2$OP), 4.12-4.38 (7H, m, Gro 2-OC***H*** + Ptd C***H***$_2$CHC***H***$_2$ + POC***H***$_2$CH$_2$CN), 5.21-5.29 (1H, m, Ptd 2-C***H***); δ_C ($CDCl_3$) 19.6 (d, *J* 7.2, ***C***H$_2$CN), 25.21 (1C), 26.73 (1C) [C(***C***H$_3$)$_2$], 61.5 (Ptd 1-***C***H$_2$), 62.2 (d, *J* 3.8, PO***C***H$_2$CH$_2$CN), 65.8 (Gro 1-O***C***H$_2$), 66.0 (Ptd 3-***C***H$_2$OP), 68.3 (Gro 3-***C***H$_2$OP), 69.27 (0.5C), 69.55 (0.5C) (Ptd 2-***C***H), 73.9 (d, *J* 7.5, Gro 2-O***C***H), 110.1 [***C***(CH$_3$)$_2$], 116.2 (***C***≡N), 172.9 (1C), 173.3 (1C) (2 × ester ***C***=O); δ_P -1.7 (***P***O$_4$).

4.4.19 3-*N*-Lysyl-1-*O*-(1,2-*O*-dipalmitoyl-*rac*-phosphatidyl)-3-aza-2,3-dideoxyglycerol, trifluoroacetate salt 1

Fully protected 3-*N*-lysyl-1-(1,2-*O*-dipalmitoyl-*rac*-phosphatidyloxy)-3-aminopropane **22a** (1.15 g, 1.06 mmol) was dissolved in triethylamine–CH_2Cl_2–acetonitrile (1:1:1 v/v/v; 9 mL) and stirred at room temperature. After 16 h, the products were concentrated under reduced pressure and stirred in trifluoroacetic acid–CH_2Cl_2–tri-isopropylsilane (35:30:1 v/v/v, 20 mL). After 1 h the mixture was concentrated under reduced pressure. The residue was twice crystallised from acetone at -20 °C and washed with cold acetone to give the *title compound* (1.04 g, 92%) as a white powder. *m/z* (HR-ESI+) found $[M+H]^+$ 834.65, $C_{44}H_{89}N_3O_9P$ requires 834.63; R_f ($CHCl_3$–MeOH–H_2O–NH_4OH, 65:25:3:2 v/v/v/v) 0.14; eight equally abundant diastereoisomers of the *title compound* were observed, resulting in several peak splits and non-integer peak integrations δ_H ($CDCl_3$–CD_3OD, 2:1 v/v) 0.89 (6H, t, *J* 6.6, 2 × Palm C***H***$_3$), 1.19-1.39 (48H, m, 2 × $CH_3(C\boldsymbol{H}_2)_{12}CH_2CH_2CO_2$), 1.49 (2H, quin, *J* 7.8, Lys δ-C***H$_2$***), 1.61 (4H, quin, *J* 7.4, 2 × Palm C***H***$_2CH_2CO_2$), 1.72 (2H, quin, *J* 7.3, Lys γ-C***H***$_2$), 1.78-1.90 (4H, m, Lys β-C***H***$_2$ + Pr $NCH_2C\boldsymbol{H}_2$), 2.32 (2H, t, *J* 7.2), 2.33 (2H, t, *J* 7.2) (2 × Palm C***H***$_2CO_2$), 2.95 (2H, t, *J* 6.4, Lys ε-C***H***$_2$), 3.40 (2H, d, *J* 5.9, Pr NC***H***$_2$), 3.83 (1H, t, *J* 6.5, Lys α-C***H***), 3.84 (1H, q, *J* 6.8), 3.94 (1H, q, *J* 6.8) (Pr C***H***$_2$OP), 3.99 (2H, t, *J* 5.9, Ptd 3-C***H***$_2$OP), 4.17 (1H, dd, *J* 12.3, 6.4), 4.41 (1H, dd, *J* 12.3, 2.6) (Ptd 1-C***H***$_2$), 5.18-5.26 (1H, m, Ptd 2-C***H***); δ_C ($CDCl_3$– CD_3OD, 2:1 v/v) 14.1 (2 x Palm ***C***H_3), 21.7 (Lys δ-***C***H_2), 22.8 (2 × Palm ***C***H_2CH_3), 25.0 (1C), 25.1 (1C) (2 × Palm ***C***$H_2CH_2CO_2$), 26.42 (0.5C), 26.45 (0.5C) (Lys γ-***C***H_2), 29.2-30.3 [21C, 2 × Palm $(\boldsymbol{C}H_2)_{10}CH_2CH_2CO_2$ + Pr $NCH_2\boldsymbol{C}H_2$], 30.1 (Lys β-***C***H_2), 32.1 (2 × Palm ***C***$H_2CH_2CH_3$), 34.2 (1C), 34.4 (1C) (2 × Palm ***C***H_2CO_2), 36.8 (0.75C), 37.0 (0.25C) (Pr N***C***H_2), 39.2 (Lys ε-***C***H_2), 53.1 (Lys α-***C***H), 62.8 (Ptd 1-***C***H_2), 63.68 (1C), 63.72 (1C) (Pr ***C***H_2OP + Ptd 3-***C***H_2), 70.39 (0.5C), 70.45 (0.5C) (Ptd 2-***C***H), 162.1 (2 × TFA ***C***=O), 171.3 (1C), 173.7 (1C), 174.1 (1C) (amide + 2 × ester ***C***=O); δ_F ($CDCl_3$–CD_3OD, 2:1 v/v) -76.3 (2 × TFA C***F***$_3$); δ_P ($CDCl_3$–CD_3OD, 2:1 v/v) -0.2 (***P***O_4).

4.4.20 3-*N*-Lysyl-1-*O*-(D_{62}-1,2-*O*-dipalmitoyl-*rac*-phosphatidyl)-3-aza-2,3-dideoxyglycerol, trifluoroacetate salt 3

Fully protected 3-*N*-lysyl-1-(D_{62}-1,2-*O*-dipalmitoyl-*rac*-phosphatidyloxy)-3-aminopropane **22b** (680 mg, 0.59 mmol), was treated as described in experiment 4.4.19. The products were crystallised from cold acetone to give the *title compound* (296 mg, 44%) as a white powder. *m/z* (ESI+) found $[M+H]^+$ 895.01, $C_{44}H_{27}D_{62}N_3O_9P$ requires 897.02; identical TLC, ^1H, ^{13}C, ^{19}F and

^{31}P NMR spectra to 3-*N*-Lysyl-1-*O*-(1,2-*O*-dipalmitoyl-*rac*-phosphatidyl)-3-aza-2,3-dideoxyglycerol, trifluoroacetate salt, except ^{1}H and ^{13}C NMR lack palmitoyl peaks. However, suspected ~15% acid catalysed hydrogen-deuterium exchange detected on deuterated CD_2 groups geminal to glycero-esters δ_H ($CDCl_3$–CD_3OD, 2:1 v/v) 2.34 (0.3H, s) 2.35 (0.3H, s) (Palm C***H***$_2CO_2$).

4.4.21 3-*N*-Lysyl-1-*O*-(1-*O*-palmitoyl-2-*O*-oleoyl-*rac*-phosphatidyl)-3-aza-2,3-dideoxyglycerol, trifluoroacetate salt 2

Fully protected 3-*N*-lysyl-1-(1-*O*-palmitoyl-2-*O*-oleoyl-*rac*-phosphatidyloxy)-3-aminopropane **24** (1.06 g, 1.19 mmol), was treated as described in experiment 4.4.19 with modifications. After deprotection, the residue was dissolved in ethanol (2 mL), then silanized silica (5 g) was added and then the slurry slowly diluted with water (100 mL) with gentle swirling and the mixture filtered. The silica was washed with water (2 × 100 mL) and ethanol–water (20:80 v/v, 100 mL). The product was then eluted from the silica with ethanol (20 mL) and concentrated under reduced pressure to yield the *title compound* (642.7 mg, 50%) as a white power. *m/z* (HR-ESI+) found $[M+H]^+$ 860.65, $C_{46}H_{91}N_3O_9P$ requires 860.65; R_f ($CHCl_3$–MeOH–H_2O–NH_4OH, 65:25:3:2 v/v/v/v) 0.18; eight equally abundant diastereoisomers of the *title compound* were observed, resulting in several peak splits and non-integer peak integrations δ_H ($CDCl_3$–CD_3OD, 2:1 v/v) 0.89 (6H, t, *J* 7.2, Palm C***H***$_3$ + Oleoyl C***H***$_3$), 1.19-1.40 [44H, m, Palm CH_3(C***H***$_2$)$_{12}$$CH_2CH_2CO_2$+ Oleoyl (C***H***$_2$)$_4$$CH_2(CH)_2$$CH_2$(C***H***$_2$)$_6$], 1.49 (2H, quin, *J* 7.8, Lys δ-C***H***$_2$), 1.62 (4H, quin, *J* 6.6, Palm C***H***$_2CH_2CO_2$ + Oleoyl C***H***$_2CH_2CO_2$), 1.72 (2H, quin, 7.1, Lys γ-C***H***$_2$), 1.79-1.92 (4H, m, Lys β-C***H***$_2$ + Pr NCH_2C***H***$_2$), 2.02 (4H, q, *J* 5.6, Oleoyl C***H***$_2$CH=CHC***H***$_2$), 2.32 (2H, t, *J* 7.0), 2.34 (2H, t, *J* 6.7) (Palm C***H***$_2CO_2$ + Palm C***H***$_2CO_2$), 2.95 (2H, t, *J* 7.0, Lys ε-C***H***$_2$), 3.40 (2H, t, *J* 5.1, Pr NC***H***$_2$), 3.78 (1H, t, *J* 6.5, Lys α-C***H***), 3.84-4.02 (4H, m, Pr C***H***$_2$OP + Ptd 3-C***H***$_2$OP), 4.18 (1H, dd, *J* 12.0, 6.8), 4.42 (1H, dd, *J* 12.0, 3.2) (Ptd 1-C***H***$_2$), 5.19-5.28 (1H, m, Ptd 2-C***H***), 5.31-5.39 (2H, m, Oleoyl C***H***=C***H***); δ_C ($CDCl_3$–CD_3OD, 2:1 v/v) 14.2 (2C) (Palm ***C***H_3 + Oleoyl ***C***H_3), 21.9 (Lys δ-***C***H_2), 23.0 (2C) (Palm ***C***H_2CH_3 + Oleoyl ***C***H_2CH_3), 25.19 (1C), 25.22 (1C) (Palm ***C***$H_2CH_2CO_2$ + Oleoyl ***C***$H_2CH_2CO_2$), 26.9 (Lys γ-***C***H_2), 27.50 (1C), 27.52 (1C) (Oleoyl ***C***H_2CH=CH***C***H_2), 29.1-30.5 (19C) [Palm (***C***H_2)$_{10}$$CH_2CH_2CO_2$ + Oleoyl (***C***H_2)$_4$$CH_2(CH)_2$$CH_2$(***C***$H_2$)$_4$ + Pr NCH_2***C***H_2], 31.4 (Lys β-***C***H_2), 32.2 (Palm ***C***$H_2CH_2CH_3$ + Oleoyl ***C***$H_2CH_2CH_3$), 34.4 (1C), 34.5 (1C) (Palm ***C***H_2CO_2 + Oleoyl ***C***H_2CO_2), 37.0 (0.75C), 37.2 (0.25C) (Pr N***C***H_2), 39.4 (Lys ε-***C***H_2), 53.23 (0.5C), 53.95 (0.5C) (Lys α-***C***H), 62.9 (Ptd 1-***C***H_2), 63.79

(1C), 63.84 (1C) (Pr ***C***H_2OP + Ptd 3-***C***H_2), 70.56 (0.5C), 70.69 (0.5C) (Ptd 2-***C***H), 129.8 (1C), 130.2 (1C) (Oleoyl C***H***=C***H***), 162.5 (2 × TFA ***C***=O), 170.0 (1C), 173.7 (1C), 174.1 (1C) (amide + 2 × ester ***C***=O); δ_F ($CDCl_3$–CD_3OD, 2:1 v/v) -76.4 (2 × TFA C***F***$_3$); δ_P ($CDCl_3$–CD_3OD, 2:1 v/v) -0.2 (***P***O_4).

4.4.22 3-*N*-lysyl-1-*O*-(1,2-*O*-dipalmitoyl-*rac*-phosphatidyl)-3-aza-3-deoxy-*rac*-glycerol, trifluoroacetate salt 4

Fully protected 3-*N*-lysyl-1-*O*-(1,2-*O*-dipalmitoyl-*rac*-phosphatidyl)-3-aza-3-deoxy-*rac*-glycerol **23** (1.11 g, 0.93 mmol) was dissolved in triethylamine–CH_2Cl_2–acetonitrile (1:1:1 v/v/v; 9 mL) and stirred at room temperature. After 16 h, the solution was then concentrated under reduced pressure and re-dissolved in trifluoroacetic acid–CH_2Cl_2–H_2O-triisopropylsilane (35:30:5:1 v/v/v, 25 mL). After stirring for 4 h, the solution was concentrated under reduced pressure. The residue was twice crystallised from acetone at -20 °C and washed with cold acetone to give the *title compound* (679 mg, 68%) as a white powder. *m/z* (HR-ESI+) found $[M+H]^+$ 850.63, $C_{44}H_{89}N_3O_{10}P$ requires 850.63; R_f ($CHCl_3$–MeOH–H_2O–NH_4OH, 65:25:3:2 v/v/v/v) 0.11; sixteen equally abundant diastereoisomers of the *title compound* were observed, resulting in several peak splits and non-integer peak integrations δ_H ($CDCl_3$–CD_3OD, 2:1 v/v) 0.88 (6H, t, *J* 6.9, 2 × Palm C***H***$_3$), 1.18-1.42 [48H, m, 2 × $CH_3(CH_2)_{12}CH_2CH_2CO_2$], 1.49 (2H, quin, *J* 7.7, Lys δ-C***H***$_2$), 1.62 (4H, quin, *J* 7.7, 2 × Palm C***H***$_2CH_2CO_2$), 1.72 (2H, quin, *J* 7.4, Lys γ-C***H***$_2$), 1.82-1.97 (2H, m, Lys β-C***H***$_2$), 2.32 (2H, t, *J* 7.1), 2.36 (2H, t, *J* 7.1) (2 × Palm C***H***$_2CO_2$), 2.96 (2H, t, *J* 6.2, Lys ε-C***H***$_2$), 3.30-3.48 (2H, m, Pr NC***H***$_2$), 3.76-4.03 (5H, m, Pr C***H***C***H***$_2$OP + Ptd 3-C***H***$_2$), 4.18 (1H, dd, *J* 12.6, 7.1), 4.41 (1H, dd, *J* 12.4, 2.2) (Ptd 1-C***H***$_2$), 5.18-5.25 (1H, m, Ptd 2-C***H***); δ_C ($CDCl_3$–CD_3OD, 2:1 v/v) 14.2 (2 x Palm ***C***H_3), 21.7 (Lys δ-***C***H_2), 22.9 (2 × Palm ***C***H_2CH_3), 25.12 (1C), 25.21 (1C) (2 × Palm ***C***$H_2CH_2CO_2$), 26.7 (Lys γ-***C***H_2), 29.2-30.6 [20C, 2 × Palm (***C***$H_2)_{10}CH_2CH_2CO_2$], 30.9 (0.5 C), 31.0 (0.5 C) (Lys β-***C***H_2), 32.2 (2 × Palm ***C***$H_2CH_2CH_3$), 34.48 (1C), 34.53 (1C) (2 × Palm ***C***H_2CO_2), 39.3 (Lys ε-***C***H_2), 42.2-42.5 (m, Pr N***C***H_2), 53.2 (Lys α-***C***H), 62.8-63.4 (m, Ptd 1-***C***H_2), 63.9 (d, *J* 3.8, Ptd 3-***C***H_2), 69.5 (0.625 C), 69.7 (1.375 C, d, *J* 5.2,) (Pr ***C***H***C***H_2OP), 70.5-70.9 (m, Ptd 2-***C***H), 162.6 (2 × TFA ***C***=O), 174.1 (1C), 174.4 (1C), 174.6 (1C) (amide + 2 × ester ***C***=O); δ_F ($CDCl_3$–CD_3OD, 2:1 v/v) -76.1 (2 × TFA C***F***$_3$); δ_P ($CDCl_3$–CD_3OD, 2:1 v/v) -0.2 (***P***O_4). Possible acid catalysed phosphate migration product (~35%) to secondary alcohol on aminopropan-di-ol was observed; δ_H ($CDCl_3$–MeOD, 2:1 v/v)

4.04-4.07 (1H, m, Pr C***H***OP), 4.14 (2H, d, *J* 5.3, Pr C***H₂***OH); δ_C ($CDCl_3$–CD_3OD, 2:1 v/v) 65.5 (Pr ***C***H_2OH), 67.7 (Pr ***C***HOP).

4.4.23 1-*O*-(D_{62}-1,2-*O*-dipalmitoyl-*rac*-phosphatidyl)-*rac*-glycerol, triethylammonium salt 5

Fully protected 1-*O*-(D_{62}-1,2-di-*O*-palmitoyl-*rac*-phosphatidyl)-*rac*-glycerol **26** (1.54 g, 1.75 mmol) was dissolved in triethylamine–CH_2Cl_2–acetonitrile (1:1:1 v/v/v, 21 mL) and stirred at room temperature. After 16 h, the solution was concentrated under reduced pressure and stirred in acetic acid (70%, 25 mL) at 40 °C. After 3 h, solvents were evaporated under reduced pressure. The residue was dissolved in CH_2Cl_2 (10 mL) and triethylamine (5 mL) was added dropwise to the stirred solution. The crude mixture was then concentrated under reduced pressure and crystallised twice from acetone at -20 °C to yield the *title compound* (1.26 g, 81%) as an off-white solid. *m/z* (HR-ESI-) found $[M]^-$ 783.89, $C_{38}H_{12}D_{62}O_{10}P$ requires 783.89; R_f (CH_2Cl_2–EtOH–H_2O–AcOH, 5:4:1:1 v/v/v/v) 0.5; eight equally abundant diastereoisomers of the *title compound* were observed, resulting in several peak splits and non-integer peak integrations δ_H ($CDCl_3$–CD_3OD, 2:1 v/v) 1.33 (9H, t, *J* 7.3, 3 × NCH_2CH_3), 3.13 (6H, q, *J* 7.3, 3 × NCH_2Me), 3.61 (2H, dd, *J* 2.4, 5.3, Gro 3-C***H₂***OP), 3.79 (1H, quin, *J* 5.1, Gro 2-C***H***), 3.89-3.96 (2H, m, Gro 1-C***H₂***OH), 4.00 (2H, t, *J* 5.8, Ptd 3-C***H₂***OP), 4.18 (1H, dd, *J* 7.0, 12.1), 4.41 (1H, dd, *J* 3.7, 12.1) (Ptd 1-C***H₂***), 5.21-5.28 (1H, m, Ptd 2-C***H***); δ_C ($CDCl_3$–MeOD, 2:1 v/v) 8.9 (3 × NCH_2CH_3), 46.6 (3 × NCH_2Me), 63.0 (2C, Gro 1-***C***H_2OH + Ptd 1-***C***H_2), 64.2 (d, *J* 5.0, Ptd 3-***C***H_2), 67.1 (d, *J* 6.2, Gro 3-***C***H_2OP), 70.83 (0.5C), 70.91 (0.5C) (Ptd 2-***C***H), 71.69 (0.5C), 71.76 (0.5C) (d, *J* 6.1, Gro 2-***C***H), 174.0 (1C), 174.5 (1C) (2 × ester ***C***=O); δ_P ($CDCl_3$–MeOD, 2:1 v/v) 0.6 (***P***O_4).

Chapter 5

Characterisation of 3-aza-lysyl lipids

5.1 Introduction

The lability of lysylphosphatidylglycerol (L-PG) under mild aqueous conditions (chapter 3.1) makes it unsuitable for use in biophysical experiments which are designed to determine its effects on membrane behaviour (Gould & Lennarz 1970, Danner *et al.* 2008). In order to resolve the problem of its degradation, two non-labile L-PG analogues, 3-aza-L-PG (3aLPG) and 3-aza-dehydroxy-L-PG (3adLPG), were synthesised with acyl chains of, 1,2-*O*-dipalmitoyl 3adLPG (DP3adLPG), 1,2-*O*-dipalmitoyl 3aLPG (DP3aLPG) and 1-*O*-dipalmitoyl-2-*O*-oleoyl 3adLPG (DP3adLPG) (Chapter 4). However, in order to be confident in using these analogues as L-PG substitutes, their structural and physicochemical properties needed to be determined and compared to those of native L-PG.

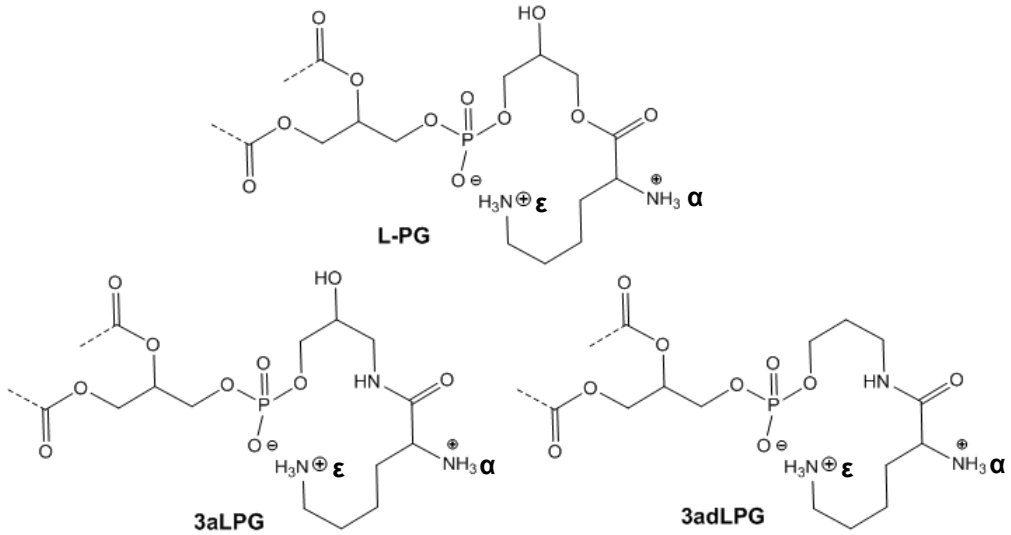

Figure 5-1 Molecular structures of the headgroups of L-PG, 3aLPG and 3adLPG.

The main difference between L-PG and both 3adLPG and 3aLPG is that the two analogues possess an amide group substituting for the ester group linking lysine to the terminal 1-CH_2 of the phosphatidylglycerol (PG) headgroup (figure 5-1). However, 3adLPG also lacks a secondary hydroxyl group along the aminopropane backbone which links its phosphate and lysine moieties together (figure 5-1). Such alterations in the headgroup structure might be expected to alter the acid-base properties of the lipids, in comparison to the native L-PG, necessitating the determination of the pKas of the ionisable groups within the analogues. For

native L-PG, the pKas of its α-amine, ε-amine and phosphate groups have been estimated by measuring the changes in lipid area per molecule when compressing L-PG monolayers on subphases ranging from pH 2.0 to pH 10.0 (Tocanne *et al.* 1974c). This same method of pKa estimation when applied to DP3aLPG and DP3adLPG, should therefore provide a means of direct comparison with the native bacterial lipid.

The phospholipids in the plasma membrane of *S. aureus* exist in the fluid L_α phase, suggesting that the physicochemical properties of the 3-aza L-PG analogues would be best studied in this phase. The most effective way to ensure that the lipids used for biophysical studies remain in the fluid phase at ambient temperatures would be to use 1-*O*-palmitoyl-2-*O*-oleoyl derivatives, whose main phase transition (T_m) is likely to be ~4 °C (Silvius 1982). However, for purposes of neutron scattering experiments it is necessary to use lipids with deuterium-labelled hydrocarbon chains in order to increase the intensity of scattering and thus improve the signal to noise ratio (Pabst *et al.* 2010). It is for this reason that a deuterated d_{62}-1,2-*O*-dipalmitoyl (d_{62}3adLPG) version of DP3adLPG was synthesised (Chapter 4), however this lipid would be expected to be in the gel ($L_{\beta'}$) phase at 25 °C (Danner *et al.* 2008). Since synthesis of a fully chain-deuterated PO3adLPG was not possible due to the non-availability of deuterated oleic acid, d_{62}3adLPG could provide a suitable alternative when studied above T_m, provided the properties of its fluid phase were comparable with those of the 1-*O*-palmitoyl-2-*O*-oleoyl version.

The main T_m of bilayers formed from the mixtures of DP3aLPG and 1,2-*O*-dipalmitoyl PG (DPPG), could be obtained using a technique such as ^{2}H-NMR to provide atomic details of lipid hydrocarbon chain order with increasing temperature (Adams *et al.* 2007). This data obtained from the ^{2}H-NMR technique could also be used to examine changes in hydrocarbon chain order in order to see how ion-pair formation between DP3aLPG and d_{62}-1,2-*O*-dipalmitoyl PG (d_{62}PG) affected bilayer hydrocarbon core viscosity. These changes in hydrocarbon core bilayer viscosity could then be related back to how ion-pairing between L-PG and PG or CL might affect the viscosity of the plasma membrane of *S. aureus* at low pH.

The high lability of L-PG under mild aqueous conditions was observed in the methicillin susceptible *S. aureus* 476 (MSSA 476) lipid extracts, where anomalous bilayer swelling was observed with increasing solvation in neutron diffraction experiments (chapter 3.3.3). The inconsistencies in bilayer swelling observed in the natural lipid extracts were attributed to L-PG

hydrolysis (chapter 3) and therefore similar swelling experiments carried out on the 3-aza analogue DP3adLPG could be used to assess its stability. The use of neutron diffraction measurements would also permit the determination of the lipid's scattering length density (SLD) profile, and provide estimates of the SLD of the lipid's headgroup and hydrocarbon core regions together with the molecular thicknesses of these two moieties along the bilayer normal.

In chapter 3.3.1 zeta potential results of multi-lamellar vesicles (MLVs) formed from *S. aureus* pH 5.5 lipid extracts showed that the lipids from strains which increased L-PG biosynthesis to ~50% of total membrane phospholipid had positive zeta potentials in a pH 5.5 buffer but negative in a pH 7.4 buffer. This change in zeta potential was attributed to the change in charge of the α-amine in L-PG (figure 5-1) where at pH 7.4 it was partially protonated but at pH 5.5 it was fully protonated (Tocanne *et al.* 1974c). Therefore, a simple way to investigate this fluctuation in zeta potential in more detail and to determine whether the α-amine in DP3adLPG behaves in an analogous manner to that of native L-PG, would be to perform zeta potential measurements on vesicles formed from DP3adLPG–DPPG mixtures in a range of buffers from pH 5.5 to 8.5.

To examine if DP3adLPG behaves in a similar fashion to L-PG in mixed monolayers containing PG and CL, synthetic replicas of the phospholipid compositions of methicillin resistant *S. aureus* G32 (MRSA G32) grown at pH 5.5 and 7.4 (chapter 2.3.1) could be readily formulated with DP3adLPG–DPPG–tetramyristoyl CL (TMCL) ratios 51.63:40:8.37 and 28.12:66.85:5.03 mol/mol/mol. The lateral compression of these synthetic monolayers could also be assessed on pH 5.5 and 7.4 subphases as a means of determining whether the substitution of L-PG with DP3adLPG could produce monolayers which behave similarly to those formed from the natural lipid extracts.

The primary aim of this study was to determine how suitable 3adLPG and 3aLPG would be as L-PG substitutes in biophysical experiments when used in conjunction with PG and CL. On the basis of this comparative study justification could then be made for the use of at least one of these analogues to replace L-PG in more detailed studies involving neutron diffraction, neutron reflectivity and small angle neutron scattering (SANS). These latter studies should then provide a better understanding of the role of L-PG in the plasma membrane of *S. aureus* for the adaptation of the bacterium to mildly acidic environments.

5.2 Materials and methods

5.2.1 Materials

Tris(hydroxymethyl)aminomethane (>99.0%), concentrated hydrochloric acid (~38%), glacial acetic acid, sodium sulphate (>99.0%), sodium hydroxide pellets (99%) and deuterium oxide (99.9%) were all purchased from Sigma-Aldrich UK, and used as supplied. Silicon discs for neutron diffraction experiments were obtained from Silicon Materials (Kaufering, Germany); diameter 50.8mm ± 0.50 mm, thickness 275 µm ± 20 µm, resistivity 1-5 Ωcm and single side polished finish. Cleaning solvents for neutron diffraction, chloroform (99.5%), methanol (99.9%) and acetone (99.9%) were all purchased from Sigma-Aldrich, international, and used as supplied. 1,1',2,2'-Tetramyristoyl cardiolipin, sodium salt, was purchased from Avanti Polar Lipids, USA, and used as supplied. 1,2-*O*-Dipalmitoyl-*sn*-glycero-3-phospho-(1'-*rac*-glycerol), sodium salt, was also purchased from Avanti Polar Lipids, USA, however was converted to the triethylammonium salt by crystallising the conjugate acid from cold acetone using 1.5 eq. HCl, then filtering off NaCl and finally crystallising the lipid-triethylammonium salt twice from cold acetone using triethylamine (>99%) purchased from Sigma-Aldrich, UK.

5.2.2 Determination of the pKas of DP3aLPG and DP3adLPG using monolayers

Both DP3aLPG and DP3adLPG were made into 1 mg/mL solutions in chloroform. To form monolayers, the lipid solutions (50 µL) were added dropwise to the surface of a 500 cm^2 (20 cm × 25 cm) NIMA technologies (Coventry, UK) KN2003 Langmuir trough containing an aqueous subphase of 10mM tris(hydroxymethyl)aminomethane (TRIS)–glacial acetic acid (AcOH) 1:1 mol/mol adjusted to either pH 2.0, 4.0, 5.5, 7.0, 8.0 or 9.0 with concentrated HCl or NaOH beads. The lipid monolayer was then equilibrated for 15 min to allow all the chloroform to evaporate and surface pressure–area isotherms were then measured at 23.4 °C through ten cycles. The barrier opening and closing speeds were set to 25 cm^2/min with a maximum surface pressure of 45 mN/m and a minimum surface pressure of 0 mN/m. The mean area per molecule of each lipid solution on each different subphase was recorded by taking the tangent from the surface pressure–area isotherm at 30 mN/m and extrapolating it back to the x-ordinate. The pKa value of each lipid's α-ammonium group was obtained by fitting a Voigt area function (eq. 24) to the maxima and minima of the titration curves between pH 5-8. The pH range between the maxima and minima provided the pKa of the α-ammonium (Tocanne *et al.* 1974c*)*.

5.2.3 Neutron diffraction of 100% DP3adLPG

One silicon disc was prepared for neutron diffraction by initially cleaning it by 5 min of bath sonication (Branson bath sonicator 3510, Danbury, USA) in chloroform, then acetone and then methanol, and finally treating it under UV light for 30 min with a UV/Ozone ProCleaner™ Plus (BioForce Nanosciences, Ames, USA). Orientated multilayers of 10 mg of DP3adLPG was then prepared for neutron diffraction by evenly coating this lipid on to the polished side of the silicon disc as a 1 mL chloroform solution, as described in chapter 3.2.6. Neutron diffraction was then performed on the sample at 25 °C with contrasts D_2O and H_2O, using the D16 neutron diffractometer at the Institut Laue-Langevin (Grenoble, France) at λ = 4.741 Å. Strong reflections were measured for short times (~30 min) whereas weaker ones were measured for ~2-3 hours to improve signal-noise of the higher orders of diffraction. Different sample humidities were employed by enclosing the sample in a sealed aluminium chamber with an outer temperature of 25 °C and heating a solvent reservoir at the bottom of the chamber up to 25 °C in increments of 0.5 °C to 1 °C from a starting temperature of 23 °C. The neutron diffraction profiles (Intensity vs. 2θ) collected for the sample were then fitted with an exponential function using Sigmaplot V 12.0 (Systat Software, San Jose, California, USA) to remove

background scattering as described in chapter 3.2.6. D-spacing calculations, and Fourier transformation of the sample neutron diffraction profile, was then performed using eq. (24-26) (chapter 3.2.6). All structure factors and assigned signs of the structure factors are published in Appendix AI.II.

5.2.4 ^{2}H Quadrupole echo NMR of mixtures of DP3adLPG and d_{62}PG

Mixtures of DP3adLPG–d_{62}PG 2:8, 3:7, 4:6 and 65:35 mol/mol (5 mg) were each dissolved in 5mL of chloroform. The lipid solutions were then evaporated to dryness under reduced pressure and re-suspended, by vortex mixing, in 1 mL of 10 mM TRIS–AcOH 1:1 mol/mol adjusted to pH 5.5 with concentrated HCl. Multi-lamellar vesicles (MLVs) of the lipid films were then formed by freeze-thaw cycling (-200 °C to 50 °C) five times using a liquid nitrogen bath and a warmed water bath. The MLVs were then centrifuged with a Beckman Coulter Microfuge (California, USA) for 30 min at 13,000 rpm and the supernatant was discarded. All of the MLV pellets formed were then examined by ^{2}H quadrupole echo NMR at 61.46 MHz on a Bruker Advance 400 NMR spectrometer using a 4 mm CP-MAS probe, at a spectral width of 100 KHz and with recycle delay, echo delay, acquisition time and 90º pulse lengths of 0.25 s, 100 µs, 2.6 ms and 3 µs respectively. The temperature was increased from 25 °C to 55 °C in increments of 1 °C. Spectra were zero filled to 1k points and 50 Hz exponential line-broadening was applied. Smoothed deuterium order parameter profiles were obtained from symmetrised and dePaked ^{2}H NMR powder spectra of d_{62}PG using published procedures (Schafer *et al.* 1995, Sternin *et al.* 1983, Davis 1983, Seelig, A. & Seelig, J. 1974) and Amix software (Bruker Karlsruhe, Germany). Order parameters of the lipid hydrocarbon chains (S_{CD}) were then calculated from the dePaked ^{2}H-NMR spectra using eq. (11) in chapter 1.6 (Vermeer *et al.* 2007).

5.2.5 Zeta potential measurements of vesicles composed of different molar ratios of DP3adLPG and DPPG

In triplicate, lipid mixtures of 500 µg of DP3adLPG–DPPG 4:6, 42:58, 44:56, 46:54, 48:52, 49:51, 51:49, 52:48, 53:47, 54:46, 55:45, 56:44, 58:42 and 6:4 mol/mol were each dissolved in 5mL of chloroform. Each lipid solution was then dried under reduced pressure and the resultant lipid films were dispersed, by vortex mixing, in 2.5 mL of either pH 5.5, 7.4 or 8.5 10mM TRIS–AcOH 1:1 mol/mol buffer. Each vesicle dispersion was probe sonicated (Soniprobe Lukas-Dawe Ultrasonics, UK) for 10 min at 26 °C to reduce the vesicle size and

polydispersity. Zeta potential measurements (Zetasizer nano ZS, Malvern, USA) were taken for each sample at 25 °C and 55 °C using Zetasizer custom software v7.03 (Malvern, Worcester, UK). Due to the effect of temperature on buffer pH, 100 mL solutions of pH 5.5, 7.4 or 8.5 10 mM TRIS–AcOH 1:1 mol/mol buffers were made for each dispersion of the vesicles and examined at 25 °C and 55 °C with appropriate pH adjustments made using concentrated HCl or NaOH beads to ensure the vesicle pH environments were the same at both temperatures.

5.2.6 Synthetic monolayers of biomimetic ratios of MRSA G32 phospholipids from the bacterium grown at pH 5.5 and 7.4

Ternary mixtures of 5 mg of DP3adLPG–DPPG–TMCL 51.63:40:8.37 and 28.12:66.85:5.03 mol/mol/mol were each dissolved in 5 mL of chloroform. To form monolayers, the lipid solutions (50 µL) were added dropwise to a NIMA technologies (Coventry, UK) KN2003 Langmuir trough, containing an aqueous subphase of TRIS–AcOH 1:1 mol/mol adjusted to either pH 5.5 or 7.4 with concentrated HCl. Surface pressure–area isotherms were then measured at 23 °C and analysed as described above (5.2.2). Compressional moduli (K^s) of each monolayer were calculated using eq. (23) in chapter 3.2.2. In order to quantitatively assess the lipid interactions in each monolayer, the excess area function (A_{ex}) (Gaines 1966) was calculated using:

$$A_{ex} = \text{ƺ} - (A_1x_1 + A_2x_2 + A_3x_3) \tag{28}$$

Where, ƺ is the experimentally determined area per molecule (Å^2), A_i is the experimental area per molecule of the individual lipids (Å^2) and x_i is the mol fraction of each lipid present in the ternary mixture.

5.2.7 Small angle neutron scattering (SANS) of mixtures of DP3adLPG–DPPG, and PO3adLPG–POPG

Vesicles dispersions (~2 mg/mL) composed of DP3adLPG–DPPG and PO3adLPG–POPG in the molar ratios of 2:8, 3:7, 4:6 and 65:35 were prepared in D_2O using the thin film solvation method described above (5.2.5). SANS data for all samples were then obtained on the LoQ small-angle diffractometer at the ISIS Pulsed Neutron Source (STFC Rutherford Appleton Laboratory, Didcot, U.K.). This is a fixed-geometry “white beam” time-of-flight instrument which utilises neutrons with wavelengths, λ, between 0.2 and 1 nm. Data were

simultaneously recorded on two, two-dimensional, position-sensitive, neutron detectors, to provide a simultaneous Q range of 0.08–16 nm^{-1}. Each sample, including one to measure the background scattering of D_2O was placed in a 2 mm pathlength quartz cell (Starna scientific, Hainault, UK) and was measured for a total of 12.5 mAh with an incident neutron flux of 160 μA. Each raw scattering data set was then corrected for the detector efficiencies, sample transmission and background scattering and converted to scattering cross-section data ($\partial\Sigma/\partial\Omega$ vs Q) using the instrument-specific software Colette (Rutherford Appleton Laboratories 2007). These data were placed on an absolute scale (cm^{-1}) using the scattering from a standard sample (a solid blend of hydrogenous and perdeuterated polystyrene). All 1,2-*O*-dipalmitoyl lipid vesicle samples were examined at 25 °C and 55 °C to assess the vesicle characteristics above and below the lipid T_m and all 1-*O*-palmitoyl-2-*O*-oleoyl lipid vesicle samples were assessed at 25 °C only. The scattering curves obtained were fitted with the software FISH using a monodisperse sheet model for samples containing only unilamellar vesicles and a one-dimensional multilayer stack model for multi-lamellar vesicle samples (Heenan 2009, Kotlarchyk & Chen 1983). Both fitting alogorithms view the vesicle bilayers as continous flat lamellar sheets which can be stacked (one-dimensional multilayer stack model). Data points are fitted along a line of best fit by the algorithms using a least squares function which then gives bilayer parameters.

5.3 Results and Discussion

5.3.1 Determination of the pKas of DP3aLPG and DP3adLPG using monolayers

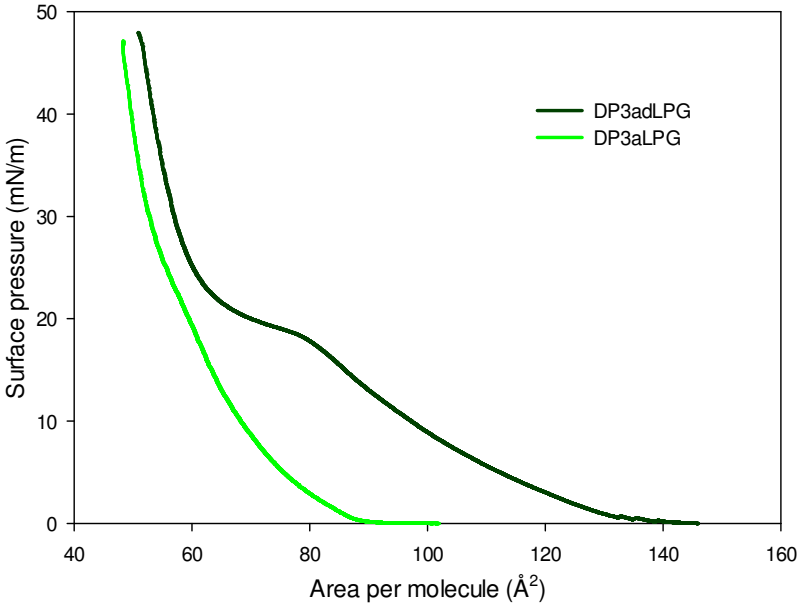

Figure 5-2 Mean surface pressure–area isotherms of DP3adLPG and DP3aLPG on a pH 7.0 subphase

The shapes of the isotherms of DP3adLPG and DP3aLPG were markedly different from one another as shown in figure 5-2. These isotherm shapes of DP3adLPG and DP3aLPG were consistent for each lipid on all of the pH subphases used, and in particular, the isotherms of DP3aLPG closely resembled the shape of the isotherm previously published for L-PG (Tocanne *et al.* 1974c). The DP3adLPG isotherm shown in figure 5-2 displayed the presence of a large liquid expanded phase (L_e) which then plateaued at ~85 Å^2 and then began to rise again to a liquid condensed phase (L_c) after ~70 Å^2. This plateau region in the isotherm of DP3adLPG suggested the monolayer co-existed in both L_c and L_e phases between 70-85 Å^2 (Gaines 1966). The reason DP3adLPG possessed an L_c/L_e phase between 70-85 Å^2 appeared to be due to the lack of a secondary hydroxyl group along its aminopropane linker molecule between lysine and phosphate, as the isotherm of DP3aLPG did not show this intermediate L_c/L_e phase (figure 5-2). Therefore, it is likely the lack of a secondary hydroxyl group in DP3adLPG reduces hydrogen bonding between neighbouring DP3adLPG headgroups and reduces its headgroup hydration which is likely to have made the monolayer more resistant to lateral compression thus causing the L_c/L_e phase shown in figure 5-2. This reduction in headgroup hydrogen bonding and hydration of DP3adLPG was also reflected in its isotherm being at higher molecular areas

compared to DP3aLPG (figure 5-2), which suggested the aminopropane secondary hydroxyl group is important for DP3aLPG to pack more closely together on a monolayer.

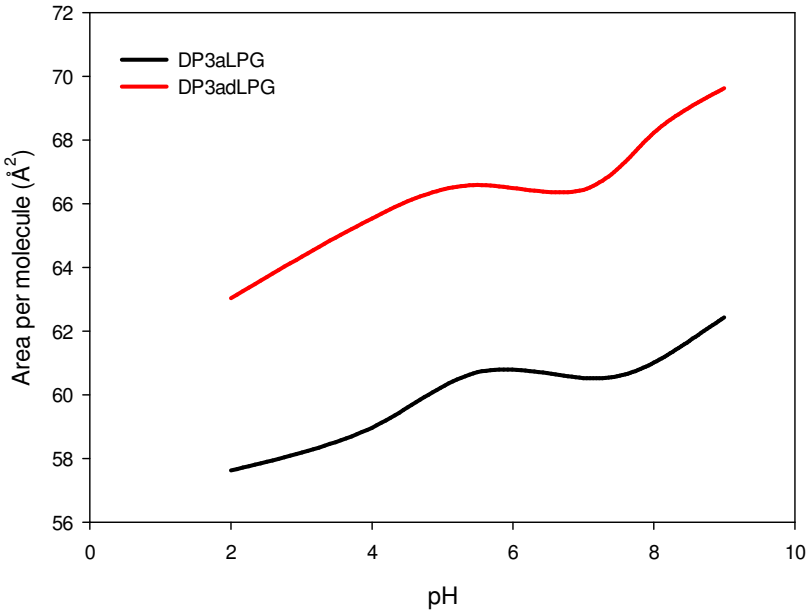

Figure 5-3 pH titration curves of DP3adLPG and DP3aLPG.

Both pH titration curves of DP3adLPG and DP3aLPG shown in figure 5-3 were analogous in shape and were also similar to the shape of the pH titration curve of L-PG with the same buffering system (figure 1-5, chapter 1.2) (Tocanne *et al.* 1974c). The pH titration curve of DP3aLPG showed the presence of a maxima at pH 6 and a minima at pH 7 which demonstrated the pKa of the α-amine in this lipid was the same as L-PG (~6-7) (Tocanne *et al.* 1974c). However, the pH titration curve of DP3adLPG in figure 5-3 varied slightly in comparison to L-PG and DP3aLPG where a maxima was observed at pH 5.5 and a minima at pH 6.7 (figure 5-3). Therefore the estimated pKa of the α-amine in DP3adLPG was slightly lower than DP3aLPG and LPG, between 5.5 and 6.7. The cause of the more acidic α-amine in DP3adLPG is unknown, as this amine should have been more basic than the α-amines in DP3aLPG and L-PG due to the lack of a secondary hydroxyl group in DP3adLPG, which normally forms hydrogen bonds to the lone pair of electrons on the α-amine in native L-PG.

The conformation of the headgroup of L-PG has previously been suggested to be in a loop structure due to the formation of an internal ionic bond between one of the lipid's protonated amines and the phosphate group (El Mashak & Tocanne 1979). This internal ionic bond in L-

PG effectively shields the anionic charge on the phosphate group of the lipid. At pHs greater than 7, the α-amine (pKa ~6-7) of L-PG would presumably become uncharged and therefore the internal ionic bond in L-PG would be formed between the protonated ε-amine and phosphate (Tocanne *et al.* 1974c). Due to the structural similarities between L-PG and both DP3adLPG and DP3aLPG it is possible the same internal ionic bond exists in both DP3adLPG and DP3aLPG at pHs greater than 7. Therefore to examine the pKa of the ε-amine in DP3adLPG and DP3aLPG, the pH of the lipid monolayers was increased above pH 7 (figure 5-3). Above pH 7 a sharp rise in lipid area per molecule was observed for both DP3adLPG and DP3aLPG and this increase in lipid area per molecule continued up until pH 9. This suggested that at pHs greater than 7 the ε-amine group in both DP3adLPG and DP3aLPG gradually became deprotonated as the lipid areas became larger as a result of phosphate anionic charge repulsion between neighbouring DP3adLPG or DP3aLPG molecules. Therefore the ε-amine in both DP3adLPG and DP3aLPG can be assumed to have a pKa greater than 9, which is consistent with the pKa of the ε-amine in L-PG (~10) (Tocanne *et al.* 1974c). With respect to the pKa of the phosphate group in both DP3adLPG and DP3aLPG, figure 5-3 showed that below pH 6 the lipid area per molecule of both monolayers declined until pH 2. Protonation of the phosphate group in both DP3adLPG and DP3aLPG would result in an increase in lipid area per molecule of both lipid monolayers as the lipid headgroups would possess a charge of +2 and therefore lipid-lipid headgroup electrostatic charge repulsion would be high. Therefore the pKa of the phosphate group in both DP3adLPG and DP3aLPG was likely to be <2, which was also consistent with the pKa of the phosphate group in L-PG (between 1 and 3) (Tocanne *et al.* 1974c).

5.3.2 Neutron diffraction of 100% DP3adLPG

Formation of orientated multilayers with only DP3adLPG was difficult to achieve as the lipid headgroups were presumably cationically charged and therefore electrostatic charge repulsion between neighbouring lipids would have been high resulting in an unstable bilayer (Hanke *et al.* 1993). However, neutron diffraction of 100% DP3adLPG showed the presence of a repeating lamellar structure with four orders of neutron diffraction (figure 5-4).

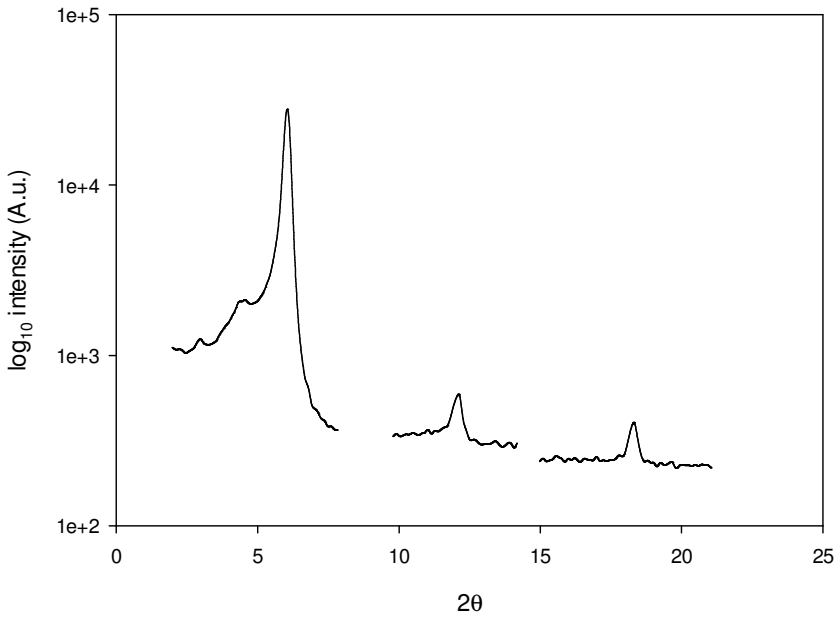

Figure 5-4 Neutron diffraction profile of the four orders of neutron diffraction of DP3adLPG at 100% humidity in a D_2O contrast.

The calculated mean d-spacing of the repeating lamellar structure in figure 5-4 was ~90 Å which was low in comparison to bilayers formed from charged lipids mixed with uncharged lipids (Pozo Navas *et al.* 2005). This low d-spacing suggested that 100% DP3adLPG in the $L_{\beta'}$ phase forms an interdigitated bilayer, which has previously been observed with 100% DPPG and 100% 1,2-*O*-dipalmitoyl L-PG (DPL-PG) in the $L_{\beta'}$ phase (Danner *et al.* 2008, Ranck *et al.* 1977). The formation of an interdigitated bilayer by DP3adLPG would presumably create a lamellar structure with a low thickness and therefore the calculated ~90 Å d-spacing from figure 5-4 was likely to contain a large water layer which is consistent with the large water layers found between charged bilayers (Pozo Navas *et al.* 2005). Figure 5-4 also detected the presence of a small peak at ~2.24° which was next to the second order peak of DP3adLPG. This peak at ~2.24° reduced in intensity and did not change in angle as the sample humidity was increased. Therefore this peak was attributed to a non-lamellar phase structure being present in the 100% DP3adLPG which has previously been observed in X-ray diffraction of DPL-PG in the $L_{\beta'}$ phase (Danner *et al.* 2008).

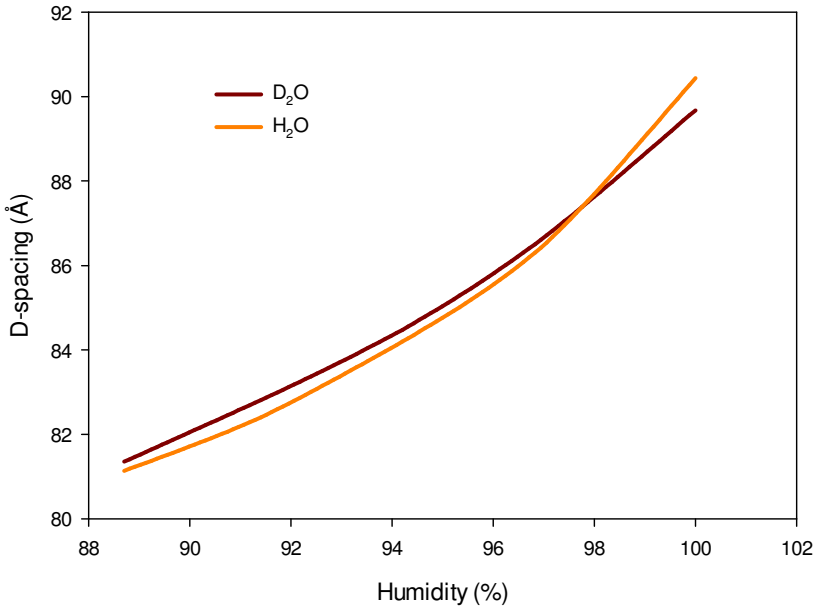

Figure 5-5 D-spacing profiles of 100% DP3adLPG at increasing humidity in both H_2O and D_2O contrasts.

The swelling behaviour of 100% DP3adLPG with increasing humidity (figure 5-5) showed a typical exponential relationship between d-spacing and humidity which was consistent with the normal swelling behaviour of phospholipid bilayers with increasing humidity (Darkes & Bradshaw 2000). This conventional swelling behaviour of the DP3adLPG interdigitated phase suggested that DP3adLPG was stable in this environment and that it was unlikely to be subject to chemical degradation.

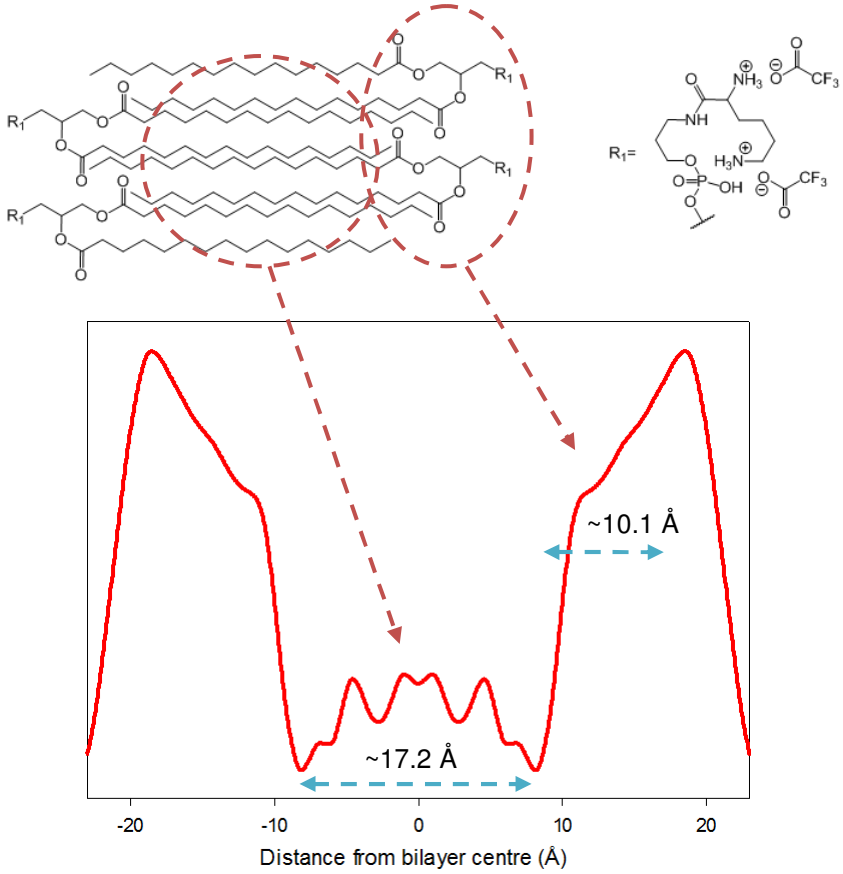

Figure 5-6 SLD profile of DP3adLPG at 100% humidity with a molecular schematic to show the possible structure of the interdigitated phase.

The formation of bilayers from dipalmitoyl phospholipids tend to show a hydrocarbon region thickness of >30 Å in the $L_{\beta'}$ phase and in neutron diffraction this is associated with a high intensity SLD negative minima at the bilayer centre as a result of the negative coherent scattering from the dipalmitoyl terminal CH_3 groups (Leonard *et al.* 2001, Buldt *et al.* 1979, Fragneto *et al.* 2000). However, the SLD profile of 100% DP3adLPG in figure 5-6 showed the hydrocarbon region of DP3adLPG to have a thickness of ~17.2 Å, with symmetrical negative SLD minima at ~8.6 Å from the bilayer centre, which validated the earlier suggestion that DP3adLPG on its own forms an interdigitated bilayer. With respect to the headgroup region of DP3adLPG, a thickness of ~10.1 Å was found (figure 5-6) which was consistent with the headgroup conformation of DP3adLPG being in a loop structure as a result of the internal ionic bond between the lipid's protonated α or ε-amine and the lipid's phosphate group (Armen *et al.* 1998). This putative conformation of the headgroup of DP3adLPG suggested that both the headgroups of L-PG (El Mashak & Tocanne 1979) and DP3adLPG exist in the same conformation which shows that the substitution of an ester in L-PG for the more rigid amide in DP3adLPG does not restrict the freedom of movement of the protonated amines in DP3adLPG

in order to form ionic bonds with the lipid's phosphate group. Therefore with respect to examining the headgroup characteristics of L-PG in biophysical assays, DP3adLPG may serve as a suitable substitute.

5.3.3 Thermal properties of mixtures of DP3adLPG and d_{62}PG

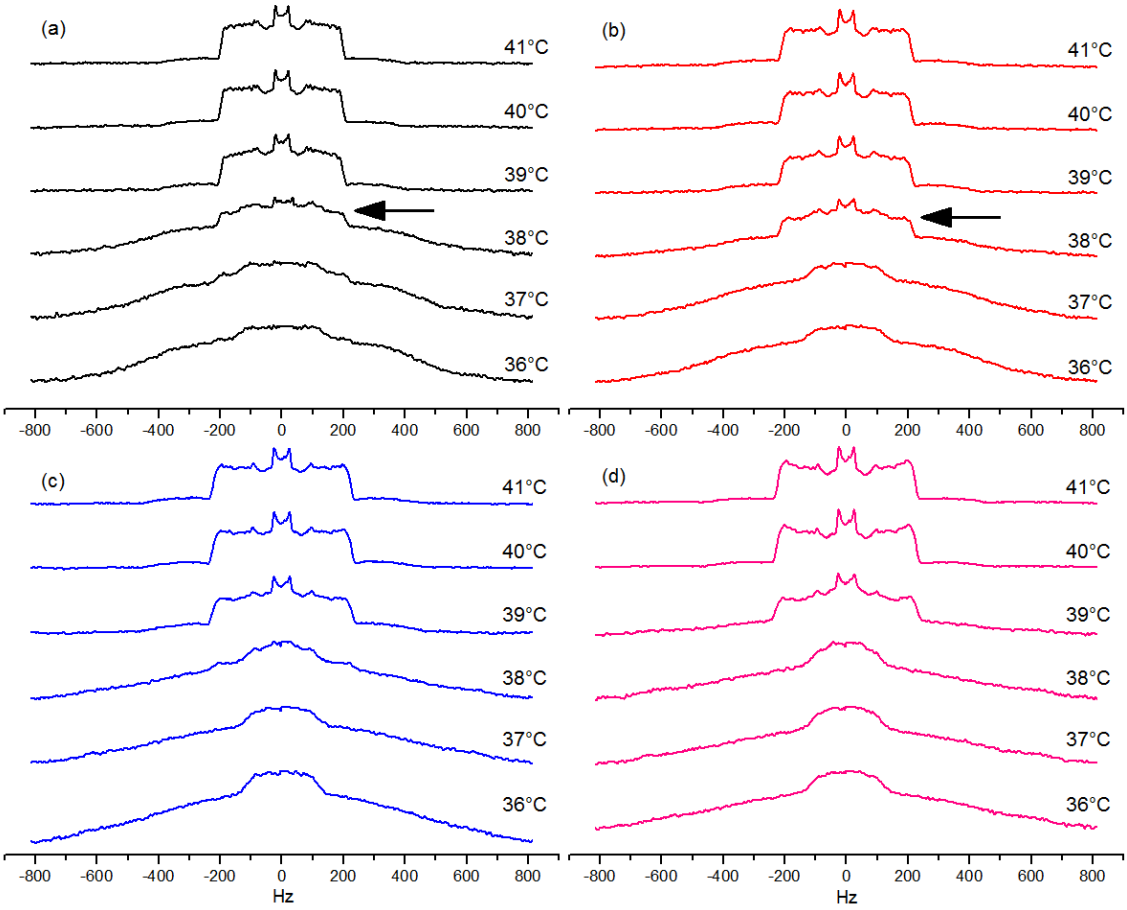

Figure 5-7 ^{2}H NMR spectra of 90°-oriented multi-bilayers consisting of mixtures of DP3adLPG–d_{62}PG (a) 2:8 (b) 3:7 (c) 4:6 and (d) 65:35 mol/mol. Arrows highlight the co-existence of both $L_{\beta'}$ and L_{α} phases in the lipid mixture.

The main $L_{\beta'}$ to L_{α} phase transition of all the DP3adLPG–d_{62}PG mixtures occurred at T_m ~39 °C (figures 5-7a-d). However, in the lipid mixtures containing ≤30% DP3adLPG (figures 5-7a and b) a possible ripple ($P_{\beta'}$) phase was observed at ~38 °C. This $P_{\beta'}$ phase was not observed in lipid mixtures containing ≥40% DP3adLPG as shown in figures 5-7c and d and therefore suggested the phase change at ~38 °C may have not been due to a $P_{\beta'}$ phase. The headgroup charge state of DP3adLPG can be presumed to be mainly +1 in these experiments due to the vesicles being prepared in a pH 5.5 buffer and thus ion-pair formation between DP3adLPG and d_{62}PG was likely to be high. The low magnitude $L_{\beta'}$ to L_{α} phase transition at ~38 °C and ≤30% DP3adLPG was therefore more likely to be due to the T_m of excess non-ion-paired d_{62}PG in the vesicle bilayers. However, previous studies have shown the sodium and potassium salts of

DPPG to have a T_m of ~41 °C at pH 5.5 (Watts *et al.* 1978), which is in contrast to the T_m ~38 °C found for the excess non-ion-paired d_{62}PG in this experiment. The discrepancy of ~3 °C, although high, may have been made possible due to the difference in ionic bonding strengths between phosphate and triethylammonium, and phosphate and sodium. The sodium cation is densely charged and associates strongly with phosphate which shields the phosphate anionic charge therefore allowing d_{62}PG to pack together more closely in a bilayer increasing its T_m (Träuble *et al.* 1976). In contrast, the triethylammonium is a bulky cation and presumably would dissociate more readily from phosphate which would leave the anionic charge unshielded on neighbouring d_{62}PG phosphate groups therefore reducing bilayer lateral density and reducing the lipid's T_m (Träuble *et al.* 1976).

The finding of two T_m results in figures 5-7a and b strongly suggested bilayers formed of DP3adLPG and d_{62}PG with ≤30% DP3adLPG contained two domains. These domains presumably were formed of ion-pairs between DP3adLPG and d_{62}PG in one domain and excess non-ion-paired d_{62}PG in the other domain. The reason the T_m results suggested the presence of two domains is because the main T_m ~39 °C was always present in figures 5-7a-d and since both DP3adLPG and d_{62}PG were present in all the lipid mixtures, this T_m could be assigned to the ion-paired domain of DP3adLPG and d_{62}PG. To support this finding, when close to equimolar mixtures of d_{62}PG and DP3adLPG were present in the vesicles the second T_m ~38 °C was no longer observed, presumably due to a reduction in non-ion-paired d_{62}PG (figures 5-7c and d). In vesicles composed of ≥60% DP3adLPG, figure 5-7d showed the presence of an additional $L_{\beta'}$ to L_α phase transition between 39 °C and 40 °C which could be assigned to the T_m of excess non-ion-paired DP3adLPG.

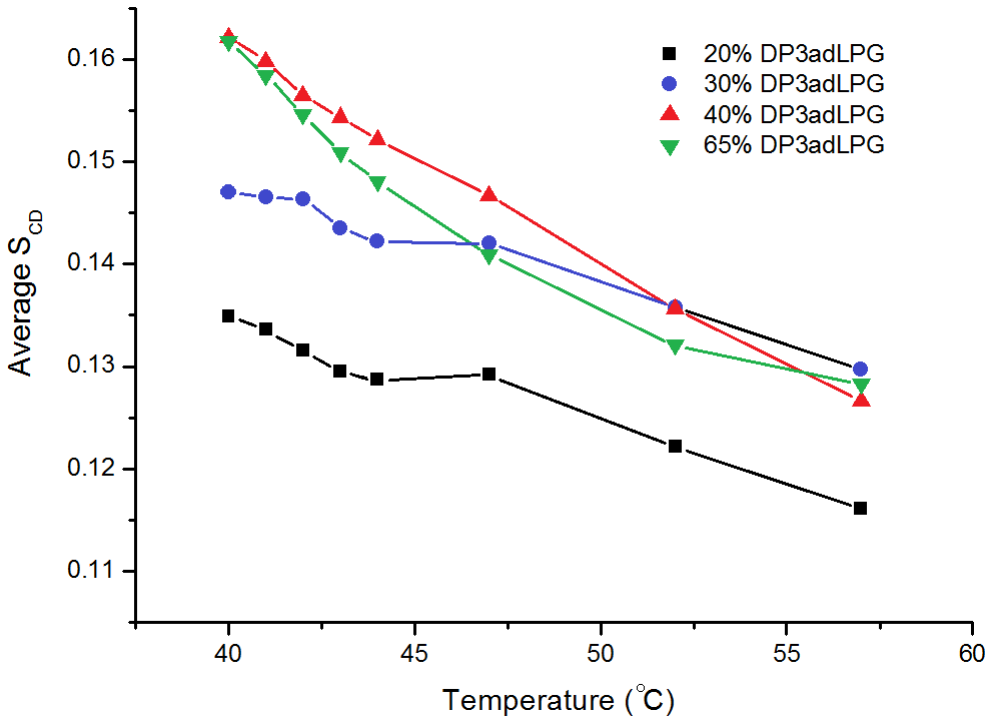

Figure 5-8 Mean lipid chain order parameters (S_{CD}) of mixtures of DP3adLPG and d_{62}PG.

The mean lipid acyl chain order (S_{CD}), in all the lipid mixtures used, decreased with increasing temperature (figure 5-8). This was to be expected as the bilayers would have expanded laterally with increasing temperature due to an increase in lipid chain mobility and flexibility (Yeagle 2012). However, as DP3adLPG content of the bilayers increased to an equimolar concentration with d_{62}PG, S_{CD} substantially increased resulting in a more ordered hydrophobic core of the bilayer (figure 5-8). This increased ordering effect suggested the ion-pairs formed between DP3adLPG and d_{62}PG headgroups were resulting in a more gel-like bilayer, possibly in the lipid ion-paired domains, which had reduced disorder. In contrast, figures 5-7a-d only showed only a small change in T_m as an equimolar mixture of the lipids was reached and does not fully correlate with the results in figure 5-8. However, it is possible the increased ordering effect between the lipid ion-pairs may have been more localised between the individual lipids and they may remain in a melted state but have a small increase in local ordering.

5.3.4 Charge properties of vesicles containing varying ratios of DP3adLPG and DPPG

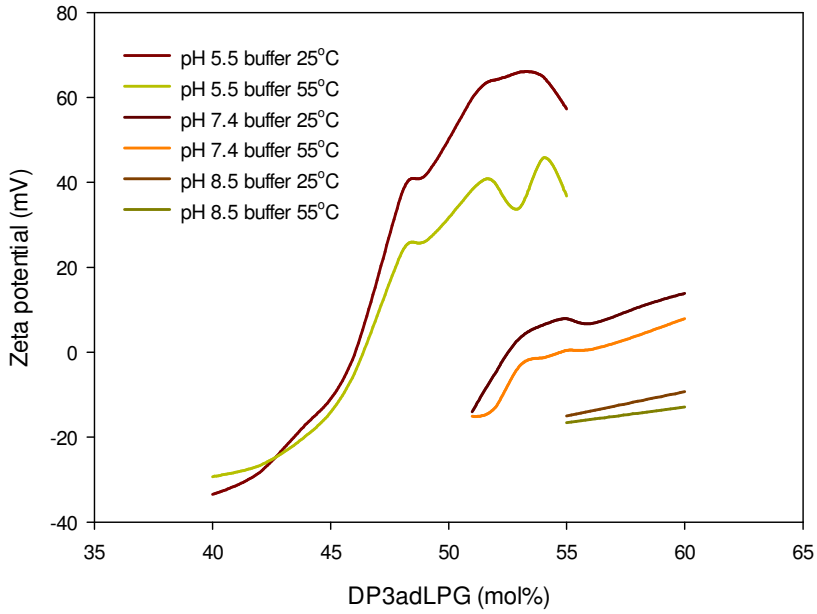

Figure 5-9 Zeta potential results of unilamellar vesicles of different DP3adLPG–DPPG mixtures in different pH buffer solutions.

A substantial change in vesicle zeta potential results was observed with the same DP3adLPG–DPPG mixtures in different pH buffers (figure 5-9). In the pH 5.5 buffer, both $L_{\beta'}$ and L_{α} phase curves in figure 5-9 intersect 0 mV at ~46% DP3adLPG vesicle content which suggested DP3adLPG was causing a large amount of charge neutralisation of the DPPG anionic headgroups. This result was unexpected as the charge adopted by the headgroup of DP3adLPG in a pH 5.5 buffer would be expected to be +1 due to the lipid's α-amine having a pKa of ~5.5-6.7 (5.3.1). Therefore a zeta potential result of 0 mV should have resulted for the equimolar mixture of DP3adLPG and DPPG. This shift in the pH 5.5 buffer curves in figure 5-9 suggested the acidity of the buffer was also causing a small amount of phosphate neutralisation therefore resulting in the zeta potential results becoming more positive. The zeta potential results of the vesicles in a pH 7.4 buffer showed a positive zeta potential was not reached until DP3adLPG was present at >52.5% in the vesicles in the $L_{\beta'}$ phase and >55% in the vesicles in the L_{α} phase (figure 5-9). This behaviour of DP3adLPG in the pH 7.4 buffer supported the finding that DP3adLPG is partly zwitterionic at pH 7.4 which is analogous to the headgroup charge state of L-PG in a pH 7.4 buffer (Tocanne *et al.* 1974c). In the pH 8.5 buffer figure 5-9 showed that even with >60 mol% DP3adLPG a positively charged vesicle was still not achieved and the vesicle surface remained predominately anionic in both $L_{\beta'}$ and L_{α} lipid phases.

However, the anionicity of these vesicles is somewhat lower than expected which may be due to the low abundance of DPPG in the vesicles as zwitterionic DP3adLPG is the predominant lipid in these samples.

The adoption of a more cationic charge state at pH 5.5 compared to pH 7.4 by the headgroup of DP3adLPG suggests the lipid has similar charge properties to the headgroup of L-PG in pH 5.5 and 7.4 environments (Tocanne *et al.* 1974c). Therefore, to examine the headgroup properties of L-PG in synthetic lipid models, DP3adLPG can serve as a suitable non-labile substitute.

5.3.5 Synthetic monolayers of biomimetic ratios of the MRSA G32 plasma membrane phospholipids under pH 5.5 and 7.4 growth conditions

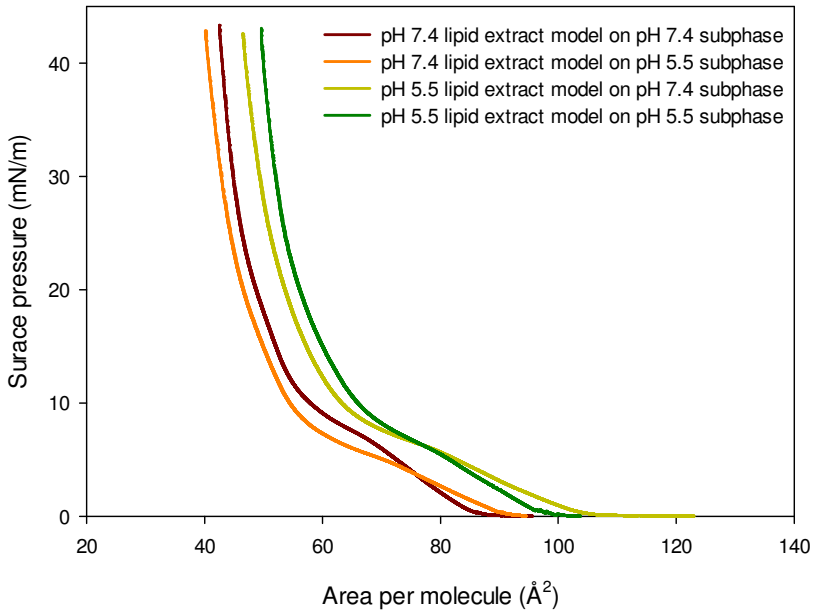

Figure 5-10 Mean surface pressure–area isotherms of mixtures of DP3adLPG–DPPG–TMCL 51.63:40:8.37 and 28.12:66.85:5.03 mol/mol/mol on pH 5.5 and 7.4 subphases.

A discernible shift in isotherm position to lower areas per molecule was observed for the pH 7.4 lipid extract model (DP3adLPG–DPPG–TMCL 28.12:66.85:5.03 mol/mol/mol) when the subphase pH was reduced from pH 7.4 to 5.5 (figure 5-10). This shift in isotherm position suggested the monolayer was more laterally condensed on the pH 5.5 subphase compared to the pH 7.4 subphase. The increased monolayer lateral density on the pH 5.5 subphase was presumably due to an increase in the proportion of cationic DP3adLPG molecules at pH 5.5 compared to pH 7.4 which resulted in more ion-pairs forming between DP3adLPG and DPPG or TMCL. The extrapolated limiting areas per molecule of the pH 7.4 lipid extract model saw a

smaller area per molecule result on the pH 5.5 subphase (~47.1 Å^2) compared to the pH 7.4 subphase (~50.1 Å^2) which also supported the finding the monolayer became more laterally condensed on the pH 5.5 subphase. The pH 5.5 lipid extract model (DP3adLPG–DPPG–TMCL 51.63:40:8.37 mol/mol/mol) results were in contrast to the pH 7.4 lipid extract model, where a small shift in the isotherm position to higher areas per molecular was observed on the pH 5.5 subphase compared to the pH 7.4 subphase (figure 5-10). This result suggested that on the pH 5.5 subphase a drop in monolayer lateral density occurred which was also reflected by a larger area per molecule on the pH 5.5 subphase (~58.1 Å^2) compared to the pH 7.4 subphase (56.1 Å^2). The reason for this occurrence was likely to have been due to the excess of cationic DP3adLPG present on the pH 5.5 subphase which resulted in cationic charge repulsion between neighbouring excess cationic DP3adLPG molecules thus causing a reduction in monolayer lateral density (Gaines 1966).

Table 5-1 Compressional moduli and excess area functions (A_{ex}) of the pH 5.5 and 7.4 lipid extract models on both pH 5.5 and 7.4 subphases.

	pH 7.4 subphase		pH 5.5 subphase	
Lipid sample	K^s (× 10^{-3} mN/m)	A_{ex} (Å^2)	K^s (× 10^{-3} mN/m)	A_{ex} (Å^2)
pH 7.4 lipid extract model	2.79 ± 0.39	-6.09 ± 1.3	2.18 ± 0.44	-7.23 ± 1.6
pH 5.5 lipid extract model	2.44 ± 0.52	-4.45 ± 0.8	2.85 ± 0.67	-1.43 ± 0.3

A reduction in monolayer elasticity of the pH 7.4 lipid extract model was observed on a pH 5.5 subphase (K^s ~2.18 mN/m) compared to the pH 7.4 subphase (K^s ~2.79 mN/m) (table 5-1). The reduction in monolayer elasticity suggested that the increase in ion-pairs between DP3adLPG and DPPG or TMCL on the pH 5.5 subphase made the monolayer more rigid and resistant to the application of lateral pressure (Gaines 1966). The elasticity of the pH 5.5 lipid extract model showed contrasting behaviour to the pH 7.4 lipid extract model where monolayer elasticity decreased on the pH 5.5 subphase (K^s ~2.85 mN/m) compared to the pH 7.4 subphase (K^s ~2.44 mN/m) (table 5-1). This increase in monolayer compressibility on a pH 5.5 subphase was attributed to the excess cationically charged DP3adLPG in this lipid mixture (>50%) where non-ion-paired excess DP3adLPG molecules will have substantial lipid-lipid electrostatic charge repulsion between one another therefore resulting in an increase in monolayer elasticity (Gaines 1966).

The A_{ex} function of the pH 7.4 lipid extract model on both pH 5.5 and pH 7.4 subphases showed a large negative deviation from ideal mixing of the lipids (table 5-1), which indicated in both lipid

models there were substantial interactions between the lipids which were reducing the mean lipid molecular areas. The most likely interaction to have occurred between DP3adLPG, DPPG and TMCL to cause a negative deviation in $A_{ex,}$ is ion-pair formation between cationic DP3adLPG and DPPG or TMCL which reduces the lipid molecular areas. Therefore, the negative deviation in A_{ex} in the pH 7.4 lipid extract model suggested both pH subphases contained DP3adLPG in a cationic state however more so on the pH 5.5 subphase as the negative value of A_{ex} was greater in magnitude compared to A_{ex} on the pH 7.4 subphase (table 5-1). With respect to the pH 5.5 lipid extract model, both pH subphases resulted in a negative A_{ex} however in contrast to the pH 7.4 lipid extract model the pH 7.4 subphase gave a more negative A_{ex} (table 5-1). The negative sign of A_{ex} in the pH 5.5 lipid extract model on both pH subphases still suggested ion-pairs were formed between DP3adLPG and DPPG or TMCL however as A_{ex} takes into account both attractive and repulsive forces between lipids the pH 5.5 subphase A_{ex} gave a less negative result as it contained an excess of cationic DP3adLPG (>50% total phospholipid). This excess of cationic DP3adLPG on the pH 5.5 subphase would presumably result in lipid-lipid charge repulsion, therefore reducing the negativity of A_{ex} as a result.

The behaviour of both pH 5.5 and 7.4 lipid extract models on pH 5.5 and 7.4 subphases is analogous to the results found with the natural lipid extracts of MRSA G32 (chapter 3.3.2). This suggests DP3adLPG must have similar structural headgroup and charge properties to L-PG on a monolayer with pH 5.5 and 7.4 subphases and therefore could serve as a suitable substitute for studying the interaction of L-PG with PG and CL in synthetic bilayers.

5.3.6 Small angle neutron scattering of different mixtures of DP3adLPG–DPPG, and PO3adLPG–POPG

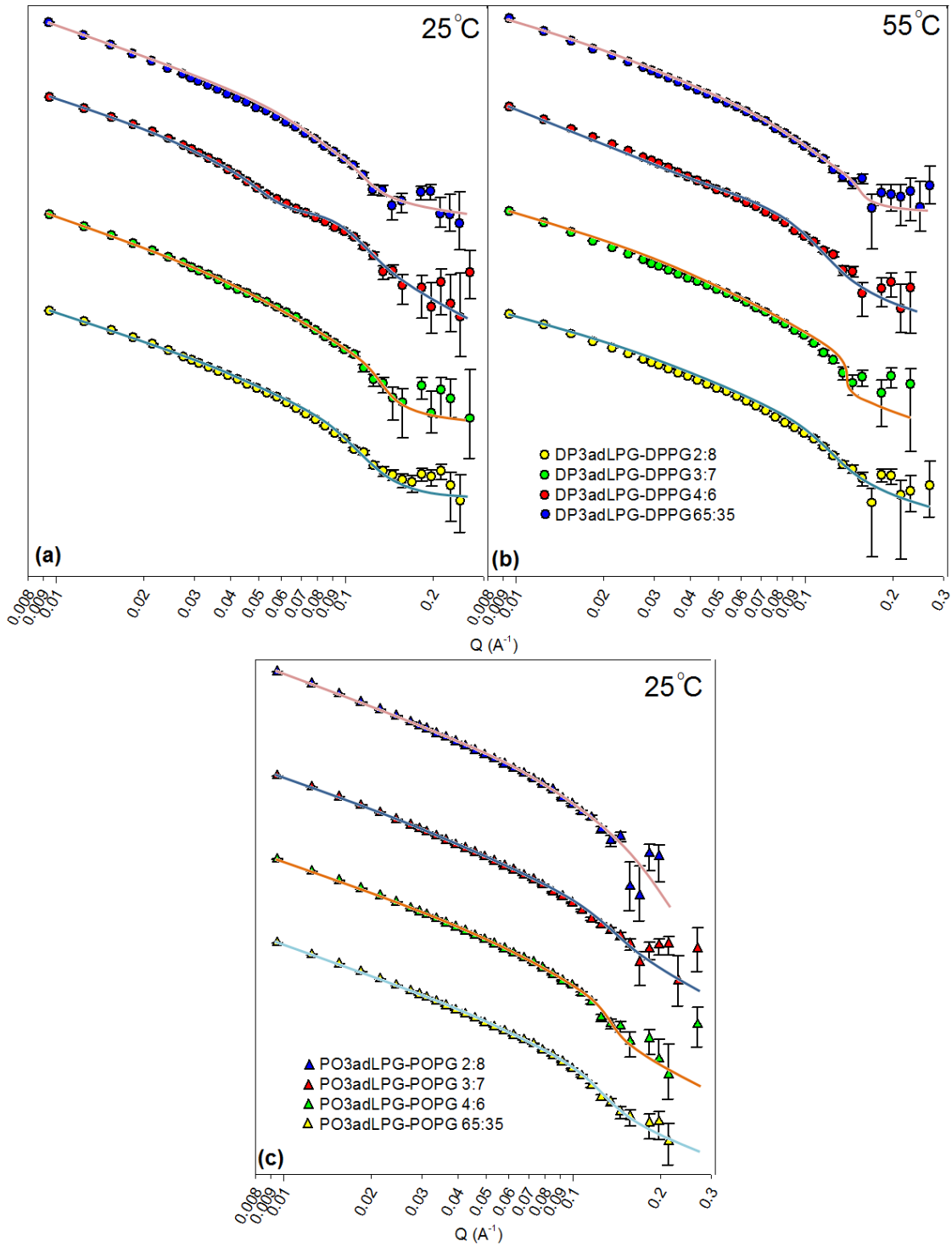

Figure 5-11 SANS curves of DP3adLPG–DPPG and PO3adLPG–POPG at different molar ratios in D_2O; (a) DP3adLPG–DPPG at 25 ℃, (b) DP3adLPG–DPPG at 55 ℃ and (c) PO3adLPG–POPG at 25 ℃.

Table 5-2 Fitted SANS parameters of mixtures of DP3adLPG–DPPG and PO3adLPG–POPG at 25 ℃ and 55 ℃ in D_2O.

		25 ℃		55 ℃	
Mol% lipid content		Bilayer thickness (Å)	D-spacing (Å)	Bilayer thickness (Å)	D-spacing (Å)
DPPG	DP3adLPG				
80	20	54.8 ± 2.6	113 ± 8.8	48 ± 3.7	123 ± 7.4
70	30	55.7 ± 3.3	116 ± 9.6	49 ± 1.1	119 ± 8.6
60	40	57.4 ± 1.9	108 ± 7.2	51 ± 4.6	111 ± 9.5
35	65	62.9 ± 4.5	111 ± 6.8	56 ± 3.2	116 ± 7.1
POPG	PO3adLPG				
80	20	47 ± 3.4	118 ± 4.6		
70	30	50 ± 2.9	117 ± 8.2		
60	40	50 ± 1.7	109 ± 6.9		
35	65	57 ± 4.2	113 ± 7.1		

All of the SANS curves of DP3adLPG–DPPG and PO3adLPG–POPG vesicles in figures 5-11a-c showed some presence of MLVs due to the appearance of a Bragg reflection at Q ~0.1 $Å^{-1}$. The fitted abundance of these MLVs in all the samples was ~2 layers which suggested the MLVs in all the lipid samples were no more than one vesicle inside of another. The fitted d-spacings of all sample MLVs shown in table 5-2 were relatively high at >110 Å, which proposed the bilayer surfaces of all the vesicles were charged resulting in substantial electrostatic charge repulsion between adjacent bilayers and a large separating water layer between bilayers as a result (Pozo Navas *et al.* 2005). This d-spacing result was expected as vesicle mixtures containing <50% DP3adLPG or PO3adLPG as total phospholipid would have had negatively charged surfaces due to the presence of non-ion-paired DPPG or POPG in them and vesicles containing >60% DP3adLPG or PO3adLPG were likely to be positively charged as they had an excess of non-ion-paired DP3adLPG or PO3adLPG. A small drop in fitted d-spacing was observed in the 40:60 molar ratio of DP3adLPG–DPPG and PO3adLPG–POPG (table 5-2) which showed these vesicle surfaces had a lower surface anionicity compared to the 20:80 and 30:70 lipid mixtures. This lower d-spacing presumably occurred due to the lipid mixtures approaching an equimolar ratio therefore their vesicle surfaces would have been less anionically charged due to ion-pair formation between 3adLPG and PG. With respect to the fitted bilayer thicknesses in table 5-2, the $L_{\beta'}$ phase DP3adLPG–DPPG lipid mixtures showed a thickness increase from 54.8 Å to 62.9 Å as DP3adLPG content of the vesicles increased. This result suggested that the thickness of the headgroup regions of these vesicles was increasing with increased DP3adLPG concentrations or that the tilt of the lipids had reduced with

increasing DP3adLPG concentrations. However, the possibility of a reduction in tilt angle of the lipids was unlikely as both the PO3adLPG–POPG and DP3adLPG–DPPG vesicle samples in the L_α phase showed the same trend of increasing fitted bilayer thickness with increasing 3adLPG concentrations (table 5-2) and lipid tilts tend not to exist in bilayers in the L_α phase as they undergo lateral expansion (Yeagle 2012). At low concentrations of DP3adLPG in the vesicles, the headgroup region would have been predominately made up of DPPG headgroups (6-7 Å, Pascher *et al.* 1987) whereas at higher concentrations of DP3adLPG (>60%) the headgroup region would have been predominately DP3adLPG headgroups (~10-11 Å) (5.3.2) (Armen *et al.* 1998). Therefore, this larger size of the DP3adLPG headgroup in comparison to the DPPG headgroup would account for the increased fitted bilayer thicknesses observed in table 5-2 at higher DP3adLPG concentrations. Comparison of the fitted bilayer thicknesses of PO3adLPG–POPG and DP3adLPG–DPPG in the L_α phase (table 5-2), showed all lipid molar ratios of both lipid samples had almost the same fitted bilayer thicknesses. This finding suggested that DP3adLPG–DPPG in the L_α phase, at higher temperatures, could serve as a suitable replacement for 1-*O*-palmitoyl-2-*O*-oleoyl lipids for future experiments, in order to study L-PG in the L_α phase. In addition to this, the fitted d-spacings of PO3adLPG–POPG and DP3adLPG–DPPG in the L_α phase (table 5-2) were also very similar in magnitude which suggested using mixtures of DP3adLPG–DPPG at higher temperatures does not alter the vesicle surface charge properties in comparison to vesicles formed from PO3adLPG–POPG at 25 °C.

5.4 Conclusion

The results from this chapter suggest that DP3adLPG could serve as a suitable non-labile substitute for L-PG when studying the behaviour of L-PG in membranes under mild aqueous environments. The charge properties of the headgroup of DP3adLPG are almost identical to those of L-PG as shown by neutron diffraction, monolayer pH titration and mixed lipid monolayer experiments. However, the monolayer pH titration did detect the α-amine of DP3adLPG to have a slightly lower pKa of between 5.5 and 6.7 in comparison to L-PG (~6-7) (Tocanne *et al.* 1974c). Nevertheless, the lower pKa of the α-amine in DP3adLPG did not appear to affect the ability of DP3adLPG to become more cationic in a pH 5.5 environment in comparison to a pH 7.4 environment therefore suggesting the α-amine pKa was closer to 6.7 than 5.5. Similar to DP3adLPG, DP3aLPG also showed similar physicochemical properties to L-PG in the monolayer pH titration experiment, however as shown in Chapter 4.4.22 this lipid contained a ~35% contaminating structural isomer of DP3aLPG caused by phosphate migration and therefore this lipid was not used any further. L-PG in the plasma membrane of *S. aureus* exists in the L_α phase which suggests the role of L-PG in the bacterial plasma membrane is best studied with a L_α phase version of 3adLPG, namely PO3adLPG. However, SANS showed both DP3adLPG and PO3adLPG in the L_α phase exhibited similar bilayer thicknesses and therefore DP3adLPG at 55 °C is able to serve as a suitable L-PG substitute to study L-PG in the L_α phase. This finding was also useful for contrast variation in neutron scattering experiments where fully deuterated palmitoyl hydrocarbon chains can be incorporated into DP3adLPG (d_{62}3adLPG). Therefore due to the numerous structural and physicochemical similarities between DP3adLPG and L-PG, d_{62}3adLPG will now be used in a series of neutron scattering experiments in order to further examine the function of L-PG in the plasma membrane of *S. aureus* in response to a mild acidic environment.

Chapter 6

High resolution structural studies of 3-aza-dehydroxy-lysylphosphatidylglycerol in biomimetic model membranes

6.1 Introduction

To determine atomic resolution details of lipid bilayer structures, focused sub-atomic radiation is required and comes either in the form of X-ray or neutron scattering techniques. X-ray scattering, although exploitable in the study of lipid bilayer structures and their interactions, can be undesirable as the high energy of bombardment and various electron excitations can lead to sample degradation (Cheng & Caffrey 1996). Neutron scattering techniques, however, use low energy thermal elastic neutrons (~0.025 eV) to analyse lipid systems which tend not to be detrimental to the sample (Fragneto-Cusani 2001). Normally, mixtures of lipids are studied using neutron scattering by forming them into bilayers, calculating the structural parameters of the bilayer and then using these parameters, elucidate the properties of the individual lipid components. For example, small angle neutron scattering (SANS) of vesicles of 1,2-dimyristol phosphatidylcholine (DMPC) demonstrated the individual lipid headgroup volume to be 325.5 $Å^3$ with 6.8 ± 0.2 associated water molecules (Kučerka *et al.* 2005). However, the use of a single neutron scattering technique is generally unreliable as system constraints (e.g. deposition onto silicon substrates) can influence the natural movement and translation of a bilayer and resolution can vary quite considerably between techniques (Hughes *et al.* 2008). Therefore, confidence in the calculated bilayer parameters can be improved by using a series of related neutron scattering techniques, such as neutron reflectivity, neutron diffraction and SANS. In this study, all three neutron scattering techniques were used to study bilayers formed from d_{62}-1,2-*O*-dipalmitoyl phosphatidylglycerol (d_{62}PG) and d_{62}-1,2-*O*-dipalmitoyl 3-aza-dehydroxy-lysyl-phosphatidylglycerol (d_{62}3adLPG) in ratios mimicking those found in the plasma membranes of methicillin susceptible *Staphylococcus aureus* 476 and methicillin resistant *S. aureus* G32 in both pH 5.5 (d_{62}PG–d_{62}3adLPG 45:55 mol/mol) and pH 7.4 (d_{62}PG–d_{62}3adLPG 7:3 mol/mol) growth environments (chapter 2.3.1). To simplify the lipid mixtures for the purposes of neutron data interpretation, cardiolipin, which is also found in the plasma membrane of *S. aureus*, was not incorporated into the model, its role being effectively taken by the d_{62}PG as cardiolipin is negatively charged at both pH 5.5 and 7.4 (Kates *et al.* 1993).

The high resolution structural information that can be determined from neutron diffraction will provide atomic details of how the interaction between d_{62}PG and d_{62}3adLPG in a bilayer at different biomimetic ratios affects the properties of the bilayer along the z-axis (the bilayer normal). However, one of the associated problems with neutron diffraction is the lack of ability to control the environmental pH, as the technique requires bilayers to be hydrated by increasing the environmental humidity (Sebastiani *et al.* 2012). The lack of pH control in neutron diffraction presents a problem when using d_{62}3adLPG as the charge state of the lipid would remain uncontrolled in such an environment, as the pKa of its α-ammonium is in the range 5.5-6.7 (chapter 5.3.1). Therefore, neutron reflectivity can also be employed with the biomimetic mixtures of d_{62}PG and d_{62}3adLPG because the bulk solvent surrounding the bilayers can be buffered at either pH 5.5 or 7.4 in order to control the charge state of the d_{62}3adLPG headgroup and mimic the effects of the culture conditions of interest. The data acquired from neutron reflectivity supports neutron diffraction by also giving SLD details of the bilayer along the z-axis plane (Hughes *et al.* 2008). The third technique, SANS, can also examine the thickness of bilayers containing d_{62}PG and d_{62}3adLPG with different buffer pHs, and since the system has no positional constraints, as no silicon substrate is required, it provides data which is more relevant to the condition of natural lipid bilayers. Therefore the SANS data can be used to support the data found with the neutron reflectivity and diffraction experiments, in order to relate it back to the natural behaviour of the lipids in the plasma membranes of *S. aureus*.

The use of these combined neutron scattering techniques to examine the interactions between d_{62}PG and d_{62}3adLPG and the effects these interactions have on bilayer structure, will provide insight into how increased biosynthesis of lysyl-phosphatidylglycerol (L-PG) in the plasma membrane of *S. aureus* aids adaptation to mildly acidic environmental conditions.

6.2 Methods and Materials

6.2.1 Materials

Tris(hydroxymethyl)aminomethane (>99.0%), concentrated hydrochloric acid (~38%), concentrated deuterium chloride (99 %D atom), glacial acetic acid, sodium sulphate (>99.0%) and deuterium oxide (99.9 %D atom) were all purchased from Sigma-Aldrich UK, and used as supplied. Cleaning solvents for neutron diffraction, chloroform (99.5%), methanol (99.9%) and acetone (99.9%) were also purchased from Sigma-Aldrich, international, and used as supplied. Ultrapure water (18.2 MΩ.cm) for all experiments was obtained from a Milli-Q 16 Ultrapure water system (Merck Millipore, Billerica, USA). Silicon substrates used for neutron reflectivity experiments measuring 38 mm × 70 mm × 10 mm with a single surface polished to a tolerance of 5 Å were purchased from Crystran Ltd, Poole, UK. Silicon discs for neutron diffraction experiments were obtained from Silicon Materials (Kaufering, Germany); diameter 50.8mm ± 0.50 mm, thickness 275 µm ± 20 µm, resistivity 1-5 Ωcm and single sided polished finish.

6.2.2 Neutron diffraction of mixtures of d_{62}PG and d_{62}3adPG

Two silicon discs were prepared for neutron diffraction by initially cleaning them by 5 min of bath sonication (Branson bath sonicator 3510, Danbury, USA) in chloroform, then acetone and then methanol, and finally treating them under UV light for 30 min with a UV/Ozone ProCleaner™ Plus (BioForce Nanosciences, Ames, USA). Orientated multilayers of 20 mg mixtures of d_{62}PG–d_{62}3adPG 7:3 and 45:55 mol/mol were then prepared for neutron diffraction by evenly coating the lipids on to the polished side of the silicon discs as 1 mL chloroform solutions, as described in chapter 3.2.6. Neutron diffraction was then performed on both samples at 25 °C and 55 °C with contrasts of D_2O and H_2O, using the D16 neutron diffractometer at the Institut Laue-Langevin (Grenoble, France) at λ = 4.741 Å. Strong reflections were measured for short times (~30 min) whereas weaker ones were measured for ~2-3 hours to improve signal-noise of the higher orders of diffraction. Both samples were analysed at 100% humidity only, using a sealed aluminium chamber as described in chapter 3.2.6. The neutron diffraction profiles (Intensity vs. 2θ) collected for the samples were then fitted with an exponential function using Sigmaplot V 12.0 (Systat Software, San Jose, California, USA) to remove background scattering as described in chapter 3.2.6. D-spacing calculations, and Fourier transformation of each sample neutron diffraction profile, was then performed using eq. (24-26) (chapter 3.2.6). All structure factors and assigned signs of the structure factors are published in Appendix AI.III–VII.

6.2.3 Neutron reflectivity of mixtures of d_{62}PG and d_{62}3adPG in different pH buffers

Directly depositing lipids onto a silicon substrate results in their localisation to the silicon (Hughes *et al.* 2008). Lipid localisation results in a loss of natural movement and translation of the bilayer and gives inaccurate results regarding the structure and behaviour of the membrane (Hughes *et al.* 2008). In order to maximise the fluidity, dynamics and translational freedom of the system (Hughes *et al.* 2008), the bilayers used in this study were deposited above a phospholipid monolayer covalently bound to the silicon substrate.

The silicon substrates were silanized using the method described by Hughes *et al.* (2008) (Hughes *et al.* 2008). 3-(trimethoxysilyl)propyl acrylate monomers (TMPA) were covalently bound by a free radical activated mechanism, using the initiator AAPD-2,2'-Azobis(2-methylpropionamidine, to the naturally formed SiO_2 layer of the polished silicon substrate. This was then followed by covalent binding of a 1-palmitoyl-2-[16-(acryloyloxy)hexadecanoyl]-*sn*-

glycero-3-phosphorylcholine (al-PC) layer to the polymerised TMPA layer by the same free radical activated mechanism. To characterise the newly formed TMPA and al-PC layers, collectively known as a self-assembled monolayer (SAM), the silanized substrate was kept immersed in H_2O (with no air exposure) and the silanized face compressed against an air-tight rubber seal attached to a plastic cell. The plastic cell with the attached silanized silicon substrate was then removed from the bulk solvent. The inside of the plastic cell contained a small solvent reservoir to keep the silanized layer fully submerged in solvent and also possessed two valves to allow solvent exchange through the cell. To hold the plastic cell and silanized substrate together two aluminium plates were attached either side of the plastic cell and silicon substrate, and were secured together tightly with aluminium screws. The whole apparatus was then mounted vertically on to an automated sample changer on the D17 reflectometer at the Institut Laue-Langevin (Grenoble, France) at 25 °C. Neutron reflectivity data was collected at two incident angles (0.8° and 3.2°), for 30 min at the lower angle (12 min for D_2O) and 50 min at the higher angle (30 min for D_2O). The overlapping data from both angles gave a total Q_z-range of 8 × 10^{-3} Å^{-1} to 0.32 Å^{-1}, although due to some incoherent scattering Q_z normally reached a maximum of ~0.3 Å^{-1}. Three solvent contrasts were employed for the SAM characterisation namely H_2O, D_2O and 4-matched water (4MW), with the latter being a mixture of H_2O and D_2O to achieve a coherent SLD of 4 × 10^{-6} Å^{-2}. Solvent contrasts were exchanged through the cell reservoir using a Knauer Smartline HPLC pump 1050 (Hegauer Weg, Germany) at a flow rate of 2 mL/min.

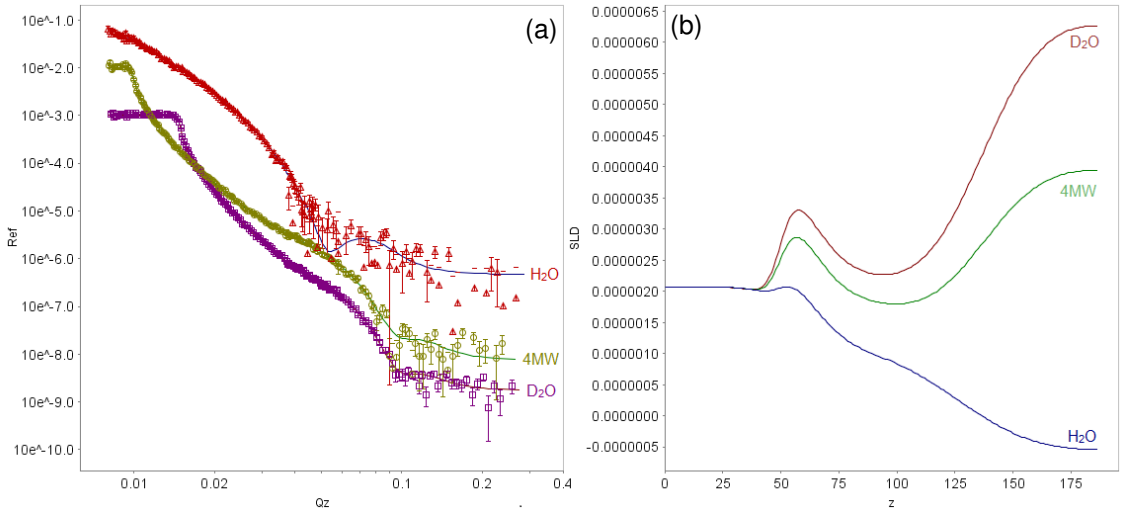

Figure 6-1 (a) Neutron reflectivity curves of the SAM layer covalently bound to the silicon substrate with the (b) accompanying fitted SLD profiles.

Due to neutron reflectivity being essentially the refractive index normal to the substrate surface (Q_z) as shown in chapter 1.7.2, the phase information of the structure is lost and therefore the z-axis plane SLD profile of the system cannot be extrapolated by Fourier transformation (Hughes *et al.* 2008). Thus the data in figure 6-1a was analysed by breaking the system into separate theoretical layers which were perpendicular to the substrate surface (chapter 1.7.2) and then fitting model parameters to these layers using a 'least squares simplex algorithm' from the program RasCal v1.0.0 (ISIS, Rutherford Appleton Laboratory). To fit the SAM layer curves in figure 6-1a, a four layer model was used (bottom four layers in figure 6-2) which from the substrate surface, in ascending order, followed silicon oxide (SiO_2), TMPA, al-PC hydrocarbon chains (al-PC Chains) and al-PC headgroups (al-PC Heads) (table 6-1). The fitted values obtained in table 6-1 were fixed for the fitting of all the floating bilayers and not modified from these values

Table 6-1 Fitted parameters for the silanized silicon substrate.

Layer	Thickness (Å)	SLD ($\times 10^{-6}$ Å^{-2})	Hydration (%)	Roughness (Å)
Si[b]				5[c]
SiO_2	12.78 ± 3.1	3.41[a]	11.79 ± 5.6	4.23 ± 0.7
TMPA	55.05 ± 8.3	1.43	17.38 ± 4.8	21.76 ± 5.1
al-PC Chains	13.71 ± 0.9	-0.41[a]	11.53 ± 6.7	21.33 ± 5.3
al-PC Heads	7.6 [a]	1.74[a]	31.87 ± 8.4	21.33 ± 5.3
Bulk			100 [c]	

[a] Values obtained from Fragneto *et al.* (2000) (Fragneto *et al.* 2000)
[b] Silicon substrate
[c] Values fixed

To prepare floating bilayers of d_{62}PG–d_{62}3adLPG 7:3 and 45:55 mol/mol, the silanized substrate was lowered into a dipping well of an automated arm adapted Nima technologies KN2003 Langmuir trough (Coventry, UK) with the silanized surface perpendicular to the air–liquid interface of the subphase. The trough was then filled with a H_2O subphase, completely submerging the silicon substrate, and 150 µL of 1 mg/mL d_{62}PG–d_{62}3adPG 7:3 or 45:55 lipid solution in chloroform was spread dropwise onto the subphase and allowed to equilibrate for 15 min at 26 °C with the trough barriers open. The trough barriers were then closed at a speed of 10 cm^2/s to achieve and maintain a surface pressure of 28 mN/m and subsequently the silanized substrate was lifted out of the well at 5 mm/min until fully emerged from the subphase (Langmuir-Blodgett deposition). The substrate was then rotated through 90° to place the

deposited monolayer parallel to the subphase surface and lowered to deposit a further monolayer of lipid (Langmuir-Schafer deposition). The substrate was then sealed with a plastic cell and two aluminium plates as described above, in order to avoid exposure to the air. Neutron reflectivity measurements were obtained according to the same procedure of the SAM layer characterisation, with solvent contrasts of H_2O, D_2O and silicon matched water (SMW) to contrast match out the silicon substrate (SLD = 2.07 × 10^{-6} $Å^{-2}$). All the solvent contrasts were buffered with Tris(hydroxymethyl)aminomethane (TRIS)–glacial acetic acid (AcOH) 1:1 mol/mol adjusted to either pH 5.5 or 7.4 with concentrated HCl or DCl, and data was acquired at 55 °C to assess the bilayer characteristics above the main lipid phase transition temperature (T_m) in order to mimic the fluid plasma membrane of *S. aureus*. The fitting of the reflectivity curves followed the same method of the SAM layer characterisation however with a further 4 layers after the al-PC headgroups, namely a solvent layer, floating bilayer inner leaflet headgroups, floating bilayer hydrocarbon chains and floating bilayer outer leaflet headgroups (figure 6-2). To simplify the fitting, the same parameters were used for the headgroups of both leaflets and the same roughness value was used for all the layers within the floating bilayer.

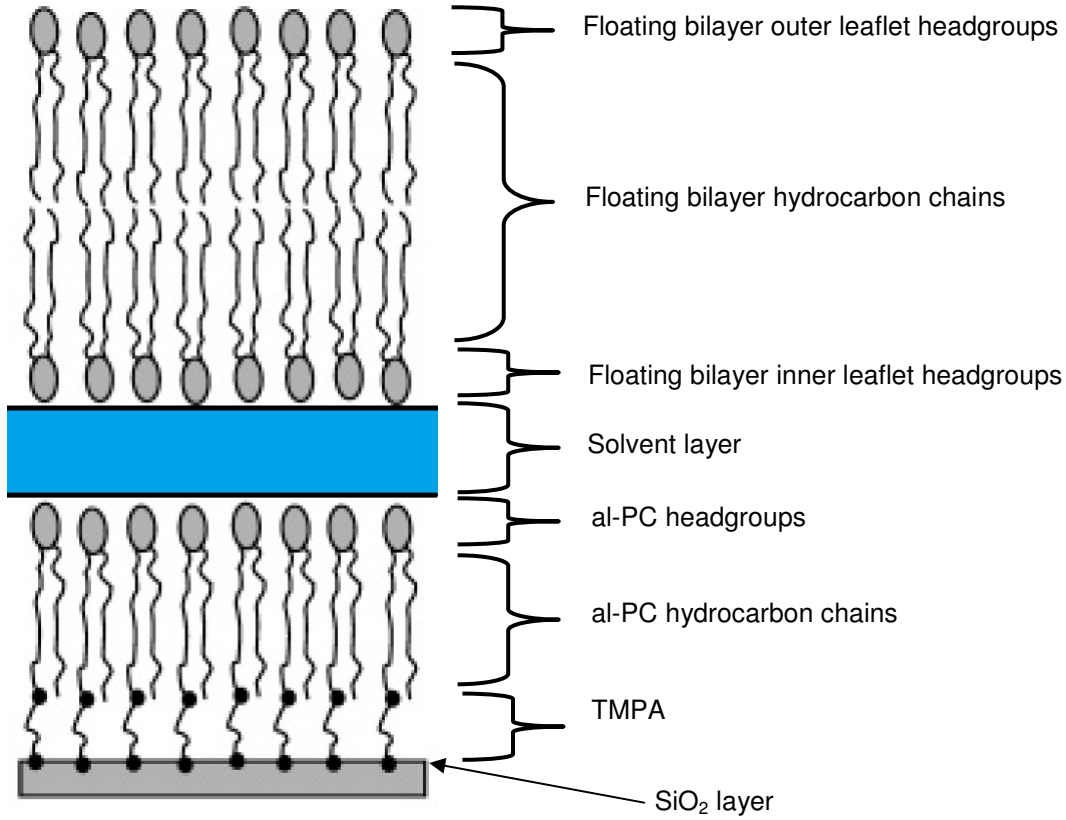

Figure 6-2 Schematic of the chemically grafted SAM layer on the silicon substrate with the deposition of a floating bilayer above the headgroups of the SAM layer.

6.2.4 Small angle neutron scattering (SANS) of mixtures of d_{62}PG and d_{62}3adPG in different pH buffers

Lipid films of d_{62}PG–d_{62}3adLPG in the molar ratios 7:3 and 45:55 were prepared by dissolving 5 mg of each lipid mixture in 5 mL of chloroform. Each sample was then evaporated to dryness under reduced pressure and resuspended, by vortex mixing, in 2.5 mL of H_2O buffered with 10mM TRIS–AcOH 1:1 mol/mol adjusted to either pH 5.5 or 7.4 with concentrated HCl. Each sample was then probe sonicated with a Soniprobe (Lukas-Dawe Ultrasonics, UK) for 10 min at 24 °C. Additional samples consisting of the same lipid mixtures were prepared in H_2O–D_2O 1:1 v/v buffered with 10mM TRIS–AcOH 1:1 mol/mol adjusted to either pH 5.5 or 7.4 with concentrated HCl–DCl 1:1 v/v. SANS data of all samples was then obtained as described in chapter 5.2.7 on the LoQ small-angle diffractometer at the ISIS Pulsed Neutron Source (STFC Rutherford Appleton Laboratory, Didcot, U.K.). Each sample including one to measure background scattering of H_2O and H_2O–D_2O 1:1 v/v was placed in a 1 mm pathlength quartz cell (Starna scientific, Hainault, UK) and was measured for a total of 13 mAh with an incident neutron flux of 160 µA. Each raw scattering data set was then corrected as described in chapter 5.2.7 and converted to scattering cross-section data ($\partial\Sigma/\partial\Omega$ vs Q) using the instrument-specific software Colette (Rutherford Appleton Laboratories 2007). All samples were examined at 55 °C to assess the vesicle bilayer characteristics above the lipid T_m in order to mimic the fluid phase of the plasma membrane lipids of *S. aureus* (L_α phase). The scattering curves obtained were fitted with the software FISH using a monodisperse sheet model for samples containing only unilamellar vesicles and a one-dimensional multilayer stack model for multi-lamellar vesicle samples (Heenan 2009, Kotlarchyk & Chen 1983).

6.3 Results

6.3.1 Neutron diffraction of mixtures of d_{62}PG and d_{62}3adPG

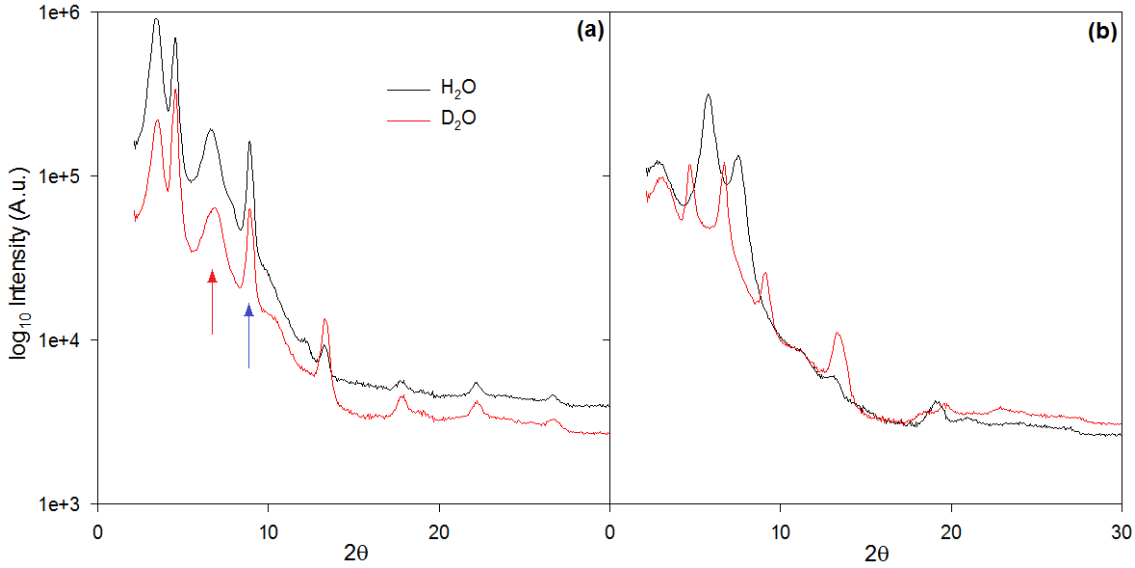

Figure 6-3 Neutron diffraction profile of d_{62}PG–d_{62}3adLPG (a) 7:3 at 25 ℃, with arrows showing the different neutron diffraction Bragg peaks of each phase and (b) 45:55 at 25 ℃. Red arrow indicates the second order diffraction peak of the d_{62}PG rich lamellar phase and the blue arrow indicates the second order diffraction peak of the d_{62}PG–d_{62}3adLPG ion-pair lamellar phase.

The neutron diffraction profile of d_{62}PG–d_{62}3adLPG 7:3 at 25 ℃ displayed the presence of two separate lamellar phases (figure 6-3a). These two lamellar phases gave d-spacings of ~82 Å and ~120 Å which were consistent in all orders of diffraction of each respective phase. In contrast, d_{62}PG–d_{62}3adLPG 45:55 at 25 ℃ showed only a single lamellar phase (figure 6-3b) with a d-spacing of ~92.5 Å and suggested the lipids in this mixture existed as an ideal mixture or that the signal for a second lamellar phase was so low it was masked by the high intensity of the first lamellar phase. The presence of lamellar phase separation in d_{62}PG–d_{62}3adLPG 7:3 suggested the lipids were not present as an ideal mixture but rather as two separate domains which were coupled either side of the bilayer leaflets and between adjacent bilayers (figure 6-4). Such lamellar phase separation has previously been found with mixtures of sphingomyelin, 1-*O*-palmitoyl-2-*O*-oleoyl phosphatidylcholine (POPC) and cholesterol, where the system formed energetically favourable interlamellar and intralamellar coupled bilayer domains of sphingomyelin and POPC (Tayebi *et al.* 2012).

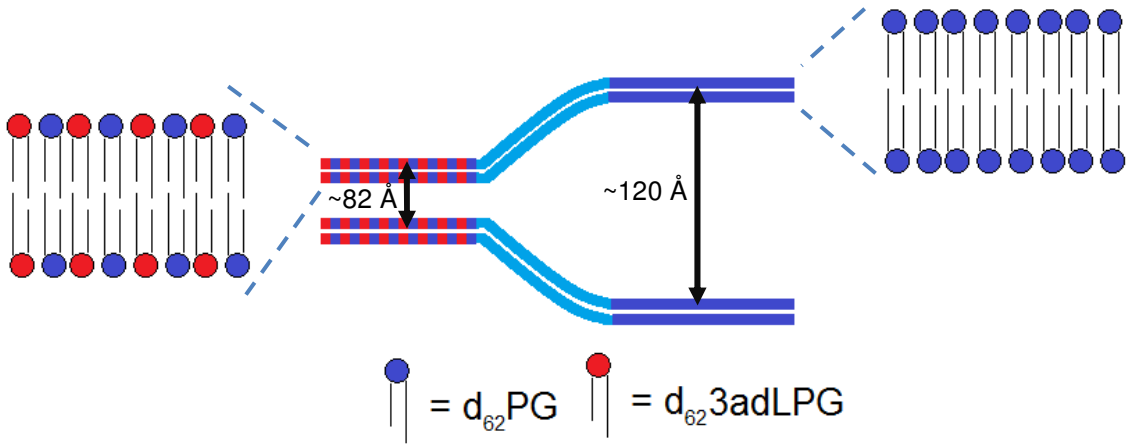

Figure 6-4 Schematic to show the lamellar phase separation of d_{62}PG–d_{62}3adLPG 7:3 in the $L_{\beta'}$ phase caused by separate lipid domains coupling between bilayer leaflets and adjacent bilayers.

The d_{62}PG–d_{62}3adLPG 7:3 lamellar phase with a d-spacing of ~82 Å is what would be expected for adjacent bilayers containing neutral lipids (Leonard *et al.* 2001) and therefore suggested this lamellar phase consisted of bilayers with neutrally charged surfaces formed from ion-pairs between d_{62}PG and cationically charged d_{62}3adLPG (figure 6-4). The second lamellar phase which had a d-spacing of ~120 Å was too large to be produced by bilayers with neutrally charged surfaces and was likely to be formed from bilayers with high adjacent electrostatic charge repulsion (Pozo Navas *et al.* 2005). Therefore the second lamellar phase was assumed to consist mainly of bilayers with non-ion-paired d_{62}PG (figure 6-4). The d-spacing of d_{62}PG–d_{62}3adLPG 45:55 at 25 °C of ~92.5 Å was also relatively large, however the lipid mixture contained an excess of non-ion-paired d_{62}3adLPG which presumably increased the d-spacing due to cationic electrostatic charge repulsion between adjacent bilayers (Pozo Navas *et al.* 2005).

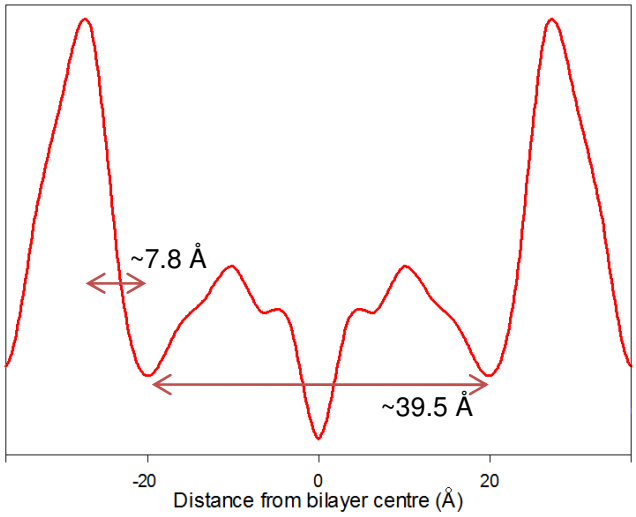

Figure 6-5 Neutron diffraction SLD profile of the d_{62}PG rich phase of d_{62}PG–d_{62}3adLPG 7:3 at 25 ℃.

Previous studies of 100% PG show the lipid interdigitates in the $L_{\beta'}$ phase (Wilkinson *et al.* 1987), which presumably should also occur with the d_{62}PG rich phase of d_{62}PG–d_{62}3adLPG 7:3. However, bilayer interdigitation was not observed in the neutron diffraction SLD profile of the d_{62}PG rich phase (figure 6-5) as a hydrocarbon core bilayer thickness of ~39.5 Å was observed which was too great in magnitude to be formed from an interdigitated bilayer (Ranck *et al.* 1977). The lack of interdigitation of the d_{62}PG rich phase suggested some zwitterionic d_{62}3adLPG may have been mixed with the excess d_{62}PG preventing bilayer interdigitation, which also occurs when mixing zwitterionic 1-*O*-palmitoyl-2-*O*-oleoyl phosphatidylethanolamine with 1-*O*-palmitoyl-2-*O*-oleoyl PG (Pozo Navas *et al.* 2005). The possibility of zwitterionic DP3adLPG being mixed with the d_{62}PG rich phase was also supported by the large headgroup thickness (~7.8 Å) of the bilayer (figure 6-5) which was greater than the headgroup thickness of crystallised DMPG (~6-7 Å) (Pascher *et al.* 1987) and as a result indicated that the bilayer headgroup region could not have been formed from d_{62}PG alone. Therefore, some zwitterionic d_{62}3adLPG must have be mixed with the d_{62}PG rich phase as d_{62}3adLPG has a larger estimated headgroup thickness of ~10-11 Å (chapter 5.3.2).

Although some zwitterionic d_{62}3adLPG was suggested to be mixed with the d_{62}PG rich phase bilayers, it does not appear to be a substantial amount as the bilayer headgroup region thickness is only slightly greater than the headgroup thickness of 100% PG therefore the quantity of zwitterionic d_{62}3adLPG in d_{62}PG–d_{62}3adLPG 7:3 was likely to be low.

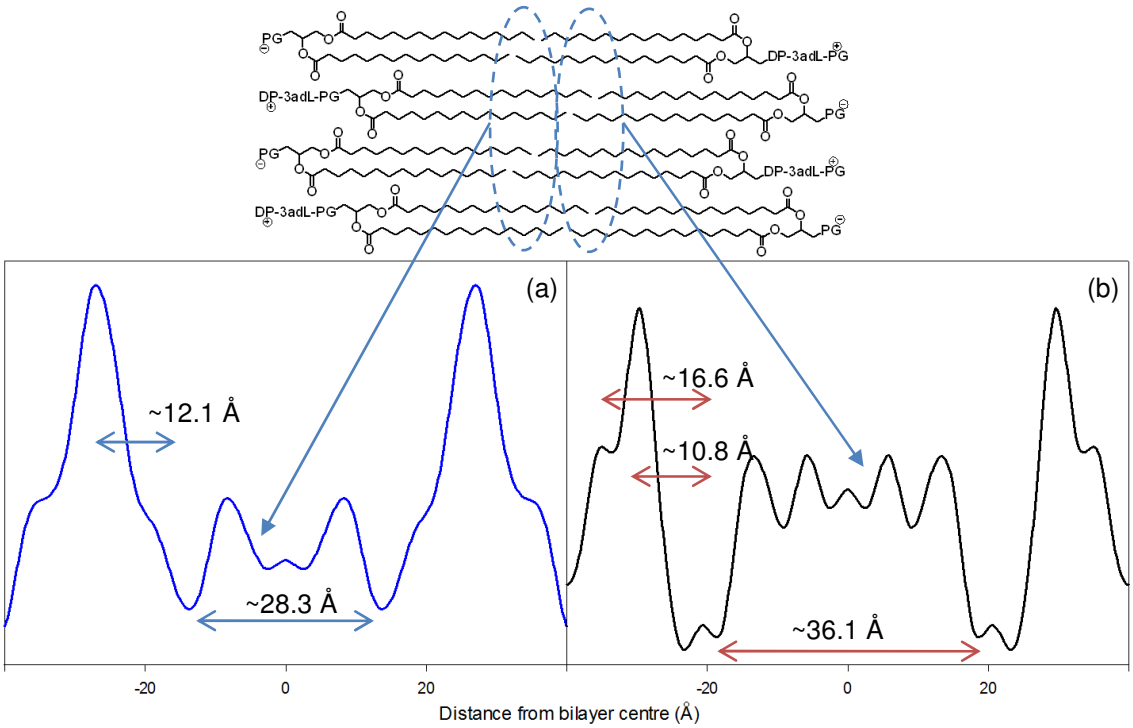

Figure 6-6 Neutron diffraction SLD profiles of d_{62}PG–d_{62}3adLPG (a) 7:3 (ion-paired phase) and (b) 45:55, at 25 °C. Molecular representation of the bilayer hydrocarbon region is shown above the neutron diffraction SLD profiles.

The neutron diffraction SLD profiles of d_{62}PG–d_{62}3adLPG 7:3 (ion-paired phase) and 45:55 in the lipid $L_{\beta'}$ phase were similar in structure as shown in figures 6-6a and b and indicated that both bilayers were composed of similar concentrations of both lipids. In contrast to the d_{62}PG rich phase of d_{62}PG–d_{62}3adLPG 7:3, d_{62}PG–d_{62}3adLPG 7:3 (ion-paired phase) and 45:55 both gave thinner hydrocarbon regions which appeared to be the result of some hydrocarbon chain overlap between the bilayer leaflets (figures 6-6a and b). The presence of a higher concentration of d_{62}3adLPG in these bilayers may have caused this overlapping effect because no hydrocarbon chain overlap was observed in the d_{62}PG rich phase (figure 6-5). The most abundant headgroup region thickness of d_{62}PG–d_{62}3adLPG 7:3 (ion-paired phase) and 45:55 was ~11-12 Å (figure 6-6a and b). This headgroup thickness was attributable to the mean thicknesses of the headgroups of d_{62}PG and d_{62}3adLPG when ion-paired. Figure 6-6b also displayed a second less abundant headgroup thickness of ~16.6 Å which suggested that the headgroup of d_{62}3adLPG was able to adopt an alternative more elongated conformation when present in amounts greater than 50 mol%, as the headgroup of d_{62}PG can only reach a maximum thickness of ~6-7 Å (Pascher *et al.* 1987).

The phospholipids found in the plasma membrane of *S. aureus*, in most cases, possess at least one anteiso hydrocarbon chain and therefore exist in the L_α phase at 37 ℃ (White & Frerman 1968). Therefore, to increase the microbiological relevance of the neutron diffraction experiments with the d_{62}PG–d_{62}3adLPG bilayers, the temperature was increased to 55 ℃ to bring the synthetic lipids into the L_α phase.

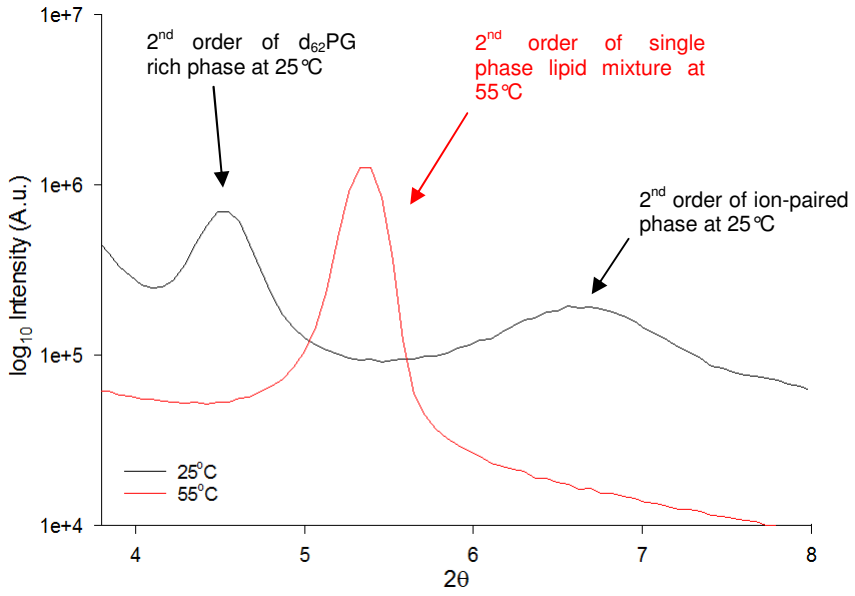

Figure 6-7 The neutron diffraction profile of d_{62}PG–d_{62}3adLPG 7:3 at 25 ℃ and 55 ℃.

Increasing of the temperature of d_{62}PG–d_{62}3adLPG 7:3 from 25 ℃ to 55 ℃ saw the two lamellar phases at 25 ℃ merge into a single lamellar phase at 55 ℃ (figure 6-7). The resultant single lamellar phase possessed a mean lamellar d-spacing of ~102 Å, which was intermediate between the d-spacing values of the two lamellar phases at 25 ℃. This d-spacing was still consistent with bilayers predominately formed from lipids with anionic or cationic charges (Pozo Navas *et al.* 2005), however it was a lot lower than the d-spacing of the d_{62}PG rich phase at 25 ℃ which presumably was due to the presence of neutral lipid ion-pairs reducing the bilayer surface anionicity.

.

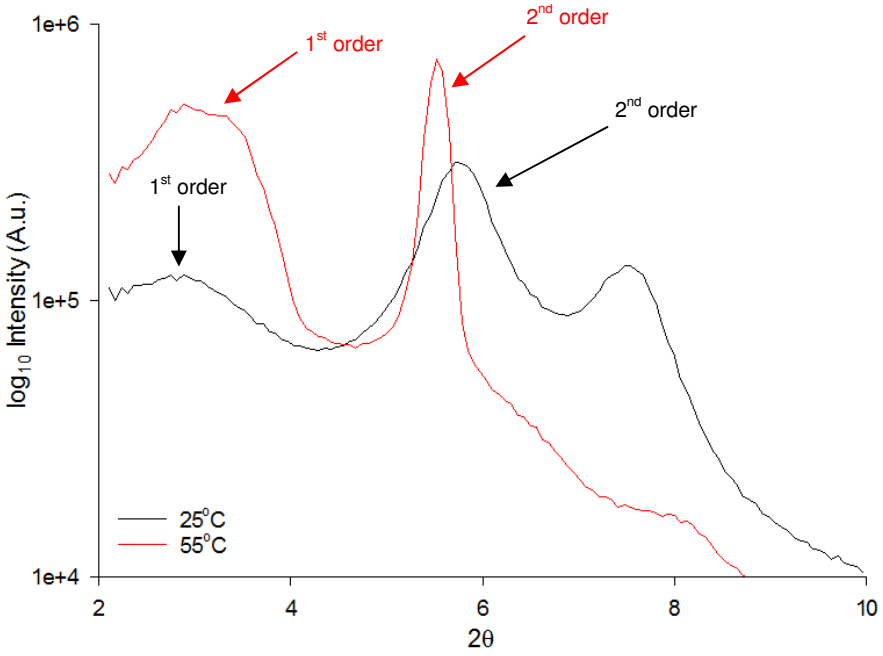

Figure 6-8 The neutron diffraction profile of d_{62}PG–d_{62}3adLPG 45:55 at 25 ℃ and 55 ℃.

In contrast, the increase in temperature of d_{62}PG–d_{62}3adLPG 45:55 from 25 ℃ to 55 ℃ saw only a minor shift in the position of the neutron diffraction peaks to lower angles at 55 ℃ (figure 6-8). This result suggested the bilayers still existed in an assumed single phase mixture in the lipid L_α phase, however the bilayers had separated further apart from each other; d-spacing of ~92.5 Å in the $L_{\beta'}$ phase increased to ~99.4 Å in the L_α phase. Presumably the increase in d-spacing was a result of increased bilayer translational freedom, as the bilayer exists in a more laterally expanded and flexible state in the L_α phase (Hanke *et al.* 1993).

The greater mobility of lipids in the L_α phase caused only a total of six orders of diffraction to be detected in both d_{62}PG–d_{62}3adLPG 7:3 and 45:55 at 55 ℃. However, most of the odd numbered orders were undetectable which resulted in the SLD profiles of the lipid mixtures being made up of a maximum of four orders. The presence of a low number of neutron diffraction orders in the L_α phase gave low resolution SLD profiles of both d_{62}PG–d_{62}3adLPG 7:3 and 45:55 (figures 6-9a and b). Such low resolution SLD profiles were expected, as L_α phase lipid bilayers scatter neutrons more erratically due to their high lipid mobility and therefore a significant amount of coherent scattering is lost as a result (Nagle & Tristram-Nagle 2000).

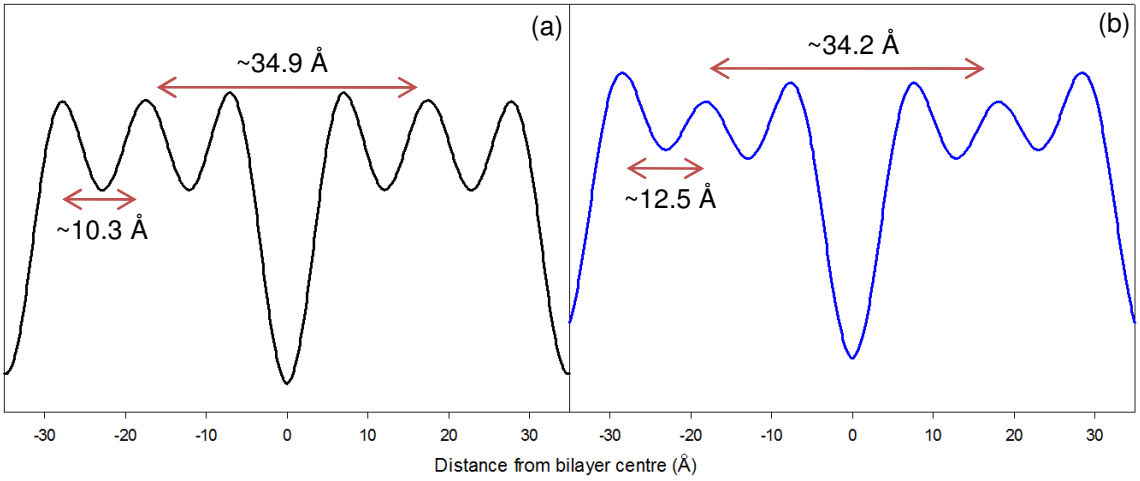

Figure 6-9 Neutron diffraction SLD profiles of d_{62}PG–d_{62}3adLPG (a) 7:3 and (b) 45:55, at 55 °C.

The L_α phase SLD profiles of d_{62}PG–d_{62}3adLPG 7:3 and 45:55 showed both bilayers to have a hydrocarbon core thickness of ~34-35 Å (figures 6-9a and b), which is ~2.5-3.5 Å greater than previous findings for d_{62}-1,2-*O*-dipalmitoyl phosphatidylcholine (d_{62}DPPC) in the L_α phase (Fragneto-Cusani 2001). The greater thickness of the hydrocarbon core was possibly due to some bilayer roughness caused by excess non-ion-paired d_{62}PG or d_{62}3adLPG in d_{62}PG–d_{62}3adLPG 7:3 and 45:55, respectively. For example, in d_{62}PG–d_{62}3adLPG 7:3 the excess non-ion-paired d_{62}PG lipid headgroups would have had high lateral electrostatic repulsion between each other and therefore to reduce this energetically unfavourable interaction some of the d_{62}PG molecules may have been forced out of the surface plane of the bilayer (Gaines 1966). The SLD profile of d_{62}PG–d_{62}3adLPG 7:3 in figure 6-9a also showed a mean bilayer headgroup thickness of ~10.3 Å which suggested the headgroup region was not made up of an average of the lipid headgroup thicknesses of d_{62}PG (~6-7 Å, (Pascher *et al.* 1987)) and d_{62}3adLPG (~10-11 Å). This finding supported the possibility that excess d_{62}PG in d_{62}PG–d_{62}3adLPG 7:3 may have had some out of plane rearrangement and increased bilayer surface roughness therefore resulting in a thicker bilayer headgroup region being observed in the bilayer SLD profile (figure 6-9a). The headgroup thickness of d_{62}PG–d_{62}3adLPG 45:55 in figure 6-9b was slightly larger than the same region in the 7:3 lipid mixture (figure 6-9a). This result was not unexpected as this lipid mixture had a greater abundance of d_{62}3adLPG, which was shown in the SLD profile of d_{62}PG–d_{62}3adLPG 45:55 in the $L_{\beta'}$ phase (figure 6-6b) to have a mean headgroup thickness from ~10.1 Å up to 16.6 Å depending on the lipid's headgroup conformation.

6.3.2 Neutron reflectivity of mixtures of d_{62}PG and d_{62}3adPG in different pH buffers

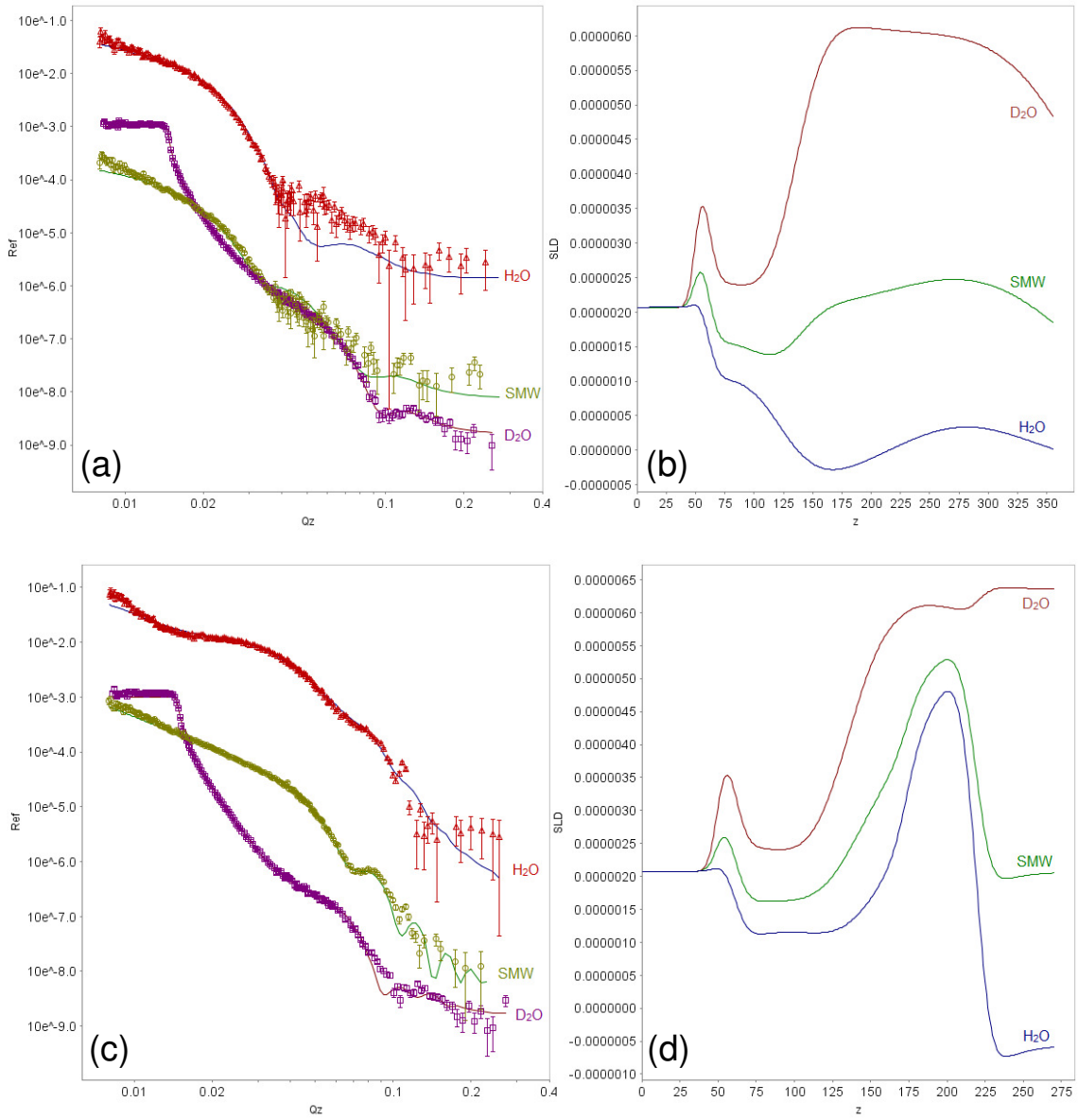

Figure 6-10 Neutron reflectivity curves of d_{62}PG–d_{62}3adLPG 7:3 at 55 ℃, with (a) a pH 7.4 buffering system and (b) the accompanying fitted SLD profiles of each contrast used and with (c) a pH 5.5 buffering system and (d) the accompanying fitted SLD profiles of each contrast used.

Table 6-2 Fitted parameters for d_{62}PG–d_{62}3adLPG 7:3 at 55 ℃, with pH 5.5 and 7.4 buffering systems.

pH	Layer	Thickness (Å)	SLD ($\times 10^{-6}$ Å^{-2})	Hydration (%)	Roughness (Å)
7.4	Water Layer	118.77 ± 19.6		100	
7.4	Head groups	8.00 ± 1.3	1.89	53.86 ± 7.4	23.14 ± 14.8
7.4	Chains	32.35 ± 3.4	6.79	26.44 ± 7.5	23.14 ± 14.8
5.5	Water Layer	28.99 ± 5.6		100	
5.5	Head groups	8.09 ± 1.3	4.08	16.23 ± 3.6	7.22 ± 2.70
5.5	Chains	31.40 ± 2.6	7.06	0.74 ± 0.4	7.22 ± 2.70

The neutron reflectivity curves of d_{62}PG–d_{62}3adLPG 7:3 in both pH environments (figures 6-10a-d) gave mean fitted hydrocarbon core thicknesses of ~31-33 Å as shown in table 6-2. These hydrocarbon core thicknesses were in good agreement with bilayers consisting of d_{62}DPPC in the L_α phase (Fragneto-Cusani 2001), and suggested the d_{62}PG–d_{62}3adLPG 7:3 bilayers in both pH environments were in the L_α phase. The fitted SLD of d_{62}PG–d_{62}3adLPG 7:3 across the whole thickness of the bilayer at pH 5.5 was substantially higher than the bilayer at pH 7.4 (table 6-2). This increase in SLD at pH 5.5 suggested the bilayer was more laterally dense at pH 5.5, presumably due to an increase in lipid ion-pair formation between d_{62}PG and d_{62}3adLPG, as a result of more d_{62}3adLPG being cationic at pH 5.5. The fitted hydrations of the bilayer at both pHs also supported the finding of increased bilayer lateral density at pH 5.5, where a low bilayer hydration was observed at pH 5.5 in contrast to pH 7.4 (table 6-2); thus showing solvent could not penetrate well into the more dense bilayer at pH 5.5. As shown in table 6-2, the fitted headgroup thicknesses of the bilayer in both pH environments were ~8 Å which suggested the headgroup regions were made up of an average headgroup thickness of d_{62}PG (~6-7 Å, (Pascher *et al.* 1987)) and d_{62}3adLPG (~10.1-16.6 Å), in the ratio of 7:3, respectively. A substantial difference in bilayer undulation was found between the pH 5.5 and 7.4 environments as indicated by the bilayer fitted roughness of ~23.14 Å at pH 7.4 and ~7.22 Å at pH 5.5 (table 6-2). The differences in bilayer undulation were attributable to the higher incidence of zwitterionic d_{62}3adLPG at pH 7.4, as bilayer undulation was less pronounced at pH 5.5 (table 6-2).

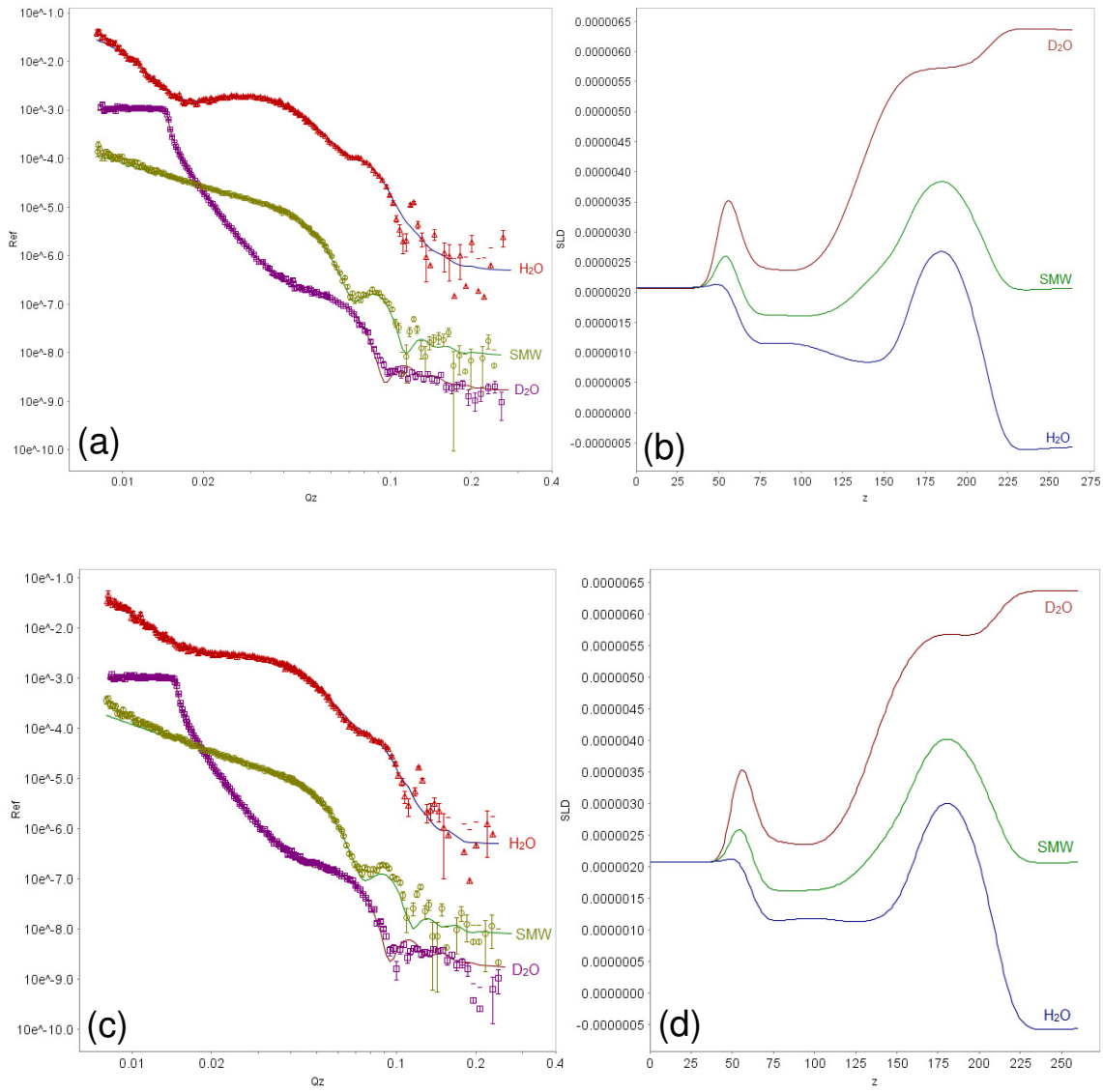

Figure 6-11 Neutron reflectivity curves of d_{62}PG–d_{62}3adLPG 45:55 at 55 ℃, with (a) a pH 7.4 buffering system and (b) the accompanying fitted SLD profiles of each contrast used and with (c) a pH 5.5 buffering system and (d) the accompanying fitted SLD profiles of each contrast used.

Table 6-3 Fitted parameters for d_{62}PG–d_{62}3adLPG 45:55 at 55 ℃, with pH 5.5 and 7.4 buffering systems.

pH	Layer	Thickness (Å)	SLD (×10^{-6} Å^{-2})	Hydration (%)	Roughness (Å)
7.4	Water Layer	14.16 ± 2.3		100	
7.4	Headgroups	14.32 ± 4.2	4.93	47.09 ± 5.1	8.00 ± 0.6
7.4	Chains	33.12 ± 4.6	5.84	34.26 ± 6.7	8.00 ± 0.6
5.5	Water Layer	18.45 ± 1.9		100	
5.5	Headgroups	16.94 ± 4.1	4.62	26.44 ± 7.9	9.48 ± 3.5
5.5	Chains	32.16 ± 4.6	5.50	8.65 ± 3.7	9.48 ± 3.5

The fitted hydrocarbon core thicknesses of the neutron reflectivity curves (figures 6-10a-d) of d_{62}PG–d_{62}3adLPG 45:55 in both pH environments (table 6-3) were similar to those found for the d_{62}PG–d_{62}3adLPG 7:3 bilayers (table 6-2), and suggested d_{62}PG–d_{62}3adLPG 45:55 was in the L_α phase at both pHs. The fitted roughness of the 45:55 lipid mixture bilayer in both pH buffers (table 6-3) showed these bilayers had analogous undulation to the 7:3 lipid mixture bilayer in a pH 5.5 buffer (table 6-2). Such similarities between the lipid mixtures supported the possibility that higher concentrations of cationic d_{62}3adLPG in d_{62}PG and d_{62}3adLPG mixtures reduces bilayer undulation and stabilises them, presumably due to more lipid ion-pair formation. With respect to the lipid ion-pairs, high positive fitted headgroup region SLDs of the bilayer in both pH environments were found (table 6-3), which suggested the bilayer headgroup regions at both pHs had high lateral density presumably as a result of substantial ion-pair formation between d_{62}PG and d_{62}3adLPG. However, the headgroup region SLD of the bilayer in the pH 5.5 buffer was markedly lower than at pH 7.4 (table 6-3), which was expected as the bilayer at pH 5.5 would have had an excess of cationic d_{62}3adLPG resulting in lipid-lipid headgroup repulsion, thus reducing bilayer lateral density (Gaines 1966). Fitted hydration of the bilayer in a pH 7.4 buffer showed ~35% hydration across the whole thickness of the bilayer whereas hydration in the pH 5.5 buffer was only 25% (table 6-3). The lack of hydration at pH 5.5 suggested that, although the bilayer had a reduction in lateral density, the bilayer was still sufficiently dense enough to reduce the traversing of solvent across it whereas at pH 7.4 the presence of zwitterionic d_{62}3adLPG may have created inhomogeneities in the bilayer surface thus making it more porous.

The fitted SLDs of the hydrocarbon regions of the bilayer in both pH buffers (table 6-3) was relatively low in comparison to the 7:3 lipid mixture in both pH buffers (table 6-2), however as explained in chapter 4.2.4, d_{62}3adLPG suffered from some deuterium-hydrogen exchange and the effect of this was more pronounced in this lipid mixture as it contained greater concentrations of d_{62}3adLPG. At pH 7.4 a fitted headgroup thickness of ~14.32 Å was found however this increased vastly to ~16.94 Å at pH 5.5 (table 6-3). The increased headgroup thickness of both bilayers was attributed to the high concentration of d_{62}3adLPG present in them. However, the more elongated headgroup conformation of d_{62}3adLPG appeared to be favoured by cationically charged d_{62}3adLPG, as the greatest headgroup region thickness was observed in the pH 5.5 buffer when d_{62}3adLPG was mostly cationic.

6.3.3 SANS of mixtures of d_{62}PG and d_{62}3adPG in different pH buffers

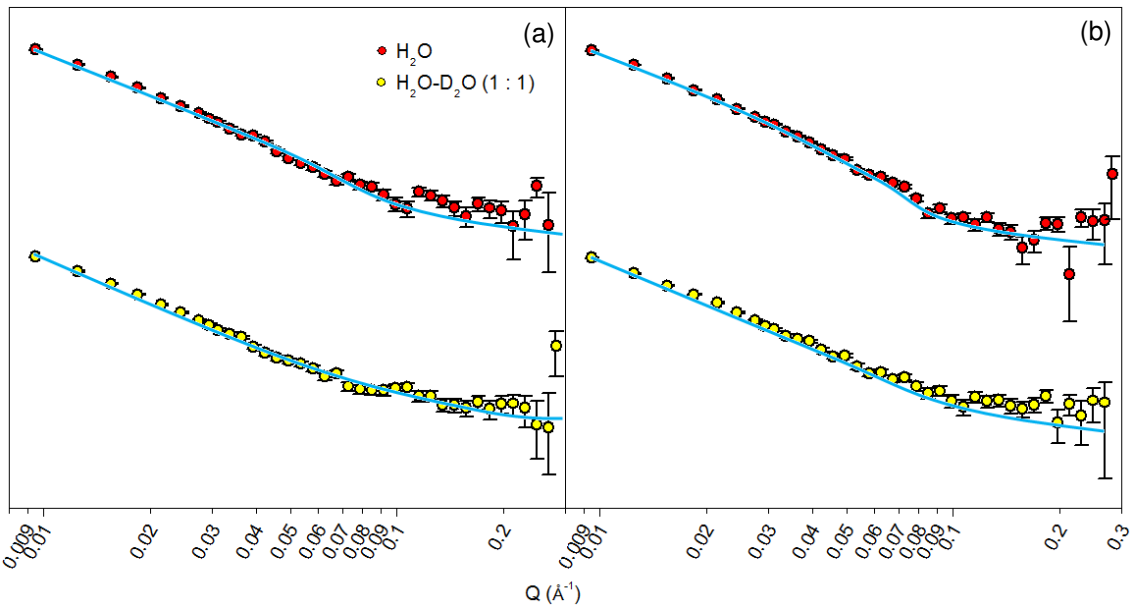

Figure 6-12 SANS curves and associated fits of d_{62}PG–d_{62}3adLPG 7:3 at 55 °C in (a) pH 7.4 and (b) pH 5.5 buffering systems, in H_2O and H_2O–D_2O 1:1 v/v contrasts.

Table 6-4 Fitted SANS parameters for d_{62}PG–d_{62}3adLPG 7:3 at 55 °C, with pH 5.5 and pH 7.4 buffering systems.

Temperature	pH	Layer thickness (Å)	D-spacing (Å)	Layers	% sample MLV
55 °C	7.4	49.93 ± 2.92	113.94 ± 12.16	2.18 ± 0.34	22.52 ± 4.45
55 °C	5.5	48.01 ± 3.03	111.09 ± 14.39	2.83 ± 0.77	29.66 ± 3.23

SANS was performed on vesicles formed from the 7:3 and 45:55 molar mixtures of d_{62}PG–d_{62}3adLPG to assess the properties of the bilayers in a structure mimetic to the plasma membrane of *S. aureus*. Both SANS curves of d_{62}PG–d_{62}3adLPG 7:3 in figures 6-12a and b showed the presence of a Bragg peak at Q ~ 0.12 Å^{-1}, which suggested some of the vesicles in each sample were multi-lamellar vesicles (MLVs) since Bragg peak formation is a feature of multilamellar structures. The fitted content of the MLVs at pH 5.5 was slightly higher than at pH 7.4 (table 6-4) which suggested the bilayer surfaces at pH 7.4 were more anionically charged due to less cationic d_{62}3adLPG being in them. Therefore electrostatic charge repulsion between adjacent MLV bilayers was likely to be high at pH 7.4, preventing preservation of stable MLV structures on sample sonication (Hope *et al.* 1986). The MLV d-spacings for both vesicle samples shown in table 6-4 were typical of highly charged bilayer surfaces (Pozo Navas *et al.* 2005), which was expected as ~70% of the vesicles consisted of anionic d_{62}PG and the remaining lipid was d_{62}3adLPG. Table 6-4 also showed the fitted thicknesses of the vesicle bilayers were similar in thickness to the bilayers of the same lipid mixtures found by neutron

reflectivity (table 6-2). The good agreement between the fitted SANS and neutron reflectivity data increase the confidence in the bilayer thickness parameters extrapolated from each model of each technique.

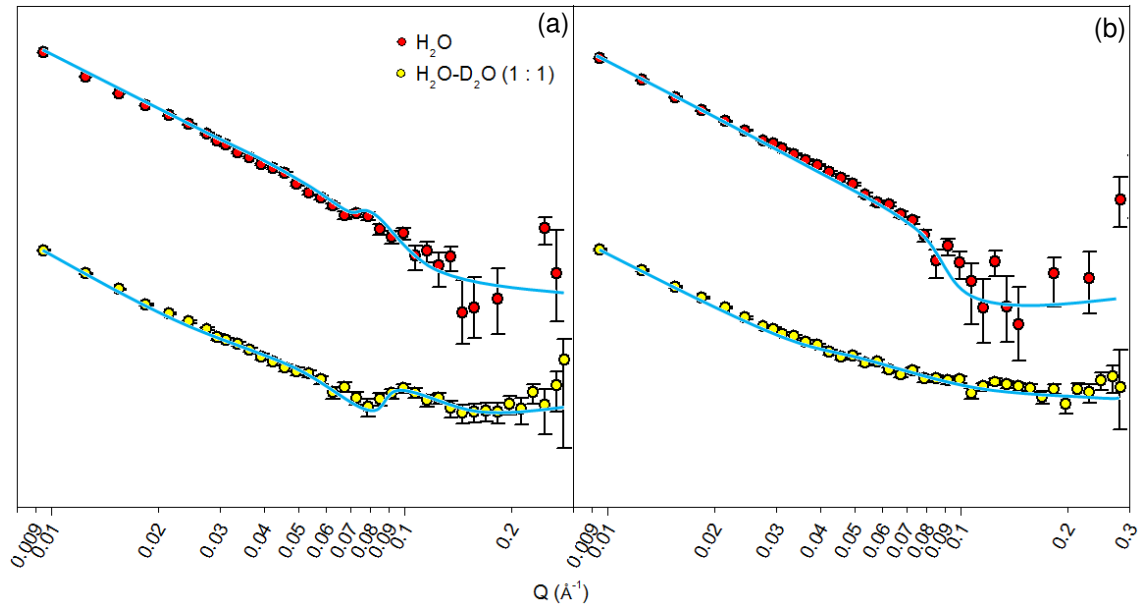

Figure 6-13 SANS curves and associated fits of d_{62}PG–d_{62}3adLPG 45:55 at 55 ℃ in (a) pH 7.4 and (b) pH 5.5 buffering systems, in H_2O and H_2O–D_2O 1:1 v/v contrasts.

Table 6-5 Fitted SANS parameters for d_{62}PG–d_{62}3adLPG 45:55 at 55 ℃, with pH 5.5 and pH 7.4 buffering systems.

Temperature	pH	Layer thickness (Å)	D-spacing (Å)	Layers	% sample MLV
55 °C	7.4	60.93 ± 3.49	101.40 ± 21.68	2.00 ± 0.06	8.37 ± 4.24
55 °C	5.5	64.34 ± 2.55	128.66 ± 17.83	1.69 ± 0.17	6.91 ± 1.98

The SANS curves of d_{62}PG–d_{62}3adLPG 45:55 (figures 6-13a and b) all showed the presence of a pronounced Bragg reflection between *Q* 0.08-0.1 $Å^{-1}$, which was similar to the 7:3 lipid mixture vesicles and suggested these vesicle dispersions also had some MLVs present in them. The fitted quantity of the MLVs of these vesicles at both pH 7.4 and 5.5 (table 6-5) were substantially less than that found for the d_{62}PG–d_{62}3adLPG 7:3 vesicle dispersions (table 6-4). The lower concentration of MLVs in these vesicle dispersions suggested that the higher concentration of d_{62}3adLPG in this lipid mixture resisted the formation of stable MLVs. The fitted MLV d-spacing shown in table 6-5 of the vesicle dispersion at pH 5.5 was similar to the MLV d-spacings of the 7:3 lipid mixture in both pH conditions (table 6-4). Such a large d-spacing was expected due to an excess of cationic d_{62}3adLPG being present in this vesicle dispersion at pH 5.5 which would have resulted in the surfaces of the vesicle bilayers being more cationically charged (chapter

5.4.4) and therefore adjacent bilayer electrostatic repulsion between bilayers would have been high (Pozo Navas *et al.* 2005). However, the MLV dispersion in the pH 7.4 buffer had a lower d-spacing in comparison to the pH 5.5 buffer (table 6-5) which suggested that the vesicle bilayer surfaces in this pH environment were not highly ionically charged and may have been close to neutral (chapter 5.4.4). This lack of vesicular surface charge was possibly due to a larger proportion of the MLVs d_{62}3adLPG lipids being zwitterionic at pH 7.4, therefore the forces governing the d-spacing of the MLV bilayers were more likely to be Van der Waal interactions rather than electrostatic ones, as observed previously for neutral PC bilayers (Lis *et al.* 1982). The bilayer thicknesses of the vesicles at both pHs were similar in thickness to that observed in neutron reflectivity of the same lipid mixture (table 6-3), which suggested both experiments data fitting models were in agreement which increased the confidence in the bilayer thickness parameters obtained. Additionally, the greater bilayer fitted thickness of the vesicles in the pH 5.5 buffer compared to the pH 7.4 buffer (table 6-5) supported data from both the neutron diffraction and reflectivity (figure 6-6b and table 6-3) of the same lipid mixture, where an alternative elongated headgroup conformation of cationic d_{62}3adLPG was proposed which increases the thickness of the bilayer.

6.4 Discussion

The headgroup conformation of L-PG in *S. aureus* has previously been thought to adopt a loop structure due to the formation of an internal ionic bond between the lipid's protonated α or ε amine of the lysyl moiety and the lipid's negatively charged phosphate group (Tocanne *et al.* 1974c, El Mashak & Tocanne 1979). Both L-PG and d_{62}3adLPG are analogous with respect to their headgroup structure and therefore it is plausible that the headgroup of d_{62}3adLPG can also form a looped structure, which was previously demonstrated in chapter 5.3.2. The neutron diffraction SLD profile (figure 6-6b) and neutron reflectivity fitted data (table 6-3) of d_{62}PG–d_{62}3adLPG 45:55 showed bilayer headgroup thicknesses of ~10-14 Å and ~16-17 Å which were attributed mainly to the thickness of the headgroup of d_{62}3adLPG in two different conformations. The smaller thickness of ~10-14 Å appeared to be the most favoured conformation of the d_{62}3adLPG headgroup as it existed at higher concentrations in both 7:3 and 45:55 molar ratios of d_{62}PG–d_{62}3adLPG in both neutron reflectivity and diffraction experiments. This headgroup thickness of ~10-14 Å of d_{62}3adLPG was able to be mapped directly onto the molecular structure of the lipid (figure 6-14) and suggested the most favourable intramolecular ionic bond in d_{62}3adLPG was formed between the protonated ε-amine of the lysyl moiety and the phosphate group. This favoured 'loop structure' headgroup conformation shown in figure 6-14 was expected as the protonated ε-amine is a much stronger base than the protonated α-amine due to it having a higher pKa of >10 (chapter 5.4.1), thus the protonated ε-amine would be expected to form stronger electrostatic bonds to the phosphate group of d_{62}3adLPG. The alternative less abundant conformation of the headgroup of d_{62}3adLPG (~16-17 Å) was most likely to be due to the lipid's protonated α-amine forming ionic bonds to its phosphate group (figure 6-14), as this gives the protonated ε-amine greater extension away from the bilayer surface into the external environment. This latter 'stretched-chain' conformation appeared to be favourable under conditions where many cationically charged d_{62}3adLPG molecules were grouped together in a bilayer (e.g. d_{62}PG–d_{62}3adLPG 45:55 in a pH 5.5 buffer), as lipid-lipid electrostatic repulsion can be minimised by protrusion of the protonated ε-amine away from the bilayer surface. The 'stretched-chain' conformation of d_{62}3adLPG was not found in neutron diffraction of 100% DP3adLPG as shown in chapter 5.3.2, presumably due to the bilayer forming an interdigitated phase which separated the lipid headgroups sufficiently to relax the lateral pressure caused by the electrostatic repulsion between adjacent headgroups.

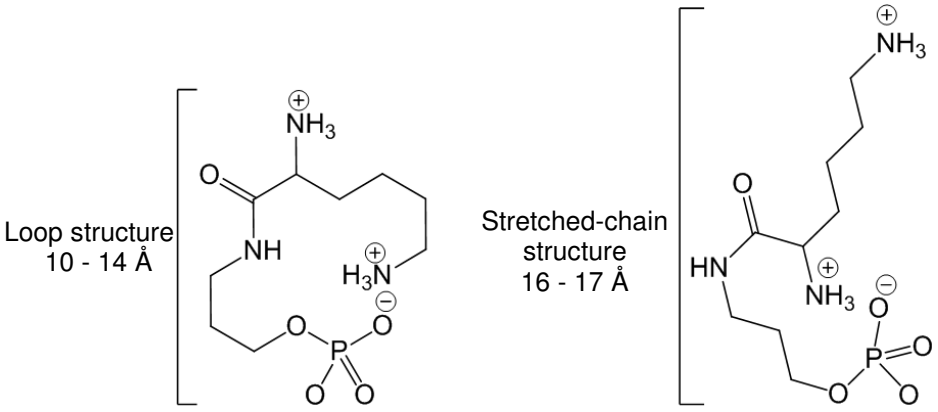

Figure 6-14 Molecular structures of the conformation of the headgroup of d_{62}3adLPG; loop structure conformation is shown on the left (most favourable) and chain stretched structure conformation is shown on the right (favourable under lateral stress conditions).

Mixing of d_{62}PG and d_{62}3adLPG led to the formation of ion-pairs between the lipids as was inferred from both neutron diffraction and neutron reflectivity experiments. However, neutron diffraction detected lamellar phase separation of d_{62}PG–d_{62}3adLPG 7:3 in the $L_{\beta'}$ phase (figure 6-3), which was caused by lipid domains coupling on either side of the bilayer leaflets and alignment of these domains in adjacent bilayers. The reason for this lamellar phase separation appears to be because intralamellar and interlamellar domain coupling reduces the tensional forces imposed upon the solvent layer between adjacent bilayers, but only when the bilayers are in a static structure such as in the lipid $L_{\beta'}$ phase (Tayebi *et al.* 2012). Therefore the alignment of lipid domains in lamellar stacks is energetically favourable, which is what appears to have occurred in d_{62}PG–d_{62}3adLPG 7:3 in the $L_{\beta'}$ phase. Increasing of the temperature, however, of d_{62}PG–d_{62}3adLPG 7:3 from 25 °C to 55 °C abolished the presence of lamellar phase separation, as the lipids in the L_{α} phase had increased kinetic energy to move laterally in the bilayer and therefore could mix more ideally. Such lipid mixing behaviour in a fluid state bilayer is thought to be more energetically favourable for the bilayer than the reduction in solvent layer tensional energy (Tayebi *et al.* 2012). With regard to if lipid domains still existed in d_{62}PG–d_{62}3adLPG 7:3 in the L_{α} phase, it currently remains inconclusive from these experiments and therefore it is possible d_{62}PG and d_{62}3adLPG may have been ideally mixed in d_{62}PG–d_{62}3adLPG 7:3 in the L_{α} phase.

The three-dimensional shape of L-PG has previously been described as 'cone-like' due to the large lateral cross-sectional area of its headgroup in comparison to the smaller lateral cross-sectional area of its hydrocarbon chains (Tocanne *et al.* 1974b). In neutron reflectivity experiments, the fitted roughness of d_{62}PG–d_{62}3adLPG 7:3 in a pH 7.4 buffer was substantially

higher than the same bilayer in a pH 5.5 buffer (table 6-2), which suggested the bilayer at pH 7.4 was more undulated than at pH 5.5. This increased undulation of the bilayer at pH 7.4 can possibly be linked to zwitterionic d_{62}3adLPG, which may adopt this suggested cone-like morphology of L-PG, and may have resulted in the substantial positive curvature of the bilayer at pH 7.4. In contrast, the lack of positive bilayer curvature at pH 5.5 suggested cationic d_{62}3adLPG does not cause bilayer curvature presumably due to the more favourable ion-pair interaction with d_{62}PG, which may align d_{62}3adLPG more parallel to the bilayer normal.

In the neutron reflectivity experiments of d_{62}PG–d_{62}3adLPG 7:3, changing of the environmental pH from 7.4 to 5.5 saw a substantial increase in the bilayer lateral density and a reduction in bilayer hydration (table 6-2). Such an effect was not observed in the lateral density of d_{62}PG–d_{62}3adLPG 45:55 when reducing the pH, presumably due to the presence of excess cationic d_{62}3adLPG, however, bilayer hydration was low in the pH 5.5 buffer which suggested the bilayer was still laterally very dense at pH 5.5 (table 6-3). The high lateral density and low hydration of both lipid mixtures at pH 5.5 was attributable to the change in charge state of d_{62}3adLPG, where the majority of the lipid's α-amines became protonated (pKa ~5.5-6.7, chapter 5.4.1). The increased number of cationic d_{62}3adLPG lipids at pH 5.5 presumably resulted in a greater number of ion-pairs being formed with d_{62}PG hence the bilayer increased in lateral density and forced out a large amount of solvent molecules. With respect to the plasma membrane of *S. aureus*, these bilayer changes suggest that the membrane becomes highly laterally dense and less susceptible to solvent penetration when the bacterium is grown in a mildly acidic environment. Therefore, it appears that not only can L-PG at >50% total phospholipid change the bacterial plasma membrane surface to cationic (chapter 3.3.1) it can also, through lipid ion-pair formation, retard the diffusion of protons through its plasma membrane by becoming more tightly packed, thus protecting the bacterial cytoplasm from the harmful effects of excess protons.

6.5 Conclusion

As a result of finding ion-pairing between d_{62}PG and d_{62}3adLPG, increases in lateral density and reduction in solvent penetration of bilayers consisting of these lipids at pH 5.5 compared to pH 7.4 gave an indication of the mechanisms by which L-PG can help *S. aureus* adapt to a mildly acidic environment. This environmental adaptation using L-PG provided insight into how *S. aureus* can survive on the mild pH environment of skin (<pH 5) and the nasal mucosa (~pH 6) (Lambers *et al.* 2006, Washington *et al.* 2000). However, a mildly acidic environment is only one of the innate defensive mechanisms of these human epithelial surfaces and both the skin and the nasal mucosa are much more complex in terms of their innate defences and tend to secrete a number of different cationic antimicrobial peptides (CAMPs) as well, which *S. aureus* can also survive in the presence of (Ong *et al.* 2002, Cole *et al.* 1999). Therefore, to investigate how L-PG can also facilitate resistance to CAMPs in the presence of a mildly acidic environment, the bilayer systems used in this chapter will be looked at after exposure to a CAMP analogue (magainin 2 F5W) in both pH 7.4 and 5.5 environments. This will help to further understand, how L-PG facilitates survival in *S. aureus* when the bacterium colonises low pH human epithelial surfaces.

Chapter 7

Study of the interaction of magainin 2 F5W with monolayers and membranes containing 3-aza-dehydroxy-lysylphosphatidylglycerol

7.1 Introduction

Since the discovery of pH-induced alterations in lysyl-phosphatidylglycerol (L-PG) biosynthesis by *Staphylococcus aureus* (Gould & Lennarz 1970), changes in the lipid's biosynthesis in *S. aureus* have primarily been examined when exposing the bacterium to sub-lethal concentrations of cationic antimicrobial peptides (CAMPs) (Thedieck *et al.* 2006, Samant *et al.* 2009, Hachmann *et al.* 2009, Salzberg & Helmann 2008, Maloney *et al.* 2009, Kleinschmidt *et al.* 1997, Nishi *et al.* 2004, Ernst *et al.* 2009, Koprivnjak *et al.* 2002, Sievers *et al.* 2010, Peschel *et al.* 2001, Kristian *et al.* 2003, Staubitz *et al.* 2004, Weidenmaier *et al.* 2005). The principal finding of these studies were that plasma membrane L-PG upregulation reduces the sensitivity of *S. aureus* to the putative membrane lytic effects of CAMPs. Therefore the function of L-PG was suggested to be primarily for resistance to CAMPs by reducing the electrostatic attraction of CAMPs to the bacterial plasma membrane (Ernst & Peschel 2011). The mechanism which causes the reduction in electrostatic attractiveness of the CAMP to the bacterial membrane was suggested to be neutralisation of the negative charge imparted by the other phospholipids in the bacterial plasma membrane, phosphatidylglycerol (PG) and cardiolipin (CL). However, to date, this mechanism is unsubstantiated due to the labile nature of L-PG under mild aqueous conditions making it difficult to study in lipid mixtures with PG and CL (Danner *et al.* 2008). To try and solve this problem, 1,2-*O*-dipalmitoyl 3-aza-dehydroxy L-PG (DP3adLPG) or d_{62}-1,2-*O*-dipalmitoyl 3-aza-dehydroxy L-PG (d_{62}3adLPG) were used as L-PG substitutes in lipid mixtures with synthetic PG and CL. These lipid mixtures, in the form of monolayers or bilayers, were then challenged with a CAMP in order to study the resistance based mechanism of L-PG. The data from these experiments were then compared to similar data obtained from *S. aureus* lipid extracts treated under the same conditions with the CAMP, in order to try and elucidate the resistance mechanism of L-PG to CAMPs.

An amphibian innate immune system CAMP analogue, magainin 2 F5W, was used to challenge monolayers and bilayers formed from both natural and synthetic lipid mixtures. With respect to the synthetic lipid mixtures, ratios of lipids that mimic those found in methicillin susceptible *S. aureus* 476 (MSSA 476), methicillin resistant *S. aureus* (MRSA) G32 and MRSA H66 grown at pH 7.4 and 5.5 were utlised (chapter 2.3.1). Examination of both the synthetic and natural lipid mixtures of *S. aureus* grown at pH 5.5 after exposure to magainin 2 F5W provided information on how the bacterial plasma membrane adapts to survive on low pH epithelial surfaces such as skin and the anterior nares of the nasal passages, where there is a rich concentration of innate immune system CAMPs such as the cathelicidin LL-37 and the defensins hBD-2 and, in the anterior nares, hBD-3 (Ong *et al.* 2002, Cole *et al.* 1999, Laudien *et al.* 2011). Assessment of the synthetic and natural lipid mixtures of *S. aureus* grown at pH 7.4 after exposure to magainin 2 F5W gave details of how the plasma membrane of *S. aureus* interacts with CAMPs at physiological pH, such as when *S. aureus* is found to be the principal pathogen in bacteremia (Klevens *et al.* 2007).

The membrane disruptive effects of magainins originate from their ability to form electrostatic bonds to the lipids on the negative surface of the bacterial plasma membrane (Zasloff *et al.* 1988). After ionic bonding of the peptide to the membrane surface, they adopt an amphiphilic α-helical conformation which allows the peptide to partition into the hydrocarbon core of the membrane (Ludtke *et al.* 1995, Zasloff *et al.* 1988). Partitioning of the peptide into the membrane disrupts the packing of the lipids and providing the concentration of the peptide is high enough on the outer leaflet of the membrane, the peptides can oligomerize and either cause membrane thinning or form pores which allow leakage of intracellular contents and disruption of membrane processes (Ludtke *et al.* 1996, Ludtke *et al.* 1995). In order to study these membrane destructive effects of magainin 2 F5W, techniques are required where the membrane lipid packing can be assessed before and after introduction of the peptide.

Previous studies with cytochrome *c* and liquid condensed phase phosphatidylethanolamine monolayers highlighted cytochrome *c* can partition into the monolayer by an increase in monolayer surface pressure after injection of cytochrome *c* under the monolayer (Quinn & Dawson 1969). This monolayer technique can be adapted to both MRSA G32 lipid extracts and synthetic lipid models of this extract with the injection of magainin 2 F5W beneath monolayers composed of these lipids. Any detected increases in surface pressure can be assumed to be

the result of the peptide partitioning into the monolayer (Quinn & Dawson 1969). Neutron diffraction is also applicable to assess the membrane disruptive effects magainin 2 F5W has on MSSA 476 lipid extracts and biomimetic synthetic lipid models of the *S. aureus* plasma membrane as alterations in the scattering length density (SLD) of the membranes along the z-axis (bilayer normal) can highlight changes in lipid packing density across the whole span of the bilayer. The disruptive effects of the peptide in the synthetic lipid bilayer are also highlightable by the use of hydrocarbon chain deuterated lipids (e.g. d_{62}3adLPG) which can clearly show the effects the peptide has on the hydrocarbon core of the bilayer as the peptide has a lower SLD of ~1-1.5 × 10^{-6} $Å^{-2}$ in comparison to the bilayer hydrocarbon core SLD which is closer to ~5-7 × 10^{-6} $Å^{-2}$ (Leonard *et al.* 2001, Armen *et al.* 1998, Fragneto *et al.* 2000).

Although neutron diffraction can provide high resolution structural details of bilayer systems with and without the presence of the peptide, the pH of the solvent surrounding the bilayers cannot be controlled as hydration of the bilayers comes in the form of humidity (Sebastiani *et al.* 2012). Therefore the charge state of d_{62}3adLPG and L-PG is largely uncontrolled in neutron diffraction due to their α-amine pKas of ~5.5-6.7 (chapter 5.3.1) and 6-7 (Tocanne *et al.* 1974c), respectively. To rectify this problem, neutron reflectivity and small angle neutron scattering (SANS) were also employed, with only the synthetic lipid models, as different pH buffers can be used to solvate the bilayers. Both SANS and neutron reflectivity collectively provide details of how the synthetic lipid bilayers, mimicking *S. aureus* grown at pH 7.4 and 5.5, change in thickness, lateral density and hydration (Fragneto *et al.* 2000) when challenged with magainin 2 F5W in both pH 5.5 and 7.4 environments, thus complimenting the diffraction data. Natural lipid extracts were not used in these experiments due to the inability to form robust long lasting stable floating bilayers and vesicles with these lipids. Therefore, the combined neutron scattering techniques and monolayer studies should provide greater insight into the mechanism by which L-PG in the membrane of *S. aureus* is able to resist the membrane destructive effects of CAMPs in both pH 5.5 and 7.4 growth environments.

7.2 Materials and methods

7.2.1 Materials

Tris(hydroxymethyl)aminomethane (>99.0%), concentrated hydrochloric acid (~38%), concentrated deuterium chloride (99 %D atom), glacial acetic acid, sodium sulphate (>99.0%) and deuterium oxide (99.9 %D atom) were all purchased from Sigma-Aldrich UK, and used as supplied. Cleaning solvents for neutron diffraction, chloroform (99.5%), methanol (99.9%) and acetone (99.9%) were purchased from Sigma-Aldrich, international, and used as supplied. Reagent grade chloroform for monolayer experiments was purchased from Fisher Scientific, Leicestershire, UK. 1,2-*O*-Dipalmitoyl-*sn*-glycero-3-phospho-(1'-*rac*-glycerol), sodium salt was purchased from Avanti Polar Lipids (Alabaster, USA), however was converted to the triethylammonium salt by crystallising the conjugate acid from cold acetone using 1.5 eq. HCl, then filtering off NaCl and finally crystallising the lipid-triethylammonium salt twice from cold acetone using triethylamine (>99%) purchased from Sigma-Aldrich, UK. 1,1',2,2'-Tetramyristoyl cardiolipin, sodium salt was also purchased from Avanti Polar Lipids (Alabaster, USA) and used as supplied. Ultrapure water (18.2 MΩ.cm) for all experiments was obtained from a Milli-Q 16 Ultrapure water system (Merck Millipore, Billerica, USA). Silicon substrates measuring 38 mm × 70 mm × 10 mm for neutron reflectivity experiments were purchased from Crystran Ltd, Poole, UK and silanized as described in chapter 6.2.3. Magainin 2 F5W was purchased from Genscript (Piscataway, New Jersey, USA). Silicon discs for neutron diffraction experiments were obtained from Silicon Materials (Kaufering, Germany); diameter 50.8mm ± 0.50 mm, thickness 275 µm ± 20 µm, resistivity 1-5 Ωcm and single sided polished finish.

7.2.2 Peptide interactions with natural and synthetic lipid monolayers

Phospholipids from MRSA G32 grown at pH 5.5 and 7.4 were extracted by the acid-modified Bligh and Dyer technique (Foreman-Wykert *et al.* 2000), as described in chapter 2.2.2. Two milligram samples of each lipid extract and DP3adLPG–1,2-*O*-diapalmitoyl PG (DPPG)–tetramyristoyl CL (TMCL) 28.12:66.85:5.03 and 51.63:40:8.37 mol/mol/mol to mimic the phospholipids expressed in these lipids extracts (chapter 2.3.1), were each dissolved in 1 mL of chloroform. A volume of ~20-30 µL of each lipid mixture was then deposited separately dropwise onto an aqueous subphase of 10 mM tris(hydroxymethyl)aminomethane (TRIS)–acetic acid (AcOH) 1:1 mol/mol adjusted to either pH 5.5 or 7.4, in a ~350 mL polytetrafluoroethane trough. The surface area of the trough was ~120 cm^2 and each lipid monolayer was maintained at a surface pressure of ~30 mN/m at 23 ℃ for 200 s under constant gentle agitation. After stable measurement of the surface pressure for 200 s, 200 µL of magainin 2 F5W at a concentration of 1 mg/mL, dissolved in the appropriate subphase, was injected underneath the monolayer and the surface pressure was recorded until no further changes were observed. All samples were run in triplicate and data was then analysed by taking 30 mN/m and 200 s as the lowest surface pressure value and injection time, respectively, and these values were set as zero on the x and y axes. A rudimentary data fit of mean surface pressure (β) vs. time (t) after injection of magainin 2 F5W was performed using a Hill function (Barnes & Chu 2010), in order to calculate the mean time taken for the surface pressure to increase by 50% (K) and the mean maximum surface pressure increase (β_{max}):

$$\beta = \frac{\beta_{max} t^n}{K^n + t^n} \tag{29}$$

Where, n is the degree of cooperativity of the peptide binding to the monolayer surfaces.

7.2.3 Neutron diffraction of natural and synthetic lipid bilayers with magainin 2 F5W

Four silicon discs were prepared for neutron diffraction by initially cleaning them by 5 min of bath sonication (Branson bath sonicator 3510, Danbury, USA) in chloroform, then acetone and then methanol, and finally treating them under UV light for 30 min with a UV/Ozone ProCleaner™ Plus (BioForce Nanosciences, Ames, USA). Orientated multilayers of 20mg of d_{62}-1,2-*O*-dipalmitoyl PG, triethylammonium salt (d_{62}PG)–d_{62}3adLPG 7:3 and 45:55 mol/mol, and 10 mg MSSA 476 lipid extracts of bacteria grown at pH 5.5 and 7.4 were then prepared for

neutron diffraction by coating these lipid mixtures on to the four silicon discs as 1 mL chloroform solutions, as described in chapter 3.2.6, with the addition of magainin 2 F5W (lipid–peptide 50:1 mol/mol) to each lipid mixture. Neutron diffraction was then performed on all samples at 25 ℃, and additionally 55 ℃ for the synthetic lipid samples only, using the D16 neutron diffractometer at the Institut Laue-Langevin (Grenoble, France) at λ = 4.741 Å. Strong reflections were measured for short times (~30 min) whereas weaker ones were measured for ~2-3 hours to improve signal-noise of the higher orders of diffraction. All samples were analysed at 100% humidity only, using a sealed aluminium chamber and D_2O and H_2O contrasts as described in chapter 3.2.6. The neutron diffraction profiles (Intensity vs. 2θ) collected for each sample were then fitted with an exponential function using Sigmaplot V 12.0 (Systat Software, San Jose, California, USA) to remove background scattering as described in chapter 3.2.6. Fourier transformation of each corrected neutron diffraction profile of each sample was then performed using eq. (24-26) (chapter 3.2.6). In order to determine the effect magainin 2 F5W had on the bilayer systems along the z-axis plane, a modified version of the Fourier transformation equation was employed (Leonard *et al.* 2001) to give the absolute scale difference SLD profile of the bilayer system with and without magainin 2 F5W:

$$p(z) = \frac{2}{\psi}\sum_{h=1}^{h_{max}}[F^M(h) - F^P(h)]\cos\left(\frac{2\pi hz}{\psi}\right) \quad (30)$$

Where, $F^M(h)$ and $F^P(h)$ are the structure factors of the bilayer without and with magainin 2 F5W, respectively, h is the order of neutron diffraction, z is the direction perpendicular to the bilayer interface and Ψ is the lamellar d-spacing.

7.2.4 Neutron reflectivity of synthetic lipid floating bilayers with magainin 2 F5W

The floating bilayers composed of d_{62}PG–d_{62}3adLPG 7:3 and 45:55 mol/mol used in chapter 6.2.3 were used again. Both samples were analysed in the presence of magainin 2 F5W (lipid–peptide 50:1 mol/mol) in pH 5.5 and 7.4 environments using contrasts of D_2O, silicon matched water (SMW) and H_2O buffered with 10 mM TRIS–AcOH 1:1 mol/mol adjusted to the appropriate pH with either concentrated HCl or DCl. Both bilayers had magainin 2 F5W introduced to them by injecting 10 mL of the peptide directly into the cell at a concentration of 0.17 μg/mL in the appropriate buffer at the appropriate pH. Excess peptide was washed away

from the bilayer with 10 mL of the appropriate contrast after injection, using a Knauer Smartline HPLC pump 1050 (Hegauer Weg, Germany) at a flow rate of 2 mL/min. Neutron reflectivity data was collected at 55 °C on the D17 reflectometer at the Institut Laue-Langevin (Grenoble, France) at two incident angles (0.8° and 3.2°), for 30 min in H_2O and SMW at the lower angle (12 min for D_2O) and 50 min in H_2O and SMW at the higher angle (30 min for D_2O). All collected neutron reflectivity curves of each sample were split into eight layers as described in chapter 6.2.3 (figure 6-2) and analysed using the 'least squares simplex algorithm' with the program RasCal v1.0.0 (ISIS, Rutherford Appleton Laboratory). Fitted parameters of the bilayer in the absence of the peptide were obtained from chapter 6.3.2.

7.2.5 SANS of synthetic lipid vesicles with magainin 2 F5W

Lipid films of d_{62}PG–d_{62}3adLPG in the molar ratios 7:3 and 45:55 were prepared by dissolving 5 mg of each lipid mixture in 5 mL of chloroform. Each sample was then evaporated to dryness under reduced pressure and re-suspended, by vortex mixing, in 2.5 mL of H_2O buffered with 10mM TRIS–AcOH 1:1 mol/mol adjusted to either pH 5.5 or 7.4 with concentrated HCl. Each sample was then probe sonicated with a Soniprobe (Lukas Dawe Ultrasonics, UK) for 10 min at 24 °C. After probe sonication, and prior to SANS, magainin 2 F5W was added to each vesicle dispersion at a lipid to peptide ratio of 50:1 mol/mol. Additional vesicle dispersions consisting of the same lipid mixtures with magainin 2 F5W were prepared in H_2O–D_2O 1:1 v/v buffered with 10mM TRIS–AcOH 1:1 mol/mol adjusted to either pH 5.5 or 7.4 with concentrated HCl–DCl 1:1 v/v. SANS data of all samples was then obtained as described in chapter 5.2.7 on the LoQ small-angle diffractometer at the ISIS Pulsed Neutron Source (STFC Rutherford Appleton Laboratory, Didcot, U.K.). Each sample, including one to measure background scattering of H_2O and H_2O–D_2O 1:1 v/v, was placed in a 1 mm pathlength quartz cell (Starna scientific, Hainault, UK) and was measured for a total of 12.5 mAh with an incident neutron flux of 160 μA. Each raw scattering data set was then corrected as described in chapter 5.2.7 and converted to scattering cross-section data ($\partial\Sigma/\partial\Omega$ vs Q) using the instrument-specific software Colette (Rutherford Appleton Laboratories 2007). All samples were examined at 55 °C to assess the vesicle bilayer characteristics above the lipid main phase transition temperature (T_m) in order to mimic the fluid phase of the plasma membrane lipids of *S. aureus* (L_α phase). The scattering curves obtained were fitted with the software FISH using a monodisperse sheet

model for samples containing only unilamellar vesicles and a one-dimensional multilayer stack model for multi-lamellar vesicle samples (Heenan 2009, Kotlarchyk & Chen 1983).

7.3 Results

7.3.1 The interaction of magainin 2 F5W with monolayers of natural lipid extracts and synthetic lipid mixtures to mimic the natural lipid extracts

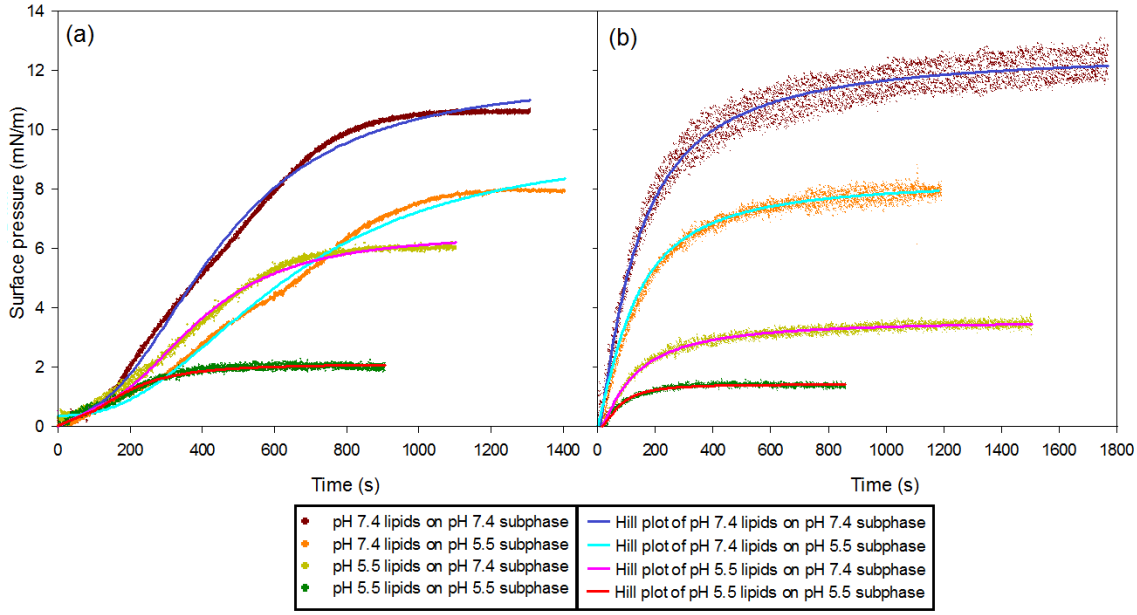

Figure 7-1 Mean increase in surface pressure vs. time of monolayers of (a) MRSA G32 lipids extracted from bacteria grown at pH 5.5 and 7.4 and (b) synthetic lipid mixtures of DP3adLPG–DPPG–TMCL 28.12:66.85:5.03 and 51.63:40:8.37 mol/mol/mol, after subphase injection of magainin 2 F5W at 0 seconds in both pH 5.5 and 7.4 subphases (lipid–peptide 50:1 mol/mol). Hill plots of each experimental data curve are also shown.

Table 7-1 Fitted Hill plot parameters β_{max} and K for mean surface pressure vs. time curves, of MRSA G32 lipids extracted from bacteria grown at pH 5.5 and 7.4 and synthetic lipid mixtures of DP3adLPG–DPPG–TMCL 28.12:66.85:5.03 and 51.63:40:8.37 mol/mol/mol, after subphase injection of magainin 2 F5W at 0 seconds on both pH 5.5 and 7.4 subphases (lipid–peptide 50:1 mol/mol).

Lipid sample	β_{max} (mN/m)	K (s^{-1})
pH 7.4 MRSA G32 on pH 7.4 subphase	11.38 ± 1.6	446.16 ± 20.3
pH 7.4 MRSA G32 on pH 5.5 subphase	9.15 ± 0.8	631.63 ± 31.9
pH 5.5 MRSA G32 on pH 7.4 subphase	5.95 ± 0.6	386.79 ± 18.6
pH 5.5 MRSA G32 on pH 5.5 subphase	2.54 ± 0.3	189.95 ± 14.7
pH 7.4 MRSA G32 model on pH 7.4 subphase	13.01 ± 0.9	135.58 ± 10.4
pH 7.4 MRSA G32 model on pH 5.5 subphase	8.64 ± 0.4	130.95 ± 8.8
pH 5.5 MRSA G32 model on pH 7.4 subphase	3.86 ± 0.6	120.21 ± 12.1
pH 5.5 MRSA G32 model on pH 5.5 subphase	1.91 ± 0.2	75.03 ± 6.6

The monolayers of the natural lipid extracts and the biomimetic synthetic lipid models of these extracts showed similar increases in surface pressure after injection of the peptide into

each subphase (figure 7-1 and table 7-1). The maximum surface pressure values obtained from the fitted curves (β_{max}) of both the pH 7.4 natural lipid extract and pH 7.4 synthetic lipid model (DP3adLPG–DPPG–TMCL 28.12:66.85:5.03 mol/mol/mol) on pH 7.4 subphases showed the largest increases of all the lipid monolayers examined (table 7-1). However, on reduction of the subphase pH to 5.5, β_{max} for both of these monolayers substantially reduced by ~3-5 mN/m after introduction of the peptide (table 7-1). A similar trend in reduction of β_{max} was also observed with monolayers of the pH 5.5 natural lipid extract and the pH 5.5 synthetic lipid model (DP3adLPG–DPPG–TMCL 51.63:40:8.37 mol/mol/mol) after introduction of the peptide and lowering of the subphase pH from 7.4 to 5.5 (table 7-1). The reductions in β_{max} of the monolayers when reducing the pH to 5.5 suggested that the lipid monolayers on pH 5.5 subphases had a reduction in the number of negatively charged lipids with which magainin 2 F5W could interact. The β_{max} of the pH 5.5 synthetic lipid model monolayer after peptide injection, on both pH 5.5 and 7.4 subphases, were lower than β_{max} of the pH 5.5 natural lipid extract monolayer on both pH subphases (table 7-1). These greater β_{max} values of the pH 5.5 natural lipid extract monolayers after peptide injection suggested there may have been some breakdown of L-PG to lysine and PG in this extract, especially in the pH 7.4 buffer, resulting in more negatively charged lipids available for the magainin 2 F5W to bind with. Apart from the pH 7.4 natural lipid extract on the pH 5.5 subphase, all monolayers showed a reduction in *K* as L-PG or DP3adLPG concentrations increased in the monolayer and subphase pH reduced to 5.5 (table 7-1). These reductions in *K* suggested that the presence of increased DP3adLPG or LPG concentrations in the monolayers retarded the time it took for the peptide to bind with the monolayer interface and this time retardation was further augmented when DP3adLPG or LPG were in a more cationically charged state on the pH 5.5 subphases. Comparison of the overall mean *K* values of all the natural lipid extracts with all the mean *K* values of the synthetic lipid models (table 7-1), showed a substantial decrease in the time of binding of the peptide to the synthetic lipid monolayers. Such time differences in peptide binding suggested there may have been non-lipidic contaminants or L-PG breakdown products in the natural lipid extract monolayers interfering with the activity of the peptide thus retarding the peptide's rate of interaction with these monolayers.

7.3.2 Neutron diffraction on natural lipid extracts and biomimetic synthetic lipid mixtures in the presence of magainin 2 F5W

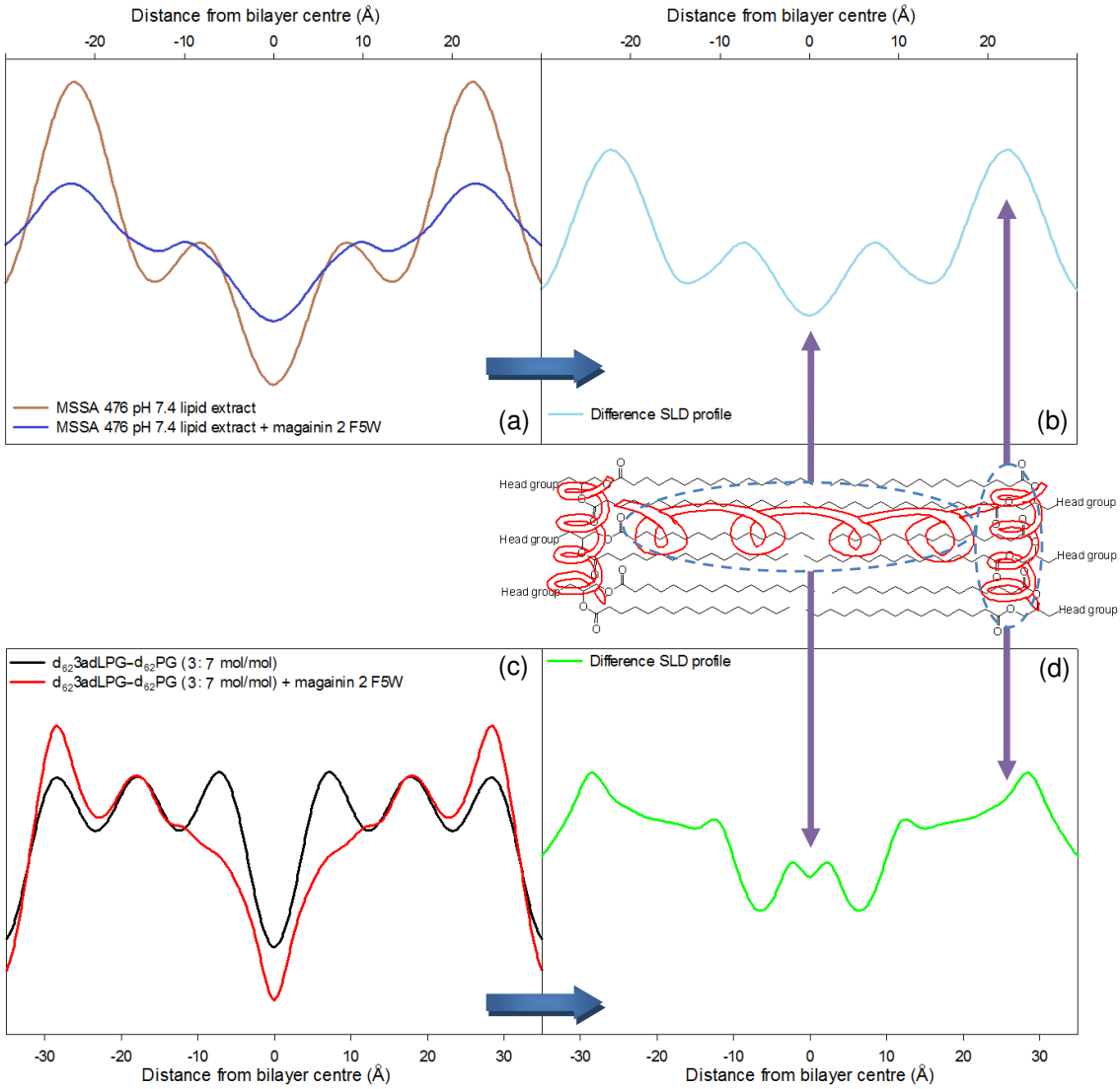

Figure 7-2 Absolute scale SLD profiles with associated difference SLD profile (b and d) of (a) MSSA 476 lipid extracts from bacteria grown at pH 7.4 at 25 °C with and without magainin 2 F5W (lipid–peptide 50:1 mol/mol) and (c) d_{62}PG–d_{62}3adLPG 7:3 mol/mol with and without magainin 2 F5W (lipid–peptide 50:1 mol/mol) at 55 °C. Molecular representation of peptide binding to the bilayer between difference SLD profiles; red coil represents magainin 2 F5W (not to scale).

In order to make comparisons between the pH 7.4 MSSA 476 natural lipid extract and its corresponding pH 7.4 synthetic lipid model (d_{62}PG–d_{62}3adLPG 7:3), neutron diffraction on the synthetic lipid model was performed at 55 °C in order to keep the lipids in the synthetic lipid model in the L_α phase, which was analogous to the lipid phase of the natural lipid extract at 25 °C. Contrast manipulation by replacing hydrogen with deuterium was not performed with the natural lipid extracts or the synthetic lipid headgroups and therefore fluctuations in SLD of the natural lipid extract bilayer or synthetic lipid bilayer headgroup regions in the presence of

magainin 2 F5W were less pronounced as the peptide had a similar SLD to these bilayer environments (Armen *et al.* 1998). As shown in figures 7-2a-d both the pH 7.4 natural lipid extract and pH 7.4 synthetic lipid model in the presence of magainin 2 F5W displayed fluctuations in SLD across the whole thickness of their bilayers. The magnitude of the SLD fluctuations across the bilayers thicknesses suggested the peptide was binding to the bilayers headgroup regions and also partitioning into their hydrocarbon core regions (figures 7-2a-d). This behaviour of the peptide in these bilayers was consistent with the mechanism of action of magainins with L_α phase negatively charged lipids and can ultimately result in pore formation or membrane thinning (Ludtke *et al.* 1996, Ludtke *et al.* 1995).

To examine this interaction of magainin 2 F5W with d_{62}PG–d_{62}3adLPG 7:3 in greater atomic detail, the sample temperature was lowered to 25 ℃ so the lipids would enter the $L_{\beta'}$ phase. However, neutron diffraction of d_{62}PG–d_{62}3adLPG 7:3 in the absence of magainin 2 F5W in the $L_{\beta'}$ phase (chapter 6.3.1) showed the existence of lamellar phase separation caused by interlamellar and intralamellar coupling of two distinct lipid domains (Tayebi *et al.* 2012). The first lamellar phase with a d-spacing of ~82 Å was assumed to be formed of neutral surface domains of ion-paired d_{62}PG and cationic d_{62}3adLPG due to its low interlamellar d-spacing. The second lamellar phase was assigned as a d_{62}PG rich phase due to a large d-spacing of ~120 Å indicating the bilayers were separated by electrostatic charge repulsion (Pozo Navas *et al.* 2005). Thus assessment to see if magainin 2 F5W had a preferential binding to one of these lamellar phases in d_{62}PG–d_{62}3adLPG 7:3 in the lipid $L_{\beta'}$ phase could also be examined.

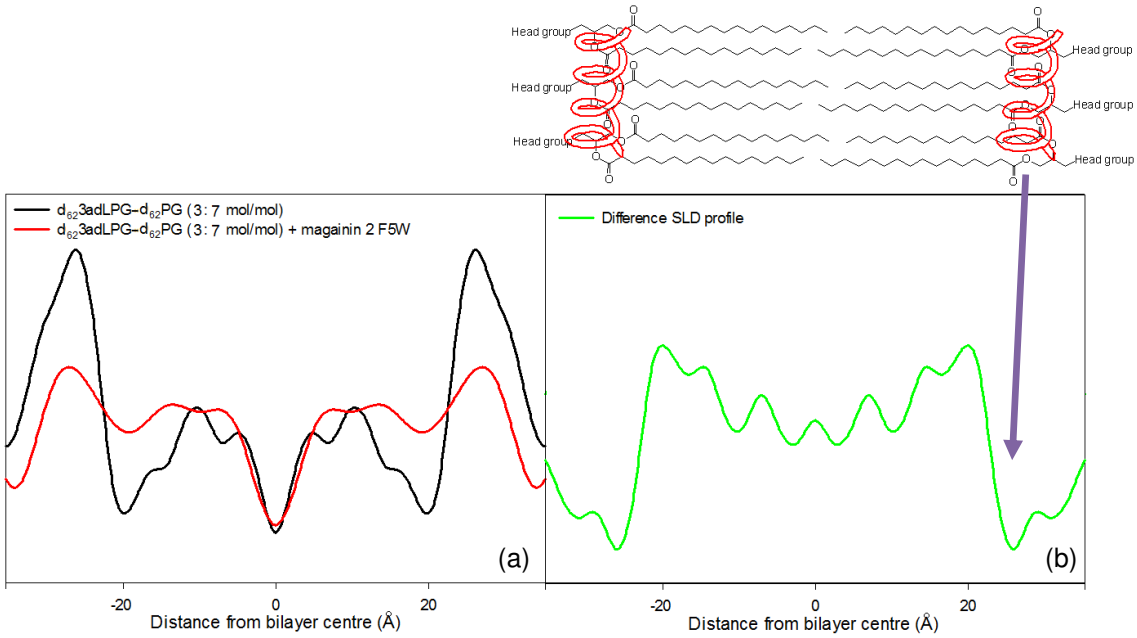

Figure 7-3 (a) Absolute scale SLD profiles of the d_{62}PG rich phase of d_{62}PG–d_{62}3adLPG 7:3 mol/mol with and without magainin 2 F5W at 25 ℃ and (b) the absolute scale difference SLD profile between the system with and without magainin 2 F5W (lipid–peptide 50:1 mol/mol). Molecular representation of peptide binding to the bilayer above difference SLD profile; red coil indicates magainin 2 F5W (not to scale).

As shown in figure 7-3a the presence of magainin 2 F5W in the d_{62}PG rich phase of d_{62}PG–d_{62}3adLPG 7:3 at 25 ℃ saw the bilayer undergo substantial changes in SLD mainly in the bilayer headgroup region. These changes in headgroup SLD in the presence of the peptide signified that there had been a change in lateral density of the bilayer headgroup region which was likely to be caused by the peptide binding to the bilayer lipid headgroups, with little evidence of the peptide partitioning into the bilayer hydrocarbon core. The difference SLD profile in figure 7-3b also supported this finding where only very negative changes in SLD were observed at distances >20 Å from the bilayer centre (bilayer headgroup region). Figure 7-3b also showed the bilayer hydrocarbon core was little affected by the presence of the peptide as only little SLD fluctuations had occurred in this region of the bilayer. The poor penetration of the peptide into the bilayer hydrocarbon core in the $L_{\beta'}$ phase was not unexpected as the peptide needs to be mobile about the bilayer leaflets to be active which was substantially limited with the viscous $L_{\beta'}$ phase d_{62}PG rich bilayer domain (Ludtke *et al.* 1996, Ludtke *et al.* 1995). Therefore the majority of the peptide in this bilayer domain was presumably sequestered in a low kinetic state by the d_{62}PG headgroups at the bilayer surfaces.

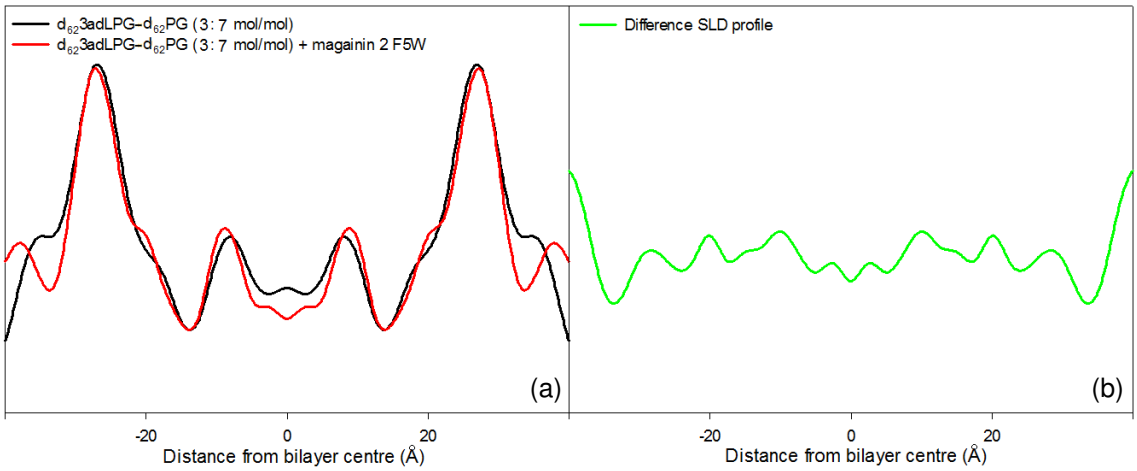

Figure 7-4 (a) Absolute scale SLD profiles of the ion-paired phase of d_{62}PG–d_{62}3adLPG 7:3 mol/mol with and without magainin 2 F5W at 25 ℃ and (b) the absolute scale difference SLD profile between the system with and without magainin 2 F5W (lipid–peptide 50:1 mol/mol).

The SLD profile of the lipid ion-paired phase of d_{62}PG–d_{62}3adLPG 7:3 at 25 ℃ with magainin 2 F5W (figure 7-4a) gave results which were in contrast to the SLD profile of the d_{62}PG rich phase with magainin 2 F5W (figure 7-3a). Figure 7-4a clearly showed the lipid ion-paired phase with magainin 2 F5W in comparison to without, fluctuated in SLD to only a minor degree and the peptide had little effect on the bilayer. The lack of interaction of the peptide with the bilayer was supported by the difference SLD profile in figure 7-4b where only small fluctuations in SLD were observed in the bilayer headgroup region ~22-25 Å from the bilayer centre. This SLD headgroup fluctuation suggested significantly less peptide was able to bind to the bilayer lipid headgroups in comparison to the d_{62}PG rich phase domains (figure 7-3b). This lack of binding of the peptide to the bilayer headgroup region suggested that the electrostatic attraction between d_{62}PG and d_{62}3adLPG was not able to be displaced by magainin 2 F5W, therefore partitioning of the peptide into the membrane was substantially reduced.

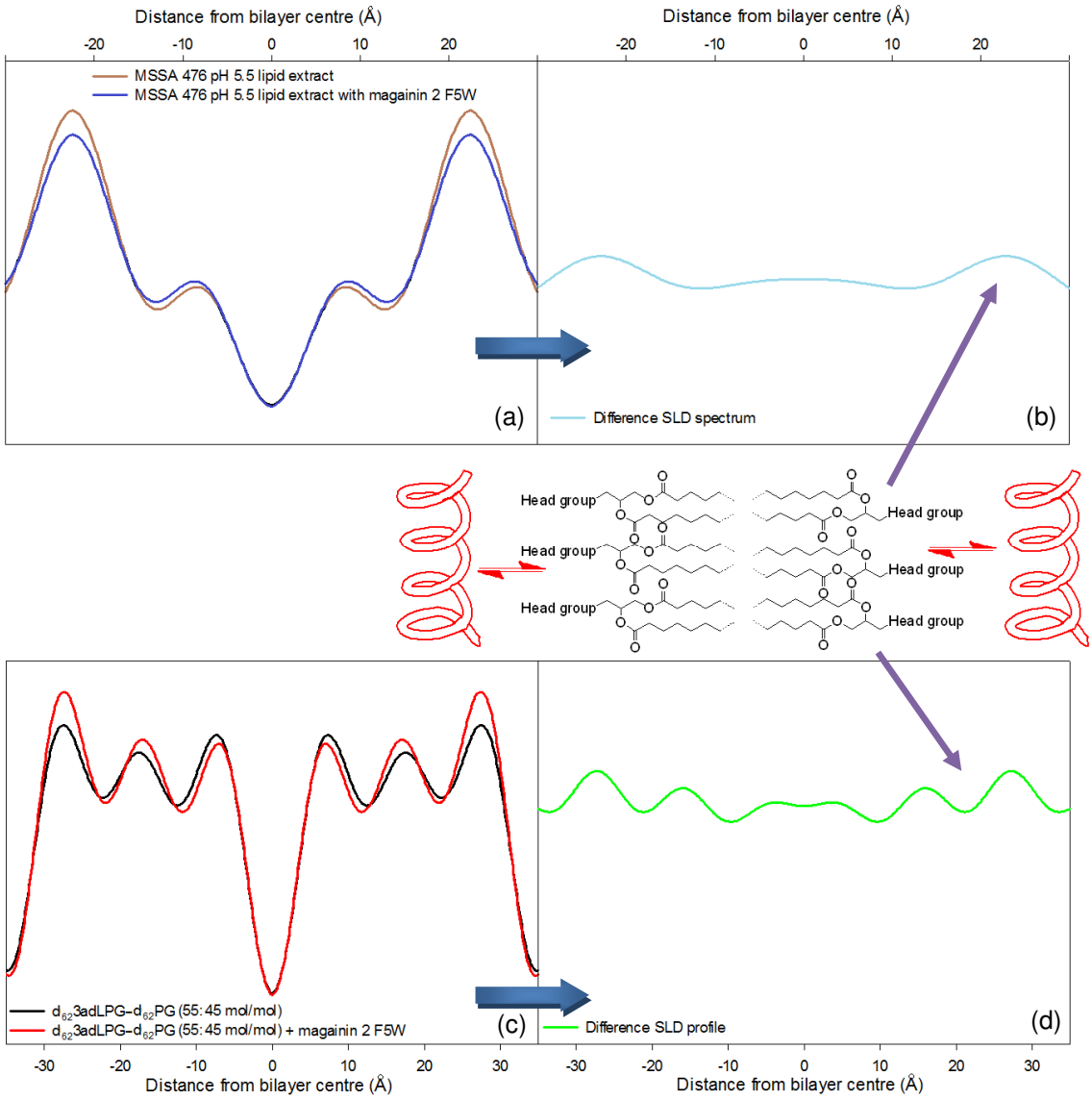

Figure 7-5 Absolute scale SLD profiles with associated difference SLD profile (b and d) of (a) MSSA 476 lipid extracts from bacteria grown at pH 5.5 at 25 ℃ with and without magainin 2 F5W (lipid–peptide 50:1 mol/mol) and (c) d_{62}PG–d_{62}3adLPG 45:55 mol/mol with and without magainin 2 F5W (lipid–peptide 50:1 mol/mol) at 55 ℃. Molecular representation of peptide interacting with the bilayer between difference SLD profiles, red coil represents magainin 2 F5W (not to scale).

As shown in the SLD profiles of d_{62}PG–d_{62}3adLPG 45:55 and the pH 5.5 MSSA 476 lipid extract, both in the L_α phase, changes in SLD of the bilayers with magainin 2 F5W in comparison to without were negligible (figures 7-5a and c). The difference SLD profiles in figures 7-5b and d also supported these findings and displayed only small SLD fluctuations in the headgroup regions of both bilayers in the presence of magainin 2 F5W. Such small headgroup SLD fluctuations suggested the peptide was only binding a small degree to the bilayer lipid headgroups and the rest of the peptide was likely to be residing in the water layers between the bilayers. This result was not unexpected as the surfaces of the membranes were

likely to be close to neutral as cationic d_{62}3adLPG or L-PG content would have been close to ~50% total phospholipid and therefore electrostatic attraction of the peptide to the surface of the membranes would have been low.

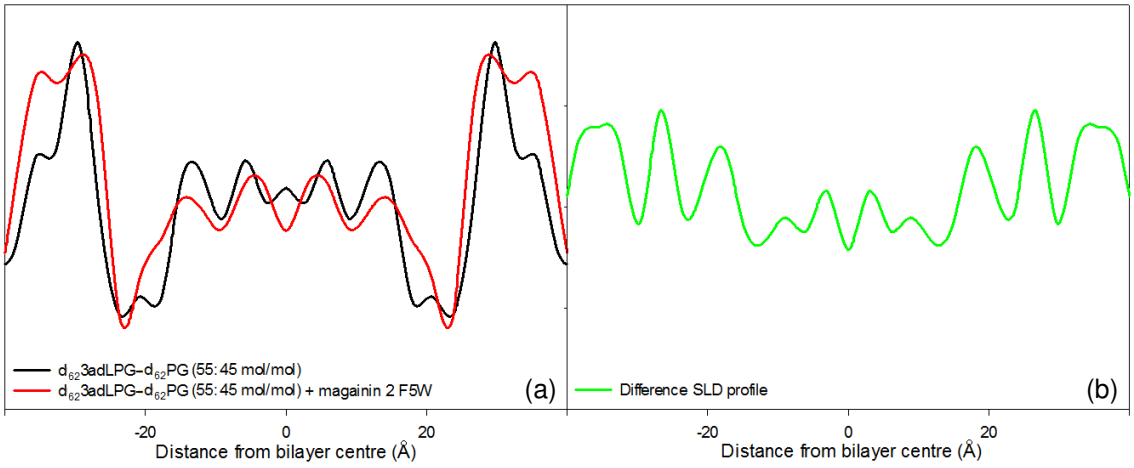

Figure 7-6 (a) True scale SLD profiles of d_{62}PG–d_{62}3adLPG 45:55 mol/mol with and without magainin 2 F5W at 25 ℃ and (b) the true scale difference SLD profile between the system with and without magainin 2 F5W (lipid–peptide 50:1 mol/mol).

In contrast, the SLD profile of d_{62}PG–d_{62}3adLPG 45:55 with magainin 2 F5W at 25 ℃ ($L_{\beta'}$ phase) showed substantial SLD fluctuations across the whole thickness of the bilayer (figure 7-6a). The difference SLD profile in figure 7-6b also indicated the whole thickness of the bilayer had undergone SLD changes in the presence of the peptide, where the largest SLD fluctuations were observed ~18-30 Å from the bilayer centre and this weakened in intensity towards the centre of the bilayer. The fluctuations in the bilayer headgroup SLD (~18-30 Å from the bilayer centre) suggested the peptide was substantially binding to the bilayer lipid headgroups and then partitioning into the bilayer to a small degree. Although figures 7-6a and b show the peptide to vastly interact with the bilayer, it appeared this interaction was an artefact as a result of the neutron diffraction preparation technique where some peptide may have been forced into the membrane causing some local disruption in the bilayer SLD. The sample preparation technique involved mixing of all the components of the bilayer stacks in a single mixture (including the peptide) and depositing the mixture over a polished silicon substrate surface. The result of this lipid and peptide co-deposition was the peptide settled within the bilayers because the lamellar bilayer stacks were not preformed before introduction of the peptide. This was not observed in the bilayer with magainin 2 F5W in the L_{α} phase as the bilayer lipids were more mobile in this lipid phase and therefore the peptide was likely to have been forced out of the membrane (figures 7-5c and d).

7.3.3 Neutron reflectivity and SANS on biomimetic synthetic lipid mixtures in the presence of magainin 2 F5W

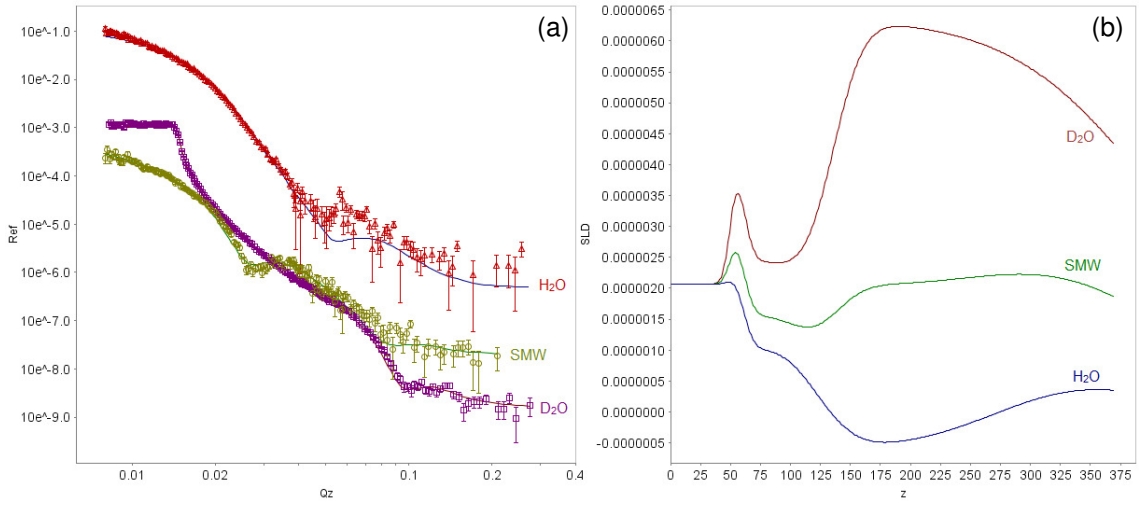

Figure 7-7 Neutron reflectivity curves of (a) d_{62}PG–d_{62}3adLPG 7:3 mol/mol with magainin 2 F5W at 55 ℃, with a pH 7.4 buffering system (lipid–peptide 50:1 mol/mol) and (b) the accompanying fitted SLD profiles of each contrast used.

Table 7-2 Fitted parameters for d_{62}PG–d_{62}3adLPG 7:3 mol/mol with (+) and without (-) magainin 2 F5W at 55 ℃, with a pH 7.4 buffering system (lipid–peptide 50:1 mol/mol).

Peptide	Layer	Thickness (Å)	SLD ($\times 10^{-6}$ Å^{-2})	Hydration (%)	Roughness (Å)
−	Water Layer	118.77 ± 19.6		100	
	Head groups	8.00 ± 1.3	1.89	53.86 ± 7.4	23.14 ± 14.8
	Chains	32.35 ± 3.4	6.79	26.44 ± 7.5	23.14 ± 14.8
+	Water Layer	154.77 ± 23.4		100	
	Headgroups	13.92 ± 3.7	1.62	60.85 ± 6.6	32.45 ± 18.4
	Chains	26.23 ± 1.7	5.15	38.63 ± 8.9	32.45 ± 18.4

The fitted bilayer parameters of the neutron reflectivity curves of d_{62}PG–d_{62}3adLPG 7:3 in a pH 7.4 buffer with magainin 2 F5W (figures 7-7a and b) showed an increase in bilayer roughness of ~9.3 Å compared to the bilayer without the peptide (table 7-2), which implied that the bilayer had become more undulated in the presence of the peptide. The increased bilayer undulation was presumably the result of the peptide binding to the surfaces of the bilayer and disrupting lipid lateral packing. This presumed binding of the peptide to the bilayer surfaces was also observed in the fitted headgroup region thickness which increased by ~6 Å in the presence of the peptide compared to without (table 7-2). Table 7-2 also showed the fitted hydration of the bilayer in the presence of the peptide increased by ~7% in the bilayer headgroup region and ~12% in the bilayer hydrocarbon core compared to the bilayer without the peptide. The increased hydration of the bilayer suggested that the binding of magainin 2 F5W

to the bilayer either reduced lateral density of the bilayer or caused some loss of lipid from the bilayer thus increasing solvent penetration into the bilayer (Ludtke *et al.* 1996). The possible disruption of the lateral lipid packing or the loss of lipid material from the bilayer by the binding of the peptide was also supported by the reduction in fitted SLD of the whole thickness of the bilayer in the presence of the peptide compared to without (table 7-2). This latter result also suggested that the peptide, which has an SLD of ~1-1.5 × 10^{-6} $Å^{-2}$ (Armen *et al.* 1998), may have been partitioning into the hydrocarbon core of the bilayer (SLD without peptide = 6.79 × 10^{-6} $Å^{-2}$, table 7-2) thus also contributing to the reduction in hydrocarbon core SLD to 5.15 × 10^{-6} $Å^{-2}$ (table 7-2). Bilayer thinning was also observed in the bilayer fitted parameters after exposure to the peptide, where a reduction in hydrocarbon core thickness of ~8 Å occurred (table 7-2). A similar result was also found in the modelled SANS data of d_{62}PG–d_{62}3adLPG 7:3 in a pH 7.4 buffer (figure 7-8a) where a reduction in bilayer thickness of ~16 Å was observed (table 7-3). Bilayer thinning by the peptide was not unexpected and is consistent with the destructive membrane effects caused by magainin 2 F5W (Ludtke *et al.* 1995).

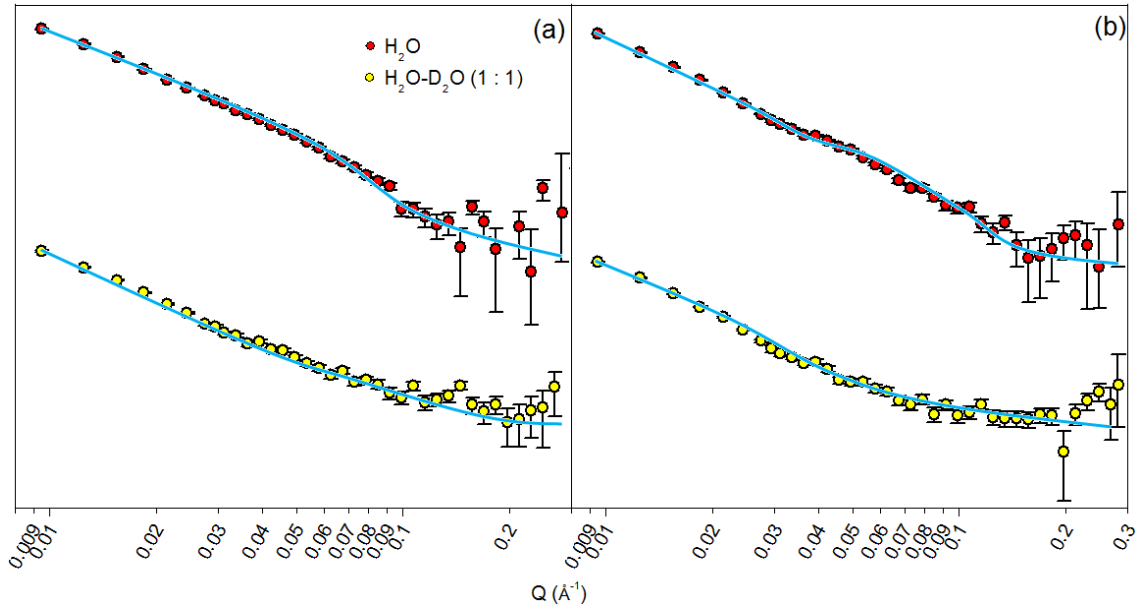

Figure 7-8 SANS curves with respective fits of d_{62}PG–d_{62}3adLPG 7:3 mol/mol with magainin 2 F5W at 55 ℃, with a (a) pH 7.4 and (b) pH 5.5 buffering system in H_2O and H_2O–D_2O (1:1 v/v) contrasts (lipid–peptide 50:1 mol/mol).

Table 7-3 SANS fitted parameters for d_{62}PG–d_{62}3adLPG 7:3 mol/mol with (+) and without (-) magainin 2 F5W at 55 ℃, with pH 5.5 and 7.4 buffering systems (lipid–peptide 50:1 mol/mol).

Peptide	pH	Layer thickness (Å)	D-spacing (Å)	Layers	% sample MLV
–	7.4	49.93 ± 2.92	113.94 ± 12.16	2.18 ± 0.34	22.52 ± 4.45
	5.5	48.01 ± 3.03	111.09 ± 14.39	2.83 ± 0.77	29.66 ± 3.23
+	7.4	33.96 ± 5.73	107.53 ± 7.40	2.18 ± 0.34	22.52 ± 4.45
	5.5	44.43 ± 1.96	110.29 ± 2.94	2.83 ± 0.77	29.66 ± 3.23

The modelled SANS data of vesicles of d_{62}PG–d_{62}3adLPG 7:3 in a pH 5.5 buffer (figure 7-8b) also showed membrane thinning in the presence of magainin 2 F5W (table 7-3). The membrane thinning effect of the peptide was ~10-11 Å less in magnitude in comparison to the vesicular bilayers in a pH 7.4 buffer (table 7-3). Such a result was also found in d_{62}PG–d_{62}3adLPG 7:3 in a pH 5.5 buffer when analysed by neutron reflectivity (figures 7-9a and b), where a reduction in bilayer fitted hydrocarbon core thickness of ~3 Å was found (table 7-4) compared to a reduction of ~8 Å in a pH 7.4 buffer (table 7-2). The reduced efficacy of the peptide with these bilayers suggested that the greater proportion of cationic d_{62}3adLPG in the bilayers in a pH 5.5 environment reduced the amount of available anionic lipids for the peptide to bind with.

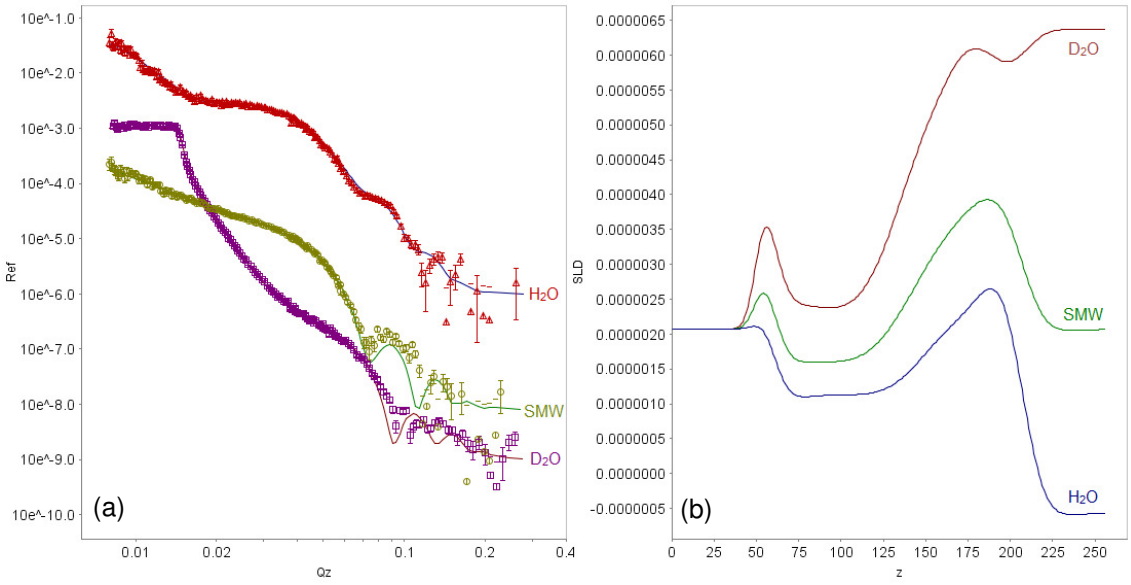

Figure 7-9 (a) Neutron reflectivity curves of d_{62}PG–d_{62}3adLPG 7:3 mol/mol with magainin 2 F5W at 55 ℃, with a pH 5.5 buffering system (lipid–peptide 50:1 mol/mol) and (b) the accompanying fitted SLD profiles of each contrast used.

Table 7-4 Fitted parameters for d_{62}PG–d_{62}3adLPG 7:3 mol/mol with (+) and without (-) magainin 2 F5W at 55 °C, with a pH 5.5 buffering system (lipid–peptide 50:1 mol/mol).

Peptide	Layer	Thickness (Å)	SLD ($\times 10^{-6}$ Å^{-2})	Hydration (%)	Roughness (Å)
–	Water Layer	28.99 ± 5.6		100	
	Headgroups	8.09 ± 1.3	4.08	16.23 ± 3.6	7.22 ± 2.70
	Chains	31.40 ± 2.6	7.06	0.74 ± 0.4	7.22 ± 2.70
+	Water Layer	17.61 ± 2.4		100	
	Headgroups	12.85 ± 2.7	4.05	41.61 ± 7.3	10.88 ± 3.6
	Chains	28.39 ± 6.4	5.87	38.09 ± 7.4	10.88 ± 3.6

The neutron reflectivity fitted roughness of d_{62}PG–d_{62}3adLPG 7:3 in a pH 5.5 buffer displayed an increase of ~3 Å after introduction of the peptide and suggested that the bilayer had become more undulated (table 7-4). This supported earlier findings of the interaction of the peptide with d_{62}PG–d_{62}3adLPG 7:3 in a pH 7.4 buffer (table 7-2), where binding of the peptide to the bilayer was suspected to cause lateral lipid packing disruption resulting in the bilayer becoming more undulated. However, it would appear that the increased cationic d_{62}3adLPG at pH 5.5 attenuated the increase in bilayer undulation caused by the peptide, as the increase in bilayer undulation at pH 5.5 (~3 Å, table 7-4) was substantially less than at pH 7.4 (~9.3 Å, table 7-2).

A noticeable increase in fitted bilayer hydration and a reduction in bilayer fitted SLD after introduction of the peptide in pH 5.5 buffer was observed (table 7-4). These changes in bilayer hydration and SLD implied that either lipid material may have been lost from the bilayer resulting in water pocket formation in the bilayer or that the peptide was partition into the bilayer and disrupting the lateral packing of the lipids. However, comparison of tables 7-2 and 7-4 showed the increase in bilayer hydration and reduction in SLD after introduction of the peptide to be to a lesser degree in the pH 5.5 buffer compared to the pH 7.4 buffer. The lower efficacy of the membrane disruptive effects of magainin 2 F5W with the bilayer in the pH 5.5 buffer was likely to be the result of increased cationic d_{62}3adLPG at pH 5.5 which would have sequestered more anionic d_{62}PG in comparison to the pH 7.4 buffer, thus reducing the amount of available d_{62}PG for the peptide to interact with.

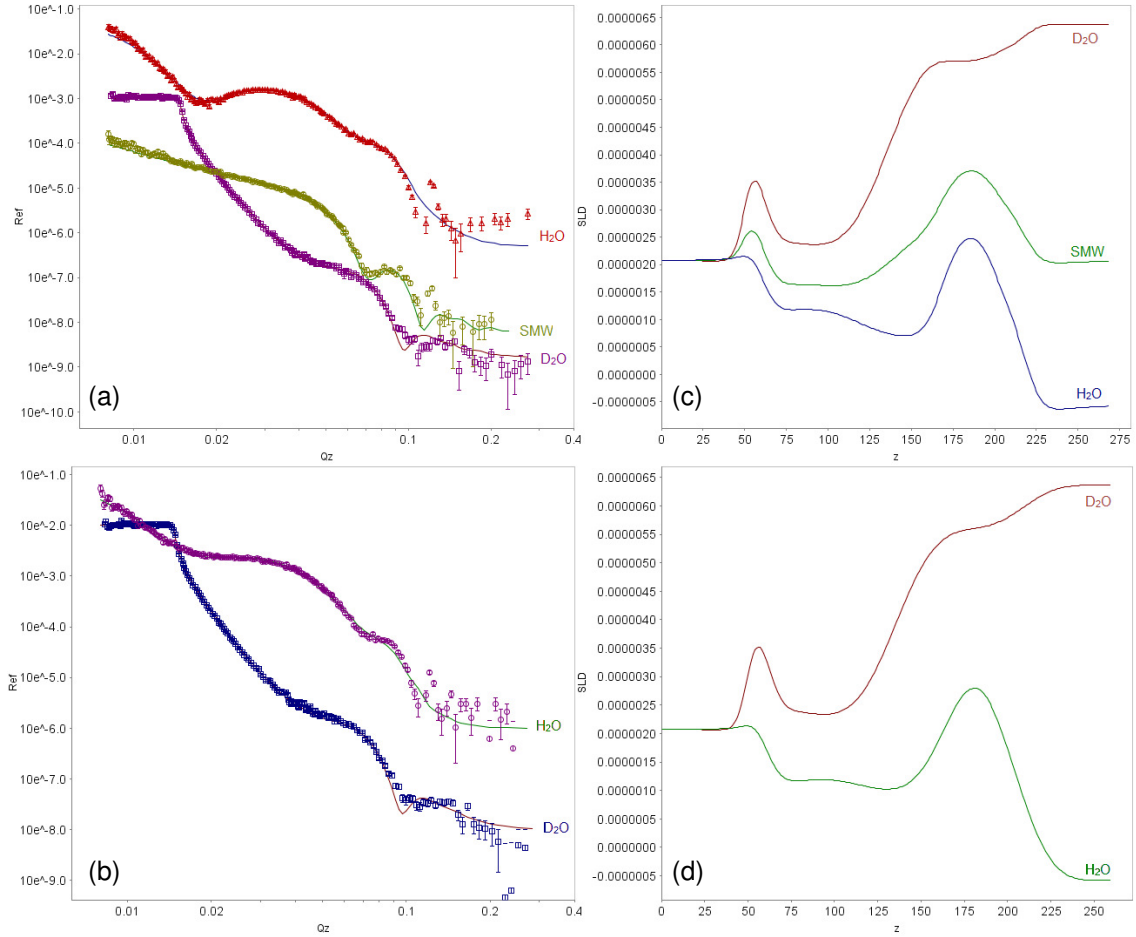

Figure 7-10 Neutron reflectivity curves of d_{62}PG–d_{62}3adLPG 45:55 mol/mol with magainin 2 F5W at 55 ℃, in (a) a pH 7.4 buffering system (lipid–peptide 50:1 mol/mol) and (b) a pH 5.5 buffer system (lipid–peptide 50:1 mol/mol), the accompanying fitted SLD profiles of each contrast used for each bilayer in (c) a pH 7.4 buffer and (d) a pH 5.5 buffer are also shown.

Table 7-5 Fitted parameters for d_{62}PG–d_{62}3adLPG 45:55 mol/mol at 55 ℃ with (+) and without (-) magainin 2 F5W in both pH 5.5 and 7.4 buffers (lipid–peptide 50:1 mol/mol).

pH	Peptide	Layer	Thickness (Å)	SLD (×10^{-6} Å^{-2})	Hydration (%)	Roughness (Å)
		Water Layer	14.16 ± 2.3		100	
7.4	–	Headgroups	14.32 ± 4.2	4.93	47.09 ± 5.1	8.00 ± 0.6
		Chains	33.12 ± 4.6	5.84	34.26 ± 6.7	8.00 ± 0.6
		Water Layer	18.45 ± 1.9		100	
5.5	–	Headgroups	16.94 ± 4.1	4.62	26.44 ± 7.9	9.48 ± 3.5
		Chains	32.16 ± 4.6	5.50	8.65 ± 3.7	9.48 ± 3.5
		Water Layer	14.85 ± 2.6		100	
7.4	+	Headgroups	12.79 ± 6.1	3.84	53.41 ± 7.2	8.03 ± 1.9
		Chains	31.97 ± 5.5	5.27	36.99 ± 5.1	8.03 ± 1.9
		Water Layer	16.80 ± 0.7		100	
5.5	+	Headgroups	15.45 ± 3.3	4.58	27.98 ± 6.4	10.03 ± 1.5
		Chains	32.68 ± 3.9	5.46	11.73 ± 5.8	10.03 ± 1.5

The reflectivity curves (figures 7-10a and b) and associated fitted SLD profiles (figures 7-10c and d) of d_{62}PG–d_{62}3adLPG 45:55 with magainin 2 F5W were similar in shape in both pH buffers in comparison to the bilayer without magainin 2 F5W (chapter 6.2.3, figures 6-11a-d).

The similarity in the reflectivity curves and SLD profiles of the bilayer in the presence and absence of magainin 2 F5W suggested that the density of the bilayer had changed by only negligible amounts after exposure to the peptide. The fitted parameters of the bilayer in a pH 7.4 buffer in the presence of the peptide showed a reduction in bilayer SLD and an increase in bilayer hydration of both the bilayer headgroup and hydrocarbon regions, in comparison to the bilayer in a pH 7.4 buffer without the peptide (table 7-5). The changes in SLD and hydration of the bilayer at pH 7.4 suggested the peptide caused some loss of lipid from the bilayer or that the peptide was inserting into the bilayer as well as disrupting the lateral lipid packing (Ludtke *et al.* 1996). Partitioning of the peptide into the bilayer at pH 7.4 was presumably possible if significant quantities of d_{62}3adLPG were not fully protonated at this pH and therefore some non-ion-paired d_{62}PG still existed in the membrane for the peptide to interact with. Changes in bilayer SLD and hydration were not observed in the pH 5.5 buffer presumably due to majority of the d_{62}3adLPG being cationically charged at this pH and all d_{62}PG in the bilayer being possibly ion-paired to cationic d_{62}3adLPG and unavailable for interaction with the peptide. Therefore d_{62}PG–d_{62}3adLPG 45:55 in a pH 5.5 buffer can be assumed to be totally resistant to the membrane destructive effects of magainin 2 F5W.

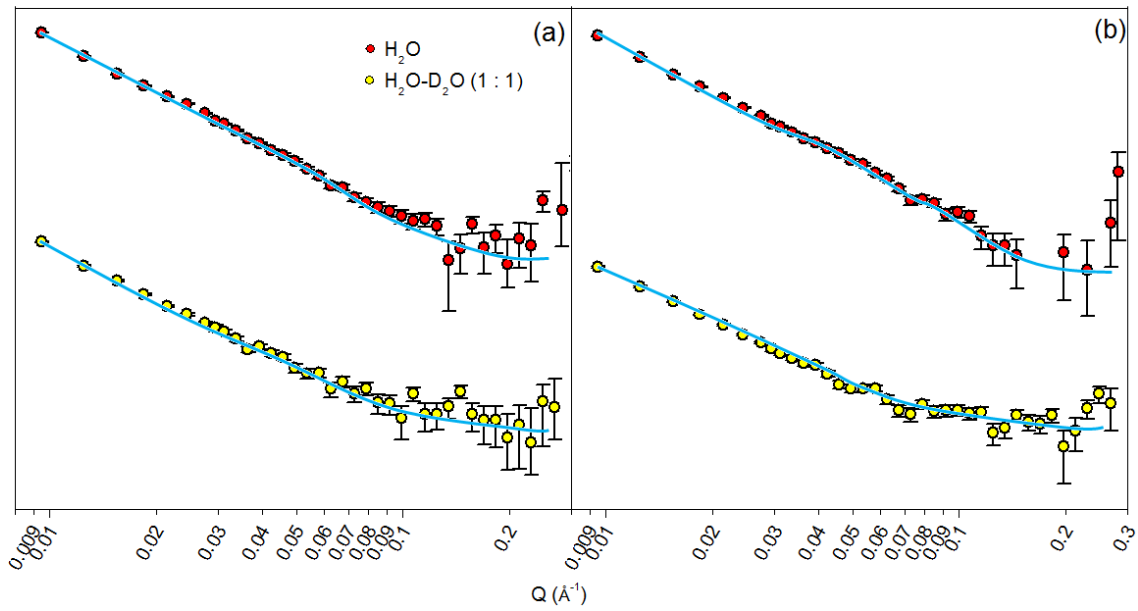

Figure 7-11 SANS curves with respective fits of d_{62}PG–d_{62}3adLPG 55:45 mol/mol with magainin 2 F5W at 55 °C, with a (a) pH 7.4 and (b) pH 5.5 buffering system in H_2O and H_2O–D_2O (1:1 v/v) contrasts (lipid–peptide 50:1 mol/mol).

Table 7-6 SANS fitted parameters for d_{62}PG–d_{62}3adLPG 45:55 mol/mol with (+) and without (-) magainin 2 F5W at 55 °C, with pH 5.5 and pH 7.4 buffering systems (lipid–peptide 50:1 mol/mol).

Peptide	pH	Layer thickness (Å)	D-spacing (Å)	Layers	% sample MLV
–	7.4	60.93 ± 3.49	101.40 ± 21.68	2.00 ± 0.06	8.37 ± 4.24
	5.5	64.34 ± 2.55	128.66 ± 17.83	1.69 ± 0.17	6.91 ± 1.98
+	7.4	57.18 ± 5.49	103.48 ± 17.61	2.00 ± 0.06	8.37 ± 4.24
	5.5	64.68 ± 4.91	127.55 ± 13.34	1.69 ± 0.17	6.91 ± 1.98

Similar to the situation with d_{62}PG–d_{62}3adLPG 7:3 in the presence of magainin 2 F5W, fitted neutron reflectivity data and fitted SANS data (figure 7-11a) of d_{62}PG–d_{62}3adLPG 45:55 showed there had been a small degree of membrane thinning in the pH 7.4 buffer in the presence of magainin 2 F5W in comparison to the bilayer without the peptide (tables 7-5 and 7-6). However, in contrast to the vesicular bilayers in the pH 7.4 buffer, peptide-induced membrane thinning was not observed with the bilayer in the pH 5.5 buffer as shown in tables 7-5 and 7-6. These findings supported the theory that some non-ion-paired d_{62}PG existed when the bilayer was in the pH 7.4 buffer due to d_{62}3adLPG being partially zwitterionic at this pH and therefore the peptide could cause some membrane thinning through electrostatic interaction with non-ion-paired d_{62}PG (Ludtke *et al.* 1995). Additionally, the lack of bilayer thinning in the pH 5.5 buffer showed this membrane to confer total resistance to the membrane destructive effects of magainin 2 F5W.

7.4 Discussion

Monolayer injection experiments of both the pH 7.4 MRSA G32 lipid extract and the pH 7.4 synthetic lipid model of this lipid extract on pH 7.4 subphases showed extensive increases in β_{max} by ~11-13 mN/m after subphase injection of magainin 2 F5W. The large increase in β_{max} signified the peptide was binding to the lipid headgroups in the monolayer and possibly inserting into the monolayer thus excluding further solvent molecules from the subphase surface and resulting in an increase in monolayer surface pressure (Quinn & Dawson 1969). Neutron reflectivity of an L_α phase floating bilayer, similar in lipid composition to these pH 7.4 lipid mixtures (d_{62}PG–d_{62}3adLPG 7:3) in a pH 7.4 buffer, showed similar disruptive effects of the peptide where binding of the peptide to the bilayer surfaces and insertion of the peptide into the bilayer hydrocarbon core was observed. Both neutron reflectivity and SANS results also found significant membrane thinning of d_{62}PG–d_{62}3adLPG 7:3 at pH 7.4 in the presence of magainin 2 F5W, which is consistent with the membrane disruptive mechanism of the peptide (Ludtke *et al.* 1995). Neutron diffraction, although unbuffered, showed the pH 7.4 MSSA 476 lipid extract and d_{62}PG–d_{62}3adLPG 7:3 in the L_α phase to undergo substantial changes in SLD across the whole thickness of the bilayer in the presence of the peptide, and also suggested the peptide was able to partition into the hydrocarbon core of the bilayer. All of these results of the pH 7.4 lipid mixtures in the unbuffered and pH 7.4 environments indicated that these lipid mixtures, with respect to the membrane destructive effects of magainin 2 F5W, were the most susceptible. Such a result was not unexpected as (d_{62} or DP)3adLPG or L-PG would have been partially zwitterionic in the unbuffered and pH 7.4 conditions employed, therefore in lipid mixtures with PG and CL, a substantial proportion of PG or CL would have been non-ion-paired and available to interact with the peptide, thus facilitating the peptides membrane disruptive effects.

To ensure magainin 2 F5W was targeting mainly the anionic lipids in the pH 7.4 lipid mixtures, neutron diffraction of d_{62}PG–d_{62}3adLPG 7:3 with magainin 2 F5W was performed in the $L_{\beta'}$ phase, where previously lamellar phase separation was observed to form a d_{62}PG rich phase and a d_{62}PG–d_{62}3adLPG ion-paired phase (chapter 6.3.1). The SLD profiles of these lamellar phases showed the peptide caused substantial changes in SLD in the d_{62}PG rich phase however little disruption in SLD was observed in the d_{62}PG–d_{62}3adLPG ion-paired phase. These findings validated the theory that the peptide was mainly targeting the non-ion-paired anionic d_{62}PG which is consistent with the mechanism of action of CAMPs with anionically

charged membranes, where electrostatic attraction of the peptide to the negatively charged surface of bacterial membranes occurs initially before the peptide partitions into the membrane (Ludtke *et al.* 1996, Ludtke *et al.* 1995, Zasloff *et al.* 1988, Hancock 2001).

In contrast to the pH 7.4 lipid mixtures in pH 7.4 environments, monolayers of the pH 7.4 MRSA G32 lipid extract and the pH 7.4 synthetic lipid model of this lipid extract when deposited on a pH 5.5 subphase with magainin 2 F5W injected underneath the monolayers showed less susceptibility to the peptide. The β_{max} of both monolayers was ~9 mN/m in the presence of the peptide and indicated less peptide was penetrating into the monolayer at this pH compared to pH 7.4. This reduction of β_{max} on the pH 5.5 subphase provided good evidence that there had been an increase in cationic DP3adLPG or L-PG in this pH environment thus the lipids formed more ion-pairs with PG or CL, resulting in less available PG or CL for the peptide to interact with. Neutron reflectivity of the floating bilayer of d_{62}PG–d_{62}3adLPG 7:3 in the L_α phase in a pH 5.5 buffer with magainin 2 F5W, also supported this finding where a reduction in membrane disruption efficacy of the peptide was observed by the bilayer's hydration and SLD deviating to a lesser extent compared to the same bilayer in a pH 7.4 buffer. Additionally, both neutron reflectivity and SANS modelled data of d_{62}PG–d_{62}3adLPG 7:3 in the L_α phase in a pH 5.5 environment showed there was a reduction in membrane thinning of d_{62}PG–d_{62}3adLPG 7:3 by the peptide compared to a pH 7.4 environment, thus also supporting the finding of reduced peptide efficacy with the bilayer in a pH 5.5 environment.

With respect to the activity of magainin 2 F5W with the pH 5.5 natural lipid extracts and the pH 5.5 synthetic lipid models of these natural lipid extracts, neutron diffraction SLD profiles of both the pH 5.5 MSSA 476 lipid extract and d_{62}PG–d_{62}3adLPG 45:55 in the L_α phase, in the presence of magainin 2 F5W, showed minor SLD fluctuations in the bilayer headgroup regions. Such activity of the peptide in these lipid bilayers suggested it was binding a small amount to the bilayer lipid headgroups but was unable to partition into the bilayer hydrocarbon core and was ejected out of the membrane. SANS and neutron reflectivity of d_{62}PG–d_{62}3adLPG 45:55 in the L_α phase in a pH 7.4 buffered environment also showed some interaction with the peptide where a loss in bilayer SLD and increase in bilayer hydration were observed, and in addition to this a membrane thinning effect was found. Monolayers of the pH 5.5 MRSA G32 lipid extract and the pH 5.5 synthetic lipid model of this lipid extract, after peptide injection, both showed β_{max} values of ~4-6 mN/m on pH 7.4 subphases which indicated the peptide was still able to bind and

partition into these monolayers even with their high contents of DP3adLPG or L-PG. It seems evident that these membrane disruptive effects of the peptide in unbuffered and pH 7.4 environments were due to d_{62}3adLPG being partly zwitterionic and therefore a small amount of non-ion-paired d_{62}PG was presumably still present for the peptide to interact with. In contrast, monolayers of the pH 5.5 MRSA G32 lipid extract and the pH 5.5 synthetic lipid model of this lipid extract showed very little peptide penetrating into the monolayers on pH 5.5 subphases, as indicated by their small increase in β_{max} on the pH 5.5 subphase. Similar lack of activity of the peptide was also observed in the modelled SANS and neutron reflectivity data of d_{62}PG–d_{62}3adLPG 45:55 in the L_α phase in a pH 5.5 buffered environment, where no membrane thinning was observed and only small fluctuations in bilayer headgroup SLD were apparent. These findings suggested that the presence of more cationically charged DP3adLPG or L-PG at concentrations >50% total phospholipid in a pH 5.5 environment resulted in total resistance of the membrane to the lytic effects of magainin 2 F5W. Therefore, it would appear that the formed ionic bond between PG or CL and cationic (d_{62} or DP)3adLPG or L-PG is more energetically favourable than the ionic bonds formed between the cationic residues on magainin 2 F5W and PG or CL. Thus total abolishment of the membrane destructive effects of magainin 2 F5W occurs when the membrane contains >50% cationic (d_{62} or DP)3adLPG or L-PG.

7.5 Conclusion

By using (d_{62} or DP)3adLPG as a substitute for L-PG in lipid mixtures with PG (and CL in some experiments), greater clarity into the mechanisms by which L-PG in *S. aureus* membranes increases resistance to CAMPs was found. From the results of both the natural lipid extracts and synthetic lipid models in different pH environments, it is clear that ion-pairs formed between cationic (d_{62} or DP)3adLPG or L-PG and anionic PG or CL are more energetically favourable than the electrostatic interaction between the cationic groups on a CAMP and anionic PG or CL and thus the peptide cannot displace the paired LPG or (d_{62} or DP)3adLPG. This finding may explain why the bacterium upregulates its expression of L-PG in the presence of CAMPs, as subsequent ion-pairing between the lipids reduces the amount of PG or CL available for the peptide to bind with. Previous studies have found that L-PG expression in *S. aureus* exposed to CAMPs can increase to up to 38% total phospholipid from ~20% total phospholipid when growing in pH 7.4 conditions (Peschel *et al.* 2001). The upregulation of L-PG to only ~38% suggests some membrane PG and CL is still available for CAMPs to interact with. However, *S. aureus* does not only produce L-PG as its only defence mechanism to CAMPs, as L-PG forms only one part of a whole range of defensive mechanisms such as the covalent binding of alanyl residues to teichoic acid carboxyl groups when exposed to CAMPs (Peschel *et al.* 2000, Fedtke *et al.* 2004). Therefore it may not be economical for *S. aureus* to over-express L-PG and expend substantial energy to do so when exposed to CAMPs, as lower levels of L-PG expression may protect the bacterium just as well as levels up to the expression of L-PG in a pH 5.5 growth environment. With regard to *S. aureus* growth on low pH epithelial surfaces, it is clear from the pH 5.5 lipid extracts and pH 5.5 synthetic lipid models, the presence of L-PG at ~50% total phospholipid in the bacterial plasma membrane is more than adequate to defend the membrane against CAMPs as well as a drop in environmental pH. This finding therefore gives insight into how *S. aureus* is able to adapt to and survive on human skin and the anterior nares of the nasal passages, which are both low pH environments rich in CAMPs.

Chapter 8

General Discussion

The main purpose of the work presented in this thesis has been to try to better understand the role, function and regulation of lysyl-phosphatidylglycerol (L-PG) in the plasma membrane of *Staphylococcus aureus* when the bacterium is grown in a low pH environment. Previous studies have shown that the biosynthesis of L-PG in the plasma membrane of *S. aureus* is increased when the bacterium is grown in a low pH environment and when it is exposed to cationic antimicrobial peptides (CAMPs) at sub-lethal concentrations (Nishi *et al.* 2004, Roy 2009, Asselineau 1991, Dossanto *et al.* 1970, Gould & Lennarz 1970, Staubitz *et al.* 2004, Thedieck *et al.* 2006, Friedman *et al.* 2006, Kosowska-Shick *et al.* 2009, Hachmann *et al.* 2009, Julian *et al.* 2007, Murthy *et al.* 2008a, Ouhara *et al.* 2008). Some preliminary physicochemical data on the ionisable groups of L-PG exists where the α-amine and ε-amine of the lipid have pKa values of ~6-7 and >10, respectively, and the phosphate has a pKa of ~1-3 (chapter 1.2, figure 1-5) (Tocanne *et al.* 1974c). There is also published data on the structural characteristics of L-PG where it forms an interdigitated bilayer when present in vesicles on its own and tends to be highly labile in mild aqueous environments (chapter 1.3) (Danner *et al.* 2008). Apart from these data no other information is currently available on the physical properties of L-PG, thus providing the impetus and starting point for the investigations presented here.

The regulation of L-PG biosynthesis in *S. aureus* is under genetic control through the genes *graXRS* and *vraFG*, known as the 'five-component system' (Falord *et al.* 2012, Li *et al.* 2007a, Li *et al.* 2007b, Meehl *et al.* 2007). Previous studies examining *graXRS* and *vraFG* expression have mainly focused on the stimulatory effects of exposure of *S. aureus* to CAMPs at sub-lethal concentrations (chapter 1.8, figure 1-28). Therefore the current consensus regarding the purpose of the five-component system in *S. aureus* is based upon a genetic resistance mediated pathway where *S. aureus* becomes less susceptible to CAMPs as a result of their challenge to the organism (Falord *et al.* 2012). However, chapter 2 of this study has suggested that a reduction in environmental growth pH to 5.5 may stimulate increased expression of *graXRS* in *S. aureus*. Examination of mRNA expression in six strains of *S. aureus* showed a strong positive correlation existed between changes in *graS* and *mprF* expression when

environmental pH was decreased from 7.4 to 5.5. The observed increased expression of *graS* and *mprF* in response to a low pH environment presumably would have resulted in more GraS and MprF being present in the bacterial plasma membrane and therefore L-PG biosynthesis would have increased. This presumption was verified by the observed increased biosynthesis of L-PG at pH 5.5 (~50% total phospholipid) compared to pH 7.4 (~30% total phospholipid) in four of the *S. aureus* strains examined (chapter 2.3.1) (Gould & Lennarz 1970). Previous studies had also suggested upregulation in expression of *graRS* is also significantly positively correlated to *vraG* expression in the presence of CAMPs (Falord *et al.* 2012), however, reduction of the pH did not produce a similar result. The degree of change in *graS* and *mprF* expression at pH 5.5 compared to pH 7.4 far exceeded any change in *vraG* expression. The original function of VraG was thought to be a peptidoglycan building block efflux pump (Meehl *et al.* 2007) however it was later also said to function as a positive feedback messenger to GraS due to it containing a 198 residue extracellular sensor loop for CAMPs to bind with (Falord *et al.* 2012). Therefore, as CAMPs were mainly shown to interact with VraG it is possible that *S. aureus* does not require it at such high concentrations in response to a low pH environment. The changes in expression of *vraF* and *graX* were also investigated in this study at pH 5.5 and 7.4 and their upregulation in expression was found to be substantially less than that of *graS* and *mprF* at pH 5.5. The function of VraF is thought to be an ATPase which mediates the efflux function of VraG, whereas GraX is thought to be a mediator protein between GraRS and VraF, however the precise mechanism of this mediation remains unsubstantiated (Falord *et al.* 2012). From this study the changes in *vraF* and *graX* expression at different pHs are difficult to interpret without gene knock-out experiments and thus their roles with regard to changes in environmental pH remain unknown.

Although some preliminary data regarding *graXRS* and *vraFG* expression at different environmental pHs was found in chapter two, *nuc* expression (reference gene) has previously been reported to be different in *S. aureus* grown under different pH conditions (Weinrick *et al*. 2004). Therefore, as explained in chapter 2.4, further work must be conducted using house keeping genes as reference internal standards to normalise the qPCR data before any definitive conclusions can be drawn from this study regarding *graXRS* and *vraFG* expression at different growth pHs.

The structure of GraS has previously been shown to consist of two membrane spanning domains and two cytoplasmic domains (Falord *et al.* 2012, Li *et al.* 2007b). The GraS cytoplasmic domains are the kinase which liberates phosphate from ATP required for GraR (regulator protein) phosphorylation and hence activation. The kinase activity of GraS is through a conformational change in the protein's membrane spanning domains. Conformational changes in these membrane spanning domains are thought to occur either through direct contact with VraG or by detection of CAMPs by the nine residue extracellular loop of GraS (Li *et al.* 2007b). This suggested mechanism of GraS activation by CAMPs would also be plausible for the mechanism of how protons activate GraS. This is because the pKa of the three aspartate residues in the nine residue extracellular loop of GraS are between 4 and 4.1 (Tollinger *et al.* 2002) and therefore some charge neutralisation of these residues would be expected to occur at pH 5.5 possibly resulting in the activation of GraS.

The end result of stimulation of the five-component system in *S. aureus* by a low pH environment is an increase in the biosynthesis of L-PG in the bacterial plasma membrane (chapter 2.3.1). This sees the plasma membrane L-PG content rise to ~50% total phospholipid which presumably would have effects on the plasma membrane charge and structure. Previous studies theorising on the charge effects L-PG has on the plasma membrane in response to CAMPs suggested that L-PG attenuated the plasma membrane outer leaflet anionicity which would result in CAMPs having a lower electrostatic attraction to the plasma membrane outer surface thus preventing their partitioning into the membrane (Peschel *et al.* 2001, Kilelee *et al.* 2010). The reason this was thought to be the role of L-PG was because L-PG has a suggested net headgroup charge of +1 at pH 7.4 and therefore could neutralise the charges on the other *S. aureus* plasma membrane phospholipids, phosphatidylglycerol (PG) and cardiolipin (CL), which have net -1 headgroup charges (Gould & Lennarz 1970, Haines 2009, Ernst *et al.* 2009). However, this suggested charge neutralisation role of L-PG through the formation of lipid ion-pairs with PG or CL was not experimentally established and no charge assessment studies have been conducted to date on membranes formed from mixtures of L-PG, PG and CL. Alas it remains unknown if lipid ion-pairs between L-PG and PG or CL actually attenuates plasma membrane anionicity and also it remains unknown what type of effects lipid ion-pairs may have on the structural properties of the plasma membrane (e.g. changes in viscosity, rigidity, elasticity and etc). Therefore this study looked at what charge and structural effects increased L-PG

biosynthesis had on the plasma membrane of *S. aureus* when the bacterium was exposed to a low pH environment.

Using *S. aureus* itself as a starting point to investigate the effects increased L-PG concentrations has on the plasma membrane of *S. aureus*, the polar lipids from six strains of *S. aureus* grown at pH 5.5 and 7.4 were extracted using the acid-modified Bligh and Dyer method (chapter 2.3.1) (Foreman-Wykert *et al.* 2000). However, this lipid extraction method gave no guarantee of purity and non-phospholipid contaminants may have been present. Also, the molecular weights of the lipids were unknown and therefore only rudimentary analytical tests could be performed on the natural lipid extracts when deposited as monolayers. Electrophoretic measurements on the pH 7.4 lipid extracts gave negative zeta potential results when the lipids were reconstituted as mutli-lamellar vesicle (MLV) dispersions in pH 7.4 buffer, however this zeta potential anionicity was reduced in buffer at pH 5.5 (chapter 3.3.1). The reduction in zeta potential anionicity at pH 5.5 was presumed to be due to a change in the charge state of L-PG from partially cationic at pH 7.4 to mostly cationic at pH 5.5 as the α-amine of L-PG possesses a pKa of between 6 and 7 (Tocanne *et al.* 1974c). Therefore the greater presence of cationic L-PG at pH 5.5 suggested that there had been an increase in the formation of ion-pairs between L-PG and PG or CL resulting in a reduction in negative zeta potential of the MLVs. This result was also supported by the observation of a monolayer condensing effect and a reduction in monolayer elasticity when the lipid extracts were deposited on a pH 5.5 subphase and compared to similar monolayers on a pH 7.4 subphase (chapter 3.3.2).

The lipids extracted from pH 5.5 cultures of methicillin susceptible *S. aureus* 476 (MSSA 476), methicillin resistant *S. aureus* G32 (MRSA G32) and MRSA H66 showed contrasting results to that of their pH 7.4 lipid extracts, where monolayer expansion and increases in monolayer lateral elasticity were observed on a pH 5.5 subphase compared with a pH 7.4 subphase (chapter 3.3.2). However as shown in chapter 2.3.1, these *S. aureus* strains contained ~50% L-PG as their total phospholipid which presumably resulted in them containing an excess of cationic L-PG on a pH 5.5 subphase resulting in lipid-lipid charge repulsion and thus lateral expansion of the monolayers (Gaines 1966). Although these results for the pH 5.5 lipid extracts showed a reduction in monolayer lateral density and an increase in elasticity on a pH 5.5 subphase, they gave positive zeta potential results when dispersed as MLVs (chapter 3.3.1). Therefore these natural lipid extract results suggest that the plasma membrane of *S. aureus*

when grown in a pH 5.5 environment becomes laterally more closely packed, more rigid and less anionically charged on the outer surface due to ion-pair formation between L-PG and PG or CL. However, there is a small reduction in membrane lateral density due to L-PG content being ~50% total phospholipid, which appears to be a compromise in order for the plasma membrane outer surface to become positively charged and thus electrostatically repel protons.

Although examination of the structural and charge properties of the *S. aureus* natural lipid extracts gave an indication as to the role of L-PG in the bacterial plasma membrane at low pH, reproducibility of the data was poor and resulted in poor statistics which gave low levels of confidence in the reported data (chapters 3.3.1 and 3.3.2). This was most obvious in the neutron diffraction data of the pH 5.5 and 7.4 lipid extracts of MSSA 476, where seemingly anomalous bilayer swelling profiles were observed (chapter 3.3.3). The poor reproducibility of the natural lipid extract data was attributed to the hydrolysis of L-PG to PG and lysine under the mild aqueous conditions, which had previously been documented for synthetic L-PG in an X-ray diffraction study (Danner *et al.* 2008). To avoid the problem of L-PG degradation, analogues of the lipid were synthesised and in order to keep the molecular structures of these analogues as biomimetic as possible only the labile ester linkage in L-PG was substituted, for a more stable amide. The L-PG analogue with the least complex synthesis, 1,2-*O*-dipalmitoyl 3-aza-dehydroxy L-PG (DP3adLPG), became the analogue of choice to act as an L-PG substitute when studying the role of L-PG in the plasma membrane of *S. aureus*. This was because, although DP3adLPG also lacked a secondary hydroxyl group along its amino-propane backbone, it displayed similar headgroup physicochemical properties to the headgroup of L-PG and did not suffer with a contaminating structural isomer as observed with 1,2-*O*-dipalmitoyl 3-aza L-PG (chapter 4.2.4).

To confirm that DP3adLPG had similar physicochemical and structural characteristics to native L-PG a series of preliminary experiments were performed with DP3adLPG and the results were compared to those in the existing literature on L-PG. The pKas of three the ionisable groups in DP3adLPG were determined, using monolayer pH titration experiments, to be 1-3 (phosphate group), 5.5-6.7 (α-amine) and >9 (ε-amine) which was almost identical to the pKa's of the same ionisable groups in L-PG (chapter 5.3.1) (Tocanne *et al.* 1974c). Charge states of DP3adLPG at pH 5.5 and 7.4 appeared to be analogous to L-PG's where zeta potential results of mixtures of DP3adLPG and 1,2-*O*-dipalmitoyl PG (DPPG) showed that the DP3adLPG existed as a

zwitterionic and cationic mixture at pH 7.4 but was significantly more cationic at pH 5.5 (chapter 5.3.4). In neutron diffraction experiments the scattering length density (SLD) profile of 100% DP3adLPG showed a headgroup thickness of ~10 Å which suggested the lipid's headgroup to be in a loop conformation. The looped headgroup conformation occurs because of an internal ion-pair formed between one of the lipid's protonated amines and its phosphate group, this being analogous to the headgroup conformation of native L-PG (El Mashak & Tocanne 1979). To ensure DP3adLPG behaved similarly to L-PG in synthetic models of the *S. aureus* phospholipid extracts, two mixtures of DP3adLPG–DPPG–tetramytristol CL (TMCL) 28.12:66.85:5.03 (pH 7.4 lipid extract model) and 51.63:40:8.37 mol/mol/mol (pH 5.5 lipid extract model) were made which replicated the phospholipid proportions measured in MRSA G32 when cultured at pH 5.5 and 7.4 (chapter 5.3.5). Monolayers formed from the pH 7.4 lipid extract model showed a lateral condensing effect and a reduction in monolayer elasticity when the subphase pH was reduced from 7.4 to 5.5. The pH 5.5 lipid extract model showed contrasting behaviour where monolayer lateral expansion and increased elasticity were observed when reducing the subphase pH from 7.4 to 5.5. This behaviour of the pH 5.5 and 7.4 lipid extract models on both subphase pHs was identical to the behaviour observed with the natural lipid extracts of MRSA G32 and therefore strongly indicated that DP3adLPG could act as a biomimetic L-PG substitute in synthetic models of the *S. aureus* plasma membrane.

In order to examine, at the atomic level, what effect ion-pairing between L-PG and PG or CL might have on the behaviour of the plasma membrane of *S. aureus* grown in a low pH environment, neutron scattering techniques (neutron diffraction, neutron reflectivity and small angle neutron scattering (SANS)) and ^{2}H-NMR were employed with synthetic lipid mixtures of hydrocarbon chain deuterium labelled DPPG (d_{62}PG) and DP3adLPG (d_{62}3adLPG) in molar ratios of 3:7 and 55:45. These ratios replicated the proportions of phospholipids found in MSSA 476, MRSA G32 and MRSA H66 grown at pH 5.5 (d_{62}3adLPG–d_{62}PG 55:45 mol/mol) and pH 7.4 (d_{62}3adLPG–d_{62}PG 3:7 mol/mol) (chapter 6). CL was deliberately omitted from these lipid mixtures in order to simplify the system for the purposes of neutron data interpretation. Both the neutron reflectivity and SANS experiments were only performed above the d_{62}3adLPG–d_{62}PG mixture main lipid phase transition temperature (T_m ~40 °C, chapter 5.3.3) at 55 °C in order to be in the same phase as the phospholipids in the plasma membrane of *S. aureus* (L_α or fluid phase). To ensure that the increased temperature did not radically alter the charge

characteristics of d_{62}3adLPG–d_{62}PG, SANS was performed to compare vesicle mixtures of 1-*O*-oleoyl-2-*O*-oleoyl (T_m ~4 °C, (Silvius 1982)) versions of 3adLPG and PG at 25 °C and DP3adLPG–DPPG at 55 °C. The SANS results showed both sets of vesicles had analogous bilayer thickness and d-spacing results therefore confirming that the DP3adLPG–DPPG mixtures were in the L_α phase at 55 °C and their surface charge characteristics had not been dramatically altered at 55 °C (chapter 5.3.6).

Neutron diffraction measurements were performed at both 25 °C and 55 °C as greater orders of neutron diffraction were detected in the $L_{\beta'}$ phase which increases the resolution of the reconstructed SLD profiles of the lipid bilayers (Pabst *et al.* 2003). Neutron reflectivity from a floating bilayer consisting of d_{62}3adLPG and d_{62}PG (3:7 mol/mol) showed a distinct increase in fitted headgroup positive SLD as the pH was reduced from 7.4 to 5.5 (chapter 6.3.2). The increase in SLD was substantial in magnitude (~3 × 10 $Å^{-2}$) between the pHs and indicated the bilayer had increased in lateral density presumably due to a higher incidence of ion-pair formation between the two lipids at pH 5.5. The observed increase in SLD in the headgroup region at pH 5.5 was also detected in the d_{62}3adLPG and d_{62}PG 55:45 mol/mol lipid mixture (chapter 6.3.2). However, in this latter lipid mixture the headgroup SLD was similarly high in both pH buffers presumably due to the higher level of d_{62}3adLPG, and the pH 7.4 buffer still containing d_{62}3adLPG in a partially cationic state therefore permitting significant ion-pair formation with the d_{62}PG. Neutron diffraction data also supported the presence of ion-pairs formed between d_{62}3adLPG and d_{62}PG in the 3:7 molar mixture of the lipids in the $L_{\beta'}$ phase, as indicated by the presence of two domains (chapter 6.3.1). The first domain had a d-spacing of ~120 Å and was assigned as a d_{62}PG rich domain due to its SLD profile having a headgroup thickness of ~8 Å and the d-spacing being large due to the electrostatic repulsion between the headgroups of adjacent bilayers (Pozo Navas *et al.* 2005, Armen *et al.* 1998). The second domain was assigned as a charge-neutral-ion-pair rich domain as it gave a d-spacing (~82 Å) which was analogous to the d-spacing of uncharged 1,2-*O*-dipalmitoyl phosphatidycholine (DPPC) bilayers (Darkes & Bradshaw 2000). In addition to this, the latter domain's SLD profile showed a much larger headgroup thickness of ~12 Å, which was assumed to be the mean thickness of the ion-paired headgroups of d_{62}3adLPG and d_{62}PG. The appearance of these two domains in neutron diffraction suggested the existence of significant intralamellar and interlamellar coupling between the domains. The reason for this domain coupling was

presumed to be to reduce the tensional strain on the water layers between the bilayers and therefore the like domains aligned in the bilayer stacks resulting in lamellar phase separation (Tayebi *et al.* 2012).

Although ion-pairing between d_{62}3adLPG and d_{62}PG had been shown to affect bilayer headgroup properties, ^{2}H-NMR, neutron reflectivity and neutron diffraction also detected substantial changes in the bilayer hydrocarbon region (chapters 5.4.3, 6.3.1 and 6.3.2). Dispersions of DP3adLPG and d_{62}PG MLVs with increasing DP3adLPG concentrations at pH 5.5 appeared to have little effect on the binary lipid mixture T_m, which remained between 39 °C and 41 °C (chapter 5.3.3). However, as an equimolar concentration of DP3adLPG and d_{62}PG was approached lateral hydrocarbon chain order (S_{CD}) increased across all 16 carbons of the palmitoyl lipid tails in the L_α phase (chapter 5.3.3). The increase in lipid tail S_{CD} with close to equimolar lipid concentrations suggested that as more ion-pairs formed between DP3adLPG and d_{62}PG, degrees of freedom of the lipid hydrocarbon tails were hindered thus resulting in a more viscous gel-phase type lipid structure in the lipid ion-pair. In addition to the increase in lipid tail S_{CD}, the lateral density of the lipid hydrocarbon tails also appeared to increase upon lipid ion-pair formation as shown by the d_{62}3adLPG–d_{62}PG 3:7 mol/mol floating bilayer neutron reflectivity data (chapter 6.3.2). A substantial increase in the hydrocarbon tail SLD occurred when the bilayer pH was reduced from 7.4 to 5.5 which indicated that the mass density of the lipid tails had increased and therefore they were occupying less volume. Although increases in hydrocarbon tail lateral density and order occurred upon lipid ion-pair formation, the neutron diffraction SLD profiles of both 3:7 (ion-paired domain) and 55:45 mol/mol mixtures of the lipids in the $L_{\beta'}$ phase showed some z-axis rearrangement of the bilayer hydrocarbon core of the ion-paired lipids (chapter 6.3.1). This rearrangement saw an overlap of the terminal hydrocarbon groups of the bilayer leaflets which was presumably due to the bulky cationic d_{62}3adLPG headgroup needing to push further into the bilayer in order for its protonated amines to form ion-pairs with their adjacent d_{62}PG headgroups.

To further investigate the headgroup properties of d_{62}3adLPG, the neutron diffraction and neutron reflectivity data of the headgroup regions of mixtures d_{62}3adLPG and d_{62}PG were examined in greater depth. DP3adLPG was shown to possess two amine groups which become cationic at different pHs as described earlier. Each protonated amine of DP3adLPG has the potential to form intramolecular ionic bonds to its own anionic phosphate group.

Previous studies with L-PG could not discern which protonated amine group bonds directly to the phosphate and it was suggested it may be a fluctuating structure between both (Tocanne *et al.* 1974c). When d_{62}3adLPG was mixed with d_{62}PG in a 3:7 molar ratio in the $L_{\beta'}$ phase the neutron diffraction SLD profile of the ion-paired domain possessed a headgroup thickness of ~12 Å which was also partly found in the d_{62}3adLPG–d_{62}PG 55:45 mol/mol mixture (chapter 6.3.1). This mean headgroup thickness of ~12 Å favours the headgroup conformation of d_{62}3adLPG to be in a loop structure where the protonated ε-amine is ionically bonded to its own phosphate and the protonated α-amine free to form ionic bonds to neighbouring d_{62}PG molecules (chapter 6.3.1). A loop conformation formed with the protonated ε-amine would certainly be the most energetically stable as the ε-amine is a stronger base than the α-amine and therefore would form a stronger electrostatic attraction to its own phosphate. In addition to this, the lipid headgroup would presumably be more flexible and entropically stable with a large loop structure formed by an ionic bond between the protonated ε-amine and phosphate whereas a loop structure formed between the protonated α-amine and phosphate would likely be more constrained and less entropically stable. However, neutron reflectivity data from d_{62}3adLPG–d_{62}PG 55:45 mol/mol at pH 5.5 possessed a headgroup thickness closer to ~16-17 Å and this was also observed in the neutron diffraction SLD profile of d_{62}3adLPG–d_{62}PG 55:45 mol/mol in the $L_{\beta'}$ phase (chapters 6.3.1 and 6.3.2). This larger headgroup thickness was likely to be the conformation formed by the d_{62}3adLPG headgroup when the protonated α-amine was bonded to its own phosphate. Such a conformation would result in a thicker headgroup because the protonated ε-amine with its long flexible hydrocarbon chain would protrude further away from the bilayer interface in order to minimise electrostatic cationic repulsion between neighbouring d_{62}3adLPG molecules. The latter conformation was not observed in neutron diffraction of 100% d_{62}3adLPG presumably due to the observed interdigitation allowing sufficient separation of the cationic charges of neighbouring lipid headgroups (chapter 5.3.2).

With respect to the behaviour of the plasma membrane of *S. aureus,* all of the combined neutron scattering and ^{2}H-NMR data support the earlier findings from the natural lipid extracts that at pH 5.5 the bacterial plasma membrane becomes more laterally condensed and more rigid. However, neutron scattering and ^{2}H-NMR also show the bacterial plasma membrane at pH 5.5 to be less disordered, rich in lipid ion-pairs, less hydrated overall and to exist mainly with the L-PG headgroup in a large loop conformation (ionic bond between protonated ε-amine and

phosphate) with the excess cationic L-PG headgroups adopting a smaller loop (more elongated) conformation (ionic bond between protonated α-amine and phosphate). There is also evidence from neutron diffraction to suggest ion-pairs between L-PG and PG or CL cause some rearrangements of the plasma membrane hydrocarbon core resulting in some hydrocarbon chain overlap between membrane leaflets.

The primary aim of the work described in the first six chapters of this thesis, with the natural lipid extracts and synthetic lipid bacterial plasma membrane models, was to try and better understand the role, function and regulation of L-PG in the plasma membrane of *S. aureus* when the bacterium is grown in a low pH environment. This is important because *S. aureus* has been found to grow on low pH human epidermal surfaces such as skin (<pH 5.0) and the anterior nares of the nasal cavity (~pH 6.0) (Lambers *et al.* 2006, Washington *et al.* 2000, Frank *et al.* 2010). With respect to the regulation of L-PG biosynthesis at pH 5.5, this appears to be under genetic control when high concentrations of protons in the environment of *S. aureus* induce an increased expression of *graS.* The increase in the expression of *graS* presumably results in the presence of more plasma membrane GraS in order to sense the increased abundance of protons in the external environment which would then stimulate an increased expression of *mprF* (chapter 1.8, figure 1-28). Increases in expression of *mprF* were shown to increase L-PG concentrations to ~50% of total membrane phospholipid when the bacterium was grown at pH 5.5, a finding which is consistent with previous studies (Gould & Lennarz 1970). The main function of L-PG in the plasma membrane of *S. aureus* at low pH has been found to be the formation ion-pairs with PG and CL as shown by neutron scattering techniques on bilayers consisting of d_{62}3adLPG and d_{62}PG. The formation of these lipid ion-pairs result in the bilayers becoming more laterally condensed, less permeable, less hydrated, less locally disordered and positively charged when >50% d_{62}3adLPG was present. Therefore it can be assumed that >50% L-PG as total plasma membrane phospholipid in *S. aureus* at pH 5.5 would also possess similar bilayer properties. The changes in plasma membrane lateral density, disorder and permeability presumably would reduce the likelihood of protons in the external growth environment from traversing the plasma membrane. The change in charge of the plasma membrane outer leaflet to positive forms an electrostatic charge barrier to repel protons away from the plasma membrane. These changes in the plasma membrane would help preserve the bacterium's cytoplasmic pH of between 7.0 to 8.0 (Collins & Hamilton 1976) and

thus minimise the risk of excess protons in the bacterial cytoplasm from interfering with internal cell processes. Additionally, the high pH of the bacterial cytoplasm would render any L-PG on the plasma membrane inner leaflet mostly zwitterionic therefore reducing the possibility of cationic L-PG also interfering with cellular processes. Therefore the role of L-PG in the plasma membrane of *S. aureus* appears to be much broader than solely for resistance to CAMPs and also appears to serve as a means for the bacterium to adapt to a low pH environment.

Although L-PG has been shown to help the plasma membrane of *S. aureus* to adapt to a low pH environment, additional stresses encountered during growth on human epithelial surfaces further compromise its survival, as the surfaces they inhabit are rich in secreted CAMPs such as the cathelicidin LL-37 and the defensins hBD-2 and hBD-3 (Ong *et al.* 2002, Cole *et al.* 1999, Laudien *et al.* 2011). The concentrations of these CAMPs are greater in the anterior nares relative to skin, however, *S. aureus* is still able to survive and grow in both environments (Lambers *et al.* 2006, Ong *et al.* 2002). In order to investigate the adaptation of *S. aureus* to these environments an analogue of an amphibian-expressed CAMP, magainin 2 F5W, was used to challenge synthetic plasma membrane models of *S. aureus* and *S. aureus* lipid extracts in both pH 5.5 and 7.4 milieux (lipid–peptide 50:1 mol/mol). MRSA G32 lipid extracts from bacteria grown at pH 7.4 and a biomimetic synthetic lipid model of the MRSA G32 lipid extract (DP3adLPG–DPPG–TMCL 28.12:66.85:5.03 mol/mol/mol) both showed an increase in monolayer surface pressure after injection of magainin 2 F5W under individual monolayers formed of these lipid mixtures (chapter 7.3.1). However, the surface pressure increase was greater on a pH 7.4 subphase (~10 mN/m) in comparison to a pH 5.5 subphase (~6-7 mN/m) which indicated greater amounts of magainin 2 F5W were binding to and penetrating into the monolayer at pH 7.4. The differences in increases of the monolayer surface pressures suggested that the amount of negative lipid headgroups available for magainin 2 F5W to bind to had reduced at the lower pH and more of the DP3adLPG (or L-PG) and PG or CL had formed ion-pairs at pH 5.5.

The system was then examined in more detail using neutron reflectivity with the floating bilayer of d_{62}3adLPG–d_{62}PG 3:7 mol/mol representing *S. aureus* grown at pH 7.4 and was challenged with magainin 2 F5W (lipid–peptide 50:1 mol/mol) (chapter 7.3.3). In the pH 7.4 buffer the peptide was observed to partition into the bilayer and bind to its interfacial regions, also an increase in bilayer solvent penetration was observed suggesting that either the peptide had

possibly formed pores in the bilayer or that the binding of the peptide to the membrane surfaces had disrupted lateral packing of the lipids making the bilayer more porous (Ludtke *et al.* 1996). In the pH 5.5 buffer the positive SLD of the whole thickness of the bilayer increased thus suggesting less magainin 2 F5W was partitioning into the bilayer, however bilayer hydration was still high indicating solvent pockets remained present in the bilayer and therefore activity of the peptide was not abolished by the formation of more ion-pairs between d_{62}3adLPG and d_{62}PG at pH 5.5. The overall bilayer thickness in both pH buffers was also shown to decrease in the presence of magainin 2 F5W and this was also observed with SANS of vesicles composed of d_{62}3adLPG–d_{62}PG 3:7 mol/mol upon peptide challenge (chapter 7.3.3). This membrane thinning effect is characteristic of the mechanism of action of magainin 2 F5W (Ludtke *et al.* 1995) and was more pronounced in the pH 7.4 buffer relative to the pH 5.5 buffer presumably due to the reduced availability of non-ion-paired d_{62}PG at pH 5.5. Neutron diffraction experiments gave higher resolution details of the interaction of magainin 2 F5W (lipid–peptide 50:1 mol/mol) with a MSSA 476 pH 7.4 lipid extract and d_{62}3adLPG–d_{62}PG at 3:7 mol/mol (chapter 7.3.2). In both lipid mixtures the SLD profiles in the L_{α} phase showed the peptide to be partitioning into the bilayer and spanning the hydrocarbon core of the bilayers to a substantial degree. However, the d_{62}3adLPG–d_{62}PG 3:7 mol/mol SLD profile in the $L_{\beta'}$ phase showed the peptide mainly altered the SLD of the d_{62}PG rich domain whereas the ion-paired domain showed only minor fluctuations in SLD.

Monolayer experiments with MRSA G32 pH 5.5 lipid extracts and a synthetic biomimetic model to represent this lipid extract (DP3adLPG–DPPG–TMCL 51.63:40:8.37 mol/mol/mol) showed very little interaction with magainin 2 F5W. On a pH 7.4 subphase an increase in surface pressure of ~3-4 mN/m was observed for both lipid mixtures however on a pH 5.5 subphase a negligible increase in surface pressure was observed, therefore suggesting total resistance to peptide binding occurred at pH 5.5 (chapter 7.3.1). On the pH 7.4 subphase the L-PG or DP3adLPG of both lipid samples would have been a mixture of cationic and zwitterionic forms of the lipids and would not interact with the cationic magainin 2 F5W which preferentially binds to negatively charged membranes (Ludtke *et al.* 1996, Ludtke *et al.* 1995). Therefore due to the availability of only a small amount of non-ion-paired DPPG or CL in these lipid samples on the pH 7.4 subphase, interaction with the magainin 2 F5W was still low. On the pH 5.5 subphase, however, all PG and CL would have been ion-paired to DP3adLPG or L-PG thus resulting in

total resistance of the monolayer to peptide challenge. However, a small discrepancy between the natural lipid extract and the synthetic lipid model was noted where greater surface pressure increases were observed after introduction of the peptide with the natural lipid extract. The greater pressure increase with the natural lipid extract suggested there had been some breakdown of L-PG to lysine and PG (Danner *et al.* 2008). SANS showed very little difference in bilayer thicknesses in both pH buffers when d_{62}3adLPG–d_{62}PG 55:45 mol/mol was dispersed as vesicles, to represent the pH 5.5 lipid extract from *S. aureus,* after exposure to magainin 2 F5W (lipid–peptide 50:1 mol/mol) (chapter 7.3.3). The bilayer thickness also remained little changed when d_{62}3adLPG–d_{62}PG 55:45 mol/mol was deposited as a floating bilayer and analysed by neutron reflectivity in a pH 5.5 buffer. However, the pH 7.4 buffer neutron reflectivity experiments did detect small changes in the SLD of the bilayer headgroups suggesting that a proportion of the peptide was able to bind to the surface of the membrane and some increased hydration of the bilayer was also apparent possibly due to this interaction. On reduction of the bulk pH to 5.5 this effect of the peptide on this membrane was reversed with the bilayer increasing in lateral density and hydration of the bilayer becoming similar to that observed for the system without the peptide. It would therefore appear the ion-pairing effect between cationic d_{62}3adLPG and anionic d_{62}PG is more energetically favourable than the binding interaction between the peptide and d_{62}PG. In the situation the peptide does manage to bind to the bilayer under favourable conditions, it appears to be forced out of the bilayer by the loss in enthalpy of the interaction between d_{62}3adLPG and d_{62}PG (Kilelee *et al.* 2010). In addition to this, in a pH 5.5 environment the d_{62}3adLPG–d_{62}PG 55:45 mol/mol bilayer presents with a cationically charged surface (chapter 5.4.4) and therefore the peptide must also overcome this electrostatic charge repulsion barrier in order to reach the membrane. These properties of the interactions between d_{62}3adLPG and d_{62}PG are also likely to be present between L-PG and PG or CL in the plasma membrane of *S. aureus* when exposed to CAMPs in a low pH environment and therefore provides a possible mechanism of how the plasma membrane of the bacterium becomes less susceptible to the cytolytic activity of membrane active CAMPs at pH 5.5.

As discussed earlier, the presence of high concentrations of L-PG in the plasma membrane of *S. aureus* appears to facilitate the bacteria's survival in a low pH environment. However, studying of magainin 2 F5W with mixtures of d_{62}3adLPG–d_{62}PG in this work also demonstrates

that the increased biosynthesis of L-PG up to ~50% of total membrane phospholipid also confers total resistance of the plasma membrane to the membrane lytic effects of the peptide in a pH 5.5 environment. In terms of the evolution of *S. aureus* it might be suggested that the primary function of L-PG was originally to facilitate adaptation to a low pH environment such as the mild acidity encountered at human mucosa (Lambers *et al.* 2006, Washington *et al.* 2000). This may be the case since the sensor, GraS, has only a small nine residue extracellular sensory loop with a proline kink and it is difficult to envisage how even a small CAMP could interact with such a small kinked sensor loop (Li *et al.* 2007a, Li *et al.* 2007b). However, this loop region appears to be ideally set up for protons to interact with as it contains three anionically charged residues with pKas of between 4.0 and 4.1 which is similar to that of the pH of healthy human skin (~4.6) (Lambers *et al.* 2006, Li *et al.* 2007a, Li *et al.* 2007b, Tollinger, Forman-Kay & Kay 2002). The 198 residue extracellular loop of VraG however is sufficiently big enough for CAMPs to interact with (Falord *et al.* 2012) and this may have evolved in the bacterium as a later adaptation to activate GraS and increase membrane L-PG in response to the selection pressure of exposure to CAMPs at mammalian mucosa. This may explain why a decrease in pH was not correlated to a large upregulation in *vraG* expression in this study but was found in other studies when *S. aureus* was exposed to sub-lethal concentrations of CAMPs (Falord *et al.* 2012).

Without further investigations involving gene knock-out, making any definitive statements about the role of GraS as an *S. aureus* pH sensor functioning independently of any CAMP-triggered mechanism will not be possible. However what is apparent from the studies presented in this thesis is that L-PG plays a dual role in the bacterial plasma membrane, since it both increases the bacterium's ability to tolerate mildly acidic environments and facilitates its intrinsic resistance to membrane-active CAMPs. This latter role of L-PG in *S. aureus* is becoming increasingly recognised in its pathogenicity and has been associated with the reduced sensitivity of *S. aureus* to vancomycin and other cationic antimicrobials with membrane-associated targets, such as daptomycin (Nishi *et al.* 2004, Meehl *et al.* 2007, Yang *et al.* 2009, Peschel *et al.* 2001, Murthy *et al.* 2008a, Kilelee *et al.* 2010). It may therefore be that one way of tackling the virulence of resistant *S. aureus* infections could be the development of antagonists or antibodies targeted at reducing MprF expression in order to prevent L-PG biosynthesis, thus attenuating the bacterium's protection to innate immune defences.

References

Adams, D., Ebsworth, E. & Lynch, R. 2007, "Nuclear quadrupole resonance spectroscopy", .

Aebersold, R. & Mann, M. 2003, "Mass spectrometry-based proteomics", *Nature,* vol. 422, no. 6928, pp. 198-207.

Altschul, S.F., Madden, T.L., Schaffer, A.A., Zhang, J.H., Zhang, Z., Miller, W. & Lipman, D.J. 1997, "Gapped BLAST and PSI-BLAST: a new generation of protein database search programs", *Nucleic acids research,* vol. 25, no. 17, pp. 3389-3402.

Anderson, G., Callahan, F. & Zimmerman, J. 1964, "Use of Esters of N-Hydroxysuccinimide in Peptide Synthesis", *Journal of the American Chemical Society,* vol. 86, no. 9, pp. 1839-&.

Armen, R.S., Uitto, O.D. & Feller, S.E. 1998, "Phospholipid component volumes: Determination and application to bilayer structure calculations", *Biophysical journal,* vol. 75, no. 2, pp. 734-744.

Asselineau, J. 1991, "Bacterial lipids containing amino acids or peptides linked by amide bonds.", *Fortschritte der Chemie organischer Naturstoffe = Progress in the chemistry of organic natural products.Progres dans la chimie des substances organiques naturelles,* vol. 56, pp. 1-85.

Avanti Polar Lipids Inc. 2013a, *,* 1,2-dipalmitoyl-sn-glycero-3-[phospho-rac-(3-lysyl(1-glycerol))] (chloride salt) [Homepage of Avanti Polar Lipids Inc.], [Online]. Available: http://avantilipids.com/index.php?option=com_content&view=article&id=839&Itemid=169&catnumber=840520 [2013, 09/04].

Avanti Polar Lipids Inc. 2013b, *,* Preparation of Liposomes [Homepage of Avanti Polar Lipids], [Online]. Available: http://avantilipids.com/index.php?option=com_content&id=1384&Itemid=372 [2013, 08/01].

Barnes, D.J. & Chu, D. 2010, *Introduction to Modeling for Biosciences,* Springer.

Bligh, E.G. & Dyer, W.J. 1959, "A Rapid Method of Total Lipid Extraction and Purification", *Canadian Journal of Biochemistry and Physiology,* vol. 37, no. 8, pp. 911-917.

Bonsen, P.P.M., Dehaas, G.H. & Van Deene, L.l. 1967, "Synthetic and Structural Investigations on 3-Phosphatidyl-1'-(3'-0-L-Lysyl) Glycerol", *Biochemistry,* vol. 6, no. 4, pp. 1114-&.

Bragg, W.H. 1959, *The Universe of Light,* Dover Publications.

Bruice, T.C. & Fife, T.H. 1962, "Hydroxyl Group Catalysis. III. 1 The nature of neighboring hydroxyl group assistance in the alkaline hydrolysis of the ester bond", *Journal of the American Chemical Society,* vol. 84, no. 10, pp. 1973-1979.

Bruzik, K.S., Salamonczyk, G. & Stec, W.J. 1986, "A general method for the synthesis of glycerophospholipids", *The Journal of Organic Chemistry,* vol. 51, no. 12, pp. 2368-2370.

Buldt, G., Gally, H., Seelig, J. & Zaccai, G. 1979, "Neutron-Diffraction Studies on Phosphatidylcholine Model Membranes .1. Head Group Conformation", *Journal of Molecular Biology,* vol. 134, no. 4, pp. 673-691.

Cheng, A. & Caffrey, M. 1996, "Free radical mediated x-ray damage of model membranes", *Biophysical Journal,* vol. 70, no. 5, pp. 2212-2222.

Cole, A.M., Dewan, P. & Ganz, T. 1999, "Innate antimicrobial activity of nasal secretions", *Infection and Immunity,* vol. 67, no. 7, pp. 3267-3275.

Collins, S.H. & Hamilton, W.A. 1976, "Magnitude of the protonmotive force in respiring *Staphylococcus aureus* and *Escherichia coli*.", *Journal of Bacteriology,* vol. 126, no. 3, pp. 1224-1231.

Corey, E. & Vemkates, A. 1972, "Protection of Hydroxyl Groups as Tert-Butyldimethylsilyl Derivatives", *Journal of the American Chemical Society,* vol. 94, no. 17, pp. 6190-6191.

Cui, L.Z., Lian, J.Q., Neoh, H.M., Reyes, E. & Hiramatsu, K. 2005, "DNA microarray-based identification of genes associated with glycopeptide resistance in *Staphylococcus aureus*", *Antimicrobial Agents and Chemotherapy,* vol. 49, no. 8, pp. 3404-3413.

Danner, S., Pabst, G., Lohner, K. & Hickel, A. 2008, "Structure and thermotropic behavior of the *Staphylococcus aureus* lipid lysyl-dipalmitoylphosphatidylglycerol", *Biophysical Journal,* vol. 94, no. 6, pp. 2150-2159.

Darkes, M.J. & Bradshaw, J.P. 2000, "Real-time swelling-series method improves the accuracy of lamellar neutron-diffraction data", *Acta Crystallographica Section D: Biological Crystallography,* vol. 56, no. 1, pp. 48-54.

Davis, J.H. 1983, "The description of membrane lipid conformation, order and dynamics by 2H-NMR", *Biochimica et Biophysica acta,* vol. 737, no. 1, pp. 117-171.

Diltmer, J.C. & Lester, R.L. 1964, "A simple, specific spray for the detection of phospholipids on thin-layer chromatograms", *Journal of Lipid Research,* vol. 5, pp. 126-127.

Dossanto. J.M., Opdenkam. J.A., Verheij, H.M. & Van Deene, L.l. 1970, "Phospholipids of *Streptococcus-Faecalis*", *Journal of Bacteriology,* vol. 104, no. 2, pp. 611-619.

Dowhan, W. 1997, "Molecular basis for membrane phospholipid diversity: Why are there so many lipids?", *Annual Review of Biochemistry,* vol. 66, pp. 199-232.

Drabkin, D.L. 1958, *Thudichum: Chemist of the Brain,* University of Pennsylvania Press.

Durham, D. & Kloos, W. 1978, "Comparative-Study of Total Cellular Fatty-Acids of *Staphylococcus* Species of Human Origin", *International Journal of Systematic Bacteriology,* vol. 28, no. 2, pp. 223-228.

El Mashak, E. & Tocanne, J. 1979, "A monolayer study of the adsorption of methyl-lysine at phosphatidylglycerol-water interfaces: A model for elucidating the conformation of the Lisylphosphatidylglycerol polar head", *Journal of Colloid and Interface Science,* vol. 70, no. 1, pp. 56-66.

Ernst, C.M. & Peschel, A. 2011, "Broad-spectrum antimicrobial peptide resistance by MprF-mediated aminoacylation and flipping of phospholipids", *Molecular Microbiology,* vol. 80, no. 2, pp. 290-299.

Ernst, C.M., Staubitz, P., Mishra, N.N., Yang, S., Hornig, G., Kalbacher, H., Bayer, A.S., Kraus, D. & Peschel, A. 2009, "The Bacterial Defensin Resistance Protein MprF Consists of Separable Domains for Lipid Lysinylation and Antimicrobial Peptide Repulsion", *Plos Pathogens,* vol. 5, no. 11, pp. e1000660.

Fadok, V., Bratton, D., Rose, D., Pearson, A., Ezekewitz, R. & Henson, P. 2000, "A receptor for phosphatidylserine-specific clearance of apoptotic cells", *Nature,* vol. 405, no. 6782, pp. 85-90.

Falord, M., Karimova, G., Hiron, A. & Msadek, T. 2012, "GraXSR Proteins Interact with the VraFG ABC Transporter To Form a Five-Component System Required for Cationic

Antimicrobial Peptide Sensing and Resistance in *Staphylococcus aureus*", *Antimicrobial Agents and Chemotherapy,* vol. 56, no. 2, pp. 1047-1058.

Fedtke, I., Gotz, F. & Peschel, A. 2004, "Bacterial evasion of innate host defenses - the *Staphylococcus aureus* lesson", *International Journal of Medical Microbiology,* vol. 294, no. 2-3, pp. 189-194.

Fell, J. 2004, "Surface and interfacial phenomena" in *Pharmaceutics: The science of dosage form design*, ed. M.E. Aulton, 2nd edn, Churchill Livingstone, Elesevier, London, pp. 59-69.

Foreman-Wykert, A.K., Weiss, J. & Elsbach, P. 2000, "Phospholipid synthesis by *Staphylococcus aureus* during (sub)lethal attack by mammalian 14-kilodalton group IIA phospholipase A2", *Infection and Immunity,* vol. 68, no. 3, pp. 1259-1264.

Fox, M.A. & Whitesell, J.K. 1997, *Organic Chemistry,* Jones and Bartlett.

Fragneto, G. & Rheinstädter, M. 2007, "Structural and dynamical studies from bio-mimetic systems: an overview", *Comptes Rendus Physique,* vol. 8, no. 7, pp. 865-883.

Fragneto, G., Graner, F., Charitat, T., Dubos, P. & Bellet-Amalric, E. 2000, "Interaction of the third helix of *Antennapedia* homeodomain with a deposited phospholipid bilayer: A neutron reflectivity structural study", *Langmuir,* vol. 16, no. 10, pp. 4581-4588.

Fragneto-Cusani, G. 2001, "Neutron reflectivity at the solid/liquid interface: examples of applications in biophysics", *Journal of Physics: Condensed Matter,* vol. 13, no. 21, pp. 4973-4981.

Franca, A., Freitas, A.I., Henriques, A.F. & Cerca, N. 2012, "Optimizing a qPCR Gene Expression Quantification Assay for S. epidermidis Biofilms: A Comparison between Commercial Kits and a Customized Protocol", *Plos One,* vol. 7, no. 5, pp. e37480.

Frank, D.N., Feazel, L.M., Bessesen, M.T., Price, C.S., Janoff, E.N. & Pace, N.R. 2010, "The Human Nasal Microbiota and *Staphylococcus aureus* Carriage", *Plos One,* vol. 5, no. 5, pp. e10598.

Friedman, L., Alder, J.D. & Silverman, J.A. 2006, "Genetic changes that correlate with reduced susceptibility to daptomycin in *Staphylococcus aureus*", *Antimicrobial Agents and Chemotherapy,* vol. 50, no. 6, pp. 2137-2145.

Gaffney, P.R.J. & Reese, C.B. 2001, "Synthesis of naturally occurring phosphatidylinositol 3,4,5-trisphosphate [PtdIns(3,4,5)P-3] and its diastereoisomers", *Journal of the Chemical Society-Perkin Transactions 1,* , no. 2, pp. 192-205.

Gaines, G.L. 1966, "Insoluble monolayers at liquid-gas interfaces", *Wiley-Interscience,*.

Geiger, O., González-Silva, N., López-Lara, I.M. & Sohlenkamp, C. 2010, "Amino acid-containing membrane lipids in bacteria", *Progress in Lipid Research,* vol. 49, no. 1, pp. 46-60.

Gould, R.M. & Lennarz, W.J. 1970, "Metabolism of Phosphatidylglycerol and Lysyl Phosphatidylglycerol in *Staphylococcus-Aureus*", *Journal of Bacteriology,* vol. 104, no. 3, pp. 1135-1144.

Gould, R.M. & Lennarz, W.J. 1967, "Biosynthesis of aminoacyl derivatives of phosphatidylglycerol.", *Biochemical and Biophysical Research Communications,* vol. 26, no. 4, pp. 512-515.

Gustavsson, L. 1986, "Densitometric quantification of individual phospholipids: improvement and evaluation of a method using molybdenum blue reagent for detection", *Journal of Chromatography B: Biomedical Sciences and Applications,* vol. 375, pp. 255-266.

Hachmann, A., Angert, E.R. & Helmann, J.D. 2009, "Genetic analysis of factors affecting susceptibility of *Bacillus subtilis* to daptomycin", *Antimicrobial Agents and Chemotherapy,* vol. 53, no. 4, pp. 1598-1609.

Haines, T.H. 2009, "A new look at Cardiolipin", *Biochimica et Biophysica acta - Biomembranes,* vol. 1788, no. 10, pp. 1997-2002.

Hancock, R.E. 2001, "Cationic peptides: effectors in innate immunity and novel antimicrobials", *The Lancet Infectious Diseases,* vol. 1, no. 3, pp. 156-164.

Hanke, W., Schulue, W.R. & Sattelle, D.B. 1993, *Planar Lipid Bilayers: Methods and Applications,* Elsevier Science.

Harkins, W.D. & Debye, P. 1952, "*The Physical Chemistry of Surface Films*", .

Heenan, R.K. 2009, *FISH*, 3.97th edn, STFC ISIS, Oxford, UK.

Hentzen, D., Mandel, P. & Garel, J. 1972, "Relation between aminoacyl-tRNA stability and the fixed amino acid", *Biochimica et Biophysica Acta (BBA)-Nucleic Acids and Protein Synthesis,* vol. 281, no. 2, pp. 228-232.

Ho, S.W., Jung, D., Calhoun, J.R., Lear, J.D., Okon, M., Scott, W.R., Hancock, R.E. & Straus, S.K. 2008, "Effect of divalent cations on the structure of the antibiotic daptomycin", *European Biophysics Journal,* vol. 37, no. 4, pp. 421-433.

Hoffman, R.V. 2004, *Organic Chemistry: An Intermediate Text,* Wiley.

Hope, M., Bally, M., Mayer, L., Janoff, A. & Cullis, P. 1986, "Generation of multilamellar and unilamellar phospholipid vesicles", *Chemistry and Physics of Lipids,* vol. 40, no. 2, pp. 89-107.

Houtsmuller, U.M.T. & Van Deenen, L.L.M. 1963, "Identification of a Bacterial Phospholipid as an O-Ornithine Ester of Phosphatidyl Glycerol", *Biochimica et Biophysica acta,* vol. 70, no. 2, pp. 211-213.

Hughes, A.V., Howse, J.R., Dabkowska, A., Jones, R.A.L., Lawrence, M.J. & Roser, S.J. 2008, "Floating lipid bilayers deposited on chemically grafted phosphatidylcholine surfaces", *Langmuir,* vol. 24, no. 5, pp. 1989-1999.

Hunter, R.J. 1988, *Zeta Potential in Colloid Science: Principles and Applications,* Academic Press.

Imae, T., Kanaya, T., Furusaka, M. & Torikai, N. 2011, *Neutrons in Soft Matter,* Wiley.com.

Iversen, O. & Grov, A. 1973, "Studies on lysostaphin", *European Journal of Biochemistry,* vol. 38, no. 2, pp. 293-300.

Jackson, A.J. 2008, "Introduction to small-angle neutron scattering and neutron reflectometry", *NIST Center for Neutron Research, Gaithersburg, MD,* .

Srivastava, A.K. & Jain, P.C. 2007, *Chemistry Vol (1 and 2),* FK Publications.

Julian, K., Kosowska-Shick, K., Whitener, C., Roos, M., Labischinski, H., Rubio, A., Parent, L., Ednie, L., Koeth, L. & Bogdanovich, T. 2007, "Characterization of a daptomycin-nonsusceptible vancomycin-intermediate *Staphylococcus aureus* strain in a patient with endocarditis", *Antimicrobial Agents and Chemotherapy,* vol. 51, no. 9, pp. 3445-3448.

Jung, D., Powers, J.P., Straus, S.K. & Hancock, R.E. 2008, "Lipid-specific binding of the calcium-dependent antibiotic daptomycin leads to changes in lipid polymorphism of model membranes", *Chemistry and Physics of Lipids,* vol. 154, no. 2, pp. 120-128.

Kaneda, T. 1991, "Iso-and anteiso-fatty acids in bacteria: biosynthesis, function, and taxonomic significance.", *Microbiological Reviews,* vol. 55, no. 2, pp. 288-302.

Kates, M., Syz, J., Gosser, D. & Haines, T. 1993, "Ph-Dissociation Characteristics of Cardiolipin and its 2'-Deoxy Analog", *Lipids,* vol. 28, no. 10, pp. 877-882.

Kilelee, E., Pokorny, A., Yeaman, M.R. & Bayer, A.S. 2010, "Lysyl-phosphatidylglycerol attenuates membrane perturbation rather than surface association of the cationic antimicrobial peptide 6W-RP-1 in a model membrane system: implications for daptomycin resistance", *Antimicrobial Agents and Chemotherapy,* vol. 54, no. 10, pp. 4476-4479.

Kim, S.J., Singh, M. & Schaefer, J. 2009, "Oritavancin Binds to Isolated Protoplast Membranes but not Intact Protoplasts of *Staphylococcus aureus*", *Journal of Molecular Biology,* vol. 391, no. 2, pp. 414-425.

Kleinschmidt, J.H., Mahaney, J.E., Thomas, D.D. & Marsh, D. 1997, "Interaction of bee venom melittin with zwitterionic and negatively charged phospholipid bilayers: A spin-label electron spin resonance study", *Biophysical Journal,* vol. 72, no. 2, pp. 767-778.

Klevens, R.M., Morrison, M.A., Nadle, J., Petit, S., Gershman, K., Ray, S., Harrison, L.H., Lynfield, R., Dumyati, G. & Townes, J.M. 2007, "Invasive methicillin-resistant *Staphylococcus aureus* infections in the United States", *JAMA: The Journal of the American Medical Association,* vol. 298, no. 15, pp. 1763-1771.

Kocienski, P.J. 2005, *Protecting Groups,* Georg Thieme Verlag.

Koprivnjak, T., Peschel, A., Gelb, M.H., Liang, N.S. & Weiss, J.P. 2002, "Role of charge properties of bacterial envelope in bactericidal action of human group IIA phospholipase A2against *Staphylococcus aureus*", *Journal of Biological Chemistry,* vol. 277, no. 49, pp. 47636-47644.

Kosowska-Shick, K., Clark, C., Pankuch, G.A., McGhee, P., Dewasse, B., Beachel, L. & Appelbaum, P.C. 2009, "Activity of telavancin against *staphylococci* and *enterococci* determined by MIC and resistance selection studies", *Antimicrobial Agents and Chemotherapy,* vol. 53, no. 10, pp. 4217-4224.

Kotlarchyk, M. & Chen, S. 1983, "Analysis of small angle neutron scattering spectra from polydisperse interacting colloids", *The Journal of Chemical Physics,* vol. 79, pp. 2461-2470.

Kotz, J.C., Treichel, P.M. & Townsend, J.R. 2009, *Chemistry & Chemical Reactivity,* Brooks/Cole.

Kristian, S.A., Dürr, M., Van Strijp, J.A., Neumeister, B. & Peschel, A. 2003, "MprF-mediated lysinylation of phospholipids in *Staphylococcus aureus* leads to protection against oxygen-independent neutrophil killing", *Infection and Immunity,* vol. 71, no. 1, pp. 546-549.

KSV NIMA 2013, *Langmuir and Langmuir-Blodgett deposition troughs*, product brochure, KSV NIMA, Coventry.

Kučerka, N., Liu, Y., Chu, N., Petrache, H.I., Tristram-Nagle, S. & Nagle, J.F. 2005, "Structure of fully hydrated fluid phase DMPC and DLPC lipid bilayers using X-ray scattering from oriented multilamellar arrays and from unilamellar vesicles", *Biophysical Journal,* vol. 88, no. 4, pp. 2626-2637.

Kuhl, O. 2008, *Phosphorus-31 NMR Spectroscopy: A Concise Introduction for the Synthetic Organic and Organometallic Chemist,* Springer.

Lambers, H., Piessens, S., Bloem, A., Pronk, H. & Finkel, P. 2006, "Natural skin surface pH is on average below 5, which is beneficial for its resident flora", *International Journal of Cosmetic Science,* vol. 28, no. 5, pp. 359-370.

Langmuir, I. 1917, "The constitution and fundamental properties of solids and liquids. II. Liquids. 1", *Journal of the American Chemical Society,* vol. 39, no. 9, pp. 1848-1906.

Laudien, M., Dressel, S., Harder, J. & Glaeser, R. 2011, "Differential expression pattern of antimicrobial peptides in nasal mucosa and secretion", *Rhinology,* vol. 49, no. 1, pp. 107-111.

Lehmann, E.L. & D'Abrera, H.J. 1975, *Nonparametrics: Statistical methods based on ranks,* Holden-Day.

Lennarz, W.J., Nesbitt, J.A. & Reiss, J. 1966, "Participation of Srna in Enzymatic Synthesis of O-L-Lysyl Phosphatidylgylcerol in *Staphylococcus Aureus*", *Proceedings of the National Academy of Sciences of the United States of America,* vol. 55, no. 4, pp. 934-&.

Leonard, A., Escrive, C., Laguerre, M., Pebay-Peyroula, E., Neri, W., Pott, T., Katsaras, J. & Dufourc, E.J. 2001, "Location of cholesterol in DMPC membranes. A comparative study by neutron diffraction and molecular mechanics simulation", *Langmuir,* vol. 17, no. 6, pp. 2019-2030.

Levitt, M.H. 2013, *Spin Dynamics,* John Wiley & Sons.

Li, M., Cha, D.J., Lai, Y., Villaruz, A.E., Sturdevant, D.E. & Otto, M. 2007a, "The antimicrobial peptide-sensing system aps of *Staphylococcus aureus*", *Molecular Microbiology,* vol. 66, no. 5, pp. 1136-1147.

Li, M., Lai, Y., Villaruz, A.E., Cha, D.J., Sturdevant, D.E. & Otto, M. 2007b, "Gram-positive three-component antimicrobial peptide-sensing system", *Proceedings of the National Academy of Sciences of the United States of America,* vol. 104, no. 22, pp. 9469-9474.

Lis, L., McAlister, M., Fuller, N., Rand, R. & Parsegian, V. 1982, "Interactions between neutral phospholipid bilayer membranes.", *Biophysical Journal,* vol. 37, no. 3, pp. 657.

Livak, K.J. & Schmittgen, T.D. 2001, "Analysis of Relative Gene Expression Data Using Real-Time Quantitative PCR and the 2−ΔΔCT Method", *Methods,* vol. 25, no. 4, pp. 402-408.

Lok, C. 1978, "Versatile methods for the synthesis of mixed-acid 1, 2-diacylglycerols", *Chemistry and Physics of Lipids,* vol. 22, no. 4, pp. 323-337.

Ludtke, S., He, K. & Huang, H. 1995, "Membrane thinning caused by magainin 2", *Biochemistry,* vol. 34, no. 51, pp. 16764-16769.

Ludtke, S., He, K., Heller, W., Harroun, T., Yang, L. & Huang, H. 1996, "Membrane pores induced by magainin", *Biochemistry,* vol. 35, no. 43, pp. 13723-13728.

Macfarlane, M.G. 1962, "Characterization of Lipoamino-Acids as O-Amino-Acid Esters of Phosphatidyl-Glycerol", *Nature,* vol. 196, no. 4850, pp. 136-138.

Maloney, E., Stankowska, D., Zhang, J., Fol, M., Cheng, Q., Lun, S., Bishai, W.R., Rajagopalan, M., Chatterjee, D. & Madiraju, M.V. 2009, "The Two-Domain LysX Protein of *Mycobacterium tuberculosis* Is Required for Production of Lysinylated Phosphatidylglycerol and Resistance to Cationic Antimicrobial Peptides", *Plos Pathogens,* vol. 5, no. 7, pp. e1000534.

Marsh, D. 1990, *CRC handbook of Lipid Bilayers,* CRC Press.

Martin, S.F., Josey, J.A., Wong, Y. & Dean, D.W. 1994, "General Method for the Synthesis of Phospholipid Derivatives of 1,2-O-Diacyl-sn-Glycerols", *The Journal of Organic Chemistry,* vol. 59, no. 17, pp. 4805-4820.

McMurry, J.E. 2012, *Organic Chemistry , Enhanced Edition, Volume 2,* .

Medimoon Ltd., 2013, *, Why is it more difficult to treat Gram negative bacteria?* [Homepage of Medimoon Ltd.,], [Online]. Available: http://medimoon.com/2013/04/why-is-it-more-difficult-to-treat-gram-negative-bacteria/ [2013, 07/25].

Meehl, M., Herbert, S., Goetz, F. & Cheung, A. 2007, "Interaction of the GraRS two-component system with the VraFG ABC transporter to support vancomycin-intermediate resistance in *Staphylococcus aureus*", *Antimicrobial Agents and Chemotherapy,* vol. 51, no. 8, pp. 2679-2689.

Metz, K. & Dunphy, L. 1996, "Absolute quantitation of tissue phospholipids using 31P NMR spectroscopy.", *Journal of Lipid Research,* vol. 37, no. 10, pp. 2251-2265.

Mischel, M., Seelig, J., Braganza, L.F. & Buldt, G. 1987, "A Neutron-Diffraction Study of the Headgroup Conformation of Phosphatidylgylcerol from *Escherichia-Coli* Membranes", *Chemistry and Physics of Lipids,* vol. 43, no. 4, pp. 237-246.

Miyashita, M., Yoshikoshi, A. & Grieco, P. 1977, "Pyridinium Para-Toluenesulfonate - Mild and Efficient Catalyst for Tetrahydropyranylation of Alcohols", *Journal of Organic Chemistry,* vol. 42, no. 23, pp. 3772-3774.

Molotkov, J.G. & Bergelso, L.D. 1968, "On Structure of Lipoamino Acids", *Chemistry and Physics of Lipids,* vol. 2, no. 1, pp. 1-10.

Mrsny, R.J., Volwerk, J.J. & Hayes Griffith, O. 1986, "A simplified procedure for lipid phosphorus analysis shows that digestion rates vary with phospholipid structure", *Chemistry and Physics of Lipids,* vol. 39, no. 1, pp. 185-191.

Mukhopadhyay, K., Whitmire, W., Xiong, Y.Q., Molden, J., Jones, T., Peschel, A., Staubitz, P., Adler-Moore, J., McNamara, P.J., Proctor, R.A., Yeaman, M.R. & Bayer, A.S. 2007, "In vitro susceptibility of *Staphylococcus aureus* to thrombin-induced platelet microbicidal protein-1 (tPMP-1) is influenced by cell membrane phospholipid composition and asymmetry", *Microbiology,* vol. 153, pp. 1187-1197.

Murthy, M.H., Olson, M.E., Wickert, R.W., Fey, P.D. & Jalali, Z. 2008a, "Daptomycin non-susceptible meticillin-resistant *Staphylococcus aureus* USA 300 isolate", *Journal of Medical Microbiology,* vol. 57, no. 8, pp. 1036-1038.

Murthy, M.H., Olson, M.E., Wickert, R.W., Fey, P.D. & Jalali, Z. 2008b, "Daptomycin non-susceptible meticillin-resistant *Staphylococcus aureus* USA 300 isolate", *Journal of Medical Microbiology,* vol. 57, no. 8, pp. 1036-1038.

Nagle, J. & Tristram-Nagle, S. 2000, "Structure of lipid bilayers", *Biochimica et Biophysica acta-Reviews on Biomembranes,* vol. 1469, no. 3, pp. 159-195.

Nesbitt, J.A. & Lennarz, W.J. 1968, "Participation of Aminoacyl Transfer Ribonucleic Acid in Aminoacyl Phosphatidylglycerol Synthesis .I. Specificity of Lysyl Phosphatidylglycerol Synthetase", *Journal of Biological Chemistry,* vol. 243, no. 11, pp. 3088-3095.

Nishi, H., Komatsuzawa, H., Fujiwara, T., McCallum, N. & Sugai, M. 2004, "Reduced content of lysyl-phosphatidylglycerol in the cytoplasmic membrane affects susceptibility to moenomycin, as well as vancomycin, gentamicin, and antimicrobial peptides, in *Staphylococcus aureus*", *Antimicrobial Agents and Chemotherapy,* vol. 48, no. 12, pp. 4800-4807.

Oivanen, M. & Lonnberg, H. 1989, "Kinetics and Mechanisms for Reactions of Adenosine 2'- and 3'-Monophosphates in Aqueous Acid - Competition between Phosphate Migration, Dephosphorylation, and Depurination", *Journal of Organic Chemistry,* vol. 54, no. 11, pp. 2556-2560.

Ong, P.Y., Ohtake, T., Brandt, C., Strickland, I., Boguniewicz, M., Ganz, T., Gallo, R.L. & Leung, D.Y. 2002, "Endogenous antimicrobial peptides and skin infections in atopic dermatitis", *New England Journal of Medicine,* vol. 347, no. 15, pp. 1151-1160.

Ouhara, K., Komatsuzawa, H., Kawai, T., Nishi, H., Fujiwara, T., Fujiue, Y., Kuwabara, M., Sayama, K., Hashimoto, K. & Sugai, M. 2008, "Increased resistance to cationic antimicrobial peptide LL-37 in methicillin-resistant strains of *Staphylococcus aureus*", *Journal of Antimicrobial Chemotherapy,* vol. 61, no. 6, pp. 1266-1269.

Pabst, G., Koschuch, R., Pozo-Navas, B., Rappolt, M., Lohner, K. & Laggner, P. 2003, "Structural analysis of weakly ordered membrane stacks", *Journal of Applied Crystallography,* vol. 36, pp. 1378-1388.

Pabst, G., Kucerka, N., Nieh, M.-., Rheinstaedter, M.C. & Katsaras, J. 2010, "Applications of neutron and X-ray scattering to the study of biologically relevant model membranes", *Chemistry and Physics of Lipids,* vol. 163, no. 6, pp. 460-479.

Pascher, I., Sundell, S., Harlos, K. & Eibl, H. 1987, "Conformation and packing properties of membrane lipids: the crystal structure of sodium dimyristoylphosphatidylglycerol", *Biochimica et Biophysica acta–Biomembranes,* vol. 896, no. 1, pp. 77-88.

Pearce, J. & Komoroski, R. 1993, "Resolution of phospholipid molecular species by 31P NMR", *Magnetic Resonance in Medicine,* vol. 29, no. 6, pp. 724-731.

Pebaypeyroula, E., Dufourc, E. & Szabo, A. 1994, "Location of Diphenyl-Hexatriene and Trimethylammonium-Diphenyl-Hexatriene in Dipalmitoylphosphatidylcholine Bilayers by Neutron-Diffraction", *Biophysical Chemistry,* vol. 53, no. 1-2, pp. 45-56.

Peschel, A., Jack, R.W., Otto, M., Collins, L.V., Staubitz, P., Nicholson, G., Kalbacher, H., Nieuwenhuizen, W.F., Jung, G., Tarkowski, A., van Kessel, K.P.M. & van Strijp, J.A.G. 2001a, "*Staphylococcus aureus* resistance to human defensins and evasion of neutrophil killing via the novel virulence factor MprF is based on modification of membrane lipids with L-lysine", *Journal of Experimental Medicine,* vol. 193, no. 9, pp. 1067-1076.

Peschel, A., Vuong, C., Otto, M. & Gotz, F. 2000, "The D-alanine residues of *Staphylococcus aureus* teichoic acids alter the susceptibility to vancomycin and the activity of autolytic enzymes", *Antimicrobial Agents and Chemotherapy,* vol. 44, no. 10, pp. 2845-2847.

Pound, R. 1950, "Nuclear electric quadrupole interactions in crystals", *Physical Review,* vol. 79, no. 4, pp. 685-702.

Pozo Navas, B., Lohner, K., Deutsch, G., Sevcsik, E., Riske, K., Dimova, R., Garidel, P. & Pabst, G. 2005, "Composition dependence of vesicle morphology and mixing properties in a bacterial model membrane system", *Biochimica et Biophysica acta–Biomembranes,* vol. 1716, no. 1, pp. 40-48.

Pynn, R. 1990, "Neutron scattering: a primer", *Los Alamos Science,* vol. 19, pp. 1-31.

Qiagen 2013, *SYBR Green Technical Manual*, Technical manual edn, Qiagen, Manchester.

Quinn, P. & Dawson, R. 1969, "The interaction of *cytochrome c* with monolayers of phosphatidylethanolamine", *Biochem.J,* vol. 113, pp. 791-803.

Ranck, J., Keira, T. & Luzzati, V. 1977, "A novel packing of the hydrocarbon chains in lipids the low temperature phases of dipalmitoyl phosphatidyl-glycerol", *Biochimica et Biophysica Acta – Lipids and Lipid Metabolism,* vol. 488, no. 3, pp. 432-441.

Rand, R. 1981, "Interacting phospholipid bilayers: measured forces and induced structural changes", *Annual Review of Biophysics and Bioengineering,* vol. 10, no. 1, pp. 277-314.

Rang, H.P., Dale, M.M., Ritter, J.M. & Moore, P.K. 2003, *Pharmacology,* 5th edn, Churchill Livingstone, London.

Reese, C.B. & Pei-Zhuo, Z. 1993, "Phosphotriester approach to the synthesis of oligonucleotides: a reappraisal", *Journal of the Chemical Society, Perkin Transactions 1,* , no. 19, pp. 2291-2301.

Renart, J. & Sandoval, I.V. 1984, "[33] Western blots", *Methods in Enzymology,* vol. 104, pp. 455-460.

Rouser, G., Fleischer, S. & Yamamoto, A. 1970, "Two dimensional thin layer chromatographic separation of polar lipids and determination of phospholipids by phosphorus analysis of spots", *Lipids,* vol. 5, no. 5, pp. 494-496.

Roy, H. & Ibba, M. 2009, "Broad range amino acid specificity of RNA-dependent lipid remodeling by multiple peptide resistance factors", *Journal of Biological Chemistry,* vol. 284, no. 43, pp. 29677-29683.

Roy, H. 2009, "Tuning the Properties of the Bacterial Membrane with Aminoacylated Phosphatidylglycerol", *IUBMB life,* vol. 61, no. 10, pp. 940-953.

Rutherford Appleton Laboratories 2007, *Colette*, ISIS, Oxford, UK.

Salzberg, L.I. & Helmann, J.D. 2008, "Phenotypic and transcriptomic characterization of *Bacillus subtilis* mutants with grossly altered membrane composition", *Journal of Bacteriology,* vol. 190, no. 23, pp. 7797-7807.

Samant, S., Hsu, F., Neyfakh, A.A. & Lee, H. 2009, "The *Bacillus anthracis* protein MprF is required for synthesis of lysylphosphatidylglycerols and for resistance to cationic antimicrobial peptides", *Journal of Bacteriology,* vol. 191, no. 4, pp. 1311-1319.

Saxena, A.M. & Schoenborn, B.P. 1977, "Correction Factors for Neutron-Diffraction from Lamellar Structures", *Acta Crystallographica Section a,* vol. 33, no. SEP1, pp. 813-818.

Schafer, H., Madler, B. & Volke, F. 1995, "De-Pake-Ing of Nmr Powder Spectra by Nonnegative Least-Squares Analysis with Tikhonov Regularization", *Journal of Magnetic Resonance Series a,* vol. 116, no. 2, pp. 145-149.

Schmittgen, T.D. & Livak, K.J. 2008, "Analyzing real-time PCR data by the comparative C-T method", *Nature Protocols,* vol. 3, no. 6, pp. 1101-1108.

Schoenborn, B.P. & Knott, R.B. 1996, *Neutrons in Biology,* Plenum Press.

Schwartz, L.H. 1977, *Diffraction From Materials,* Elsevier Science.

Sebastiani, F., Harvey, R., Khanniche, S., Artero, J., Haertlein, M. & Fragneto, G. 2012, "Diffraction studies on natural and model lipid bilayers", *The European Physical Journal Special Topics,* vol. 213, no. 1, pp. 355-365.

Seelig, A. & Seelig, J. 1974, "Dynamic Structure of Fatty Acyl Chains in a Phospholipid Bilayer Measured by Deuterium Magnetic-Resonance", *Biochemistry,* vol. 13, no. 23, pp. 4839-4845.

Sheehan, J., Boshart, G. & Cruickshank, P. 1961, "Convenient Synthesis of Water-Soluble Carbodiimides", *Journal of Organic Chemistry,* vol. 26, no. 7, pp. 2525-2528.

Sheehan, J. & Hess, G. 1955, "A New Method of Forming Peptide Bonds", *Journal of the American Chemical Society,* vol. 77, no. 4, pp. 1067-1068.

Short, S.A. & White, D.C. 1971, "Metabolism of Phosphatidylglycerol, Lysylphosphatidylglycerol, and Cardiolipin of *Staphylococcus-Aureus*", *Journal of Bacteriology,* vol. 108, no. 1, pp. 219-226.

Sievers, S., M Ernst, C., Geiger, T., Hecker, M., Wolz, C., Becher, D. & Peschel, A. 2010, "Changing the phospholipid composition of *Staphylococcus aureus* causes distinct changes in membrane proteome and membrane-sensory regulators", *Proteomics,* vol. 10, no. 8, pp. 1685-1693.

Silvius, J. 1982, *Thermotropic Phase Transitions of Pure Lipids in Model Membranes and Their Modifications by Membrane Proteins,* John Wiley & Sons, Inc, 1982.

Skipski, V., Peterson, R. & Barclay, M. 1964, "Quantitative analysis of phospholipids by thin-layer chromatography", *Biochemical Journal,* vol. 90, no. 2, pp. 374-378.

Slavetinsky, C.J., Peschel, A. & Ernst, C.M. 2012, "Alanyl-phosphatidylglycerol and lysyl-phosphatidylglycerol are translocated by the same MprF flippases and have similar capacities to protect against the antibiotic daptomycin in *Staphylococcus aureus*", *Antimicrobial Agents and Chemotherapy,* vol. 56, no. 7, pp. 3492-3497.

Snyder, L.R. 2008, "Solvent selectivity in normal-phase TLC", *JPC-Journal of Planar Chromatography-Modern TLC,* vol. 21, no. 5, pp. 315-323.

Sohlenkamp, C., Galindo-Lagunas, K.A., Guan, Z., Vinuesa, P., Robinson, S., Thomas-Oates, J., Raetz, C.R. & Geiger, O. 2007, "The lipid lysyl-phosphatidylglycerol is present in membranes of *Rhizobium tropici* CIAT899 and confers increased resistance to polymyxin B under acidic growth conditions", *Molecular Plant-Microbe Interactions,* vol. 20, no. 11, pp. 1421-1430.

Sorrell, T.N. 2006, *Organic Chemistry,* University Science Books.

Squires, G.L. 2012, *Introduction to the theory of thermal neutron scattering,* Cambridge University Press.

Staubitz, P., Neumann, H., Schneider, T., Wiedemann, I. & Peschel, A. 2004, "MprF-mediated biosynthesis of lysylphosphatidylglycerol, an important determinant in *staphylococcal* defensin resistance", *FEMS Microbiology Letters,* vol. 231, no. 1, pp. 67-71.

Sternin, E., Bloom, M. & Mackay, A.L. 1983, "De-Pake-Ing of Nmr-Spectra", *Journal of Magnetic Resonance,* vol. 55, no. 2, pp. 274-282.

Suits, B. & Slichter, C. 1984, "Nuclear-quadrupole-resonance study of the 145-K charge-density-wave transition in $NbSe_3$", *Physical Review B,* vol. 29, no. 1, pp. 41-51.

Sung, W., Seok, S., Kim, D., Tian, C. & Shen, Y. 2010, "Sum-frequency spectroscopic study of Langmuir monolayers of lipids having oppositely charged headgroups", *Langmuir,* vol. 26, no. 23, pp. 18266-18272.

Systat software 2012, *Peakfit*, 4.12th edn, Systat software, San Jose, USA.

Tarbell, D., Yamamoto, Y. & Pope, B. 1972, "New Method to Prepare N-t-Butoxycarbonyl Derivatives and the Corresponding Sulfur Analogs from di-t-Butyl Dicarbonate or di-t-Butyl Dithiol Dicarbonates and Amino Acids", *Proc Natl Acad Sci U S A,* vol. 69, no. 3, pp. 730-732.

Tayebi, L., Ma, Y., Vashaee, D., Chen, G., Sinha, S.K. & Parikh, A.N. 2012, "Long-range interlayer alignment of intralayer domains in stacked lipid bilayers", *Nature materials,* .

Thedieck, K., Hain, T., Mohamed, W., Tindall, B.J., Nimtz, M., Chakraborty, T., Wehland, J. & Jänsch, L. 2006, "The MprF protein is required for lysinylation of phospholipids in listerial

membranes and confers resistance to cationic antimicrobial peptides (CAMPs) on *Listeria monocytogenes*", *Molecular Microbiology,* vol. 62, no. 5, pp. 1325-1339.

Theis, T., Skurray, R.A. & Brown, M.H. 2007, "Identification of suitable internal controls to study expression of a *Staphylococcus aureus* multidrug resistance system by quantitative real-time PCR", *Journal of Microbiological Methods,* vol. 70, no. 2, pp. 355-362.

Thomas, L.C., Gidding, H.F., Ginn, A.N., Olma, T. & Iredell, J. 2007, "Development of a real-time *Staphylococcus aureus* and MRSA (SAM-) PCR for routine blood culture", *Journal of Microbiological Methods,* vol. 68, no. 2, pp. 296-302.

Tocanne, J.F., Verheij, H.M., Op Den Kamp, J.A.F. & Van Deenen, L.L.M. 1974a, "Chemical and physicochemical studies of lysylphosphatidylglycerol derivatives. Occurrence of A2′ → 3′ lysyl migration", *Chemistry and Physics of Lipids,* vol. 13, no. 4, pp. 389-403.

Tocanne, J.F., Ververga. P.H.J.T., Verkleij, A.J. & Vandeene, L.l. 1974b, "Monolayer and Freeze-Etching Study of Charged Phospholipids .2. Ionic Properties of Mixtures of Phosphatidylglycerol and Lysylphosphatidylglycerol", *Chemistry and Physics of Lipids,* vol. 12, no. 3, pp. 220-231.

Tocanne, J.F., Ververgaert, P.H.J.T., Verkleij, A.J. & Van Deenen, L.L.M. 1974c, "A monolayer and freeze-etching study of charged phospholipids I. Effects of ions and pH on the ionic properties of phosphatidylglycerol and lysylphosphatidylglycerol", *Chemistry and Physics of Lipids,* vol. 12, no. 3, pp. 201-219.

Tollinger, M., Forman-Kay, J. & Kay, L.E. 2002, "Measurement of Side-Chain Carboxyl pKa Values of Glutamate and Aspartate Residues in an Unfolded Protein by Multinuclear NMR Spectroscopy", *Journal of the American Chemical Society,* vol. 124, no. 20, pp. 5714-5717.

Traïkia, M., Warschawski, D.E., Recouvreur, M., Cartaud, J. & Devaux, P.F. 2000, "Formation of unilamellar vesicles by repetitive freeze-thaw cycles: characterization by electron microscopy and 31P-nuclear magnetic resonance", *European Biophysics Journal,* vol. 29, no. 3, pp. 184-195.

Träuble, H., Teubner, M., Woolley, P. & Eibl, H. 1976, "Electrostatic interactions at charged lipid membranes: I. Effects of ph and univalent cations on membrane structure", *Biophysical Chemistry,* vol. 4, no. 4, pp. 319-342.

Ulrich, H. 2008, *Chemistry and Technology of Carbodiimides,* Wiley.

Vaskovsky, V. & Kostetsky, E. 1968, "Modified spray for the detection of phospholipids on thin-layer chromatograms", *Journal of Lipid Research,* vol. 9, no. 3, pp. 396-396.

Vermeer, L.S., De Groot, B.L., Réat, V., Milon, A. & Czaplicki, J. 2007, "Acyl chain order parameter profiles in phospholipid bilayers: computation from molecular dynamics simulations and comparison with 2H NMR experiments", *European Biophysics Journal,* vol. 36, no. 8, pp. 919-931.

Von Eiff, C., Becker, K., Machka, K., Stammer, H., Peters, G. & Study Grp 2001, "Nasal carriage as a source of *Staphylococcus aureus* bacteremia.", *New England Journal of Medicine,* vol. 344, no. 1, pp. 11-16.

Walther, T.C. & Mann, M. 2010, "Mass spectrometry–based proteomics in cell biology", *The Journal of Cell Biology,* vol. 190, no. 4, pp. 491-500.

Ward, J.B. & Perkins, H.R. 1968, "Chemical Composition of Membranes of Protoplasts and L-Forms of *Staphylococcus Aureus*", *Biochemical Journal,* vol. 106, no. 2, pp. 391-400.

Washington, N., Steele, R.J.C., Jackson, S.J., Bush, D., Mason, J., Gill, D.A., Pitt, K. & Rawlins, D.A. 2000, "Determination of baseline human nasal pH and the effect of intranasally administered buffers", *International Journal of Pharmaceutics,* vol. 198, no. 2, pp. 139-146.

Watts, A., Harlos, K., Maschke, W. & Marsh, D. 1978, "Control of the structure and fluidity of phosphatidylglycerol bilayers by pH titration", *Biochimica et Biophysica acta–Biomembranes,* vol. 510, no. 1, pp. 63-74.

Weinrick, B., Dunman, P.M., McAleese, F., Murphy, E., Projan, S.J., Fang, Y. & Novick, R.P. 2004, "Effect of mild acid on gene expression in *Staphylococcus aureus*", *Journal of Bacteriology,* vol. 186, no. 24, pp. 8407-8423.

Weidenmaier, C., Peschel, A., Kempf, V.A., Lucindo, N., Yeaman, M.R. & Bayer, A.S. 2005, "DltABCD-and MprF-mediated cell envelope modifications of *Staphylococcus aureus* confer resistance to platelet microbicidal proteins and contribute to virulence in a rabbit endocarditis model", *Infection and Immunity,* vol. 73, no. 12, pp. 8033-8038.

Wey, S., Augustyniak, M.E., Cochran, E.D., Ellis, J.L., Fang, X., Garvey, D.S., Janero, D.R., Letts, L.G., Martino, A.M., Melim, T.L., Murty, M.G., Richardson, S.K., Schroeder, J.D., Selig, W.M., Trocha, A.M., Wexler, R.S., Young, D.V., Zemtseva, I.S. & Zifcak, B.M. 2007, "Structure-based design, synthesis, and biological evaluation of indomethacin derivatives as cyclooxygenase-2 inhibiting nitric oxide donors", *Journal of Medicinal Chemistry,* vol. 50, no. 25, pp. 6367-6382.

White, D.C. & Frerman, F.E. 1968, "Fatty Acid Composition of Complex Lipids of *Staphylococcus Aureus* during Formation of Membrane-Bound Electron Transport System", *Journal of Bacteriology,* vol. 95, no. 6, pp. 2198-2209.

Wilkinson, D., Tirrell, D., Turek, A. & McIntosh, T. 1987, "Tris buffer causes acyl chain interdigitation in phosphatidylglycerol", *Biochimica et Biophysica acta–Biomembranes,* vol. 905, no. 2, pp. 447-453.

Williams, D. & Fleming, I. 2008, *Spectroscopic methoids in organic chemistry,* 6th edn, McGraw-Hill Education (UK), New York.

Wilson, C.C. & Myles, D.A. 2006, "Single Crystal Neutron Diffraction and Protein Crystallography" in Springer Berlin Heidelberg, , pp. 21-42.

Wilson, W.W., Wade, M.M., Holman, S.C. & Champlin, F.R. 2001, "Status of methods for assessing bacterial cell surface charge properties based on zeta potential measurements", *Journal of Microbiological Methods,* vol. 43, no. 3, pp. 153-164.

Woodle, M.C. & Papahadjopoulos, D. 1989, "Liposome preparation and size characterization", *Methods in Enzymology,* vol. 171, pp. 193-217.

Worcester, D.L. & Franks, N.P. 1976, "Structural analysis of hydrated egg lecithin and cholesterol bilayers II. Neutron diffraction", *Journal of Molecular Biology,* vol. 100, no. 3, pp. 359-378.

Wuts, P.G.M. & Greene, T.W. 2006, *Greene's Protective Groups in Organic Synthesis,* Wiley.

Yang, S., Xiong, Y.Q., Dunman, P.M., Schrenzel, J., Francois, P., Peschel, A. & Bayer, A.S. 2009, "Regulation of mprF in Daptomycin-Nonsusceptible *Staphylococcus aureus* Strains", *Antimicrobial Agents and Chemotherapy,* vol. 53, no. 6, pp. 2636-2637.

Ye, J., Coulouris, G., Zaretskaya, I., Cutcutache, I., Rozen, S. & Madden, T.L. 2012, "Primer-BLAST: A tool to design target-specific primers for polymerase chain reaction", *Bmc Bioinformatics,* vol. 13, pp. 13-134.

Yeagle, P. 2012, *The Structure of Biological Membranes,* CRC Press.

Yoshioka, S. & Stella, V.J. 2000, *Stability of Drugs and Dosage Forms,* Springer.

Zagorevskii, V. & Kirsanova, Z. 1970, "Migration of the tosyl group in 7-O-tosylesculetins", *Chemistry of Heterocyclic Compounds,* vol. 6, no. 3, pp. 288-289.

Zasloff, M., Martin, B. & Chen, H.C. 1988, "Antimicrobial Activity of Synthetic Magainin Peptides and several Analogs", *Proceedings of the National Academy of Sciences of the United States of America,* vol. 85, no. 3, pp. 910-913.

Appendix I Neutron diffraction structure factors

In order to determine the signs of the structure factors for all scattering length density (SLD) profiles, the linear dependence model was utlised (Pebaypeyroula *et al.* 1994).

AI.I *Staphylococcus aureus* lipid extracts

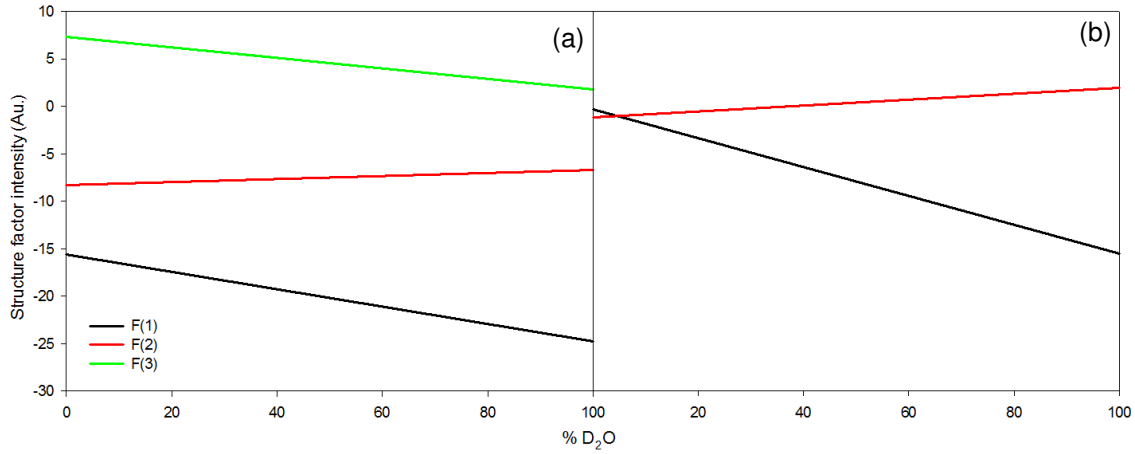

Figure A-1 Structure factor linear dependence profiles for the sign assignment of the structure factors of MSSA 476 lipid extracts of bacteria grown at (a) pH 7.4 and (b) pH 5.5.

Table A-1 Absolute structure factors with signs of the lipid extracts from MSSA 476 grown at pH 5.5 and 7.4.

	pH 7.4		pH 5.5	
h	D_2O	H_2O	D_2O	H_2O
1	-15.6	-24.8	-7.8	-19.2
2	-8.3	-6.7	-8.4	-6.1
3	7.3	1.8		

AI.II 100% DP3adLPG

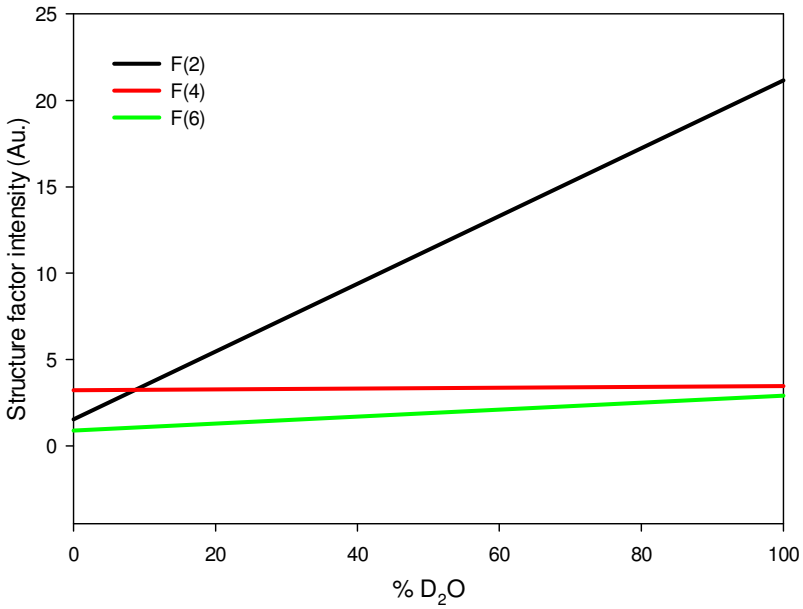

Figure A-2 Structure factor linear dependence profile for the sign assignment of the structure factors of 100% DP3adLPG.

Table A-2 Absolute structure factors with signs of 100% DP3adLPG.

h	D_2O	H_2O
2	1.53	21.16
4	3.46	3.48
6	0.88	2.91

AI.III d_{62}3adLPG–d_{62}PG 3:7 at 25 °C, d_{62}PG rich phase

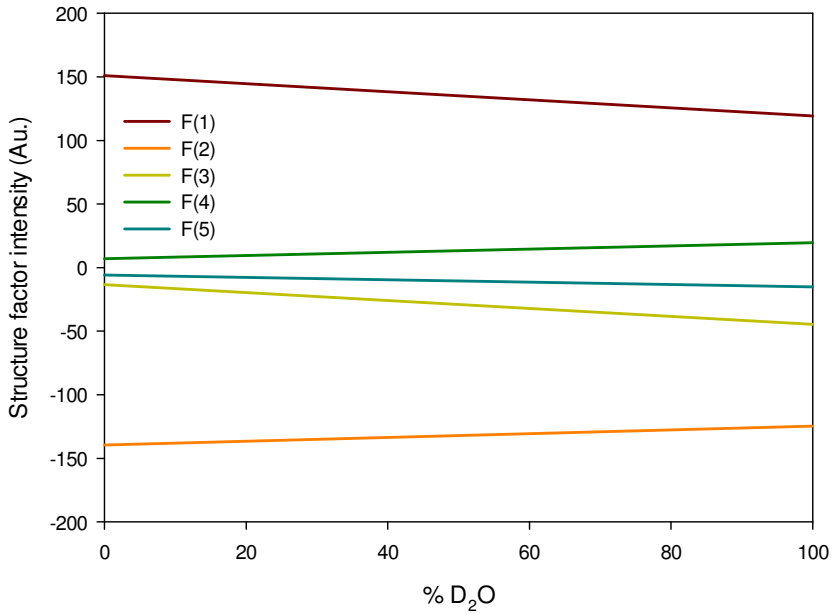

Figure A-3 Structure factor linear dependence profile for the sign assignment of the structure factors of d_{62}3adLPG–d_{62}PG 3:7 at 25 °C, d_{62}PG rich phase.

Table A-3 Absolute structure factors with signs of d_{62}3adLPG–d_{62}PG 3:7 at 25 °C, d_{62}PG rich phase.

h	D_2O	H_2O
1	150.94	119.32
2	-139.40	-124.64
3	-13.30	-44.60
4	6.96	19.66
5	-5.87	-14.96
6		
7		
8		-11.19

AI.IV d_{62}3adLPG–d_{62}PG 3:7 at 25 °C, d_{62}3adLPG–d_{62}PG ion-pair phase

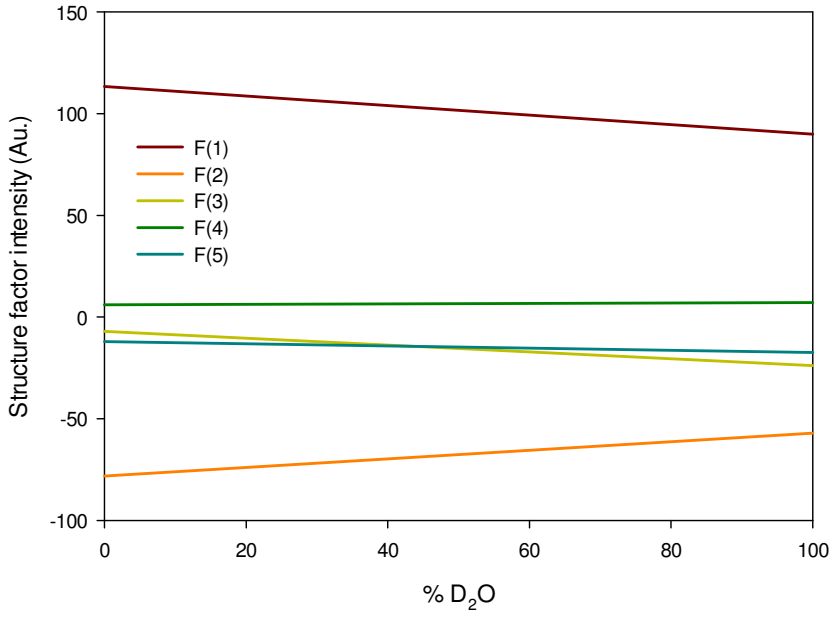

Figure A-4 Structure factor linear dependence profile for the sign assignment of the structure factors of d_{62}3adLPG–d_{62}PG 3:7 at 25 °C, d_{62}3adLPG–d_{62}PG ion-pair phase.

Table A-4 Absolute structure factors with signs of d_{62}3adLPG–d_{62}PG 3:7 at 25 °C, d_{62}3adLPG–d_{62}PG ion-pair phase.

h	D_2O	H_2O
1	113.40	90.01
2	-78.20	-57.01
3	-7.02	-23.74
4	7.16	6.05
5	-11.98	-17.44
6		8.85

AI.V d_{62}3adLPG–d_{62}PG 55:45 at 25 °C

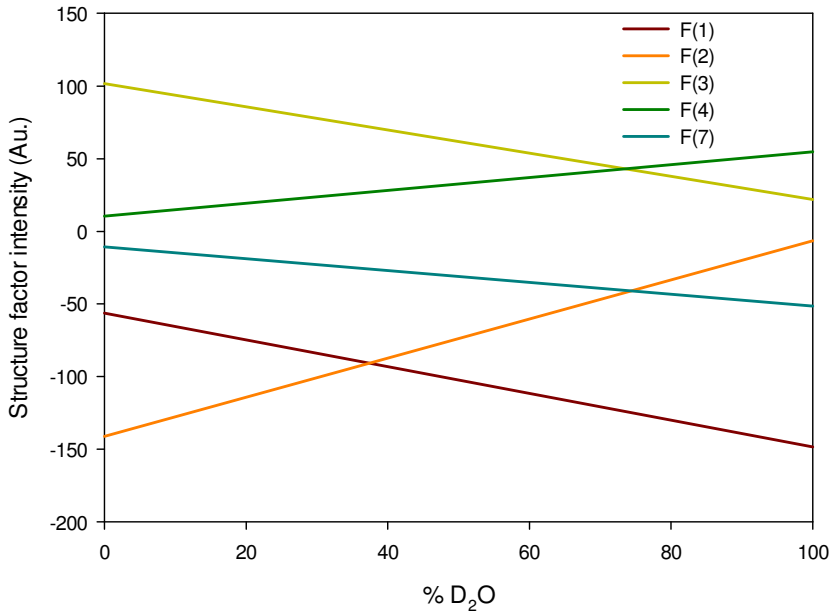

Figure A-5 Structure factor linear dependence profile for the sign assignment of the structure factors of d_{62}3adLPG–d_{62}PG 55:45 at 25 °C.

Table A-5 Absolute structure factors with signs of d_{62}3adLPG–d_{62}PG 55:45 at 25 °C.

h	D_2O	H_2O
1	-56.41	-148.43
2	-141.10	-6.54
3	101.78	21.81
4	10.37	54.70
5	-6.91	
6		-21.76
7	-10.68	-51.46
8	-2.86	

AI.VI d_{62}3adLPG–d_{62}PG 3:7 at 55 °C

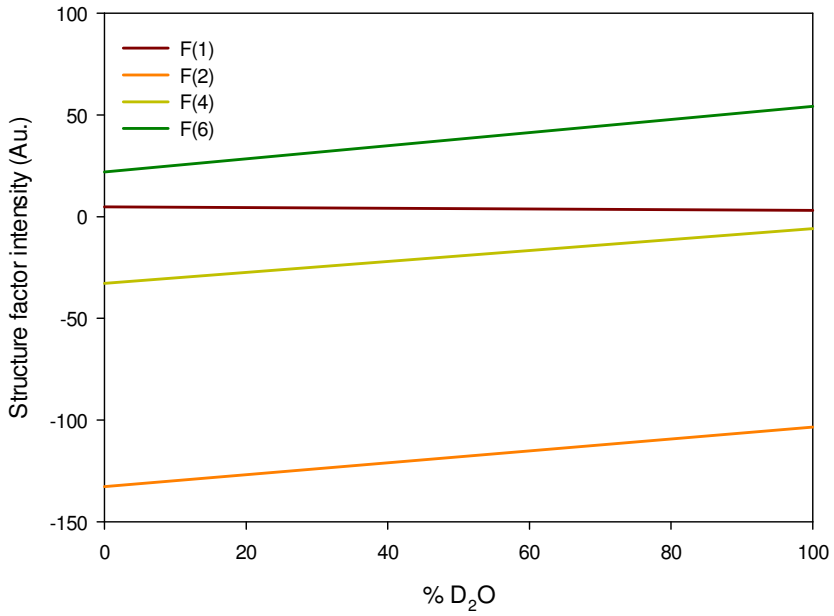

Figure A-6 Structure factor linear dependence profile for the sign assignment of the structure factors of d_{62}3adLPG–d_{62}PG 3:7 at 55 °C.

Table A-6 Absolute structure factors with signs of d_{62}3adLPG–d_{62}PG 3:7 at 55 °C.

h	D_2O	H_2O
1	3.16	4.94
2	-132.72	-103.36
4	-32.68	-5.79
6	22.01	54.37

AI.VII d_{62}3adLPG–d_{62}PG 55:45 at 55 °C

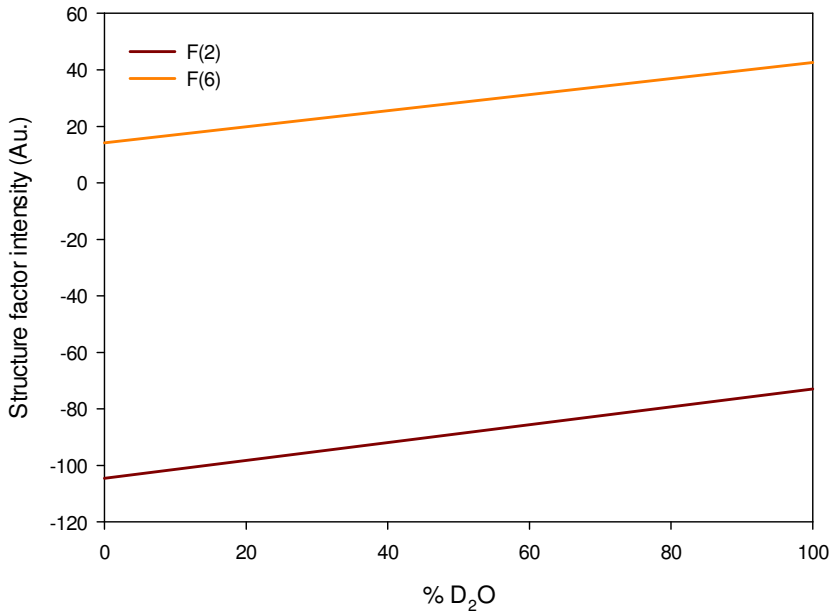

Figure A-7 Structure factor linear dependence profile for the sign assignment of the structure factors of d_{62}3adLPG–d_{62}PG 55:45 at 55 °C.

Table A-7 Absolute structure factors with signs of d_{62}3adLPG–d_{62}PG 55:45 at 55 °C.

h	D_2O	H_2O
2	-104.52	-72.96
4	-32.99	
6	14.13	42.65

Appendix II Bacterial lipid extract surface pressure-area isotherms

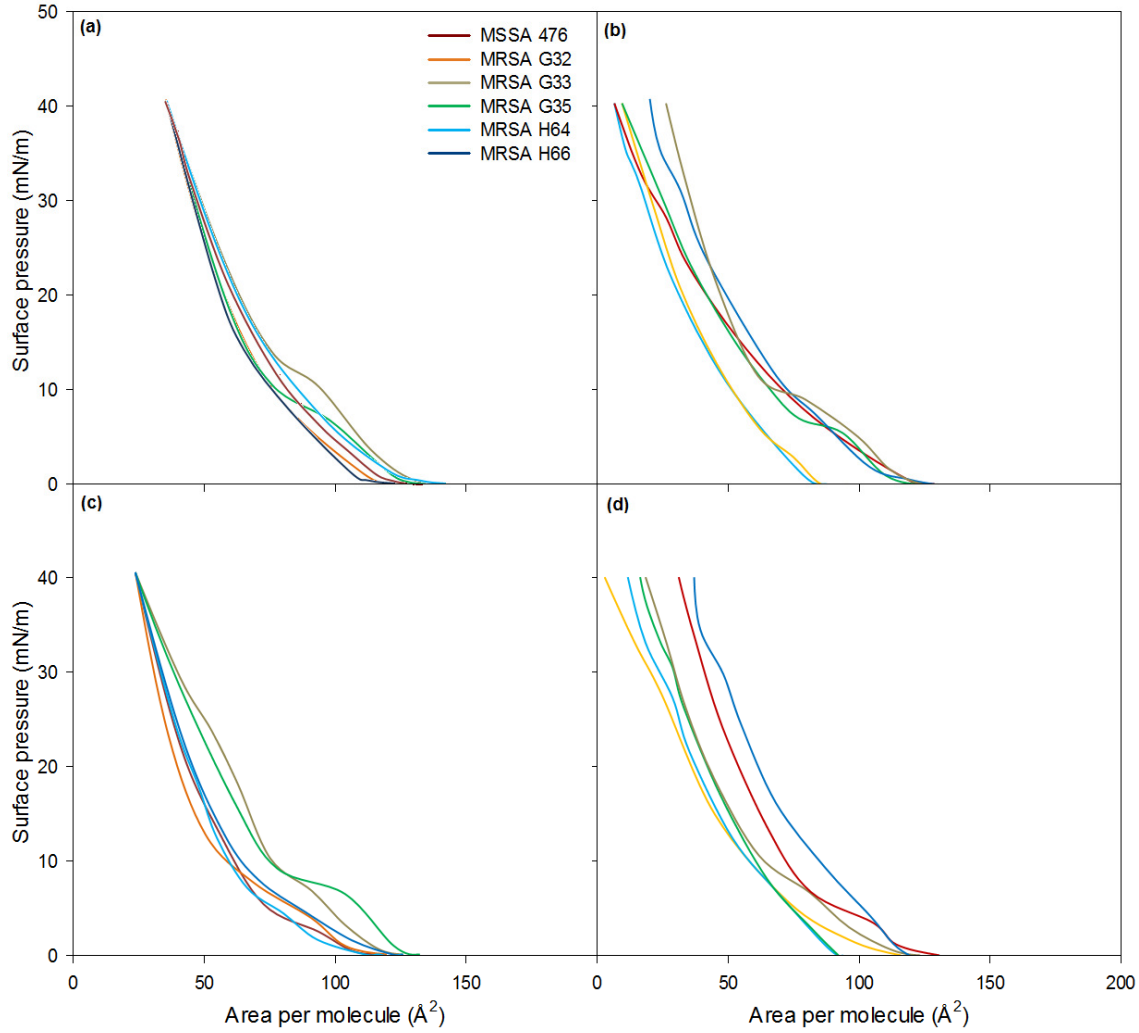

Figure A-8 *Staphylococcus aureus* lipid extract surface pressure-area isotherms; (a) pH 7.4 lipid extracts on a pH 7.4 subphase, (b) pH 7.4 lipid extracts on a pH 5.5 subphase, (c) pH 5.5 lipid extracts on a pH 7.4 subphase and (d) pH 5.5 lipid extracts on a pH 5.5 subphase.